Engineering Proceedings P-42

WAVE INTERACTION AND DYNAMIC NONLINEAR PHENOMENA IN PLASMAS

Papers presented at a conference at
The Pennsylvania State University
February 4 to 6, 1963

September 1963

THE PENNSYLVANIA STATE UNIVERSITY
College of Engineering
University Park, Pennsylvania

Engineering Proceedings P-42

WAVE INTERACTION AND DYNAMIC NONLINEAR PHENOMENA IN PLASMAS

Papers presented at a conference at
The Pennsylvania State University
February 4 to 6, 1963

Conducted by
The Department of Electrical Engineering
and
Continuing Education

Sponsored by
The Ionosphere Research Laboratory
and
The National Aeronautics and Space Administration

Cooperating organizations
Center for Radiophysics and Space Research, Cornell University
Courant Institute of Mathematical Sciences, New York University
Department of Electrical Engineering, University of Michigan
Electron Physics Laboratory, University of Michigan
General Electric Research Laboratory, Schenectady
Microwave Associates, Inc.
Plasma Physics Laboratory, Princeton University
RCA Laboratories, Princeton
Research Laboratory of Electronics, Chalmers University of Technology

Conference chairman
Anthony J. Ferraro, Associate Professor
Department of Electrical Engineering

THE PENNSYLVANIA STATE UNIVERSITY
College of Engineering
University Park, Pennsylvania

September 1963

ORDER FROM: Engineering Publications
227 Hammond Building
The Pennsylvania State University
University Park, Pa. 16802

Checks or money orders should be payable to THE PENNSYLVANIA STATE UNIVERSITY. If your address is in Pennsylvania, please add 5% sales tax. We pay postage at the minimum book rate.

PREFACE

Presented here, as complete papers or abstracts, are the major contributions to a conference held at The Pennsylvania State University in February 1963. The speakers were invited, and their lectures were mainly concerned with the following subject areas:

I. Linearly interacting waves of physically different kinds:
   A. Space-charge waves and magnetoionic-type waves encountered in plasma amplifying devices.
   B. Whistlers produced by interacting streams.

II. Nonlinearly interacting waves that are normally of the same nature but of different frequency:
   A. High power and low power waves in stationary and streaming ionized media.
   B. Parametric wave interaction as it may occur in propagation through the solar corona.
   C. Nonlinear optics of ionized media.

The conference was designed to bring together outstanding workers in the fields of weak interactions and dynamic nonlinear phenomena in ionized media such as the solar corona and exospheric and ionospheric plasmas, and prominent workers engaged in developing high power microwave and plasma devices. It was our hope that in sharing a discussion of fundamental problems in plasma physics, scientists and engineers from these related but quite different fields would recognize the possibility of coordinating the two distinct bodies of literature evolving from geophysical interests and device engineering.

The presence of Dr. O. E. H. Rydbeck as a distinguished visiting professor of electrical engineering at this University provided the basic motivation for the conference. His great influence is indicated by his large contribution to this volume. Dr. A. J. Ferraro, associate professor of electrical engineering, undertook the numerous duties of conference chairman. The University is greatly indebted to the contributors whose work is reported herein.

It is a great pleasure to acknowledge the financial support of the Office of Space Sciences of the National Aeronautics and Space Administration, which made the conference possible and permitted the publication of these papers.

ARTHUR H. WAYNICK, Head
Department of Electrical Engineering
and Director of
The Ionosphere Research Laboratory

University Park, Pennsylvania
June 28, 1963

CONTENTS

Page

ELECTROMAGNETIC NONLINEAR INTERACTION AND
REFLECTION FROM A PLANE IONIZED MEDIUM 3
O. E. H. Rydbeck
Chalmers University of Technology

DYNAMIC NONLINEAR ELECTROMAGNETIC WAVE PROPAGATION
AND HARMONIC RADIATION IN MAGNETOIONIC MEDIA 42
O. E. H. Rydbeck

WHISTLER MODE AND IONIZED STREAM INTERACTIONS 71
O. E. H. Rydbeck and J. Askne

NONLINEAR WAVE PHENOMENA IN PLASMAS (abstract) 115
P. A. Sturrock
Stanford University

THE QUASI-LINEAR THEORY OF PLASMA OSCILLATIONS
AND INSTABILITIES (abstract) 117
S. E. Bodner and E. A. Frieman
Princeton University

RADIO BURSTS FROM THE SUN (abstract) 118
M. H. Cohen
Cornell University

SOME INVESTIGATIONS OF INSTABILITIES
IN ONE-DIMENSIONAL PLASMAS (abstract) 121
John Dawson
Princeton University

SURVEY OF PROPAGATION PHENOMENA, LINEAR AND NONLINEAR,
IN AN INFINITELY CONDUCTING COMPRESSIBLE FLUID (abstract) 123
J. Bazer
New York University

ON THE NONLINEAR THEORY OF MULTISTREAM ELECTRONIC DEVICES 125
C. L. Dolph and R. J. Lomax
The University of Michigan

BEAM-PLASMA AMPLIFIER EXPERIMENTS 138
Paul Chorney
Microwave Associates, Inc.

EFFECT OF NONUNIFORM PLASMA DENSITY ON
ELECTRON BEAM-PLASMA INTERACTION 147
G. A. Swartz and L. S. Napoli
RCA Laboratories

(CONTINUED)

CONTENTS (Continued)

Page

NONPLANAR PHENOMENA IN SINGLE AND MULTIPLE ELECTRON BEAMS 157
Theodore G. Mihran
General Electric Research Laboratory

MULTIDIMENSIONAL NONLINEAR THEORY OF MICROWAVE INTERACTIONS . . . 189
J. E. Rowe
The University of Michigan

ON THE NONLINEAR THEORY OF THE PLANE TRAVELING-WAVE TUBE 205
S. Olving
Chalmers University of Technology

NOTE

In text, numbers in parentheses relate to the references at the end of each paper.

Page

I
3 . . . . . ELECTROMAGNETIC NONLINEAR INTERACTION AND REFLECTION FROM A PLANE IONIZED MEDIUM

II
42 . . . . . DYNAMIC NONLINEAR ELECTROMAGNETIC WAVE PROPAGATION AND HARMONIC RADIATION IN MAGNETOIONIC MEDIA

III
71 . . . . . WHISTLER MODE AND IONIZED STREAM INTERACTIONS

by

O. E. H. RYDBECK

Distinguished Visiting Professor
Department of Electrical Engineering
The Pennsylvania State University

on leave from
Research Laboratory of Electronics
Chalmers University of Technology
Gothenburg, Sweden

J. ASKNE, Research Laboratory of Electronics,
Chalmers University of Technology, collaborated
with Dr. Rydbeck on paper III.

The research reported in these papers was sponsored by the Ionosphere Research Laboratory, The Pennsylvania State University; the National Science Foundation, under Grant G-18983; and the Geophysics Research Directorate, Air Force Cambridge Research Laboratories, Office of Aerospace Research, L. G. Hanscom Field, Bedford, Massachusetts, under Contract AF19(604)-4563.

NOTE

Equations in the three papers by Dr. Rydbeck are reproduced photographically from typewriter copy prepared under his supervision.

In the text, numbers in parentheses relate to the references at the end of each paper.

I. ELECTROMAGNETIC NONLINEAR INTERACTION AND REFLECTION FROM A PLANE IONIZED MEDIUM*

1. SUMMARY

The study of the dynamic nonlinear reflection of radio waves from ionized media has recently become a subject of practical importance, apart from the interesting theoretical problems involved in such studies. Rocket-borne transmitters and ionospheric topside sounders now make it possible to generate dynamic ionospheric nonlinearities and to obtain in situ recordings of the results produced. These experiments will doubtless yield important ionospheric propagation information, especially in the upper ionosphere where losses are small and nonlinear resonance effects may be quite important.

It is the purpose of the research reported in this communication to study the reflection properties of an isotropic ionized medium in the presence of nonlinear effects produced in the medium by a separate, very powerful "pump" wave of angular frequency ω_p. It is shown, to the first order, that if a primary signal or probing wave of angular frequency ω_o impinges on the disturbed ionized medium at some specified angle, waves of frequencies ω_o, $\omega_o + \omega_p$, and $\omega_o - \omega_p$ are returned from the layer.

The laws of reflection and refraction deduced for these waves may be considered as typical expressions for the nonlinear optics of the system. These relations have very interesting properties. They show, for example, that the difference frequency wave is returned in the direction of the incident primary wave if $\omega_p = 2\omega_o$ and if the pump wave is normally incident. Since this makes the difference frequency equal (in magnitude) to the signal frequency, the peculiar situation arises wherein the reflected wave direction is that of the incident primary wave.

It is furthermore shown that the sum and difference frequency waves may be very much enhanced by "nonlinear" or parametric resonances of the system. When conditions prevail for degenerate parametric resonance of the difference frequency wave, the medium acts as a parametric amplifier with the remarkable property that the amplified wave is returned in the primary incidence direction. The energy providing this amplification is furnished by the powerful pump wave.

The properties of the sum and difference frequency waves, also called "secondary waves," have likewise been investigated inside the ionized medium. It is shown that four types of secondary waves are produced in the medium, two of which are associated with the primary waves and two of which exhibit the properties of "independent" electromagnetic waves. It is waves of the latter type that leave the interaction region and are observable from the "outside."

---

*Scientific Report No. 183, Ionosphere Research Laboratory, The Pennsylvania State University, April 15, 1963.

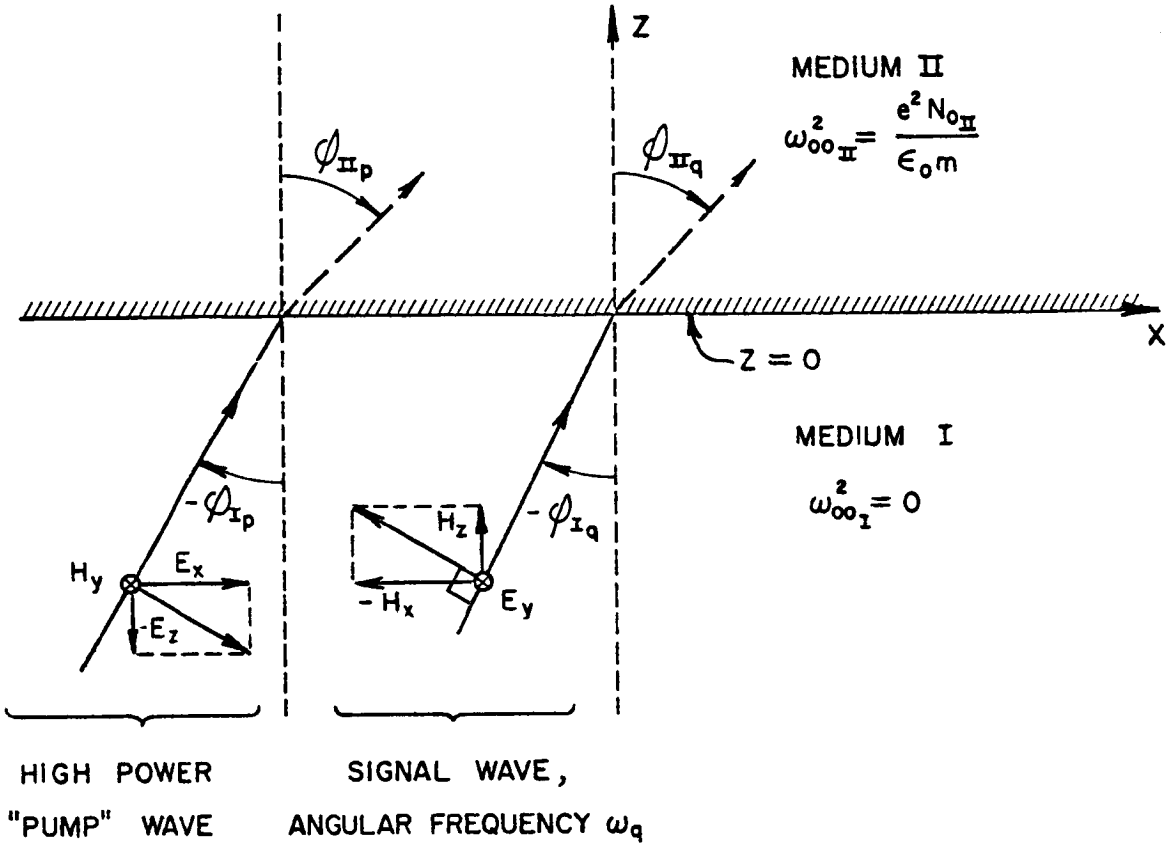

FIG. 1. Polarizations and angles of incidence of signal and high power pump waves.

To show how the secondary waves leave the interaction region, the theory has been extended, in approximate form, to the practically important but now very difficult case of a slowly varying inhomogeneous medium. When the interaction region is small, counted in pump wavelengths, the resonance effects become much less pronounced. The smaller the primary partial reflection, the greater the nonlinear resonance interaction.

Problems of this kind are of considerable interest in connection with harmonic or subharmonic radio wave radiation from the solar corona. Now that ionospheric topside sounders are available, it should be possible to check experimentally some of the results presented in this report. It might also be worthwhile to pump-irradiate ionized meteor trails and observe the effects of the echoes then obtained.

The results of the present investigation are of a fairly general nature, in spite of the fact that magnetoionic effects have been excluded. Some of the results may, in principle, find direct application in the nonlinear laser field.

The investigations reported in this communication are presently being extended to the nonlinear magnetoionic medium, on the basis of the dynamic nonlinear magnetoionic theory recently published by the author (5).

2. WAVE EQUATION OF THE OSCILLATING MEDIUM

We assume that the signal or probing wave, of angular frequency ω_o, and the high power pump wave or waves producing the nonlinear oscillations have polarizations and angles of incidence upon the ionized layer, as shown in Fig. 1.

In an earlier communication Rydbeck (1) showed that the high power wave or waves produce a nonlinear variation ΔN_{II} of the mean electron density $N_{o_{II}}$, and a longitudinal electron velocity v_L in the wave normal direction φ_{II_p}. These electron density and velocity fluctuations travel through the medium, locked to the high power wave, and can be written as follows (1):

$$\Delta N_{II} = \eta N_{o_{II}} \cos(\omega_p t - \bar{k}_p \bar{r}) \tag{1}$$

$$v_L = v_L^o \cos(\omega_p t - \bar{k}_p \bar{r}) \tag{2}$$

where ω_p and k_p depend upon the frequency or frequencies of the high power waves. Besides the nonlinear plasma wave (Eqs. 1 and 2), one must also consider the linear transverse electron velocities v_{T_x} and v_{T_z} produced

by the high power waves. The velocities produced by this high power or pump wave thus become

$$v_{P_x} = v_{T_x} + v_{L_x} = v_T \cos\varphi_{II_P} + v_L \sin\varphi_{II_P}$$

$$v_{P_z} = v_{T_z} + v_{L_z} = -v_T \sin\varphi_{II_P} + v_L \cos\varphi_{II_P} \qquad (3)$$

If v_y denotes the electron velocities of the signal wave (it will be split up in a spectrum of frequency components), its wave equation can be written (note: $\partial/\partial_y = 0$)

$$\left(\frac{\partial^2}{\partial x^2} + \frac{\partial^2}{\partial z^2} - \frac{1}{c_o^2} \frac{\partial^2}{\partial t^2} \right) E_y + \mu_o e \frac{\partial}{\partial t} (N_{II} v_y) = 0 \qquad (4)$$

where $c_o = 1/\sqrt{\mu_o \epsilon_o}$ and

$$N_{II} = N_{o_{II}} + \Delta N_{II} \qquad (5)$$

If the Lorentz forces are taken into account, the equation of motion of the electrons becomes (collisional friction neglected)

$$\frac{\partial v_y}{\partial t} + v_{P_x} \frac{\partial v_y}{\partial x} + v_{P_z} \frac{\partial v_y}{\partial z} = - \frac{e}{m} E_y + \mu_o \frac{e}{m} (v_{P_x} H_z - v_{P_z} H_x) \qquad (6)$$

From Maxwell's equations, Eq. 6 can be written

$$\frac{\partial}{\partial t} \frac{dv_y}{dt} = - \frac{e}{m} \frac{dE_y}{dt} \qquad (6a)$$

where

$$\frac{d}{dt} = \frac{\partial}{\partial t} + v_{P_x} \frac{\partial}{\partial x} + v_{P_z} \frac{\partial}{\partial z} \qquad (7)$$

We notice that for a streaming medium ($\partial v_p/\partial t = 0$), $\partial v_y/\partial t = -(eE_y/m)$.

If we introduce

$$\omega_{o_{II}}^2 = \omega_{oo_{II}}^2 \left(1+\frac{\Delta N_{II}}{N_{o_{II}}}\right) = \omega_{oo_{II}}^2 \left[1+\eta\cos(\omega_p t-\bar{k}_p\bar{r})\right] \tag{8}$$

$$\xi = \frac{\omega_{oo_{II}}^2}{\omega_{o_{II}}^2} \tag{9}$$

$$P_e^2 = \frac{\partial^2}{\partial x^2} + \frac{\partial^2}{\partial z^2} - \frac{1}{c_o^2}\frac{\partial^2}{\partial t^2} \qquad \text{(electromagnetic wave operator for vacuum)} \tag{10}$$

$$\frac{\partial\psi}{\partial t} = E_y \tag{11}$$

the wave equation (Eq. 4) can be written (12)

$$\frac{\partial}{\partial t}\frac{d}{dt}\left[\left(\xi P_e^2 - \frac{\omega_{oo_{II}}^2}{c_o^2}\right)\psi\right] = -\frac{\omega_{oo_{II}}^2}{c_o^2}\left(\frac{\partial v_{P_x}}{\partial t}\frac{\partial}{\partial x} + \frac{\partial v_{P_z}}{\partial t}\frac{\partial}{\partial z}\right)\psi$$

In detail, Eq. 12 becomes

$$\left(\frac{\partial^2}{\partial t^2} + \frac{\partial v_{P_x}}{\partial t}\frac{\partial}{\partial x} + \frac{\partial v_{P_z}}{\partial t}\frac{\partial}{\partial z} + v_{P_x}\frac{\partial^2}{\partial t\partial x} + v_{P_z}\frac{\partial^2}{\partial t\partial z}\right)(\xi P_e^2\psi)$$

$$-\frac{\omega_{oo_{II}}^2}{c_o^2}\left(\frac{\partial^2}{\partial t^2} + v_{P_x}\frac{\partial^2}{\partial t\partial x} + v_{P_z}\frac{\partial^2}{\partial t\partial z}\right)\psi = 0 \tag{12a}$$

3. WAVE REFLECTION, ONLY ELECTRON DENSITY OSCILLATIONS CONSIDERED

To distinguish between the two nonlinear effects, we first study the reflection property of the layer when the velocity fluctuations are

neglected. We assume $v_P = 0 = v_T$, and disregard for the moment the fact that these velocities, in reality, always differ from zero when ΔN_{II} does so. Equation 12 now simplifies to

$$\left\{ \frac{\partial^2}{\partial x^2} + \frac{\partial^2}{\partial z^2} - \frac{1}{c_o^2} \frac{\partial^2}{\partial t^2} - \frac{\omega_{oo_{II}}^2}{c_o^2} \left[1 + \eta \cos(\omega_p t - \bar{k}_p \bar{r}) \right] \right\} \psi = 0 \quad (13)$$

We introduce

$$k_p = \frac{\omega_p}{c_o} n_p$$

$$k_{p_x} = \frac{\omega_p}{c_o} n_{p_x} = k_p \sin\varphi_{II_p} \quad (14)$$

$$k_{p_z} = \frac{\omega_p}{c_o} n_{p_z} = k_p \cos\varphi_{II_p}$$

where n_p is assumed to be a known function of the angular pump frequency ω_p. Furthermore, we introduce the variable

$$\tau = t - \frac{n_{p_x}}{c_o} x - \frac{n_{p_z}}{c_o} z \quad (15)$$

and assume that ψ can be written as

$$\psi_q = e^{+j(\omega_q t - \bar{k}_q \bar{r})} \pi_{q_1}(\tau) \quad (16)$$

where

$$k_q^2 = \frac{\omega_q^2}{c_o^2} \left(1 - \frac{\omega_{oo_{II}}^2}{\omega_q^2} \right) = \frac{\omega_q^2}{c_o^2} n_q^2 = k_{o_q}^2 n_q^2 \quad (17)$$

in which $k_{o_q} = \omega_q/c_o$, and ω_q denotes the angular frequency of an unperturbed wave with the following notations:

$$\omega_{\pm 1} = \omega_o \pm \omega_p \; ; \; \omega_{\pm 2} = \omega_o \pm 2\omega_p \; , \text{ etc.} \tag{18}$$

The wave equation (Eq. 13) now becomes

$$\left(\frac{d^2}{d\tau^2} + j2\omega_q \frac{1-d_q}{1-n_p^2} + \frac{\omega_{oo_{II}}^2}{1-n_p^2} \eta \cos \omega_p \tau \right) \Pi_{q_1} = 0 \tag{19}$$

where

$$d_q = n_{q_x} n_{p_x} + n_{q_z} n_{p_z} = n_q n_p \cos(\varphi_{II_p} - \varphi_{II_q})$$

$$= n_q n_p \cos \Delta\varphi_q \tag{20}$$

We next introduce

$$\Pi_{q_2} = e^{+j\omega_q \frac{1-d_q}{1-n_p^2} \tau} \Pi_{q_1} \tag{21}$$

and, with

$$u = \omega_p \tau/2 \tag{22}$$

we obtain the final (Mathieu) equation

$$\left(\frac{d^2}{du^2} + \theta_{o_q} + 2\theta_1 \cos 2u \right) \Pi_{q_2} = 0 \tag{23}$$

where

$$\theta_{o_q} = \frac{4\omega_q^2}{\omega_p^2} \left(\frac{1-d_q}{1-n_p^2} \right)^2, \text{ and } \theta_1 = \eta \frac{2\omega_{oo_{II}}^2}{\omega_p^2} \frac{1}{1-n_p^2} \tag{24}$$

If we use the notations of Rydbeck (2), the solution to Eq. 23 can be written, for our purposes,

$$\pi_{q_2} = e^{(\mu_q + j)u} \sum_{n=-\infty}^{n=+\infty} b_{q_n} e^{+j2nu} \tag{25}$$

where the amplitude coefficients are obtained from the equations

$$\left\{ \left[\mu_q + j(2n+1) \right]^2 + \theta_{o_q} \right\} b_{q_n}$$

$$+ \theta_1 (b_{q_{n-1}} + b_{q_{n+1}}) = 0 \qquad (n=..,-2,-1,0,1,2,...) \tag{26}$$

and with an accuracy sufficient for our purpose (2), μ_q is obtained from the relation

$$\mu_q^2 = -(\sqrt{\theta_{o_q}} - 1)^2 + \left(\frac{\theta_1}{2} \right)^2 \tag{27}$$

which, for the present case, is conveniently written

$$\mu_q = +j(\sqrt{\theta_{o_q}} - 1) \sqrt{1 - \left[\frac{\theta_1}{2(\sqrt{\theta_{o_q}} - 1)} \right]^2} = j(\sqrt{\theta_{o_q}} - 1 - \delta_{\mu_q}) \tag{28}$$

or

$$\mu_q + j = j(\sqrt{\theta_{o_q}} - \delta_{\mu_q}) \tag{28a}$$

That is,

$$\psi_q = e^{+j(\omega_q t - \bar{k}_q \bar{r} - \delta_{\mu_q} \omega_p \frac{\tau}{2})} \sum_{n=-\infty}^{n=+\infty} b_{q_n} e^{+jn\omega_p \tau} \tag{29}$$

By Eq. 26 we furthermore obtain, neglecting the second order terms $b_{q_{+2}}$ and $b_{q_{-2}}$,

$$b_{q_{+1}} = b_{q_o} \frac{\theta_1/4}{1+(\sqrt{\theta_{o_q}} - \delta_{\mu_q}/2)}$$

$$b_{q_{-1}} = b_{q_o} \frac{\theta_1/4}{1-(\sqrt{\theta_{o_q}} - \delta_{\mu_q}/2)} \qquad (30)$$

When

$$(\sqrt{\theta_{o_q}} - 1)^2 < (\frac{\theta_1}{2})^2 \qquad (31)$$

the medium becomes unstable, and exponentially growing or evanescing waves may result.

We find from Eq. 24 that

$$\sqrt{\theta_{o_q}} \mp 1 = \frac{\omega_q}{\omega_p}\left(2 \mp \frac{\omega_p}{\omega_q} + 2n_p \frac{n_p - n_q \cos\Delta\varphi_q}{1-n_p^2}\right)$$

$$= \frac{\omega_q/\omega_p}{1-n_p^2}\left[2 \mp \frac{\omega_p}{\omega_q}(1-n_p^2) - 2n_p n_q \cos\Delta\varphi_q\right] \qquad (32)$$

If we neglect $\delta_{\mu_q}/2$ in Eq. 30 (well outside the instability range), we we obtain from Eq. 30

$$b_{\substack{q \\ +1 \\ -1}} = \pm b_{q_o} \frac{\eta}{2} \frac{\omega^2_{oo_{II}}}{\omega_q \omega_p} \frac{1}{2 \mp \frac{\omega_p}{\omega_q}(1-n_p^2) - 2n_q n_p \cos\Delta\varphi_q} \qquad (33)$$

In the center of the instability or resonance range $\sqrt{\theta_{o_q}} = \pm 1$, we obtain

$$\left(b_{q_{-1}}\right)_{\sqrt{\theta_{o_q}} = \pm 1} = \mp j b_{q_o} \tag{34}$$

which is a finite large value.

We note from Eq. 33 that the magnitude of the $b_{q_{-1}}$ coefficients depends upon the difference in propagation angles between the signal and pump waves. Furthermore, as is obvious from Eq. 8, we consider only propagating pump waves ($n_p^2 > 0$).

The denominator in Eq. 33 is zero for

$$\omega_q = \omega_{q_{res}} = \frac{1-n_p^2}{1-n_p^2\cos^2\Delta\varphi_q}\left[\frac{\omega_p}{2} + n_p\cos\Delta\varphi_q\sqrt{\frac{\omega_p^2}{4} - \omega_{oo_{II}}^2\frac{1-n_p^2\cos^2\Delta\varphi_q}{(1-n_p^2)^2}}\right] \tag{35}$$

If we assume that $n_p = 0$ can be realized physically -- that the ΔN_{II} oscillations do not travel or propagate -- we find that

$$\omega_{q_{res}} = \frac{\omega_p}{2} \quad (n_p = 0) \tag{36}$$

which is a degenerate parametric resonance. If the pump and signal waves travel perpendicularly to each other, Eq. 35 assumes the simple form

$$\omega_{q_{res}} = (1-n_p^2)\frac{\omega_p}{2} \qquad (\Delta\varphi_q = \pm\pi/2) \tag{37}$$

It is important and interesting to note that resonance interaction also takes place in this case. When $\Delta\varphi_q = \pm\pi/2$, we speak of transverse resonance interaction; and when $\Delta\varphi_q = 0 \pm \pi$, of longitudinal resonance interaction.

Since

$$\left[R_e(\mu_q)\right]_{max} \cong \frac{\theta_1}{2} = \eta \frac{\omega_{oo_{II}}^2}{\omega_p^2} \frac{1}{1-n_p^2} \qquad (\omega_q \cong \omega_{q_{res}}) \qquad (38)$$

we note that maximum exponential growth, or decay, in the instability region is <u>independent</u> of the angle $\Delta\varphi_q$ between the waves.

Furthermore, from Eq. 35 it appears that a physical resonance is possible only if

$$\omega_{oo_{II}}^2 < \frac{\omega_p^2}{4} \frac{(1-n_p^2)^2}{1-n_p^2\cos^2\Delta\varphi_q}$$

Since n_p^2 is in reality a function of both ω_p^2 and $\omega_{oo_{II}}^2$, this condition can not always be satisfied. If we assume (1) that $n_p^2 = 1 - 4\omega_{oo_{II}}^2/\omega_p^2$, we find that Eq. 35 can be written

$$\omega_{q_{res}} = \frac{\omega_p}{2} \frac{4\omega_{oo_{II}}^2}{4\omega_{oo_{II}}^2\cos^2\Delta\varphi_q + \omega_p^2\sin^2\Delta\varphi_q}$$

$$\cdot\left[1+j\sin\Delta\varphi_q\left(1-\frac{4\omega_{oo_{II}}^2}{\omega_p^2}\right)\right] \qquad \left(n_p^2 = 1-\frac{4\omega_{oo_{II}}^2}{\omega_p^2}\right) \qquad (35a)$$

When $\Delta\varphi_q = 0$ this resonance is possible, in principle, for any value of $\omega_{oo_{II}}^2$. When $\Delta\varphi_q \neq 0$ it is possible only when $\omega_p^2 = 4\omega_{oo_{II}}^2$, that is, when $n_p^2 = 0 = n_q^2$, which is a true degenerate parametric resonance.

Finally, we find that the relative interaction bandwidth, determined by the condition $\sqrt{\theta_{o_q}} - 1 = \pm\,\theta_1/2$, approximately becomes

$$\frac{\Delta\omega_{q_{res}}}{\omega_{q_{res}}} \cong \eta \frac{\omega_{oo_{II}}^2}{\omega_{q_{res}}\omega_p} \frac{1}{1-\frac{d_q}{n_q^2}} \qquad (39)$$

In the instability range $\Delta\omega_{q_{res}}$, the ionized medium needs only the slightest primary triggering (expressed by b_{q_o}) in order to radiate at the (difference) frequency $\omega_{q_{res}} - \omega_p$.

Next, let us consider the final field,

$$\psi_{tot} = \sum_{q=-\infty}^{q=+\infty} \psi_q \tag{40}$$

If we limit ourselves to the first "sidebands" or secondary waves, that is, to $q = 0 \pm 1$, and assume that ω_o is the angular frequency of the primary signal wave reaching the medium from outside (see Fig. 1 and Eq. 18), we obtain

$$\psi_o = e^{-j\left[\bar{k}_o\bar{r} - \frac{\delta\mu_o}{2}(\omega_p t - \bar{k}_p\bar{r})\right]}\left[b_{o_o}e^{+j\omega_o t} + b_{o_{+1}}e^{+j(\omega_{+1}t - \bar{k}_p\bar{r})} + b_{o_{-1}}e^{+j(\omega_{-1}t + \bar{k}_p\bar{r})} + \ldots\right] \tag{41}$$

$$\psi_{+1} = e^{-j\left[\bar{k}_{+1}\bar{r} - \frac{\delta\mu_{+1}}{2}(\omega_p t - \bar{k}_p\bar{r})\right]}\left[b_{+1_o}e^{+j\omega_{+1}t} + b_{+1_{-1}}e^{+j(\omega_o t + \bar{k}_p\bar{r})} + \ldots\right] \tag{42}$$

$$\psi_{-1} = e^{-j\left[\bar{k}_{-1}\bar{r} - \frac{\delta\mu_{-1}}{2}(\omega_p t - \bar{k}_p\bar{r})\right]}\left[b_{-1_o}e^{+j\omega_{-1}t} + b_{-1_{+1}}e^{j(\omega_o t - \bar{k}_p\bar{r})}\right] \tag{43}$$

If we further assume that we are sufficiently far outside any interaction range $\Delta\omega_{q_{res}}$, we can neglect δ_{μ_q} in the preceding relations and sum up terms of equal angular frequency. For $z \geqq 0$, the total field thus becomes

$$\psi_{tot} = e^{+j\omega_o t}\left[b_{o_o} e^{-j\bar{k}_o\bar{r}} + b_{+1_{-1}} e^{-j(\bar{k}_{+1}-\bar{k}_p)\bar{r}} + b_{-1_{+1}} e^{-j(\bar{k}_{-1}+\bar{k}_p)\bar{r}} + \ldots\right]$$

$$+ e^{+j\omega_{+1} t}\left[b_{o_{+1}} e^{-j(\bar{k}_o+\bar{k}_p)\bar{r}} + b_{+1_o} e^{-j\bar{k}_{+1}\bar{r}} + \ldots\right]$$

$$+ e^{-j\omega_{-1} t}\left[b_{o_{-1}} e^{-j(\bar{k}_o-\bar{k}_p)\bar{r}} + b_{-1_o} e^{-j\bar{k}_{-1}\bar{r}} + \ldots\right] + \ldots \qquad (44)$$

In order to satisfy the boundary condition at $z = 0$, we must require that

$$\begin{aligned} k_{+1}\sin\varphi_{II_{+1}} &= k_o\sin\varphi_{II_o} + k_p\sin\varphi_{II_p} \\ k_{-1}\sin\varphi_{II_{-1}} &= k_o\sin\varphi_{II_o} - k_p\sin\varphi_{II_p} \end{aligned} \qquad (45)$$

Expressed in terms of the incidence angles in medium I, these relations assume the very simple form

$$\sin\varphi_{I_{\substack{+1\\-1}}} = \frac{1}{\omega_o \pm \omega_p}\left(\omega_o\sin\varphi_{I_o} \pm \omega_p\sin\varphi_{I_p}\right) \qquad (46)$$

Thus if $\varphi_{I_p} = \varphi_{I_o}$, then $\varphi_{I_{\substack{+1\\-1}}} = \varphi_{I_o}$ for all ω_p values. If ω_p is very large and $\varphi_{I_p} \neq 0$, then $\varphi_{I_{\substack{+1\\-1}}} \rightarrow \varphi_{I_p}$. It is particularly interesting to to note that $\varphi_{I_{\substack{+1\\-1}}}$ may differ in sign from φ_{I_o}. If we assume that $\sin\varphi_{I_p} = 0$, Eq. 46 becomes

$$\sin\varphi_{I_{\substack{+1\\-1}}} = \frac{\omega_o}{\omega_o \pm \omega_p}\sin\varphi_{I_o} \qquad (\varphi_{I_p} = 0) \qquad (46a)$$

From this relation it appears that $\sin\varphi_{I_{+1}}$ is always smaller than $\sin\varphi_{I_o}$, but $\varphi_{I_{-1}}$ behaves in an entirely different manner. If ω_p lies in the range $\omega_o(1 + \sin\varphi_{I_o}) > \omega_p > \omega_o(1 - \sin\varphi_{I_o})$, then $|\sin\varphi_{I_{-1}}| > 1$, and a surface wave

$$e^{\left\{ j\left[(\omega_o-\omega_p)t - \frac{\omega_o}{c_o}\sin\varphi_{I_o}x\right] + \frac{\omega_o}{c_o}\sin\varphi_{I_o}\sqrt{1-\left(\frac{\omega_o-\omega_p}{\omega_o\sin\varphi_{I_o}}\right)^2}\ z\right\}} \qquad (47)$$

for $z \leqq 0$, is generated at the difference frequency in medium I. This surface wave travels in the positive x direction when $\omega_o > \omega_p > \omega_o(1 - \sin\varphi_{I_o})$, and in the <u>negative</u> x direction when $\omega_o(1 + \sin\varphi_{I_o}) > \omega_p > 1$.

When $\omega_p > \omega_o(1 + \sin\varphi_{I_o})$, the difference frequency wave becomes

$$e^{j\left[(\omega_o-\omega_p)t - \frac{\omega_o}{c_o}\sin\varphi_{I_o}x + \frac{\omega_o-\omega_p}{c_o}\sqrt{1-\left(\frac{\omega_o\sin\varphi_{I_o}}{\omega_o-\omega_p}\right)^2}\ z\right]} \qquad (48)$$

for $z \leqq 0$. Since $\omega_p > \omega_o(1 + \sin\varphi_{I_o})$, this wave leaves the medium at a <u>negative</u> angle, in the same quadrant as the incident primary signal wave of frequency ω_o. At the degenerate parametric resonance frequency $\omega_p = 2\omega_o$ and $\varphi_{I_{-1}} = -\varphi_{I_o}$, a peculiar phenomenon occurs that has previously been considered by the author (3).

Figure 2, sketched for $\omega_p < \omega_o(1 - \sin\varphi_{I_o})$, depicts how the three characteristic waves, with frequencies ω_o and $\omega_o \pm \omega_p$, leave the pumped ionized medium.

It should be added that if higher sidebands (that is, higher order terms) had been considered throughout, we would have obtained the general reflection laws

$$\sin\varphi_{I_{\pm n}} = \frac{1}{\omega_o \pm n\omega_p}(\omega_o\sin\varphi_{I_o} \pm n\omega_p\sin\varphi_{I_p}) \qquad (49)$$

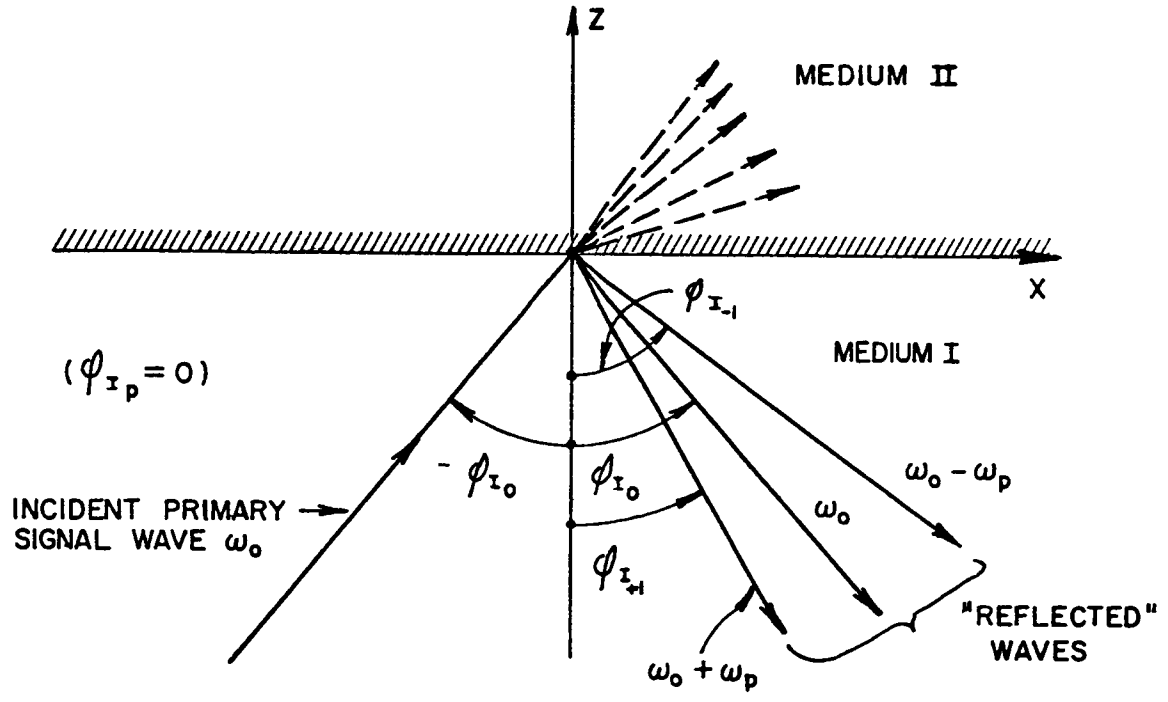

FIG. 2. First order wave spectrum obtained from the pumped ionized medium.

If we write $E_y = (1/\omega_o)(\partial\psi/\partial t)$ from Eq. 11, the electric field -- so far unmatched to the incident primary field of angular frequency ω_o -- can be written

$$E_{y_{tot}} = e^{+j(\omega_o t - k_{o_x} x)} \left[b_{o_o} e^{-jk_{o_z} z} + b_{+1_{-1}} e^{-j(k_{+1_z} - k_{p_z})z} + b_{-1_{+1}} e^{-j(k_{-1_z} + k_{p_z})z} + \cdots \right]$$

$$+ e^{+j(\omega_{+1} t - k_{+1_x} x)} \frac{\omega_{+1}}{\omega_o} \left[b_{o_{+1}} e^{-j(k_{o_z} + k_{p_z})z} + b_{+1_o} e^{-jk_{+1_z} z} + \cdots \right]$$

$$+ e^{+j(\omega_{-1} t - k_{-1_x} x)} \frac{\omega_{-1}}{\omega_o} \left[b_{o_{-1}} e^{-j(k_{o_z} - k_{p_z})z} + b_{-1_o} e^{-jk_{-1_z} z} + \cdots \right] \qquad (50)$$

for $z \geqq 0$. If we neglect the second order terms $b_{+1_{-1}}$ and $b_{-1_{+1}}$ of the ω_o wave, we note that two different ω_{+1} and ω_{-1} waves appear in medium II. The $\omega_{+1_{-1}}$ waves have components which, in certain frequency regions, have the properties of backward waves, as will be discussed later in this section. Nevertheless the group velocity, if referred to ω_o, is positive.

Next, let us match the interior field of Eq. 50 to the exterior field, still neglecting the second order terms $b_{+1_{-1}}$ and $b_{-1_{+1}}$ for the sake of logical convenience. If the incident primary field is written

$$E_{y_{inc}} = E_{y_o} e^{+j(\omega_o t - \bar{k}_o \cdot \bar{r})} \qquad (51)$$

remembering that E_y and $\partial E_y/\partial_z$ must be continuous at z = 0 (for each frequency component), then b_{o_o} becomes

$$b_{o_o} = E_{y_o} \frac{2k_{o_{o_z}}}{k_{o_{o_z}} + k_{o_z}} = E_{y_o} T_{o,o} \tag{52}$$

in which $T_{o,o}$ is the primary transmission coefficient. For the reflected ω_o component we similarly introduce the primary reflection coefficient

$$R_{o,o} = \frac{k_{o_{o_z}} - k_{o_z}}{k_{o_{o_z}} + k_{o_z}} \tag{53}$$

Since no waves reach the layer from the outside at the sum and difference frequencies, the relevant field components in medium I must be written (see Fig. 2)

$$\alpha_{+1} e^{+j(\omega_{+1} t - k_{+1_{o_x}} x + k_{+1_{o_z}} z)}$$

$$\alpha_{-1} e^{+j(\omega_{-1} t - k_{-1_{o_x}} x + k_{-1_{o_z}} z)}$$

We therefore obtain

$$\frac{\omega_{+1}}{\omega_o} (b_{o_{+1}} + b_{+1_o}) = \alpha_{+1}$$

$$\frac{\omega_{-1}}{\omega_o} (b_{o_{-1}} + b_{-1_o}) = \alpha_{-1}$$

$$\frac{\omega_{+1}}{\omega_o} \left[(k_{o_z} + k_{p_z}) b_{o_{+1}} + k_{+1_z} b_{+1_o} \right] = -k_{+1_{o_z}} \alpha_{+1}$$

$$\frac{\omega_{-1}}{\omega_o} \left[(k_{o_z} - k_{p_z}) b_{o_{-1}} + k_{-1_z} b_{-1_o} \right] = -k_{-1_{o_z}} \alpha_{-1}$$

These relations yield

$$b_{+1_o} = -b_{o_{+1}} \frac{k_{+1_{o_z}} + k_{o_z} + k_{p_z}}{k_{+1_{o_z}} + k_{+1_z}} = -b_{o_{+1}} T_{o,+1} \tag{54}$$

$$b_{-1_o} = -b_{o_{-1}} \frac{k_{-1_{o_z}} + k_{o_z} - k_{p_z}}{k_{-1_{o_z}} + k_{-1_z}} = -b_{o_{-1}} T_{o,-1} \tag{55}$$

$$a_{+1} = b_{o_{+1}} \frac{\omega_{+1}}{\omega_o} \frac{k_{+1_z} - k_{o_z} - k_{p_z}}{k_{+1_{o_z}} + k_{+1_z}} = b_{o_{+1}} \frac{\omega_{+1}}{\omega_o} R_{o,+1} \tag{56}$$

$$a_{-1} = b_{o_{-1}} \frac{\omega_{-1}}{\omega_o} \frac{k_{-1_z} - k_{o_z} + k_{p_z}}{k_{-1_{o_z}} + k_{-1_z}} = b_{o_{-1}} \frac{\omega_{-1}}{\omega_o} R_{o,-1} \tag{57}$$

It is interesting to note that for $k_p = 0$ (nontraveling pump wave), these transmission and reflection coefficients are the regular ones for a frequency shifting network.

We are now in a position to write down the complete expression for the traveling fields in media I and II. By Eq. 33 we obtain the following results.

Medium I ($z \leqq 0$):

$$E_y = E_{y_o} \Big[e^{+j(\omega_o t - k_{o_{o_x}} x - k_{o_{o_z}} z)} + R_{o,o} e^{+j(\omega_o t - k_{o_{o_x}} x + k_{o_{o_z}} z)} + T_{o,o} R_{o,+1} \frac{\omega_{+1}}{\omega_o} \cdot \frac{\eta}{2} \frac{\omega^2_{o o_{II}}}{\omega_o \omega_p} \frac{1}{2 + \frac{\omega_p}{\omega_o}(1 - n_p^2) - 2 n_o n_p \cos\Delta\varphi_o} e^{+j(\omega_+ t - k_{o_{+1_x}} x + k_{o_{+1_z}} z)}$$

(CONTINUED)

$$- T_{o,o} R_{o,-1} \frac{\omega_{-1}}{\omega_o} \frac{\eta}{2} \frac{\omega_{oo_{II}}^2}{\omega_o \omega_p} \frac{1}{2 - \frac{\omega_p}{\omega_o}(1-n_p^2) - 2n_o n_p \cos\Delta\varphi_o}$$

$$\cdot e^{+j(\omega_{-1} t - k_{o_{-1}x} x + k_{o_{-1}z} z)} + \ldots \Big] \qquad (58)$$

(ω_o outside $\Delta\omega_{o_{res}}$ range).

Medium II ($z \geqq 0$):

$$E_y = E_{y_o} T_{o,o} \Big\{ e^{+j(\omega_o t - k_{o_x} x - k_{o_z} z)} + \frac{\omega_{+1}}{\omega_o} \frac{\omega_{oo_{II}}^2}{\omega_o \omega_p}$$

$$\cdot \frac{1}{2 + \frac{\omega_p}{\omega_o}(1-n_p^2) - 2n_o n_p \cos\Delta\varphi_o} e^{+j(\omega_{+1} t - k_{+1_x} x)}$$

$$\cdot \Big[e^{-j(k_{o_z} + k_{p_z}) z} - T_{o,+1} e^{-jk_{+1_z} z} \Big] + \frac{\omega_{-1}}{\omega_o} \frac{\omega_{oo_{II}}^2}{\omega_o \omega_p}$$

$$\cdot \frac{1}{2 - \frac{\omega_p}{\omega_o}(1-n_p^2) - 2n_o n_p \cos\Delta\varphi_o} e^{+j(\omega_{-1} t - k_{-1_x} x)}$$

$$\cdot \Big[e^{-j(k_{o_z} - k_{p_z}) z} - T_{o,-1} e^{-jk_{-1_z} z} \Big] + \ldots \Big\} \qquad (59)$$

(ω_o outside $\Delta\omega_{o_{res}}$ range).

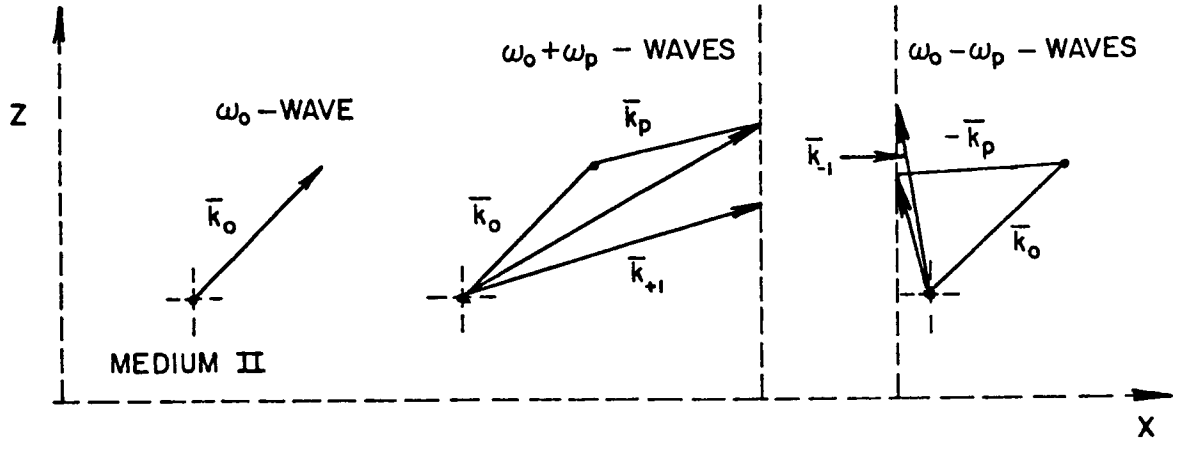

FIG. 3. First order waves in medium II.

If, finally, we introduce

$$\mu_{+1_{-1}} = \frac{\omega_{+1_{-1}}}{\omega_o} \frac{\omega_{oo_{II}}^2}{\omega_o \omega_p} \frac{1}{2 \pm \frac{\omega_p}{\omega_o}(1-n_p^2) - 2 n_o n_p \cos \Delta\varphi_o} \tag{60}$$

and remember Eqs. 44 and 45, then Eq. 59 can also be written

$$E_y = E_{y_o} T_{o,o} \left\{ e^{+j(\omega_o t - \bar{k}_o \bar{r})} \left[1 + \sqrt{\mu_{+1}\mu_{-1}} \left(\sqrt{\frac{\mu_{+1}}{\mu_{-1}}} e^{+j(\omega_p t - \bar{k}_p \bar{r})} \right.\right.\right.$$

$$\left.\left.\left. - \sqrt{\frac{\mu_{-1}}{\mu_{+1}}}\, e^{-j(\omega_p t - \bar{k}_p \bar{r})} \right) \right] - T_{o,+1} \mu_{+1} e^{+j(\omega_{+1} t - \bar{k}_{+1} \bar{r})} \right.$$

$$\left. + T_{o,-1} \mu_{-1} e^{-j(\omega_p t - \bar{k}_{-1} \bar{r})} + \cdots \right\} \tag{61}$$

From this relation it appears that the peculiar first components of the sum and difference frequency waves, which may appear as backward waves, can be considered as a traveling-wave modulation of the primary wave. The remaining sum and difference frequency waves have completely normal characteristics; that is, they satisfy Maxwell's equations for the unperturbed medium, and thus propagate in medium II with phase velocities corresponding to their frequencies. To further illustrate the physical properties of Eqs. 60 and 61, Fig. 3 depicts in vector form the various waves in medium II.

Let us now reexamine the resonance conditions on the basis of the results so far obtained. It is not difficult to show that the following relations hold:

$$\frac{c_o^2}{\omega_p^2} \left(k_{+1}^2 - \left| \bar{k}_o + \bar{k}_p \right|^2 \right) = (1-n_p^2)(1+\sqrt{\theta_{o_o}}) \tag{62}$$

$$\frac{c_o^2}{\omega_p^2} \left(k_{-1}^2 - \left| \bar{k}_o - \bar{k}_p \right|^2 \right) = (1-n_p^2)(1-\sqrt{\theta_{o_o}}) \tag{63}$$

These relations finally yield the interesting general results (δ_{μ_o} neglected)

$$b_{o_{+1}} = b_{o_o} \frac{\eta}{2} \frac{\omega^2_{oo_{II}}/c_o^2}{k_{+1}^2 - |\bar{k}_o + \bar{k}_p|^2} \tag{64}$$

$$b_{o_{-1}} = b_{o_o} \frac{\eta}{2} \frac{\omega^2_{oo_{II}}/c_o^2}{k_{-1}^2 - |\bar{k}_o - \bar{k}_p|^2} \tag{65}$$

which demonstrate that, as expected, the system resonances are traveling-wave resonances (5). Hence

$$\left|b_{o_{+1}}\right| \to \infty \qquad \text{if } k_{+1} \longrightarrow \pm |\bar{k}_o + \bar{k}_p|$$

$$\left|b_{o_{-1}}\right| \to \infty \qquad \text{if } k_{-1} \longrightarrow \pm |\bar{k}_o - \bar{k}_p| \tag{66}$$

In these relations one must be careful to use the proper signs. Our boundary conditions (see Fig. 3) required that $k_{+1_x} = k_{o_x} + k_{p_x}$ and $k_{-1_x} = k_{o_x} - k_{p_x}$, which means that the resonance conditions should be written

$$k_{+1_z} = k_{o_z} + k_{p_z} \qquad \text{(sum frequency wave)}$$

$$k_{-1_z} = k_{o_z} - k_{p_z} \qquad \text{(difference frequency wave)} \tag{66a}$$

At the resonance levels, the traveling-wave modulations or associated waves with propagation exponents $\bar{k}_o \pm \bar{k}_p$ always travel in the same direction and with the same phase velocity as the independent sum and difference frequency waves, which thereby are excited to very large amplitudes.

The associated sum frequency wave always travels in positive z direction when k_{p_z} is positive. If k_{p_z} is negative and $-k_{p_z} > k_{o_z}$, this wave appears as a backward wave.

When $\omega_p < \omega_o$, the associated difference frequency wave has the property of a backward wave if $k_{p_z} > k_{o_z}$. When $\omega_p > \omega_o$, this wave appears

as a backward wave only if $k_{p_z} < k_{o_z}$. In the resonance regions, therefore, the independent sum and difference frequency waves may be generated as forward or backward waves. To generate a forward wave at the difference frequency resonance, which in our specific case would call for $\omega_p > \omega_o$, k_{p_z} must be larger than k_{o_z}.

In our isotropic ionized medium, the independent waves have the group velocities $c\,n_{\substack{+1\\-1}}$, quite independent of the original modulation, which may be effected on the pump or the primary wave. The situation is different as far as the associated waves are concerned. In our special case, if the primary wave is modulated, we obtain $c_o n_o$ in the $\bar{k}_o$ direction. If the pump carries the modulation, we obtain $c_o/[n_p + \omega_p (dn_p/d\omega)]$ in the $\bar{k}_p$ direction.

A complete discussion of the total power flow in the first order multiwave system would necessitate the evaluation of the $b_{\substack{+1\\-1}}$ and $b_{\substack{-1\\+1}}$ coefficients. Interesting as this may be, it is outside the scope and aim of the present communication.

Traveling-wave resonance coefficients quite like those presented in Eqs. 64 and 65 appear also in the nonlinear magnetoionic medium (5). The resonance interactions in this much more complicated medium will be discussed in a later scientific report.

4. WAVE REFLECTION, BOTH ELECTRON DENSITY AND ELECTRON VELOCITY OSCILLATIONS CONSIDERED

We must now resort to the complete wave equation, Eq. 12. Since it cannot be transformed to a Mathieu equation, we neglect the possible instabilities and write

$$\psi_q = e^{+j(\omega_q t - \bar{k}_q \bar{r})} \left(b_{q_o} + b_{q_{+1}} e^{+j\tau} + b_{q_{-1}} e^{-j\tau} + \ldots \right) \tag{67}$$

where τ is defined by Eq. 15.

We recall from Eq. 9 that ξ of Eq. 12 can be written

$$\xi = \frac{1}{1+\eta \cos\tau} \tag{68}$$

and put

$$v_{p_z} = v_p \cos\varphi_{II_p}^{(v)} \cos\tau \; ; \; v_{p_x} = v_p \sin\varphi_{II_p}^{(v)} \cos\tau \tag{69}$$

where $\varphi_{II_p}^{(v)}$ is the angle that the electron velocity of the pump wave makes with the z axis. We have used τ as the general pump wave propagation factor, although this is not correct (1) if both linear and nonlinear pump wave quantities are considered. The ΔN_{II} and the longitudinal velocity oscillations, which are the nonlinear components of the high power (pump) wave, generally have a τ value different from that of the transverse and linear pump wave velocity. For the sake of simplicity, however, and since it is natural to treat separately the effects of the former upon the probing or signal wave, we use the same τ throughout and later adjust the velocity angle $\varphi_{II_p}^{(v)}$ and τ to the relevant case under study.

Remembering that

$$P_e^2 \Psi_{q_o} = \frac{\omega_{oo}^2 {}_{II}}{c_o^2} \tag{70}$$

and making use of Eqs. 62, 63, and 64 in Eq. 12, retaining only the linear η and v_p terms, we obtain after some rearrangement of terms the final relation

$$b_{\substack{o+1 \\ -1}} = b_{o_o} \frac{\omega_{oo}^2 {}_{II}}{2\omega_o\omega_p} \frac{\pm\eta + \frac{\omega_o\omega_p}{(\omega_o \pm \omega_p)^2} \mathcal{M}_o \cos(\varphi_{II_p}^{(v)} - \varphi_{II_o})}{2 \pm \frac{\omega_p}{\omega_o}(1-n_p^2) - 2n_o n_p \cos\Delta\varphi_o} \tag{71}$$

where

$$\mathcal{M}_o = \frac{v_p n_o}{c_o} = \frac{v_p}{v_{phase}} \tag{72}$$

Comparing Eq. 71 with Eq. 33, we immediately note the <u>important</u> fact that the denominator of $b_{\substack{o+1 \\ -1}}$ remains unchanged. Therefore, the electron velocities of the pump wave do not influence the system resonances (to first order), even though the magnitude of $b_{\substack{o+1 \\ -1}}$ depends upon the former.

We next study the two velocity cases separately.

Case 1 considers only the nonlinear plasma wave. As has been shown by Rydbeck (1), we now have

$$\eta = \frac{1}{4} \frac{v_t^{(1)}}{v_{phase_{p/2}}} R(\omega_p, \omega_{oo_{II}}) \cos\tau \tag{73}$$

where $v_t^{(1)}(\omega_p/2)$ is the linear transverse velocity of the pump wave (angular frequency $\omega_p/2$), $v_{phase_{p/2}}$ is the corresponding phase velocity $\left[= c_o/(n)_{\omega_{p/2}}\right]$, and the nonlinear plasma resonance factor is

$$R(\omega_p, \omega_{oo_{II}}) = \frac{\omega_p^2}{\omega_p^2 - \omega_{oo_{II}}^2} = \frac{1}{n_p^2} \tag{74}$$

Furthermore

$$\varphi_{II_p}^{(v)} = \varphi_{II_p} \tag{75}$$

and

$$k_p = \frac{\omega_p}{c_o}(n)_{\omega_{p/2}} \tag{76}$$

It should be added that

$$\frac{v_p}{v_{phase_{p/2}}} = \eta \tag{77}$$

That is, by Eq. 72,

$$\mathcal{M}_o = \frac{v_p}{v_{phase_o}} = \eta \frac{n_o}{(n)_{\omega_{p/2}}} \tag{78}$$

These relations yield

$$b_{o_{+1\,-1}} = b_{o_o} \frac{\eta}{2} \frac{\omega^2_{oo_{II}}}{\omega_o \omega_p} \frac{\pm 1 + \frac{\omega_p \omega_p}{(\omega_o \pm \omega_p)^2} \frac{n_o}{(n)_{\omega_p/2}} \cos\Delta\varphi_o}{2 \pm \frac{\omega_p}{\omega_o}(1-n_p^2) - 2n_o n_p \cos\Delta\varphi_o} \tag{79}$$

when $\omega_o \neq \omega_p$. From this relation it is evident that it is not permissible to neglect the nonlinear longitudinal velocity produced by the pump wave. The effects of ΔN_{II} and v_p are of the same magnitude, even though the system resonance is not displaced. As expected, it appears that in the case of transverse pumping, that is, when $\Delta\varphi_o = \pm\pi/2$, the effect of velocity pumping is zero.

Case 2 considers only the transverse linear pump wave velocity. We now have $\eta = 0$ and $\varphi^{(v)}_{II_p} = \varphi_{II_p} (\pm)\pi/2$. Assuming that the primary wave angular frequency now is ω_p, instead of $\omega_p/2$ as in Case 1, we obtain

$$b_{o_{+1\,-1}} = b_{o_o} \frac{\omega^2_{oo_{II}}}{(\omega_o \pm \omega_p)^2} \frac{v_t^{(1)}(\omega_p)}{v_{phase_p}}$$

$$\frac{n_o}{n_p} \sin\Delta\varphi_o \frac{1}{2 \pm \frac{\omega_p}{\omega_o}(1-n_p^2) - 2n_o n_p \cos\Delta\varphi_o} \tag{80}$$

when $\omega_p \neq \omega_o$. Here we note that for transverse pumping ($\Delta\varphi_o = \pm\pi/2$) -- that is, the pump wave and the signal wave crossing each other perpendicularly -- the interaction will be approximately at a maximum. For longitudinal pumping, the effect is zero, as expected. Case 2 is, of course, much more effective than Case 1, since $b_{o_{+1\,-1}}$ is here proportional to $v_t^{(1)}/v_{ph_p}$ instead of to $(v_t^{(1)}/v_{ph_{p/2}})^2$.

Since $v_t^{(1)}/v_{ph_p}$ is always a small quantity unless one has airborne pump transmitters in or very near to the ionized medium, it is obvious

that $b_{o_{+1}}$ and $b_{o_{-1}}$ are always extremely small in practical ionospheric cases, except near system resonances, of which there could be a number in the magnetoionic medium (5). The resonance effects naturally depend upon the collisional losses of the electrons, which are very small in the exosphere. A brief survey of the effects of collisional losses has therefore been made in Section 5.

If at any ω_o or ω_p the medium becomes unstable (in our thinking we are not now limiting ourselves as to the nature of the various n values), only a slight triggering, for example by b_{o_o}, would cause the medium to go into self-oscillations and to radiate, assuming that the pump wave energy input overcomes the collisional losses of the system. For this case a complete transient analysis of the system becomes necessary. It should therefore be emphasized that our results, as expressed in Eq. 71 for example, are steady state results for a medium that is <u>infinitely</u> extended from z = 0 in the positive z direction. Our present results thus summarize infinitely extended interaction effects, what happens after "infinite" time. It is the purpose of Section 6 to show that intense resonances of the type found here for the infinite homogeneous medium are appreciably reduced, though present, in an inhomogeneous medium.

A few remarks should be made concerning degenerate parametric resonance. Whenever $n_p = 0$ or $n_p = n_o \cos \Delta\varphi_o$ (the latter condition will not be attainable for an isotropic ionized medium), the denominator of $b_{o_{-1}}$ is zero for $\omega_p = 2\omega_o$. If we assume vertical incidence pumping ($\varphi_{I_p} = 0$), we note from Eq. 46a that $\varphi_{I_{-1}} = -\varphi_{I_o}$. The pumped ionized medium then acts as a <u>parametric amplifier</u>, with the peculiar and interesting property that the amplified signal (angular frequency ω_o) is <u>always</u> returned in its incidence direction. The reflection medium now acts very much like a degenerate-type reflection cavity parametric amplifier.

5. EFFECTS OF COLLISIONAL LOSSES AT SYSTEM RESONANCES

To estimate the pump power necessary to generate appreciable nonlinear resonance effects, one has to consider the effects of electronic collisional friction at or near the resonance level. If we introduce a constant collisional frequency ν, we obtain

$$n_{-1}^2 = 1 - \frac{\omega_{oo_{II}}^2}{\omega_{-1}(\omega_{-1} - j\nu)}, \text{ and } n_o^2 = 1 - \frac{\omega_{oo_{II}}^2}{\omega_o(\omega_o - j\nu)} \qquad (81)$$

if the medium is isotropic.

If we also, for the sake of completeness, consider an attenuated pump wave, we write instead of Eq. 1

$$\frac{\Delta N_{II}}{N_{o_{II}}} = \eta e^{-k_{z_i} z} \cos(\omega_p t - \bar{k}_p^o \bar{r}) \tag{82}$$

where k_p^o indicates the real part of k_p. For the difference frequency wave, the only one we will study in what follows, $\bar{k}_p$ thus has the components $k_{p_z}^o + jk_{z_i}$ and $k_{p_x}^o$. We can also express k_{z_i} in the loss angle δ_p of the pump wave, defined by the relation

$$k_p = k_p^o (1 + j\delta_p) \tag{83}$$

and obtain

$$k_{z_i} = \delta_p \frac{k_p^o}{\cos\varphi_{II_p}} \qquad (\cos^2\varphi_{II_p} \gg \delta_p^2) \tag{84}$$

To make an approximate study of the influence of losses at or near resonance, we next introduce Eqs. 81, 83, and 84 in Eq. 63. The first order result (ν^2 and δ_p^2 terms neglected) for the difference frequency wave then becomes

$$\sqrt{\theta_{o_o}} - 1 \cong \frac{\omega_o}{\omega_p} \frac{1}{1-n_p^{o^2}} \left\{ 2 - \frac{\omega_p}{\omega_o}(1-n_p^{o^2}) - 2n_o^o n_p^o \cos\Delta\varphi_o \right. \tag{85}$$

$$\left. - j\left[\frac{\omega_{oo_{II}}^2}{\omega_o^2} \frac{\nu}{\omega_p} \left(\frac{\omega_p}{\omega_p - \omega_o} - \frac{k_{p_z}^o}{k_{o_z}^o} \right) - 2\delta_p n_p^{o^2} \frac{\omega_p}{\omega_o} \left(1 - \frac{k_{o_z}^o}{k_{p_z}^o} \right) \right] \right\}$$

$[\cos^2 \varphi_{II_p} \gg \delta_p^2,\ \cos^2 \varphi_{II_o} \gg (\nu/\omega_o)^2]$ where $k^o_{o_z}$ denotes the z component of the real part of k_o, which is labeled k^o_o, and so on. The resonance value of $\sqrt{\theta_{o_o}}$ thus becomes

$$(\sqrt{\theta_{o_o}})_{res} \cong 1-j \frac{\omega^2_{oo_{II}}}{\omega_p^2} \frac{1}{1-n_o^{o2}} \cdot \Delta \qquad (85a)$$

where

$$\Delta = \frac{\nu}{\omega_o} \left(\frac{\omega_p}{\omega_p - \omega_o} - \frac{k^o_{p_z}}{k^o_{o_z}} \right) - 2\delta_p n_p^{o2} \frac{\omega_p^2}{\omega^2_{oo_{II}}} \left(1 - \frac{k^o_{o_z}}{k^o_{p_z}} \right) \qquad (85b)$$

It is to be remembered that at least for small $\omega^2_{oo_{II}}$, $\delta_p n_p^{o2}$ is proportional to this quantity.

If we next introduce Eq. 85a in Eq. 27, and this is quite an approximation, we find that

$$(\mu_o)_{res} \approx \frac{\omega^2_{oo_{II}}}{\omega_p^2} \frac{1}{1-n_p^{o2}} \sqrt{\eta^2+\Delta^2} \qquad (86)$$

By Eq. 30 we furthermore obtain

$$(b_{o_{-1}})_{res} \approx -jb_{o_o} \frac{\eta}{\Delta + \sqrt{\eta^2+\Delta^2}} \qquad (87)$$

When losses are large, $b_{o_{-1}}$ is proportional to $\eta/2\Delta$. Since the order of Δ is ν/ω_o, η must approach this value if one wants to obtain strong resonance effects.

Let us now look at the possible growth of waves in the instability region, remembering that the discussion is highly approximate since no transient analysis is used. By Eq. 21 we can write

$$\Pi_{o_1} = e^{-j\sqrt{\theta_{o_o}}u} e^{(\mu_o+j)u} \sum_{m=-\infty}^{+\infty} b_{o_n} e^{+j2nu} \tag{88}$$

At the resonance level this approximately yields, for its difference frequency component,

$$(\Pi_{o_1})_{res} \approx e^{-\frac{\omega_{o_o}^2}{\omega_p^2}\frac{1}{1-n_p^{o^2}}\left(\Delta-\sqrt{\Delta^2+\eta^2}\right)u_o} b_{o_{-1}} e^{-k_{z_i}z-j2u_o} \tag{89}$$

where

$$u_o = \frac{1}{2}(\omega_p t - \bar{k}_p^o \bar{r}) \tag{90}$$

If losses dominate, that is, if pumping is weak, the wave amplitude grows with time like

$$\exp\left\{\omega_{o_o}^2 \eta^2 / \left[4\omega_p \Delta(1-n_p^{o^2})\right]\right\} t$$

If Δ is positive, the difference frequency wave, in this very approximate second order form, slowly grows with time. If Δ is negative, its amplitude decreases with time in this approximation. But Eq. 89 cannot be made to satisfy any stationary boundary conditions.

For the isotropic medium, $1 - n_p^{o^2}$ is proportional to $\omega_{o_o}^2$ Its frequency dependence, however, is a function of the type of pumping that is used (see Cases 1 and 2 of Section 4).

If Δ could be made equal to zero at the resonance level, very strong interactions would result, even if the medium is lossy. One could then speak of complete traveling-wave resonance interaction. If we neglect pump wave losses, such an interaction would take place at degenerate parametric resonance ($\omega_p = 2\omega_o$) if $k_{p_z}^o = 2k_{o_z}^o$, that is, if $n_{p_z}^o = n_{o_z}^o$.

Since degenerate parametric resonance is possible in the isotropic medium only if $n_p^o = 0$, we have to require pumping as described in Case 1 of Section 4 and that $\varphi_{I_p} = 0 = \varphi_o$, a truly degenerate case because the primary pump wave frequency now is equal to $\omega_p/2 = \omega_o$. But remember that Eq. 85b, on which we based our discussions, is valid only when $\cos^2 \varphi_{II_p} \gg \delta_p^2$ and $\cos^2 \varphi_{II_o} \gg \delta_o^2$.

A more detailed study of the behavior of Δ under resonance conditions lies outside the scope of the present investigations. Such studies should be especially interesting in the case of the magnetoionic medium, for which the refractive indices vary widely with the medium parameters.

A few remarks should be made concerning the pumping power necessary to obtain observable dynamic nonlinear interaction effects. Since η or the equivalent velocity term in Eq. 80 has to approach the magnitude ν/ω_o, one finds that in the upper ionosphere, pumping according to Case 2 could be done by strong ground stations with pulse power of about 50 kw and an antenna surface of approximately $(40\lambda)^2$. Pumping according to Case 1 would at present have to be done by satellite- or rocket-borne transmitters.

6. DYNAMIC NONLINEAR REFLECTION FROM A PUMPED INHOMOGENEOUS IONIZED MEDIUM

We finally approach the much more difficult problem of dynamic nonlinear interactions in an inhomogeneous medium. What is the nature of the nonlinear resonance in such a medium, and when does actual radiation take place at the sum or difference frequencies?

For obvious reasons our study will be limited to a very slowly varying medium, in which partial reflections of the various waves can be neglected in the main interaction region, where $|\sqrt{\theta_o}_o| \approx 1$. We assume that the electron density is zero for $z = 0$ and increases monotonically, and very slowly, from this level in positive z direction. Since we will primarily limit our study to an analysis of the difference frequency wave, when $\omega_p > \omega_o$, and of its possible radiation in the forward or positive z direction, we assume that $k_{p_z} > k_{o_z}$ in the interaction region. It will later be shown that our results can easily be extended to the equally important case of backward radiation, for which $k_{p_z} < k_{o_z}$.

To make our discussions more general we do not assume special relations between n_o, n_p, and the medium parameters, except that for convenience $1 - n_p^2$ is assumed to be positive and proportional to $\omega_{oo_{II}}^2$ when $\omega_{oo_{II}}^2 \ll \omega_p^2$.

In Fig. 4, which approximately depicts the situation, z_o is the level of resonance interaction for the difference frequency wave. That is,

$$\left(\sqrt{\theta_{o_o}}\right)_{z=z_o}=1$$

Figure 4 is based on the following assumptions: $\omega_p > \omega_o$, $k_{p_z} > k_{o_z}$, and $k_{p_x} > k_{o_x}$.

From Section 4 it appears to be unnecessary to take special account of the electron velocities from the pump wave in order to make an approximate study of the interaction, since they do not influence the resonance condition. Furthermore, since we are dealing with a slowly varying medium, we may let the primary or signal wave have the approximate form

$$e^{+j(\omega_o t-\int^r \bar{k}_o d\bar{r})} \tag{91}$$

Similarly, the electron density fluctuation may be expressed as

$$\frac{\Delta N_{II}}{N_{II}} = \eta\cos(\omega_p t-\int^r \bar{k}_p d\bar{r}) \tag{92}$$

For definite reasons we have not included the usual WBK coefficient $1/\sqrt{k_q}$. Rydbeck (4) has shown that in a multiwave system the WKB-type approximations assume a very different form, owing to the fact that energy is now exchanged between a group of waves. Under these circumstances, and since we wish to carry out only a qualitative study of the interaction in an inhomogeneous medium (which actually is a very complicated problem), the best and most adequate approximations for our present purpose are those represented by Eqs. 91 and 92.

Neglecting terms like $\partial\omega^2_{oo_{II}}/\partial z$, we now make use of Eq. 23, which may be written

$$\left(\frac{d^2}{du^2}+\theta_{o_o}\right)\pi_{o_2} = -(2\theta_1\cos 2u)\pi_{o_2} \tag{93}$$

where

$$u = \frac{1}{2}(\omega_p t-\int^r \bar{k}_p d\bar{r}) \tag{94}$$

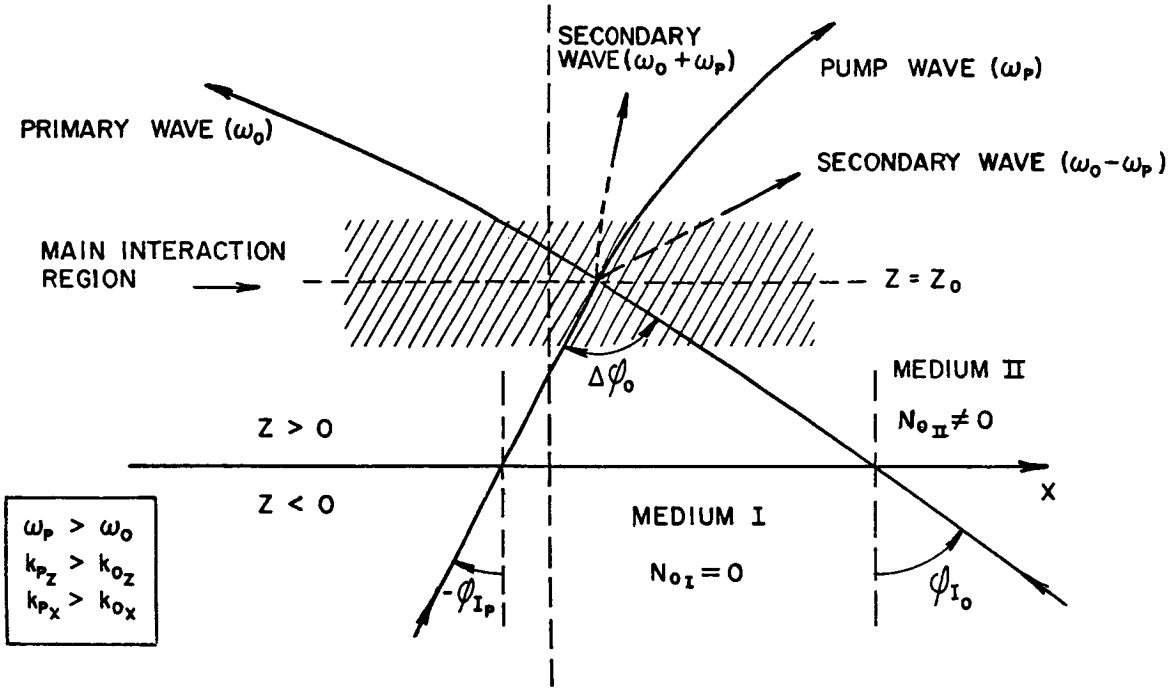

FIG. 4. Dynamic nonlinear wave interaction in a plane inhomogeneous ionized medium.

If we introduce $\xi = 2\theta_1 \cos 2u$, and $\pi^{(1)}_{o_2}$ representing the up-going unperturbed primary wave as defined by

$$\left(\frac{d^2}{du^2} + \theta_o^2\right)\pi^{(1)}_{o_2} = 0 \tag{95}$$

where θ_o denotes θ_{o_o}, the approximate solution of Eq. 93 can be written as

$$\pi_{o_2} \cong b_{o_o}\left\{\pi^{(1)}_{o_2} - \pi^{(1)}_{o_2}\int_{u_1}^{u}\frac{du}{\left[\pi^{(1)}_{o_2}\right]^2}\int_{u_2}^{u}\left[\pi^{(1)}_{o_2}\right]^2\xi\,du\right\} \tag{96}$$

Here b_{o_o} is the amplitude of the unperturbed primary wave, and u_1 and u_2 must be adjusted to fit the actual physical conditions, such as that there is no down-coming primary wave.

Since the linearly independent second solution to Eq. 95 can be written

$$\pi^{(2)}_{o_2} = \alpha\pi^{(1)}_{o_2}\int^{u}\frac{du}{\left[\pi^{(1)}_{o_2}\right]^2} \tag{97}$$

where α is a constant, π_{o_2} can now be expressed in terms of two "coupling" integrals:

$$\pi_{2_o} = b_{o_o}\left\{\pi^{(1)}_{o_2} - \frac{1}{\alpha}\pi^{(2)}_{o_2}\int_{u_3}^{u}\left[\pi^{(1)}_{o_2}\right]^2\xi\,du\right.$$

$$\left. + \frac{1}{\alpha}\pi^{(1)}_{o_2}\int_{u_1}^{u}\pi^{(2)}_{o_2}\pi^{(1)}_{o_2}\xi\,du\right\} \tag{98}$$

If we make the approximation by writing

$$\pi_{o_2}^{(1),(2)} \sim e^{\pm j\int^{u}\sqrt{\theta_o}\,du} \tag{99}$$

which yields

$$\alpha \approx j2\sqrt{\theta_o} \tag{100}$$

the total field by Eqs. 16 and 21 becomes, in appropriate inhomogeneous form,

$$\psi_o - b_{o_o}\psi_{o_o} \cong \frac{b_{o_o}\theta_1}{4\sqrt{\theta_o}} \left\{ e^{+j\left[\omega_{+1}t - \int^{r}(\bar{k}_o+\bar{k}_p)\bar{dr}\right]} \left[\frac{\sqrt{\theta_o}}{\sqrt{\theta_o}+1} - e^{+j\int_{u_z}^{u_{z_3}} 2du_z} \right.\right.$$

$$\left. \cdot \left(1 - \frac{e^{+j\int_{u_z}^{u_{z_3}} 2\sqrt{\theta_o}du_z}}{\sqrt{\theta_o}+1} \right) \right] - e^{+j\left[\omega_{-1}t - \int^{r}(\bar{k}_o-\bar{k}_p)\bar{dr}\right]}$$

$$\left. \cdot \left[1-e^{-j\int_{u_z}^{u_{z_1}} 2du_z} + 2je^{-j\int^{u_z} 2(\sqrt{\theta_o}-1)du_z} \cdot Q \right] \right\} \tag{101}$$

where

$$Q = \int_{u_{z_1}}^{u_z} e^{+j\int^{u_z} 2(\sqrt{\theta_o}-1)du_z} du_z \tag{101a}$$

and

$$u_z = -\frac{\omega_p}{2} n_{p_z} z = -\frac{1}{2} k_{p_z} z \tag{102}$$

Relation 91 has been deduced under the assumptions that all parameters vary quite slowly and that the main interaction takes place for only the difference frequency wave. If the reverse were to take place, Eq. 101 could readily be used with the proper permutation of signs.

If no sum and difference frequency waves impinge upon the layer from the outside, we put $u_{z_3} = +j\infty$ and note from Eq. 101 that the amplitude coefficient of the sum frequency wave gets the "correct" value $b_{o_{+1}}$ for the slowly varying medium (without strong interactions at any point). Similary, we find that $u_{z_1} = -j\infty$.

Next we have to evaluate the integral Q in Eq. 101. To that end we introduce the following linear approximation, which we assume to hold through the main interaction region:

$$\sqrt{\theta_o} \cong 1 + \left(\frac{\partial \sqrt{\theta_o}}{\partial u_z}\right)_{u_{z_o}} (u_z - u_{z_o}) = 1 + \mathcal{H}(u_z - u_{z_o}) \qquad (103)$$

where $\mathcal{H}$ is a positive quantity if we assume $\sqrt{\theta_o} < 1$ for $z > z_o$. (Note: n_p^2 is assumed to be less than 1 throughout). Furthermore, according to our assumptions about n_p^2, $\sqrt{\theta_o}$ is a large quantity at or near the layer boundary, where n_o^2 is assumed equal to 1. Now Q becomes a Fresnel integral (with $u_{z_1} = -j\infty$):

$$Q = \frac{1}{\sqrt{\mathcal{H}}} \int_{+j\infty}^{w_z} e^{-jw^2} dw = \frac{1}{\sqrt{\mathcal{H}}} \left(\int_0^{w_z} e^{-jw^2} dw + \frac{\sqrt{\pi}}{2} e^{-j\,\pi/4} \right) \qquad (104)$$

where

$$w = -\sqrt{\mathcal{H}}(u_z - u_{z_o}) \qquad (105)$$

That is, w is positive for $z > z_o$.

If we next make use of the asymptotic expression of the Fresnel integral for large $|w|$ values ($w \gg 1$, $w \ll 1$),

$$\int_0^w e^{-jw^2} dw = \pm \frac{\sqrt{\pi}}{2} \left[e^{-j\,\pi/4} \pm j \frac{1}{\sqrt{\pi w}} e^{-jw^2} + O\left(\frac{1}{w^2}\right) \right] \qquad (106)$$

we obtain

$$Q \sim \frac{1}{2\sqrt{\mu}\, w} \begin{cases} 2\sqrt{\pi w}\, e^{-j\,\pi/4} + j e^{-jw^2} & (w \gg 1) \\ j e^{-jw^2} & (w \ll 1) \end{cases} \tag{106a}$$

Remembering the resonance conditions (Eq. 66) and that Eq. 45 must hold throughout, we now obtain the following final approximate results if we assume that $|w|$ is large at the top and bottom of the interaction region:

$z < z_o$, <u>at the bottom of the main interaction region</u>

$$\psi_o - \psi_{o_o} b_{o_o} \sim b_{o_o} \frac{\theta_1}{4} \left\{ e^{+j\left[\omega_{+1} t - \int^r (\bar{k}_o + \bar{k}_p)\, d\bar{r}\right]} \frac{1}{\sqrt{\theta_o} + 1} \right.$$

$$\left. - e^{+j\left[\omega_{-1} t - \int^r (\bar{k}_o - \bar{k}_p)\, d\bar{r}\right]} \frac{1}{\sqrt{\theta_o} - 1} \right\} \qquad (\sqrt{\theta_o} \neq 1;\ |w| \gg 1) \tag{107}$$

$z > z_o$, <u>at the top of the main interaction region</u>

$$\psi_o - \psi_{o_o} b_{o_o} \sim b_{o_o} \frac{\theta_1}{4} \left\{ e^{+j\left[\omega_{+1} t - \int^r (\bar{k}_o + \bar{k}_p)\, d\bar{r}\right]} \frac{1}{\sqrt{\theta_o} + 1} \right.$$

$$- e^{+j\left[\omega_{-1} t - \int^r (\bar{k}_o - \bar{k}_p)\, d\bar{r}\right]} \frac{1}{\sqrt{\theta_o} - 1}$$

$$\left. - \frac{2\sqrt{\pi}}{\left(\dfrac{\partial \sqrt{\theta_o}}{\partial u_z}\right)^{1/2}_{z_o}} e^{+j\left(\omega_{-1} t - \int^r \bar{k}_{o_{-1}}\, d\bar{r} - \pi/4\right)} \right\} \qquad (\sqrt{\theta_o} \neq 1;\ |w| \gg 1) \tag{108}$$

It is interesting to note that the emerging difference frequency radiation, the last term in Eq. 108, has finite amplitude when it approaches the top of the interaction region. Apparently $\theta_1\sqrt{\pi}/[2(\partial\sqrt{\theta_o}/\partial u_z)_{z_o}]$, the ratio between the radiated and the primary field, is a first order measure of the nonlinear radiation efficiency.

The amplitude of the emerging independent difference frequency wave, which is a solution of Maxwell's equation for the unperturbed medium, thus tends to infinity, to first order, provided that

$$\left(\frac{\partial\sqrt{\theta_o}}{\partial u_z}\right)_{z_o} \to 0$$

and that, at the same time, the optical width of the interaction region at the difference frequency is so large that

$$\left|\left(\frac{\partial\sqrt{\theta_o}}{\partial u_z}\right)_{z_o}\left(u_{z_{top}} - u_{z_{bottom}}\right)\right| \gg 1$$

The layer must be infinitely wide and $|n_{p_z}| > 0$, which agrees with our original assumption that there should be no partial reflection of any wave within the interaction region.

This throws some interesting light on our relations of Sections 3 and 4, and clearly demonstrates that they represent a stationary result, after infinite time, for the infinitely thick homogeneous medium II. Only a very extended and monotonically varying medium would exhibit strong nonlinear signal pump-wave resonance interactions. The conditions in this respect are therefore entirely the reverse of those for strong partial reflections, which is an interesting observation. That any boundary discontinuities, like the one between media I and II in Sections 3 and 4, will produce sum and difference frequency radiations is, of course, an entirely different matter.

The expression for the total phase of the radiating difference frequency wave is very approximate. A more accurate phase determination, which is outside the scope of the present communication, would require a more stringent solution of the original wave equation for the perturbed inhomogeneous medium. A first order ray tracing of the radiating difference frequency wave is possible, however, on the basis of our present results.

REFERENCES

1. O. E. H. Rydbeck, Dynamic Non-linear Wave Propagation in Ionized Media: 1, The Isotropic Medium, Research Rept. No. 27, Research Laboratory of Electronics, Chalmers Univ. Technol., Gothenburg, 1961.

2. O. E. H. Rydbeck and B. Agdur, The Propagation of Electronic Space Charge Waves in Periodic Structures, Trans. Chalmers Univ. Technol., No. 138, 1954.

3. O. E. H. Rydbeck, Wave Propagation Research, Progress Rept., 1961, Research Laboratory of Electronics, Chalmers Univ. Technol.

4. O. E. H. Rydbeck, The Propagation and Coupling of Waves in Inhomogeneous Media, Research Rept. No. 7, Research Laboratory of Electronics, Chalmers Univ. Technol., 1960 (also Arkiv Fysik, Roy. Swed. Acad. Sci.).

5. O. E. H. Rydbeck, Dynamic Non-linear Wave Propagation in Ionized Media: 2, The Magneto-ionic Medium, Research Rept. No. 28, Research Laboratory of Electronics, Chalmers Univ. Technol., 1962.

6. O. E. H. Rydbeck, The Non-linear Magneto-ionic Theory, Arkiv Geofysik, Roy. Swed. Acad. Sci., in press.

N63-15741

II. DYNAMIC NONLINEAR ELECTROMAGNETIC WAVE PROPAGATION AND HARMONIC RADIATION IN MAGNETOIONIC MEDIA*

1. SUMMARY

The preceding paper considered nonlinear wave interaction and its associated wave generations, at various combination frequencies, in an isotropic ionized medium. To make the results as general as possible, the interaction and the nonlinear reflection laws were expressed in terms of unspecified refractive indices. Among other things, this made it possible to express in vector form the conditions for traveling-wave resonance, permitting a study of the interaction between two waves that have arbitrary and different angles of incidence upon the medium, such as the generation of sum or difference frequency radiation.

This paper extends the nonlinear propagation studies to a magnetoionic medium, the limitation being that all wave normals are assumed to be parallel. The general theory involving arbitrary wave normals is dealt with in the third paper of this group.

It is shown that, as expected, traveling-wave resonances occur in the magnetoionic medium, not only between waves of the same kind (for example, between waves of ordinary polarization) but also between waves of opposite kinds. From the viewpoint of nonlinear interaction there is not much difference, at least in principle, between the ordinary and the extraordinary waves. It is also of interest that the second order nonlinear waves are characterized by two different kinds of polarization, which become equal only at traveling-wave resonance.

Traveling-wave resonances should be very efficient in the "topside" ionosphere, where both losses and electron density gradients are small. Most of them take place in regions where $X > 1 - Y$, in the usual notation, which are accessible to both types of waves from a "topside" sounder. Interaction instabilities are likely to be strong in regions near or close to fourth reflection level conditions, where the electron velocities become very large, especially for $Y^2 = 1$, and $Y^2 = 1 - X$. Parametric harmonic pumping of cyclotron-type resonances is particularly probable, in agreement with recent experimental results.

Under certain conditions, second harmonic or echo generation is possible at or near the combined fundamental and second harmonic reflection levels $X = 1$, 2, and 4. Similar levels can be established for the higher harmonics.

The author believes that if future "topside" sounders are equipped with harmonic sweep recording devices, our knowledge of dynamic nonlinear "topside" phenomena will be greatly extended.

---

*Scientific Report No. 186, Ionosphere Research Laboratory, The Pennsylvania State University, June 1, 1963.

The results here reported can also be used to study and evaluate parametric amplification, or second harmonic generation, of exospheric whistler modes.

2. ELECTRON VELOCITIES AND DIFFERENTIAL SPACE-CHARGE DENSITY OF LINEAR MAGNETOIONIC WAVES

Let us assume that the static magnetic field, of strength H_o and cyclotron frequency ω_H, is oriented with respect to the wave normal (z direction) and the coordinate system as shown in Fig. 1.

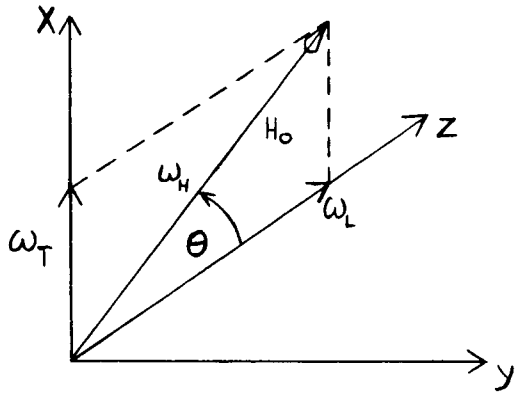

FIG. 1. Orientation of the static magnetic field.

If we let $E_y = E^{(1)}_{y_q}$, and so forth, denote the linear field, of angular frequency ω_q, the transverse linear electron velocities can be written (1) as

$$v^{(1)}_{q_y} = - \frac{1-n_q^2}{X_q} \frac{eE^{(1)}_{q_y}}{j\omega_q m} \qquad \left(\frac{\partial}{\partial x} = 0 = \frac{\partial}{\partial y}\right) \qquad (1)$$

$$v^{(1)}_{q_x} = - \frac{1-n_q^2}{X_q} \frac{eE^{(1)}_{q_x}}{j\omega_q m}$$

where n_q is the refractive index of the wave in question, and $X_q = \omega_p^2/\omega_q^2$ in which ω_p is the angular (electronic) plasma frequency of the ionized

medium. Introducing the cyclotron frequency ratio $Y_q = \omega_H/\omega_q$, its transverse and longitudinal components $Y_{T_q} = Y_q \sin\theta_q$ and $Y_{L_q} = Y_q \cos\theta$, and and the plasma resonance factor

$$R_q = \frac{1}{1-X_q-j\delta_q} \qquad (\delta_q = \nu/\omega_q) \tag{2}$$

the Appleton-Hartree expression for n_q^2 assumes the convenient form

$$1-n_{q_o}^2 = \frac{X_q}{1-j\delta_q - \frac{1}{2}Y_{T_q}^2 R_q \pm \sqrt{\frac{1}{4}Y_{T_q}^4 R_q^2 + Y_{L_q}^2}} \tag{3}$$

which demonstrates the influence of the transversely coupled plasma oscillation upon the propagation of the linear wave.

The longitudinal velocity component can be written as

$$v_{q_z}^{(1)} = Y_{T_q} R_q \frac{1-n_q^2}{X_q} \frac{eE_{q_y}^{(1)}}{\omega_q m} \tag{4}$$

and is thus in phase with $E_{q_y}^{(1)}$ for a lossless medium. By Eq. 1, this relation can also be expressed as

$$v_{q_z}^{(1)} = -jY_{T_q} R_q v_{q_y}^{(1)} \tag{4a}$$

Consequently $v_{q_z}^{(1)}$ and $v_{q_y}^{(1)}$ are of the same order of magnitude ($Y_{q_T} \neq 0$) <u>except</u> near the plasma resonance level, where R_q may be very large. In this region, therefore, $v_{q_z}^{(1)}$ may give rise to appreciable nonlinear effects, provided that $\delta_q^2 \ll 1$, even if the transverse velocities remain small.

The a-c space-charge density can be written (1) as

$$\frac{\rho_{1_q}}{\rho_o} = \frac{\Delta N_q}{N_o} = \frac{v_{q_z}^{(1)}}{c_o/n_q} = \frac{v_{q_z}^{(1)}}{v_{phase_q}} \tag{5}$$

where $\rho_o = -eN_o$, N_o is the mean electron density, and c_o is the electromagnetic velocity in vacuum. By Eq. 4 we can now give Eq. 5 the alternate and in this case important form:

$$\frac{\rho_{1_q}}{\rho_o} = -jY_{T_q}\left[R_q \frac{v_{q_y}^{(1)}}{v_{ph_q}}\right] \tag{5a}$$

Thus ρ_{1_q} is zero when $Y_T = 0$ (longitudinal propagation) and when $R_q n_q = 0$. Relation 5a furthermore shows that as far as the charge bunching is concerned, the measure of nonlinearity is $R_q v_{q_y}^{(1)}/v_{ph_q}$, and not $v_{q_y}^{(1)}/v_{ph_q}$. From Eq. 5 it also appears that ρ_{1_q}/ρ_o may become very large for the extraordinary wave (the Z component) at or very near the plasma resonance level.

According to Eqs. 1, 4, and 5 we can regard the magnetoionic wave as composed of a transverse electromagnetic wave, represented by $v_y^{(1)}$ and $v_x^{(1)}$, and an associated plasma wave, represented by $v_z^{(1)}$ and $\rho_1^{(1)}$, coupled to each other by the transverse magnetic field. This plasma wave disappears when $\theta = 0$, and therefore does not appear in the linear theory, when the propagation is purely longitudinal. The plasma wave may become very large at the plasma resonance level, and is physically instrumental in producing the triple split coupling.

In the linear magnetoionic theory we consider only the linear convection current density $\rho_o \bar{v}_q^{(1)}$. At the plasma resonance level, however, we may also have to consider the nonlinear term $\rho_q^{(1)}\bar{v}_q^{(1)}$, which produces a second harmonic. The moment the ionized medium drifts, we must also deal with the linear drift component $\rho_q^{(1)}\bar{v}_o$, where $\bar{v}_o$ is the drift velocity. Different types of waves, such as space-charge waves, may then be generated in the medium. These are discussed in the following paper on electron stream whistler mode interaction.

To make the linear field survey complete, we should perhaps recall that

$$H_{q_y}^{(1)} = \frac{n_q}{Z_o} E_{q_x}^{(1)} \qquad H_{q_x}^{(1)} = -\frac{n_q}{Z_o} E_{q_y}^{(1)} \tag{6}$$

and

$$E_{q_x}^{(1)}/E_{q_y}^{(1)} = S_{q_{o_x}}^{(1)} = jQ_{q_{o_x}}^{(1)} = -jY_{L_q} \frac{1}{-\frac{1}{2}Y_{T_q}{}^2 R_q \pm \sqrt{\frac{1}{4}Y_{T_q}{}^4 R_q{}^2 + Y_{L_q}{}^2}}$$

$$= jY_{L_q} R_q \frac{1-n_q{}^2}{1-R_q n_q{}^2(1-j\delta_q)} \qquad (7)$$

which is the linear (or first order) polarization ratio. The polarization of the nonlinear field components is generally different from $S_q^{(1)}$ (see Eq. 33 and the preceding paper).

In the study of nonlinear effects one is naturally interested in regions where the linear velocity fields, and for that matter also $\rho_1^{(1)}$, generated by a high power wave such as a pump wave become very large. We have seen that $v_z^{(1)}$ and $\rho_1^{(1)}$ behave in this manner at or near the plasma resonance level, whereas the other components remain small.

It appears from our previous relation that there is another and very important resonance level, when <u>all</u> velocities and the a-c space-charge density may become very large in a medium with small losses. This is at or near the so-called fourth reflection level, where $|n_q^2| \to \infty$. It is well known, as is easily verified by Eq. 3, that this "resonance" occurs when

$$Y_q{}^2 = Y_{R_q}{}^2 = \frac{1-X_q}{1-X_q \cos^2\theta_q} \qquad (8)$$

or expressed in X_q, when

$$X_q = X_{R_q} = \frac{1-Y_q{}^2}{1-Y_q{}^2 \cos^2\theta_q} \qquad (8a)$$

When X_q is small, Eq. 8 approximately yields

$$Y_{R_q}{}^2 \simeq 1 - X_q \sin^2\theta_q$$

which is very close to "cyclotron resonance," especially when θ_q is small. The latter case is especially important when one considers the excitation of cyclotron harmonics, or near harmonics, in the "topside" ionosphere.

Equation 9 can also be written as

$$\underbrace{(\omega_q{}^2-\omega_H{}^2)}_{\text{cyclotron osc. term}} \quad \underbrace{(\omega_q{}^2-\omega_p{}^2)}_{\text{plasma osc. term}} = \underbrace{\omega_H{}^2\omega_p{}^2\sin^2\theta}_{\text{coupling term}} = \omega_T{}^2\omega_p{}^2 \qquad (9)$$

which shows that the fourth reflection resonance can be considered as a transverse coupling between the plasma and cyclotron oscillations.

Let us summarize the results of this section. As far as the linear driving forces are concerned, we have two important resonance levels in the ionized medium:

$$X_q = 1 \text{ , and } X_q = \frac{1-Y_q{}^2}{1-Y_q{}^2\cos^2\theta}$$

Besides these resonance there are, of course, nonlinear traveling-wave resonances. These will be discussed in Section 4.

3. NONLINEAR DRIVING FORCES

If we retain the nonlinear terms in the equation of motion, we have

$$\frac{\partial \bar{v}}{\partial t} = -\frac{e}{m}\bar{E} + \frac{e}{m}\mu_o\left[(\bar{H}_o+\bar{H}) \times \bar{v}\right] - (\bar{v}\cdot\nabla)\bar{v}$$

$$= -\frac{e}{m}\bar{E} + \bar{\omega}_H \times \bar{v} + \bar{P} \qquad (10)$$

where $\bar{P}$ is the nonlinear force on the oscillating electrons. These are assumed to have zero drift motion in the linear theory (a stationary magnetoionic medium).

For the moment, consider only self-nonlinearities (for example, with a powerful primary wave). The second order force term can be written in the instructive form

$$\bar{P}^{(2)} = -\frac{1}{2}\,\text{grad}\,\left|\bar{v}^{(1)}\right|^2 + \left\{\bar{v}^{(1)} \times \left[\text{curl}\;\bar{v}^{(1)} + \int^{t} \frac{e}{m}\,\bar{E}^{(1)}\,dt\right]\right\} \tag{11}$$

Since $-\mu_o \frac{\partial \bar{H}}{\partial t} = \text{curl}\;\bar{E}$, this relation can also be written as

$$\bar{P}^{(2)} = -\frac{1}{2}\,\text{grad}\,\left|\bar{v}^{(1)}\right|^2 + \left\{\bar{v}^{(1)} \times \left[\text{curl}\;\bar{v}^{(1)} - \bar{\omega}_{H_1}^{(1)}\right]\right\} \tag{11a}$$

where $\bar{\omega}_{H_1}^{(1)}$ is the a-c cyclotron frequency. This yields the following basic relation for the isotropic nonlinear medium:

$$\bar{P}^{(2)} = -\frac{1}{2}\,\text{grad}\,\left|\bar{v}^{(1)}\right|^2 \qquad (H_o = 0) \tag{11b}$$

In this case the nonlinear force (second order) is proportional to the gradient of the <u>first order kinetic energy</u> of the oscillating electrons.

If we next assume that two waves are present in the medium (q = 1, 2), it can be shown (1) that $\bar{P}^{(2)}$ has the following components (ν = 0).

$$P_z^{(2)} = \underbrace{-\frac{1}{2}\frac{\partial}{\partial z}\left\{v_{z_1}^{(1)^2} + \frac{X_1}{1-n_1^2}\left[v_{y_1}^{(1)^2} + v_{x_1}^{(1)^2}\right]\right\}}_{P_{z_1}^{(2)}}$$

$$\underbrace{-\frac{1}{2}\frac{\partial}{\partial z}\left\{v_{z_2}^{(1)^2} + \frac{X_2}{1-n_2^2}\left[v_{y_2}^{(1)^2} + v_{x_2}^{(1)^2}\right]\right\}}_{P_{z_2}^{(2)}}$$

$$\underbrace{-\frac{\partial}{\partial z}\left[v_{z_1}^{(1)} v_{z_2}^{(1)}\right] - \frac{X_1}{1-n_1^2}\left[\frac{\partial v_{y_1}^{(1)}}{\partial z} v_{y_2}^{(1)} + \frac{\partial v_{x_1}^{(1)}}{\partial z} v_{x_2}^{(1)}\right] - \frac{X_2}{1-n_2^2}\left[\frac{\partial v_{y_2}^{(1)}}{\partial z} v_{y_1}^{(1)} + \frac{\partial v_{x_2}^{(1)}}{\partial z} v_{x_1}^{(1)}\right]}_{P_{z_{12}}^{(2)}} \tag{12}$$

$$P_y^{(2)} = \underbrace{-\frac{1}{2} v_{z_1}^{(1)} \frac{\partial v_{y_1}^{(1)}}{\partial z}\left(1 - \frac{X_1}{1-n_1^2}\right)}_{P_{y_1}^{(2)}} \underbrace{-\frac{1}{2} v_{z_2}^{(1)} \frac{\partial v_{y_2}^{(1)}}{\partial z}\left(1 - \frac{X_2}{1-n_2^2}\right)}_{P_{y_2}^{(2)}}$$

$$\underbrace{- v_{z_1}^{(1)} \frac{\partial v_{y_2}^{(1)}}{\partial z}\left(1 - \frac{X_2}{1-n_2^2}\right) - v_{z_2}^{(1)} \frac{\partial v_{y_1}^{(1)}}{\partial z}\left(1 - \frac{X_1}{1-n_1^2}\right)}_{P_{y_{12}}^{(2)}} \tag{13}$$

$$P_x^{(2)} = \underbrace{-\frac{1}{2} v_{z_1}^{(1)} \frac{\partial v_{x_1}^{(1)}}{\partial z}\left(1 - \frac{X_1}{1-n_1^2}\right)}_{P_{x_1}^{(2)}} \underbrace{-\frac{1}{2} v_{z_2}^{(1)} \frac{\partial v_{x_2}^{(1)}}{\partial z}\left(1 - \frac{X_2}{1-n_2^2}\right)}_{P_{x_2}^{(2)}}$$

$$\underbrace{- v_{z_1}^{(1)} \frac{\partial v_{x_2}^{(1)}}{\partial z}\left(1 - \frac{X_2}{1-n_2^2}\right) - v_{z_2}^{(1)} \frac{\partial v_{x_1}^{(1)}}{\partial z}\left(1 - \frac{X_1}{1-n_1^2}\right)}_{P_{x_{12}}^{(2)}} \qquad (14)$$

Complex values of the electron velocities cannot be used in these relations. The real velocity values are easily obtained from the various field relations in the previous section.

For the ionosphere it is usually sufficient to use the second order relations, Eqs. 12, 13, 14. In a physical plasma device this is not always permissible, but the second order relations are still very useful, since they can be applied to demonstrate how and when wave instabilities tend to build up (see the preceding paper).

It is important to note that the transverse nonlinear forces $P_y^{(2)}$ and $P_x^{(2)}$ disappear if $v_{z_{1,2}}^{(1)} = 0$. When all waves travel longitudinally, there are second order nonlinear driving forces in the longitudinal or z direction only. This case is therefore simpler to treat, but it is much less interesting from the interaction point of view.

The $\bar{P}_1^{(2)}$ and $\bar{P}_2^{(2)}$ terms contain the second harmonic forces, of angular frequencies $2\omega_1$ and $2\omega_2$, and a nonlinear static force term. Since $v_z^{(1)}$ differs in phase from $v_y^{(1)}$ by $\pm\pi/2$ ($\nu=0$), it appears from Eqs. 12, 13, and 14 that there is a second order static nonlinear force term in the y direction only. As the total direct current must be zero in the infinite-plane medium, we must require that the mean value,

denoted by $\langle\ \rangle$, of the second order convection current be zero. That is,

$$\left\langle \rho_{1\,\frac{1}{2}}^{(1)}\ \bar{v}_{1\,\frac{1}{2}}^{(1)} + \rho_o\ \bar{v}_{1\,\frac{1}{2}}^{(2)} \right\rangle = 0 \tag{15}$$

which, by the $\bar{v}$ and ρ_1 relations of Section 2, yields

$$\left\langle v_{x_{1\,\frac{1}{2}}}^{(2)} \right\rangle = -R_{1\,\frac{1}{2}}\, Y_{T_{1\,\frac{1}{2}}}\, Q_{1\,\frac{1}{2}}^{(1)}\ \frac{1}{2}\left[\frac{v_{y_{max}}^{(1)\ 2}}{v_{ph}}\right]_{1\,\frac{1}{2}}$$

$$\left\langle v_{z_{1\,\frac{1}{2}}}^{(2)} \right\rangle = \left\langle v_{x_{1\,\frac{1}{2}}}^{(2)} \right\rangle R_{1\,\frac{1}{2}}\, Y_{T_{1\,\frac{1}{2}}} / Q_{1\,\frac{1}{2}}^{(1)} \tag{16}$$

$$\left\langle v_{y_{1\,\frac{1}{2}}}^{(2)} \right\rangle = 0$$

when $\nu = 0$. Since $\left\langle v_{z_{1\,\frac{1}{2}}} \right\rangle$ is always positive, the higher power wave, to second order, pushes the medium ahead. There is no transverse drift, and it should be noted that $\left\langle \bar{v}^{(1)} \right\rangle$ has the same direction in the x-z plane as the linear electron velocity.

From the second order equation of motion we next obtain (indices 1 and 2 dropped)

$$\frac{e}{m}\left\langle E_x^{(2)} \right\rangle = -\omega_L \left\langle v_y^{(2)} \right\rangle + \left\langle P_x^{(2)} \right\rangle$$

$$\frac{e}{m}\left\langle E_y^{(2)} \right\rangle = \omega_L \left\langle v_x^{(2)} \right\rangle - \omega_T \left\langle v_z^{(2)} \right\rangle + \left\langle P_y^{(2)} \right\rangle \tag{17}$$

$$\frac{e}{m}\left\langle E_z^{(2)} \right\rangle = \omega_T \left\langle v_y^{(2)} \right\rangle + \left\langle P_z^{(2)} \right\rangle$$

This yields

$$\langle E^{(2)}_{x_{1_2}} \rangle = 0 = \langle E^{(2)}_{z_{1_2}} \rangle$$

$$\frac{e}{\omega_{1_2} m} \langle E^{(2)}_{y_{1_2}} \rangle = -R_{1_2} Y_{T_{1_2}} \left\{ Y_{L_{1_2}} \left[Q^{(1)}_{1_2} - \frac{1}{Q^{(1)}_{1_2}} \right] + R_{1_2} Y^2_{T_{1_2}} \right\} \frac{1}{2} \left[\frac{v^{(1)\,2}_{y_{max}}}{v_{ph}} \right]_{1_2} \tag{18}$$

Thus a static nonlinear electric field is generated in the y direction only. It has the right magnitude and direction to permit the electrons to drift in a straight line in spite of the presence of the static magnetic field.

In a system with one high power wave only,

$$P^{(2)}_x / P^{(2)}_y = \frac{\partial v^{(1)}_x}{\partial z} \Big/ \frac{\partial v^{(1)}_y}{\partial z} \tag{19}$$

Besides the nonlinear force on the electrons, we must also consider the nonlinear a-c convection densities in the system,

$$\bar{i}^{(2)}_a = \rho^{(1)}_{1_1} \bar{v}^{(1)}_1 + \rho^{(1)}_{1_2} \bar{v}^{(1)}_2 + \rho^{(1)}_{1_1} \bar{v}^{(1)}_2 + \rho^{(1)}_{1_2} \bar{v}^{(1)}_1 - \langle i^{(2)}_a \rangle \tag{20}$$

$$\bar{i}^{(2)}_b = \rho_o \left[\bar{v}^{(2)}_1 + \bar{v}^{(2)}_2 \right] + \langle i^{(2)}_a \rangle$$

which also contain second harmonics and sum and difference frequency terms.

4. NONLINEAR WAVE EQUATION

For the second order nonlinear fields, Maxwell's equations can now be written as

$$p_e^2 E_x^{(2)} = -\frac{1}{\varepsilon_o}\frac{\partial}{\partial t}\left[\bar{i}_a^{(2)}+\bar{i}_b^{(2)}\right]_x$$

$$p_e^2 E_y = -\frac{1}{\varepsilon_o}\frac{\partial}{\partial t}\left[\bar{i}_a^{(2)}+\bar{i}_b^{(2)}\right]_y \qquad (21)$$

$$\frac{\partial^2}{\partial t^2} E_z^{(2)} = -\frac{1}{\varepsilon_o}\frac{\partial}{\partial t}\left[\bar{i}_a^{(2)}+\bar{i}_b^{(2)}\right]_z$$

where

$$p_e^2 = -\frac{1}{\mu_o \varepsilon_o}\frac{\partial^2}{\partial z^2}+\frac{\partial^2}{\partial t^2} \qquad \text{(electromagnetic wave operator in vacuum)} \qquad (22)$$

If we introduce the additional operators

$$p_p^2 = \frac{\partial^2}{\partial t^2}+\omega_p^2 \qquad \text{(plasma oscillation operator)} \qquad (23)$$

$$p_{e_m}^2 = p_e^2+\omega_p^2 \qquad \text{(electromagnetic wave operator for the isotropic ionized medium)}$$

and make use of the various expressions for the $\bar{P}^{(2)}$ components of the previous section, we obtain (after some transformations) the following nonlinear wave equation for $v_y^{(2)}$:

$$Dv_y^{(2)} = p_p^2\left(\omega_L p_e^2 \psi_x + p_{em}^2\frac{\partial \psi_y}{\partial t}\right) - \omega_T p_{em}^2 p_e^2 \psi_z = \pi_d \qquad (24)$$

where

$$\psi_x = p_e^2 P_x^{(2)} - \omega_p^2 \frac{\partial W_x^{(2)}}{\partial t}$$

$$\psi_y = p_e^2 P_y^{(2)} - \omega_p^2 \frac{\partial W_y^{(2)}}{\partial t} \qquad (25)$$

$$\psi_z = \frac{\partial^2}{\partial t^2} P_z^{(2)} - \omega_p^2 \frac{\partial W_z^{(2)}}{\partial t}$$

Here $W_x^{(2)}$, $W_y^{(2)}$, and $W_z^{(2)}$ are the x, y, and z components of

$$\bar{W}^{(2)} = \frac{1}{\rho_o} \bar{i}_a^{(2)} \qquad (26)$$

and

$$D = p_{em}^2 \left(p_p^2 p_{em}^2 + \omega_T^2 p_e^2 \right) \frac{\partial^2}{\partial t^2} + \omega_L^2 p_p^2 p_e^4 \qquad (27)$$

We furthermore obtain

$$p_{em}^2 \frac{\partial v_x^{(2)}}{\partial t} = - \omega_L p_e^2 v_y^{(2)} + \psi_y \qquad (28)$$

$$p_p^2 \frac{\partial v_z^{(2)}}{\partial t} = \omega_T \frac{\partial^2 v_y^{(2)}}{\partial t^2} + \psi_z \qquad (29)$$

Since $v_y^{(2)}$ is also related to $v_x^{(2)}$ by the following relation

$$\left(p_p^2 p_{em}^2 + \omega_T^2 p_e^2 \right) \frac{\partial^2 v_y^{(2)}}{\partial t^2} = \omega_L p_p^2 p_e^2 \frac{\partial v_x^{(2)}}{\partial t}$$

$$- \omega_T p_e^2 \psi_z + p_p^2 \frac{\partial \psi_y}{\partial t} \qquad (30)$$

one is induced to introduce the two "symbolic" second order polarization ratios (compare Eq. 7)

$$S_1^{(2)} = \frac{\left(p_p^2 p_{em}^2 + \omega_T^2 p_e^2\right)\partial/\partial t}{\omega_L p_p^2 p_e^2} \tag{31}$$

and

$$S_1^{(2)} = - \frac{\omega_L p_e^2}{p_{em}^2 \partial/\partial t} \tag{32}$$

By Eq. 27 it can immediately be shown that

$$S_1^{(2)} = S_2^{(2)} \left(1 - \frac{D}{\omega_L^2 p_p^2 p_e^4}\right) \tag{33}$$

The two second order polarization ratios are therefore equal only when $D = 0$, that is, when we have resonances in the system.

By our previous relations the wave equation for $v_x^{(2)}$ now can be written as

$$D \frac{\partial v_x^{(2)}}{\partial t} = \left(p_p^2 p_{em}^2 + \omega_T^2 p_e^2\right) \frac{\partial^2 \psi_x}{\partial t^2}$$

$$- \omega_L p_e^2 p_p^2 \frac{\partial \psi_y}{\partial t} + \omega_L \omega_T p_e^4 \psi_z \tag{34}$$

which by Eqs. 31 and 32 transforms to

$$D v_x^{(2)} = p_p^2 \left[\omega_L p_e^2 S_1^{(2)} \psi_x + p_{em}^2 S_2^{(2)} \frac{\partial \psi_y}{\partial t}\right]$$

$$- \omega_T p_{em}^2 p_e^2 S_2^{(2)} \psi_z \tag{35}$$

This relation demonstrates the meaning of the two polarization terms: $S_1^{(2)}$ applies to the nonlinear ψ_x forces, and $S_2^{(2)}$ to the ψ_y and ψ_z forces. Therefore $v_x^{(2)}/v_y^{(2)} = S_1^{(2)} = S_2^{(2)}$ when we have resonance in the system.

The wave equation for the second order longitudinal velocity finally becomes

$$D\frac{\partial v_z^{(2)}}{\partial t} = \omega_T\left(\omega_L p_e^{\,2}\frac{\partial^2\psi_x}{\partial t^2} + p_{em}^{\,2}\frac{\partial^3\psi_y}{\partial t^3}\right)$$

$$+ \overbrace{\left(p_{em}^{\,4}\frac{\partial^2}{\partial t^2} + \omega_L^{\,2}p_e^{\,4}\right)}^{\alpha}\psi_z \qquad (36)$$

where it is of interest that α annihilates the longitudinal magnetoionic modes.

From Eq. 27 we find that D can be written as

$$p_p^{\,2}D = \left[p_e^{\,2}\left(p_p^{\,2}\,\frac{\omega_T^{\,2}}{2}\right) + p_p^{\,2}\omega_p^{\,2}\right]^2\frac{\partial^2}{\partial t^2}$$

$$- p_e^{\,4}\left(\frac{\omega_T^{\,4}}{4}\frac{\partial^2}{\partial t^2} - \omega_L^{\,2}p_p^{\,4}\right) \qquad (37)$$

whence we symbolically obtain

$$p_p^{\,2}D = \underbrace{p_p^{\,2}\left\{\left[p_e^{\,2}\left(1+\frac{\omega_T^{\,2}/2}{p_p^{\,2}}\right)+\omega_p^{\,2}\right]\frac{\partial}{\partial t} - p_e^{\,2}\sqrt{\left(\frac{\omega_T^{\,2}/2}{p_p^{\,2}}\right)^2\frac{\partial^2}{\partial t^2} - \omega_L^{\,2}}\right\}}_{D_o}$$

Ordinary Electromagnetic Wave and Plasma Oscillation Operator

$$\cdot\, \underbrace{p_p^{\,2}\left[\left\{p_e^{\,2}\left(1+\frac{\omega_T^{\,2}/2}{p_p^{\,2}}\right)+\omega_p^{\,2}\right\}\frac{\partial}{\partial t} + p_e^{\,2}\sqrt{\left(\frac{\omega_T^{\,2}/2}{p_p^{\,2}}\right)^2\frac{\partial^2}{\partial t^2} - \omega_L^{\,2}}\right]}_{D_x}$$

Extraordinary Electromagnetic Wave Operator (38)

and

$$p_p^2 D = D_o D_x \tag{38a}$$

Note that D_o annihilates both an ordinary wave and a plasma oscillation ($p_p^2 = 0$), whereas D_x annihilates only an extraordinary wave.

Subject to proper boundary conditions, $D_o D_x \bar{v}^{(2)} = 0$ yields the linear transients of the system and its self-oscillations ($\nu = 0$, $\partial/\partial z = 0$) $X = \omega_p^2/\omega^2 = 1 + Y$, 1, and $1 - Y$.

If we assume that two high power waves, represented by $\bar{v}_1^{(1)}$ and $\bar{v}_2^{(1)}$, are present in the system, the nonlinear driving forces ψ_x, ψ_y, and ψ_z may contain terms with the propagation factors

$$\begin{gathered}
\exp\,(2\omega_1 t \pm 2\omega_1 n_1 z/c_o) \\
\exp\,(2\omega_2 t \pm 2\omega_2 n_2 z/c_o) \\
\exp\left[(\omega_1+\omega_2)t \pm (\omega_1 n_1+\omega_2 n_2) z/c_o\right] \\
\exp\left[(\omega_1+\omega_2)t \pm (\omega_1 n_1-\omega_2 n_2) z/c_o\right] \\
\exp\left[(\omega_1-\omega_2)t \pm (\omega_1 n_1-\omega_2 n_2) z/c_o\right] \\
\exp\left[(\omega_1-\omega_2)t \pm (\omega_1 n_1+\omega_2 n_2) z/c_o\right]
\end{gathered} \tag{39}$$

where $n_1 = n(\omega_1)$ and $n_2 = n(\omega_2)$. It should be remembered that a primary high power wave is defined as a "pure" magnetoionic mode. Two different magnetoionic modes have to be treated as <u>two</u> primary waves, even if their wave frequency happens to be the same.

According to Eq. 29 the "effective" refractive indices of the second harmonic driving forces are $2n(\omega_1)$ and $2n(\omega_2)$. The effective refractive indices n_+ and n_- of the sum and difference frequency waves become

$$n_+ = \frac{\omega_1 n_1 \pm \omega_2 n_2}{\omega_1 + \omega_2} = \frac{\omega_1 n_1 \pm \omega_2 n_2}{\omega_+}$$

$$n_- = \frac{\omega_1 n_1 \mp \omega_2 n_2}{\omega_1 - \omega_2} = \frac{\omega_1 n_1 \mp \omega_2 n_2}{\omega_-} \qquad (40)$$

where the upper signs correspond to the situation that both primary waves propagate in the same direction, and the lower signs to propagation in opposite directions.

Next let us introduce the self-explanatory operator equivalents

$$p_{e_\pm}^2 = \omega_\pm^2 (n_\pm^2 - 1) \qquad p_{em_\pm}^2 = p_{e_\pm}^2 + \omega_p^2 \qquad (41)$$

and

$$p_{p_\pm}^2 = \omega_p^2 - \omega_\pm^2 \qquad (42)$$

Making use of these relations and Eq. 40, we can prove that the following important relation holds,

$$D_\pm = -p_{e_\pm}^2 \, p_{p_\pm}^2 \, \Gamma_\pm \qquad (43)$$

where

$$\boxed{\Gamma_\pm = \omega_p^2 \left[\frac{1}{1-n_o^2(\omega_\pm)} - \frac{1}{1-n_\pm^2}\right] \left[\frac{1}{1-n_x^2(\omega_\pm)} - \frac{1}{1-n_\pm^2}\right]} \qquad (44)$$

This relation shows that we obtain traveling-wave resonance D = 0 in the system when $n_\pm^2 = n_o^2(\omega_\pm)$ or $n_\pm^2 = n_x^2(\omega_\pm)$. (Compare the preceding paper.)

In principle, therefore, the nonlinear driving forces, irrespective of the type of polarization of the high power primary waves, may excite sum and/or difference frequency waves of either polarization. The only factor of importance, apart from the difference in magnitude of the nonlinear driving forces in the various cases, is the traveling-wave resonance, that is, equality in phase velocity and in phase velocity direction between the excited and the exciting waves. This is a characteristic feature of the dynamic nonlinear magnetoionic theory.

If collisional losses had been introduced in the system, we would have found that $\Gamma_{\pm}$ contained the same resonance terms but now with complex refractive indices. It is interesting to recall that maximum triple split coupling occurs when $[n_o(\omega) = n_x(\omega)]_{X=1}$, which is possible only when collisional losses are introduced. Triple split coupling can therefore be regarded as a kind of traveling-wave resonance in the coupling region. When $n_o(\omega_{\pm}) \approx n_x(\omega_{\pm})$, $\Gamma_{\pm}$ and $D_{\pm}$ must be used with great care, since the nonlinear driving forces now could excite both an o wave and a z wave at the same time. A detailed discussion of this complicated resonance case lies outside the scope of the present communication.

Let us focus our attention on Eq. 24 for a moment. From the previous relations it appears that $\psi_x = 0 = \psi_y$ if $\omega_T = 0$. In purely longitudinal propagation no second order electromagnetic waves are excited in the system. By Eq. 27, $D = p_p^2 \alpha$ in this case. We then find from Eq. 26 that a second order longitudinal plasma wave, determined by the relation

$$p_p^2 \frac{\partial v_z^{(2)}}{\partial t} = (\psi_z)_{\omega_T=0} \qquad (\omega_T=0) \tag{45}$$

is excited in the system. Since $1 - n_q^2 = X_q$ for the isotropic medium ($\omega_H = 0$), Eq. 45 yields a very simple result in this case, and $v_z^{(2)}$, which become large when $p_p^2 \rightarrow 0$, is proportional to the gradient of the first order kinetic energy of the oscillating electrons (Ref. 1; see also Eqs. 11b and 12). It consequently appears that no interesting second order nonlinear interaction effects take place unless $\omega_T \neq 0$.

The present theory is based on the limiting assumption that the wave normals of the high power waves and the system waves are parallel. The more general case when the wave normal directions differ by certain specified angles will be discussed in the following paper. One finds that Eq. 40 holds, provided it is written in vector form. (See also the preceding paper.) If the medium is stratified in the z direction, then $\bar{n}_1$, $\bar{n}_2$, $\bar{n}_+$, and $\bar{n}_-$ in Eq. 40 "simply" have to be replaced by their z components.

5. GENERATION OF SUM AND DIFFERENCE FREQUENCY WAVES

From Eqs. 30 and 44 it appears that intense sum and difference frequency waves will be excited in the magnetoionic medium if (a) the high power or pump waves experience a medium resonance, that is, if $X_{\frac{1}{2}} = 1$ or $Y^2_{\frac{1}{2}} = Y^2_{R\frac{1}{2}}$ (Eq. 8); or (b) if there is traveling-wave resonance in the medium, that is, $n^2_{\pm} = n^2_o(\omega_{\pm})$ or $n^2_x(\omega_{\pm})$. If both (a) and (b) happen at the same time, which is possible, one can expect extra-strong excitation of the resonant waves.

For the homogeneous medium the associated sum and difference frequency waves (for nomenclature see also the preceding paper) are easily obtained from Eq. 30 when ψ_x, ψ_y, and ψ_z have been evaluated by means of the various relations of Sections 2 and 3. When the medium is not homogeneous, which is the physically important case, the problem is more difficult. What we wish to determine is not only the amplitude and phase of the associated waves, but also the same quantities for the radiating sum and difference frequency waves.

It is possible, however, to obtain an approximate but useful solution if the medium parameters vary so slowly that partial reflection can be neglected. To that end we proceed as follows.

It can easily be verified that $D_{\pm}$ can be written

$$D_{\pm} = \underbrace{-\frac{\left(\omega_{\pm}^2-\omega_p^2\right)\left(\omega_{\pm}^2-\omega_H^2\right)-\omega_T^2\omega_p^2}{\omega_{\pm}^2-\omega_p^2}\, c_o^4}_{\beta} \left(\frac{d^2}{dz^2}+k_{o_{\pm}}^2\right)\left(\frac{d^2}{dz^2}+k_{x_{\pm}}^2\right) \qquad (46)$$

where $k_{o_{\pm}} = \frac{\omega_{\pm}}{c_o} n_o(\omega_{\pm})$ and $k_{x_{\pm}} = \frac{\omega_{\pm}}{c_o} n_x(\omega_{\pm})$. The factor β preceding the operators is zero at the fourth reflection point (Eq. 9) for an "independent" sum or difference frequency wave.

Let us assume, in order to study the radiation of the difference frequency wave only (the procedure to obtain the sum frequency wave is quite analogous), that Π_d of Eq. 24 can be written

$$\Pi_{\underline{d}} = b_o e^{+j\left[\omega_- t - \frac{\omega_-}{c_o}\int_{z_a}^{z} n(\omega_-)\,dz\right]} = b_o e^{+j\left(\omega_- t - \int_{z_a}^{z} k_- dz\right)} \qquad (47)$$

where k_{-1} is considered to be positive, that is, the nonlinear driving force travels in the positive z direction. The driving force amplitude b_o is assumed to vary so slowly that it can be regarded as constant in the main interaction region. (Note: Resonances of the driving force, $X_{\frac{1}{2}} = 1$ or $Y^2_{\frac{1}{2}} = Y^2_{R_{\frac{1}{2}}}$, are assumed <u>not</u> to appear within the traveling-wave resonance region.) Furthermore, we assume that resonance takes place between the driving (nonlinear) wave and the extraordinary wave of the system, and that $k_{o_-} \neq k_{x_-}$; that is, we avoid the triple split region.

At some medium level $z = z_o$, traveling-wave resonance takes place. For the very slowly varying medium we therefore write

$$k_{-1} - k_{x_{-1}} = \mathscr{k}(z - z_o) \tag{48}$$

which we assume to hold within the main interaction region $z_o - z_m/2$ to $z_o + z_m/2$, where z_m is the width of the region.

If we next assert that z_m is so large that

$$|w_m| = \left| \int_{z_o - z_m/2}^{z_o + z_m/2} (k_{-1} - k_{x_{-1}})\, dz \right| \gg 1 \tag{49}$$

and make use of the asymptotic properties of the Fresnel integral (see the preceding paper), the first order solutions to Eq. 24 become

$$v_y^{(2)} \simeq \frac{b_o\, e^{+j\omega_- t}}{\beta(k_{o_-}^2 - k_-^2)(k_{x_-}^2 - k_-^2)}\, e^{-j\int_{z_a}^{z} k_{-1}\, dz} \tag{50}$$

when $z \approx z_o - z_m/2$, and

$$v_y^{(2)} \simeq \frac{b_o\, e^{+j\omega_- t}}{\beta(k_{o_-}^2 - k_-^2)(k_{x_-}^2 - k_-^2)} \cdot \left[e^{-j\int_{z_a}^{z} k_{-1}\, dz} + \sqrt{\frac{2\pi}{\mathscr{k}}}(k_{x_-} - k_-)\, e^{-j\left(\int_{z_a}^{z} k_{x_-}\, dz - \frac{\pi}{4}\right)} \right] \tag{51}$$

when $z \approx z_o + z_m/2$. At the bottom of the interaction region we have only one "associated" wave, which is not an independent or radiating wave, since it does not satisfy Maxwell's equations for the unperturbed magnetoionic medium. At the top of the interaction region, $z \approx z_o + z_m/2$, we still obtain the same associated wave but also an "independent" radiating wave

$$\exp\left[j(\omega_- t) - \int_{z_a}^{z} k_{x_{-1}}\, dz\right]$$

which is a solution of Maxwell's equations, at the difference frequency, for the unperturbed magnetoionic medium. We can regard the amplitude ratio $\left|(k_- - k_{x_-})\sqrt{2\pi/\mathcal{H}}\right|$ between these two waves as a measure of the radiation efficiency at the difference frequency.

Since by Eq. 51 the amplitude of the radiating wave varies as $\sqrt{2\pi/\mathcal{H}}$, we note that only a small gradient of the refractive index difference is required in order to generate a strong difference frequency radiation. Since $|w_m|$ of Eq. 49 must also be large, a very wide medium is required at the same time. If $|\mathcal{H}| \longrightarrow 0$, then z_m must $\longrightarrow \infty$ so fast that Eq. 49 holds. Therefore, to first order, instabilities develop only in a very extended interaction region.

Relation 51 can be used to evaluate the first order second harmonic radiation of a high power primary wave. According to the previous relations, this takes place at the levels where

$$n^2(\omega) = n_o^2(2\omega) \qquad \text{or} \qquad n^2(\omega) = n_x^2(2\omega) \tag{52}$$

Here $n(\omega)$ is the refractive index of the high power wave and can have index x or o, as the situation may be.

Next let us investigate the possibilities of second harmonic traveling-wave resonances according to Eq. 52. We immediately find that in the longitudinal case $Y_T = 0$,

$$Y_T^2 = 0 \begin{cases} n_x^2(\omega) = n_x^2(2\omega) = 1 + \dfrac{X}{2}\,, \quad (X = \omega_p^2/\omega^2), \quad \text{if } Y_L = \dfrac{\omega_L}{\omega} = 3 & (53) \\[2ex] n_o^2(\omega) = n_x^2(2\omega) = 1 - \dfrac{X}{2}\,, \quad \text{if } Y_L = \dfrac{\omega_L}{\omega} = 1 & (54) \end{cases}$$

These resonances are particularly interesting because they hold for any X value and are therefore likely to generate strong second harmonics when $Y_T^2 = 0$, in spite of the fact that the nonlinear driving forces must be of the third order. The case of Eq. 54 corresponds to "cyclotron resonance" and should be observable, for example by "topside" sounders.

Putting $Y_L = 0$, the case of completely transverse propagation, we find that

$$Y_T^2 = 0 \begin{cases} n_x^2(\omega) = n_x^2(2\omega) = 1 - \frac{X^2}{4} & (55) \\ \qquad \text{if } Y_T^2 = \frac{\omega_T^2}{\omega^2} = -\frac{(1-X)(1-X/4)}{X/4} = Y_{T_{III}}^2 \\ \qquad \text{(Physically possible only if } 1 \leq X \leq 4) \\ n_o^2(\omega) = n_x^2(2\omega) = 1 - X \\ \qquad \text{if } Y_T^2 = 3(1-X/4) = Y_{T_{IV}}^2 \qquad (X \leq 4) & (56) \end{cases}$$

and

$$n_x^2(\omega) = n_o^2(2\omega) = 1 - X/4, \text{ if } Y_T^2 = 3(X-1) = Y_{T_V}^2 \qquad (X \geq 1) \quad (57)$$

We further notice that Eq. 55 yields physically propagating resonant waves only when $1 \leq X < 4$ ($0 \leq Y_{T_{III}}^2 < 1$); Eq. 56 when $X < 4$ ($3 \geq Y_{T_{IV}}^2 > 0$); and Eq. 57 when $1 \leq X < 4$ ($0 \leq Y_{T_V}^2 < 9$). Thus, only Eq. 56 is physically possible when $X < 1$.

The corresponding traveling-wave resonance frequencies are

$$\omega^2 = \frac{1}{8}\left(5\omega_p^2 \pm \sqrt{9\omega_p^4 - 16\omega_p^2\omega_T^2}\right) \qquad \left(\omega_T^2 \leq \frac{9}{16}\,\omega_p^2\right) \qquad (55a)$$

$$\omega^2 = \frac{\omega_p^2}{4} + \frac{\omega_T^2}{3} \qquad (56a)$$

$$\omega^2 = \omega_p^2 - \frac{\omega_T^2}{3} \qquad (\omega_T^2 < 3\omega_p^2)$$

which do not always correspond to propagating conditions $[n^2(\omega) = n^2(2\omega) > 0]$.

It is interesting that traveling-wave resonances can also be obtained at or near the fourth reflection level, where all electron velocities become very large. For this resonance to hold, we must require that $Y_R^2(\omega) = Y_R^2(2\omega)$. That is,

$$1 - X = \frac{Y_T^2}{1-Y_L^2} \qquad 1 - \frac{X}{4} = \frac{Y_T^2/4}{1-Y_L^2/4}$$

which yields, when $|n^2(\omega)| = |n^2(2\omega)| = \infty$,

$$Y_{L_R}^2 = \frac{4}{X} \qquad Y_{T_R}^2 = \frac{(4-X)(X-1)}{X} \qquad (1 \leq X \leq 4)$$

$$Y_R^2 = 5-X \qquad (Y_{T_{R_{max}}}^2 = 1, \text{ for } X = 2) \tag{58}$$

This resonance takes place only when X lies in the range 1 to 4, and Y_R^2 is never less than one. At these resonance levels an exospheric whistler may produce second harmonics. Conversely, a 2ω whistler "pump" wave may amplify (or generate) an ω whistler by parametric traveling-wave interaction.

In the general case where the wave normal makes an arbitrary angle with the static magnetic field, the refractive index relations become more complicated. Introducing the parameter

$$\lambda = -Y_T^2/Y_{T_{III}}^2 \tag{59}$$

the equalized refractive indices become

$$n_1^2(\omega) = n_1^2(2\omega) = 1 + \frac{X^2/2}{\lambda + \sqrt{\lambda^2+(\lambda+1)X^2}} \tag{60}$$

$$n_2^2(\omega) = n_2^2(2\omega) = 1 - \frac{X^2/2}{\underbrace{-\lambda+\sqrt{\lambda^2+(\lambda+1)X^2}}_{\mu}} \tag{61}$$

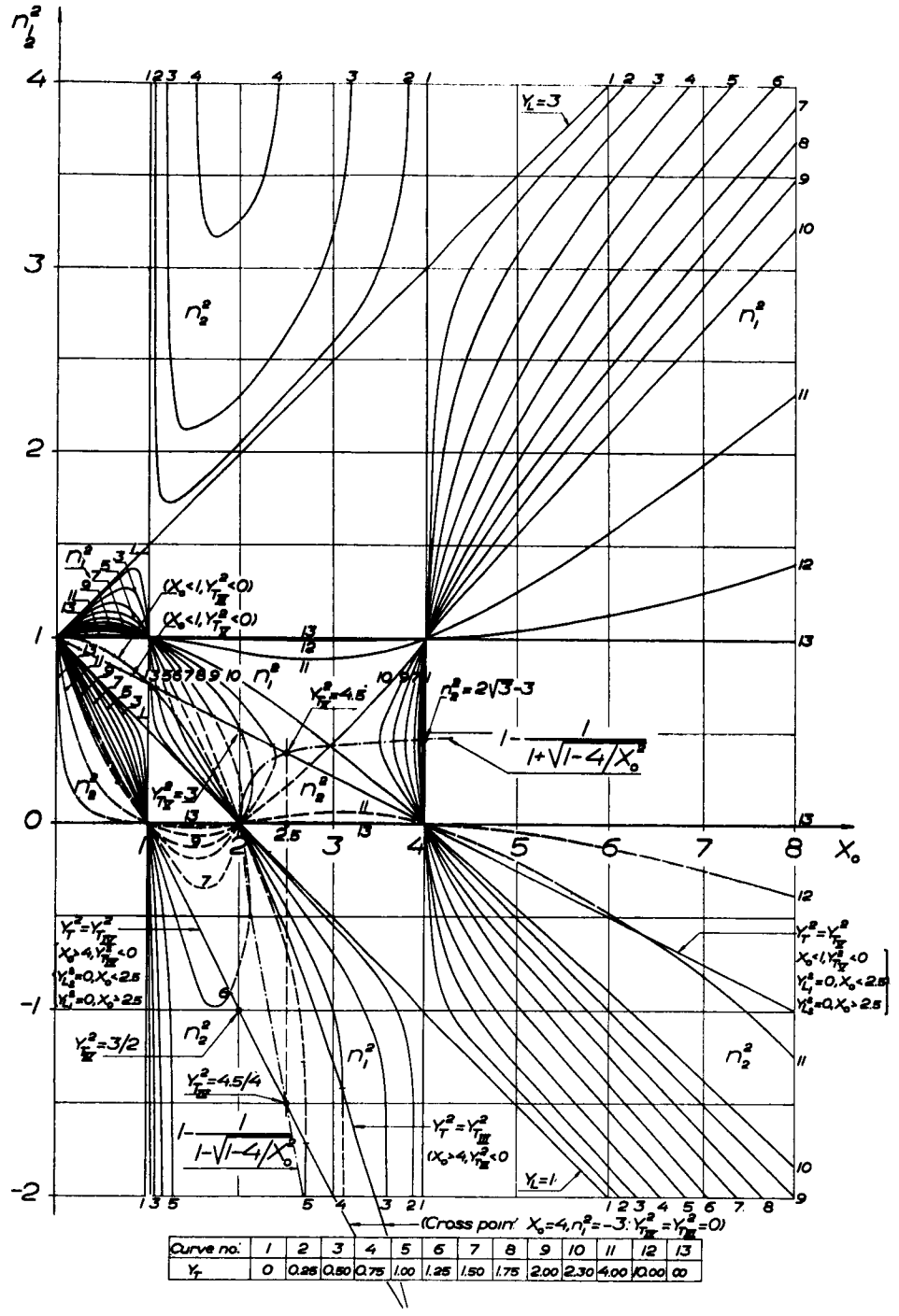

Curve no.	1	2	3	4	5	6	7	8	9	10	11	12	13
Y_T	0	0.25	0.50	0.75	1.00	1.25	1.50	1.75	2.00	2.30	4.00	10.00	∞

FIG. 2. Demonstration of $n^2(\omega) = n^2(2\omega)$ as functions of $X = \omega_p^2/\omega^2$ (denoted by X_o) for various values of Y_L and Y_T.

with the corresponding longitudinal cyclotron frequency components

$$Y_{L_{\frac{1}{2}}^{2}} = \frac{1}{X}\left[2\lambda^2+5(\lambda+1)X\pm 2(2+\lambda)\mu\right] \tag{62}$$

For graphical presentation (Fig. 2) we have labeled the equalized refractive indices 1 and 2. Only a more detailed investigation will reveal to which polarization the equalized indices may correspond. This varies with X and is of no immediate concern, since there is no difference in principle between the various states of polarization from the point of view of nonlinear interaction.

A closer examination of Eqs. 60 and 61 reveals that most of the traveling-wave resonances take place in a region where $X > 1 - Y$. In Fig. 2, which depicts the equalized refractive indices as functions of X, there are three levels for which $n^2(\omega) = 0 = n^2(2\omega)$: X = 1, 2, and 4. Generation of a fairly strong second harmonic echo can be anticipated at these levels. A detailed analysis of the radiation efficiency in this case, which must be based on a more rigorous wave treatment to replace Eq. 51, is outside the scope of the present communication. It should be noted, however, that the following refractive indices are equal to zero at these levels:

$$\begin{aligned} X = 1 \qquad & n_o(\omega) = n_x(2\omega), \text{ for } Y = 3/2 \\ X = 2 \qquad & n_z(\omega) = n_x(2\omega), \text{ for } Y = 1 \\ X = 4 \qquad & n_z(\omega) = n_o(2\omega), \text{ for } Y = 3 \end{aligned} \tag{63}$$

where $n_z(\omega)$ denotes $n_x(\omega)$, for $X > X_R$.

According to Fig. 2 there are a number of levels, of special interest in the "topside" ionosphere, where traveling-wave excitation of second harmonics is possible. The same applies to the exosphere, where wave interaction takes place in regions where $Y > 1$. But the different resonance levels may differ in efficiency, since the nonlinear driving forces (represented by b_o in Eq. 50) may vary widely with X and Y.

6. NONLINEAR INTERACTION, PUMP WAVE CHARGE BUNCHING

In order to briefly discuss the parametric interaction in the magnetoionic medium, let us limit ourselves to the effects of pump wave

charge bunching only (see also the preceding paper). We then have (ω_p is the angular pump frequency)

$$\psi_x = -\omega_p^2 \frac{\partial}{\partial t}(\eta v_x^{(2)})$$

$$\psi_y = -\omega_p^2 \frac{\partial}{\partial t}(\eta v_y^{(2)}) \qquad (64)$$

$$\psi_z = -\omega_p^2 \frac{\partial}{\partial t}(\eta v_z^{(2)})$$

where

$$\eta = \frac{\Delta N(z,t)}{N_o} = \frac{\Delta N_m}{N_o} \cos\left[\omega_p t - \omega_p n_{ox}(\omega_p) z\right] \qquad (65)$$

represents the charge bunching. If $\omega_T \neq 0$, then η is linearly proportional to the pump field amplitude (Eq. 5a). When $\omega_T = 0$, it is proportional to the square of this (see Eq. 45 and the preceding paper). Equation 24 and associated relations now yield the following coupled equations:

$$\left(\frac{\partial^2}{\partial t^2} p_{em}^2 \left\{ p_p^2 \left[p_e^2 + \omega_p^2 (1+\eta) \right] + \omega_T^2 p_e^2 \right\} + \omega_L^2 p_p^2 p_e^4 \right) v_y^{(2)}$$

$$= -\omega_p^2 p_e^2 \frac{\partial}{\partial t} \left[p_p^2 \omega_L \eta v_x^{(2)} - p_{em}^2 \omega_T \eta v_z^{(2)} \right] \qquad (66)$$

$$\left[\frac{\partial^2}{\partial t^2} + \omega_p^2 (1+\eta) \right] v_z^{(2)} = \omega_T \frac{\partial v_y^{(2)}}{\partial t} \qquad (67)$$

$$\frac{\partial}{\partial t} \left[p_e^2 + \omega_p^2 (1+\eta) \right] v_x^{(2)} = -\omega_L p_e^2 v_y^{(2)} \qquad (68)$$

The left-hand side of Eq. 67 is a Mathieu equation, and the left-hand side of Eq. 68 can be reduced to one. Both operators describe oscillations in a periodically perturbed isotropic ionized medium.

To study the instabilities in this medium, we would have to solve the coupled Mathieu-type equations, a very complicated matter. The spectral terms of the steady state can always be obtained, of course,

from Eqs. 66, 67, and 68. We then obtain the parametric resonance conditions already described (Eq. 40). If the fundamental mode easily becomes nonlinear, for example at the fourth reflection level, we can pump the medium with a higher frequency than 2ω (3ω, 4ω, etc.) corresponding to the higher order Mathieu instabilities. If losses are very small, as in the uppermost ionosphere, harmonic traveling-wave pumping and generation of the more easily excited modes should be possible, provided the resonance conditions are satisfied.

7. NONLINEARITIES IN THE "TOPSIDE" IONOSPHERE

Even though the theory presented in the previous sections is based on the assumption that infinite-plane magnetoionic waves travel in the system, which is not true within a wavelength or so of a "topside" sounder, it should be possible to draw some general conclusions concerning the nature of the wave instabilities recorded by such a device.

At the normal total-reflection or self-oscillation levels $X = 1 - Y$, 1, and $1 + Y$, one only expects fundamental plasma "spikes" except at levels where any of the traveling-wave resonances of Eq. 63 would take place. At these levels harmonic pumping should also be possible; that is, plasma "spikes" could be recorded when the sounder emits at twice the resonance frequency.

Instabilities are likely to be very strong at the fourth reflection levels, at least as far as plane waves are concerned. These levels, which lie in the following Y^2 range (Eq. 8),

$$Y^2 = Y_R^2 = \frac{1-X}{1-X\cos^2\theta} \qquad (X < 1)$$

$$Y^2 = Y_R^2 = \frac{X-1}{X\cos^2\theta-1} \qquad (X > 1/\cos^2\theta)$$

depend upon the angle θ. Since the "topside" sounder acts almost as a point source in the medium, plasma "spikes" at the Y_R^2 levels are likely to be strong only in wave normal directions for which $(1/n)(dn/d\theta) = 0$, which means that the Poynting vector is parallel to the wave normal. Since $\cos^2\theta$ is equal to 0 or 1 in these directions (longitudinal or transverse propagation), strong fundamental plasma "spikes" are likely only when $Y_R^2 = 1$ ($\theta = 0$), and $Y_R^2 = 1 - X$ ($\theta = \pi/2$). This agrees with the experimental results so far reported. Harmonic pumping of these resonances (see Section 6) should also be possible, especially for the one at $Y_R^2 = 1$ (cyclotron resonance), since traveling-wave resonances are easily obtained at this level (see Eq. 54).

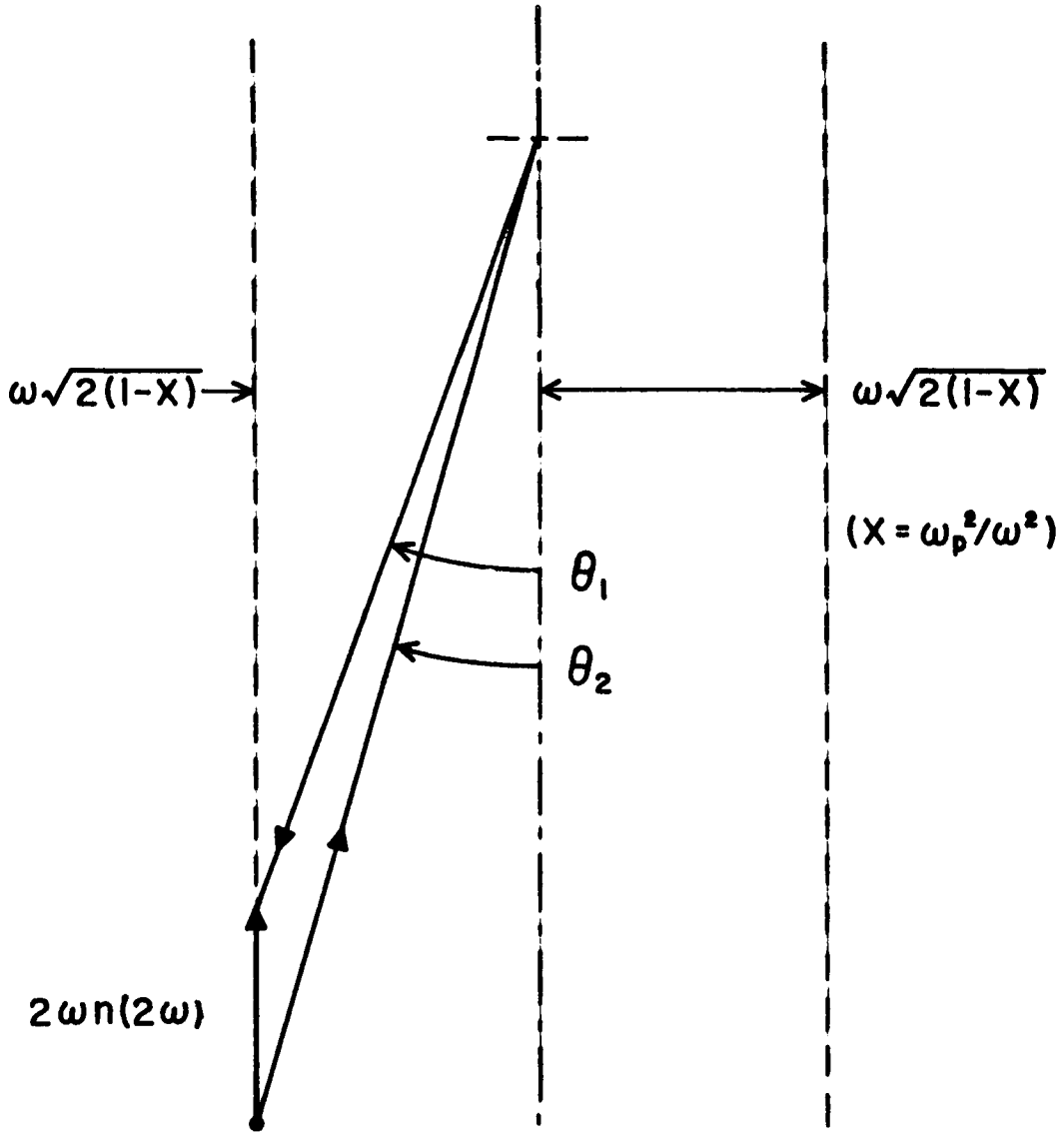

FIG. 3. Second harmonic pumping at $Y_R^2 = 1$.

If $Y^2 = 1$, we obtain for small values of θ

$$n_x^2(\omega) \approx 1 + \frac{2(1-X)}{\sin^2\theta} \tag{69}$$

which means that for small angles the transverse component of n_x is practically independent of θ, or

$$n_x(\omega)\sin\theta \approx \sqrt{2(1-X)} \tag{70}$$

Second harmonic traveling-wave resonances (now shown in vector form) are thus easily obtainable in the direction around $\theta = 0$, as sketched in Fig. 3. The second harmonic pump wave continuously builds up forward and backward waves at the fundamental frequency, which in their turn generate a backward second harmonic wave. The system becomes unstable at complete traveling-wave resonance (see Section 6 and the preceding paper), and "cyclotron spikes" will be recorded at both the fundamental and the second harmonic. Similar pumping schemes would also be effective at the higher harmonics, provided ν is small enough (as in the "topside" ionosphere). Harmonic "spikes" related to $Y_R^2 = 1$ have been recorded by "topside" sounders, but to the authors knowledge, none related to $Y^2 = 1 - X$.

Unfortunately, present "topside" sounders are not equipped to record harmonics and fundamentals simultaneously. A recorder with such features would no doubt yield very interesting and important results, and is almost a necessity if we wish to study the "topside" nonlinearities thoroughly.

REFERENCES

1. O. E. H. Rydbeck, Dynamic Non-linear Wave Propagation in Ionized Media, II, Research Rept. No. 28, Research Laboratory of Electronics, Chalmers Univ. Technol., Gothenburg, 1962 (also to appear in Arkiv for Geofysik, Roy. Swed. Acad. Sci.).

See also papers I and II herein.

III. WHISTLER MODE AND IONIZED STREAM INTERACTIONS*

O. E. H. Rydbeck and J. Askne

1. SUMMARY

Gallet and Helliwell (1) suggested in 1959 that selective traveling-wave amplification caused by interactions between an ionized stream and whistler modes could generate low frequency emissions in the exosphere. Rydbeck in 1959 (2) showed that no such amplification is possible when the wave normal is parallel to the stream and the exospheric magnetic field, but that another and probably very important interaction takes place, by which the incoming fast cyclotron waves of the stream are totally or partially reflected as backward whistler modes. This mode transformation, which has a fairly large "gyromagnetic" interaction bandwidth, occurs in a region where $\omega_H/\omega > 1$ and the fast cyclotron wave has a negative phase velocity. The efficiency of this transformation depends upon the square root of the stream current density, in such a fashion that the amplitude of the fast cyclotron wave decreases approximately as exp. $(\mathcal{H}\sqrt{i_o}z)$, where i_o is the current density and z the axial distance.

The nature of this wave transformation is studied in more detail in the present communication, as well as interactions for arbitrary values of θ, the angle between the wave normal and the static magnetic field, which is initially assumed to be parallel to the infinitely wide ionized stream.

It is shown that the forward whistler mode and the slow cyclotron wave do not interact when $\theta = 0$, even if their phase velocities are equal, because they are oppositely (circularly) polarized. Equivalence of phase velocities, or wave "synchronism," therefore is not always a sufficient condition for linear wave interaction.

When $\theta \neq 0$, there are no less than eight waves that can interact in the system: four magnetoionic waves, two cyclotron waves, and two space-charge waves. It is shown that the backward whistler mode excitation is practically independent of θ as long as $\theta < \arccos [\omega/\omega_p^{(2)}]$, where $\omega_p^{(2)}$ is the electronic plasma frequency of the streaming medium. Backward whistler mode generation should therefore be a very probable phenomenon in the exosphere, especially since the gyromagnetic bandwidth is so large that one can "allow" some velocity spread in the stream and still obtain reasonably strong interaction.

When $\theta \neq 0$, the streaming medium can actually amplify the forward whistler mode, as postulated by Gallet and Helliwell. This is a traveling-wave interaction between the fast cyclotron wave and the forward

---

*Part I, Scientific Report No. 187, Ionosphere Research Laboratory, The Pennsylvania State University, June 15, 1963 (with authors' revisions to September 6, 1963).

whistler mode. It increases in strength as θ approaches arc cos $[\omega/\omega_p^{(2)}]$, but its gyromagnetic bandwidth is very small. For this amplification to take place, one must therefore have a stream with an extremely small velocity spread.

The space-charge waves play no essential role in the whistler mode range. Their general interaction properties are, however, quite thoroughly discussed in the present report.

As a by-product of the present investigations, the wave propagation properties of a moving magnetoionic medium are also discussed in some detail. It is shown, for example, that the normal fourth reflection level disappears for the moving medium. Furthermore, it is found that magnetoionic waves are not always totally reflected, and may partly proceed as cyclotron waves in the moving medium. This combined reflection-transformation level corresponds to an ω_H/ω value somewhat larger than $1 - \omega_p^{(1)^2}/\omega^2$, where $\omega_p^{(1)}$ is the angular plasma frequency of the streaming medium, for the perturbed extraordinary wave.

Finally, the very general case when the stream makes some angle θ_s with the magnetic field (assuming electrostatic field conditions that make this flow direction possible) is briefly considered. The general nature of the interaction between the whistler mode and the stream does not change appreciably when $|\theta - \theta_s|$ has moderate values.

[Deletion in press by authors.]

Nonlinear whistler phenomena are likely to be important at various exospheric traveling-wave resonance levels. Problems of a related nature are dealt with in Ref. 3 and the preceding paper.

2. THE LONGITUDINAL CASE

We shall first consider whistler mode and ionized stream interaction when the wave normal and the stream are parallel to the static magnetic field.

As shown in Fig. 1, we assume that the neutral ionized medium, electron and ion density $N^{(2)}$, and the neutral ionized stream, electron and ion density $N^{(1)}$, are infinitely wide. We also assume that they are homogeneous, and for the present, that the strength H_o of the static magnetic field does not vary with z, the drift direction.

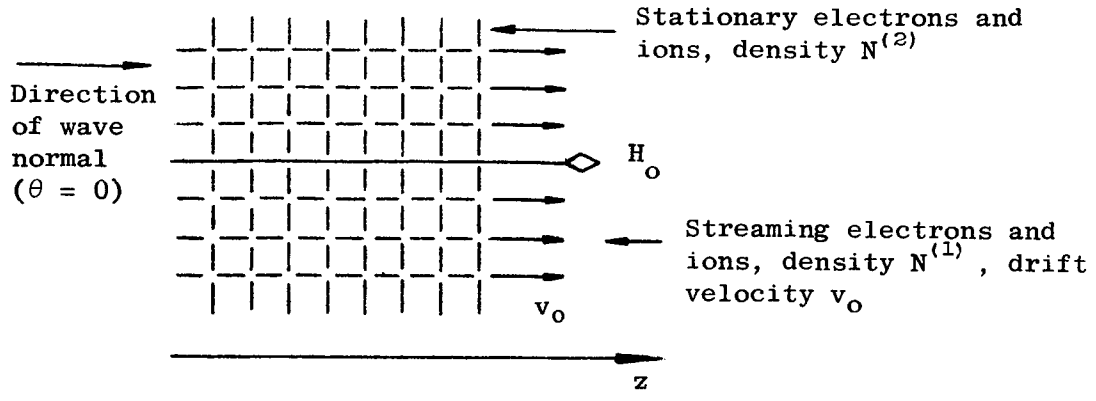

FIG. 1. Electron-ion stream in the stationary magnetoionic medium, longitudinal case.

Since the differential space-charge densities $\Delta N^{(1)}$ and $\Delta N^{(2)}$ are equal to zero in the longitudinal case -- that is, no charge bunching takes place -- Maxwell's equations yield ($E_z = 0$)

$$p_e^2 E_x = \mu_o \frac{\partial}{\partial t}\left(q_e^{(1)} v_{x_e}^{(1)} + q_j^{(1)} v_{x_j}^{(1)} + q_e^{(2)} v_{x_e}^{(2)} + q_j^{(2)} v_{x_j}^{(2)}\right)$$

$$p_e^2 E_y = \mu_o \frac{\partial}{\partial t}\left(q_e^{(1)} v_{y_e}^{(1)} + q_j^{(1)} v_{y_j}^{(1)} + q_e^{(2)} v_{y_e}^{(2)} + q_j^{(2)} v_{y_j}^{(2)}\right) \qquad (1)$$

where p_e^2 is the one-dimensional vacuum electromagnetic wave operator,

$$p_e^2 = \frac{\partial^2}{\partial z^2} - \mu_o \varepsilon_o \frac{\partial^2}{\partial t^2} \qquad (2)$$

$v_{x_e}^{(1)}$ and $v_{x_j}^{(1)}$ are the x-direction a-c velocities of the streaming electrons and ions, etc., and

$$q_e^{(1)} = -eN^{(1)} = -q_j^{(1)} \qquad q_e^{(2)} = -eN^{(2)} = -q_j^{(2)} \qquad (3)$$

We next introduce the drift operator

$$p_t = \frac{\partial}{\partial t} + v_o \frac{\partial}{\partial z} \tag{4}$$

which annihilates a synchronous wave; the gyro-oscillation operators, which annihilate cyclotron oscillations,

$$p_{c_e}^2 = \frac{\partial^2}{\partial t^2} + \omega_{H_e}^2 \qquad p_{c_j}^2 = \frac{\partial^2}{\partial t^2} + \omega_{H_j}^2 \tag{5}$$

where ω_{H_e} and ω_{H_j} are the angular cyclotron frequencies of the electrons and ions; and the cyclotron wave operators, which annihilate cyclotron waves,

$$p_{g_e}^2 = p_t^2 + \omega_{H_e}^2 \qquad p_{g_j}^2 = p_t^2 + \omega_{H_j}^2 \tag{6}$$

The equations of motion can then be written

$$\begin{aligned} p_{g_e}^2 \frac{\partial}{\partial t} v_{x_e}^{(1)} &= -\frac{e}{m_e} p_t (p_t E_x - \omega_{H_e} E_y) \\ p_{c_e}^2 \frac{\partial}{\partial t} v_{x_e}^{(2)} &= -\frac{e}{m_e} \frac{\partial}{\partial t} \left(\frac{\partial}{\partial t} E_x - \omega_{H_e} E_y \right) \end{aligned} \tag{7}$$

and so forth, in which m_e = mass of electrons.

Relations 1 and 7 now yield the coupled transverse field equations

$$\begin{aligned} &\left\{ p_{g_e}^2 p_{g_j}^2 \left[p_e^2 - \mu_o \varepsilon_o \frac{\partial^2}{\partial t^2} \left(\frac{\omega_{p_e}^{(2)^2}}{p_{c_e}^2} + \frac{\omega_{p_j}^{(2)^2}}{p_{c_j}^2} \right) \right] - \mu_o \varepsilon_o p_t^2 \left(\omega_{p_e}^{(1)^2} p_{g_j}^2 + \omega_{p_j}^{(1)^2} p_{g_e}^2 \right) \right\} \begin{matrix} E_x \\ E_y \end{matrix} \\ &= \mp \mu_o \varepsilon_o \left[\frac{\partial}{\partial t} p_{g_e}^2 p_{g_j}^2 \left(\omega_{H_e} \frac{\omega_{p_e}^{(2)^2}}{p_{c_e}^2} - \omega_{H_j} \frac{\omega_{p_j}^{(2)^2}}{p_{c_j}^2} \right) \right. \\ &\left. + p_t \left(\omega_{H_e} \omega_{p_e}^{(1)^2} p_{g_j}^2 - \omega_{H_j} \omega_{p_j}^{(1)^2} p_{g_e}^2 \right) \right] \begin{matrix} E_y \\ E_x \end{matrix} \end{aligned} \tag{8}$$

where $\omega_{p_e}^{(1)}$ and $\omega_{p_j}^{(1)}$ are the angular plasma frequencies of the streaming electrons and ions, and $\omega_{p_e}^{(2)}$ and $\omega_{p_j}^{(2)}$ are the same quantities for the stationary electrons and ions [$\omega_{p_e}^{(1)^2} = e^2 N^{(1)}/m_e \epsilon_o$, etc.].

If the medium parameters are constant, Eq. 8 implies that $(E_x/E_y)^2 = -1$; that is, <u>all</u> wave motions are circularly polarized. This yields two uncoupled wave equations,

$$p^*_{g_e} p^*_{g_j} p^2_{em_x} E_x = +\mu_o \varepsilon_o p_t (p^*_{g_j} \omega_{p_e}^{(1)^2} + p^*_{g_e} \omega_{p_j}^{(1)^2}) E_x \tag{9}$$

when $E_y = -jE_x$, and

$$p_{g_e} p_{g_j} p^2_{em_o} E_x = +\mu_o \varepsilon_o p_t (p_{g_j} \omega_{p_e}^{(1)^2} + p_{g_e} \omega_{p_j}^{(1)^2}) E_x \tag{10}$$

when $E_y = +jE_x$. In these equations

$$\begin{aligned} p_{g_e} &= p_t + j\omega_{H_e} \qquad & p^*_{g_e} &= p_t - j\omega_{H_e} \\ p_{c_e} &= \frac{\partial}{\partial t} + j\omega_{H_e} \qquad & p^*_{c_e} &= \frac{\partial}{\partial t} - j\omega_{H_e} \end{aligned} \tag{11}$$

and so on, and

$$p^2_{em_x} = p^2_e - \mu_o \varepsilon_o \frac{\partial}{\partial t} \left(\frac{\omega_{p_e}^{(2)^2}}{p^*_{c_e}} + \frac{\omega_{p_j}^{(2)^2}}{p^*_{c_j}} \right) \tag{12}$$

$$p^2_{em_o} = p^2_e - \mu_o \varepsilon_o \frac{\partial}{\partial t} \left(\frac{\omega_{p_e}^{(2)^2}}{p_{c_e}} + \frac{\omega_{p_j}^{(2)^2}}{p_{c_j}} \right) \tag{13}$$

are the operators annihilating the extraordinary and ordinary longitudinal magnetoionic waves.

The right-hand sides of Eqs. 9 and 10 couple the electron and ion cyclotron waves to the magnetoionic waves. This coupling tends to zero when $N^{(1)} \rightarrow 0$.

Since the $p^*_{g_e}$ and $p^*_{g_j}$ operators annihilate fast cyclotron waves and p_{g_e} and p_{g_j} annihilate slow cyclotron waves, we infer from Eqs. 9 and 10 that the backward waves only couple to fast-electron cyclotron waves and fast-ion cyclotron waves; that is, the interacting waves must have the same sense of polarization in the homogeneous and linear medium. From these equations it also appears that the moving electrons and ions are stationary whenever $|\partial/\partial z| \ll \omega/v_o$ -- when the phase velocity of the waves is much larger than the drift velocity. Often, therefore, the ordinary magnetoionic wave barely "notices" the drift motion of the streaming electrons and ions. The situation is entirely different as far as the extraordinary waves are concerned. Because whistler modes travel slowly, they readily interact with the streaming medium.

If we assume conditions such that $p^*_{g_e} E_x \approx 0$, Eq. 9 then yields

$$p^*_{g_e} p^2_{em_x} E_x \approx +\mu_o \varepsilon_o p_t \omega^{(1)2}_{p_e} E_x \tag{14}$$

If $p^2_{em_x} E_x \approx 0$ at the same time, strong coupling takes place between the fast-electron cyclotron wave and the backward extraordinary magnetoionic wave (the whistler mode), practically independently of the streaming ions. On the other hand, if $p^*_{g_j} E_x \approx 0$ and $p^2_{em_x} E_x \approx 0$ at the same time, strong coupling takes place between the ion cyclotron wave and the whistler mode. Hence, the ionic and electronic cyclotron wave interactions with the whistler mode can be analyzed separately with very good accuracy. In the following discussion we will limit ourselves to a study of the electron cyclotron wave interaction; the ionic case will be dealt with in a later report.

Considering electrons only and replacing $\partial/\partial z$ by

$$\frac{\partial}{\partial z} = -j\gamma \tag{15}$$

[that is, Re (γ) positive indicates a forward wave if the time factor is exp. ($j\omega t$)], Eqs. 9 and 10 can be thrown into the instructive forms

$$\gamma^2_{x_o} = \frac{1}{c_o^2}\left[\omega^2 + \frac{\omega^{(1)2}_{p_e}(\omega - \gamma v_o)}{(\pm\omega_{H_e} - \omega + \gamma v_o)} + \frac{\omega^{(2)2}_{p_e}\omega}{(\pm\omega_{H_e} - \omega)}\right] \tag{16a}$$

(16b)

where $1/c_o^2 = \mu_o \epsilon_o$. This demonstrates the effect of the drift-Doppler shift of the transversely oscillating streaming electrons.

Let us next, on the basis of Eq. 16a, study the interaction between the whistler mode and the fast cyclotron wave. Relation 16 can now be written

$$\underbrace{[\gamma-(\alpha-k_H)]}_{\substack{\text{Fast}\\ \text{cyclotron}\\ \text{wave}}}\underbrace{(\gamma^2-k_x^2)}_{\substack{\text{Eo}\\ \text{magneto-}\\ \text{ionic}\\ \text{waves}}} = \underbrace{k^2X_1(\alpha-\gamma)}_{\text{Coupling term}} \tag{17}$$

where

$$k_x^2 = k^2\left(1+\frac{X_2}{Y-1}\right) = k^2n_x^2 \qquad (k^2 = \omega^2/c_o^2)$$

$$X_2 = \omega_{p_e}^{(2)^2}/\omega^2 \qquad X_1 = \omega_{p_e}^{(1)^2}/\omega^2 \qquad k_H = \omega_{H_e}/v_o \tag{18}$$

$$\alpha = \omega/v_o \qquad Y = \omega_{H_e}/\omega$$

Thus, if the coupling is neglected, we have the three independent roots

$$\gamma_1 = \gamma_1^o = \alpha-k_H \qquad \gamma_2 = \gamma_2^o = +k_x \qquad \gamma_3 = \gamma_3^o = -k_x \tag{17a}$$

It is interesting to note that Eq. 17 can also be written

$$[\gamma-(\alpha-k_H)](\gamma^2-k_{21}^2) = k^2X_1k_H \tag{19}$$

where

$$k_{21}^2 = k_x^2 - k^2X_1 \tag{19a}$$

This relation demonstrates the influence of the static magnetic field upon the coupling. If the electron stream is underdense, $k_{21}^2 \cong k_x^2$.

Now let us introduce the notations

$$\Delta = \frac{k_H - \alpha - k_{21}}{2} \qquad k_m = \frac{k_H - \alpha + k_{21}}{2} \tag{20}$$

where Δ can be regarded as a measure of the phase velocity difference, from synchronism, between the fast cyclotron wave and the k_{21} wave (a slightly perturbed backward whistler mode). Relation 19 then becomes

$$(\Psi+\Delta)(\Psi-\Delta)(\Psi-k_m) = k^2 X_1 k_H \tag{21}$$

where

$$\Psi = \gamma + k_m \tag{21a}$$

In the interaction or traveling-wave resonance region, where Δ^2 is small compared to k_m^2 if the electron stream is not too dense, Eq. 21 becomes approximately

$$\Psi^2 \cong -\frac{k^2 X_1 k_H}{k_m} + \Delta^2 \qquad (X_1 << 1) \tag{22}$$

which yields

$$\gamma_{1\atop 3} \cong -k_m \pm \sqrt{\Delta^2 - \Delta_o^2} \qquad (X_1 << 1) \tag{22a}$$

where

$$\Delta_o^2 = \frac{k^2 X_1 k_H}{k_m} \tag{22b}$$

The remaining root of Eq. 21 becomes

$$\gamma_2 \cong k_x \left[1 - \frac{1}{n_x^2}\frac{X_1}{2}\left(1 + \frac{1}{2}\frac{k_H}{k_x}\right)\right] \qquad (\Delta = 0;\ X_1 << 1) \tag{23}$$

representing a forward whistler mode slightly perturbed by the underdense stream.

The two interacting waves experience traveling-wave resonance. Both are backward waves, since the fast cyclotron wave is a backward wave when $Y > 1$. In the center of the interaction or coupling region, $\Delta = 0$. That is,

$$k_H = k_{H_o} = \alpha + (k_{21})_{k_{H_o}} \qquad \text{or } Y = Y_o \cong 1 + \beta(n_x)_{Y_o} \tag{24}$$

where $\beta = v_o/c_o$. If $(n_x^2)_{Y_o} \gg 1$, Eq. 24 reduces to

$$Y_o = \frac{\omega_{H_o}}{\omega} \cong 1 + \beta^{2/3} X_2^{1/3} \tag{24a}$$

This demonstrates how the gyromagnetic interaction-band center varies with the stream velocity and the plasma frequency of the stationary medium.

In the center of the interaction band,

$$|\mathrm{Im}(\gamma_1)| \cong \Delta_o = k_o \sqrt{X_1 \frac{k_H}{k_m}} \qquad (\Delta = 0) \tag{25}$$

which is thus proportional to the square root of the electron current density. The higher the current density, the stronger the interaction.

The gyromagnetic interaction bandwidth is determined by the relation

$$\Delta = \pm k_o \sqrt{X_1 \frac{k_H}{k_m}} \tag{26}$$

corresponding to two k_H values, k_{H_1} and k_{H_2}. Relation 26 yields

$$k_{H_2} - k_{H_1} = \alpha(Y_2 - Y_1) = \frac{\Delta\omega_H}{v_o} = 4\Delta_o \sqrt{1 + \Delta_o \mu^2} \qquad (X_1 \ll 1) \tag{27}$$

where

$$\mu = \left[\frac{1}{k_H} - \frac{1}{2k_x}\left(1 + \frac{\partial k_x}{\partial k_H}\right)\right]_{Y_o} \qquad (X_1 \ll 1) \tag{27a}$$

From Eq. 27 one obtains the approximate relative gyromagnetic bandwidth,

$$\frac{\Delta\omega_H}{\omega} \approx 4\beta\sqrt{X_1 \frac{k_H}{k_m}} \qquad (X_1 << 1) \tag{27b}$$

which can be quite large, as accurate solutions of Eq. 21 would show, when the stream is fast and dense (X_1 of the order of 0.5, for example). It should also be pointed out that Eq. 27b can be written

$$\Delta\omega_H \approx \frac{4}{c_o}\sqrt{\frac{e}{m_e \varepsilon_o}|i_o|\frac{\omega_H}{k_m}} \qquad (X_1 << 1;\ Y = Y_o) \tag{27c}$$

$$\frac{\Delta\omega_H}{\omega_{H_o}} \approx 4\sqrt{\frac{|i_o|}{H_o k_m}} \qquad (X_1 << 1;\ Y = Y_o) \tag{27d}$$

The magnetic bandwidth thus depends upon only the stream density if the $k_o^2 X_1$ term in k_m is neglected.

It should be added that Eq. 17 has the following simple solutions when $k_x = \alpha$:

$$\gamma_{1,3} = \frac{1}{2}\left[-k_H \pm \sqrt{(2\alpha - k_H)^2 - 4k^2 X_1}\right]$$
$$\gamma_2 = \alpha \tag{28}$$

To demonstrate the details of the wave interaction, we have plotted in Fig. 2 the normalized γ values, $\Gamma = \gamma/k$, as functions of Y for $X_1 = 2/3$, $X_2 = 9$ (a whistler mode value), and $\beta = 1/3$. We have also included the roots Γ_4, Γ_5, and Γ_6 of Eq. 16b, which, similarly to Eq. 17, can be written

$$[\gamma - (\alpha + k_H)](\gamma^2 - k_o^2) = k^2 X_1 (\alpha - \gamma) \tag{29}$$

where

$$k_o^2 = k^2\left(1 - \frac{X_2}{1+Y}\right) = k^2 n_o^2 \tag{30}$$

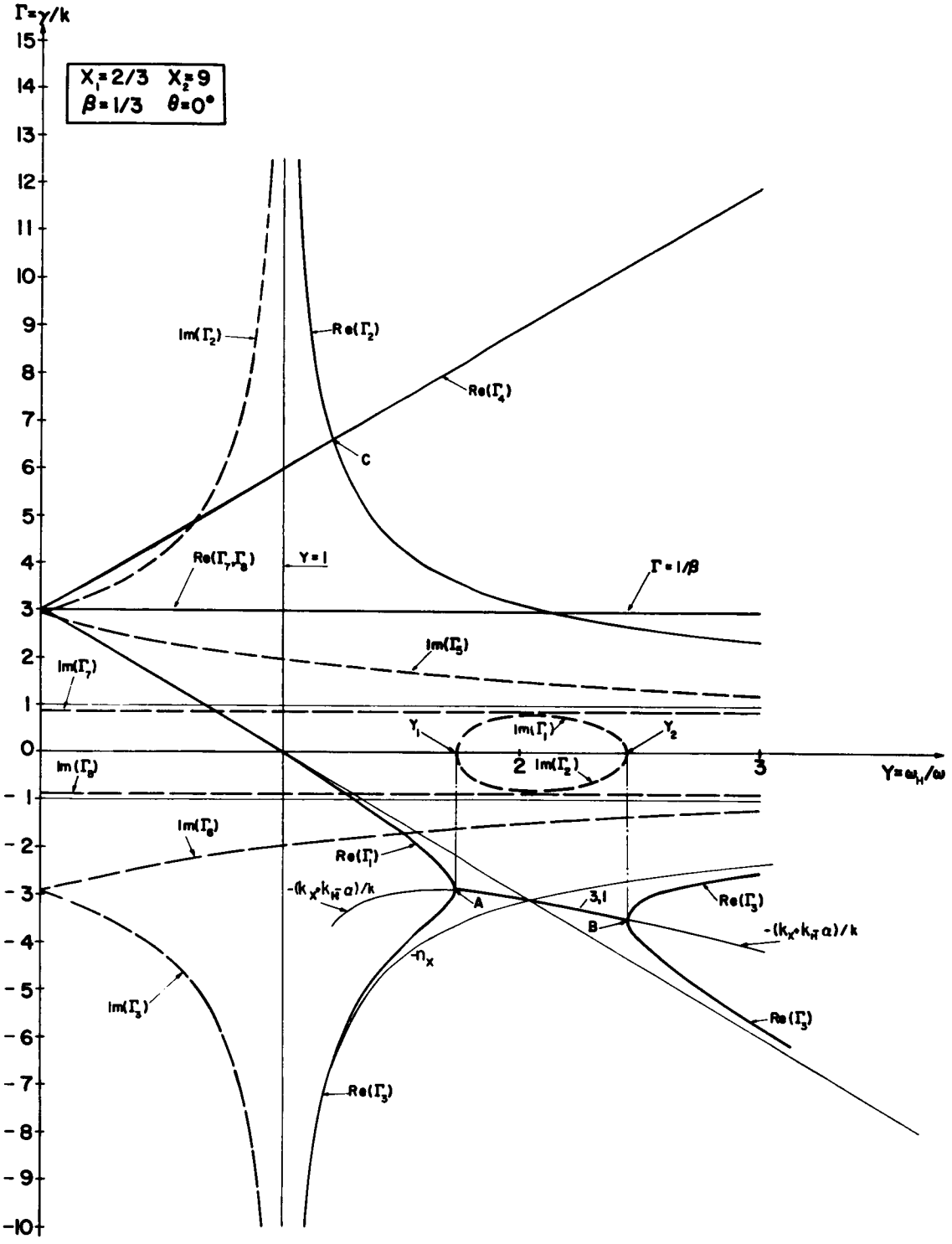

FIG. 2. γ_1, γ_2, and γ_3 as functions of $Y = \omega_H/\omega$ for $X_1 = 2/3$, $X_2 = 9$, $\beta = 1/3$, and $\theta = 0°$.

For completeness we have also included the space-charge waves of the system,

$$\Gamma_{\substack{7\\8}} = \frac{1}{\beta}\left(1 \pm \sqrt{\frac{X_1}{1-X_2}}\right) \tag{31}$$

which do not interact with the other waves when $\theta = 0$.

Let us assume that a fast cyclotron wave Γ_1 travels in the positive z direction, which for the moment is supposed to be the direction of increasing ω_H, or Y. When the Γ_1 wave passes the level Y = 1, it acquires a negative phase velocity and has the property of a backward wave. As it approaches the interaction range A-B, its negative phase velocity gradually decreases until it meets the perturbed backward whistler mode Γ_3. At A and through the interaction region, these two waves travel with the same negative phase velocity.

At and around A, strong interaction takes place between the waves. If the interaction distance $Y_2 - Y_1$ is long enough, the fast cyclotron wave is almost totally reflected at A, but now in terms of a backward whistler mode. This means that the electron stream is practically stripped of its transverse kinetic energy. The remainder of the first cyclotron wave leaves the interaction region at B and follows the Γ_1 branch. For large Y values it will almost be a pure cyclotron wave, as it was in its initial phase (Y < 1).

Using the coupled analysis method of Rydbeck (4) and assuming that ω_H varies linearly with z throughout the interaction region, we find that the reflection coefficient, defined as the ratio between incident cyclotron-wave power flow and reflected whistler-wave power, becomes

$$R_{13}^2 \approx \frac{P_3^{(i)}}{P_1} = \frac{1}{1+e^{-2\Delta_o(z_2-z_1)\pi/4}} \qquad (X_1 \ll 1) \tag{32}$$

where z_2 and z_1 are the z values corresponding to Y_2 and Y_1. The reduction in cyclotron-wave power flow through the coupling barrier is

$$\frac{P_3^{(o)}}{P_3^{(i)}} = 1 - R_{13}^2 \tag{32a}$$

If $\Delta_o(z_2 - z_1)$ is of the order of unity or more, the reflection or mode transformation is almost total. It is important to note that the traveling-wave interaction produces only a mode transformation in this case; no amplification takes place.

Let us next investigate what happens if a whistler mode travels in negative z direction and approaches B from the region $Y > Y_2$. At B it is partially or totally reflected in the form of a fast cyclotron wave (which follows branch Γ_1 to high Y values) or partially transmitted through the coupling barrier, emerging at A with much reduced amplitude as a perturbed whistler mode following branch Γ_3.

Actually, the wave reflection mechanism at levels A and B is almost the same as normal wave reflection in stationary media. One easily sees that this is so if the drift factor $-\frac{1}{k}(k_x + k_H - \alpha)$, drawn as a thin line in Fig. 2, is subtracted from the Γ_1 and Γ_3 curves.

It should be emphasized that the results presented in Fig. 2 are based on the concept of a monovelocity stream. If the velocity distribution of the stream is taken into account, for example by using the methods of Rydbeck and Wilhelmsson (5) and assuming a rectangular velocity distribution of velocity width Δv_o, we find, as expected, that the main features of the interaction effects are preserved as long as $(\Delta v_o/v_o)^2 \ll (4\Delta_o/\alpha)^2$, which by Eq. 27 means that $(\Delta v_o/v_o)^2 \ll (\Delta\omega_H/\omega_{H_o})^2$. Thus, for the traveling-wave interaction to take place efficiently, the relative velocity spread should be appreciably smaller than the relative magnetic bandwidth. Since this bandwidth increases with the square root of the stream current density, we infer that dense streams are less susceptible to velocity spread effects.

Returning to Fig. 2 for a moment, we notice that there is no coupling between the Γ_2 and Γ_4 waves at C, where they should experience traveling-wave resonance. The reason is that these waves have <u>opposite</u> senses of circular polarization and no component of a-c electric field in the direction of the wave normal. This example typically illustrates the fact that traveling-wave resonance alone is not a sufficient condition for interaction in the linear theory. That is also clearly borne out by our theory, since Γ_4 is a root of Eq. 29, Γ_2 a root of Eq. 17, and these equations are uncoupled.

When $\theta \neq 0$, however, both Γ_2 and Γ_4 have an E_z component in the direction of the wave normal. In this case, both waves will interact at and near the C level, as will be shown in the following section.

3. WAVE NORMAL AT ANGLE TO STREAM AND STATIC MAGNETIC FIELD

The wave normal is now assumed to make an arbitrary angle θ with the direction of the static magnetic field, which is parallel to the drift direction of the electron-ion stream (see Fig. 3).

As is well known from the magnetoionic theory, the magnetoionic modes now have a longitudinal component of the a-c electric field, which means that waves with opposite senses of polarization can interact at traveling-wave resonance and that longitudinal interaction with the space-charge waves may also take place. We have in this system four magnetoionic modes (one forward and one backward mode of each kind), two cyclotron waves, and two space-charge waves, and will therefore obtain an eighth order wave equation.

Since ionic oscillations will not be discussed in this section, we drop the e-charge indices and introduce the notation

$$q_1 = \frac{\Delta N^{(1)}}{N^{(1)}}\, q^{(1)} \tag{33}$$

for the differential charge density of the electron stream. Maxwell's equations can then be written as follows (assuming the wave normal to lie in the x-z plane).

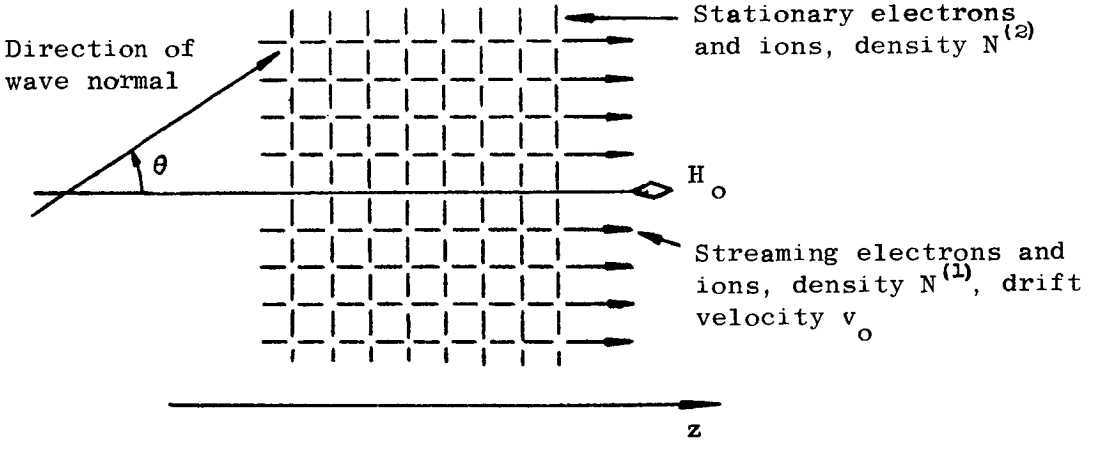

FIG. 3. Electron-ion stream in the stationary magnetoionic medium, wave normal at angle θ.

$$\frac{\partial H_y}{\partial x} = \varepsilon_o \frac{\partial E_z}{\partial t} + q_1 v_o + q^{(1)} v_z^{(1)} + q^{(2)} v_z^{(2)}$$

$$-\frac{\partial H_z}{\partial x} + \frac{\partial H_x}{\partial z} = \varepsilon_o \frac{\partial E_y}{\partial t} + q^{(1)} v_y^{(1)} + q^{(2)} v_y^{(2)}$$

$$-\frac{\partial H_y}{\partial z} = \varepsilon_o \frac{\partial E_x}{\partial t} + q^{(1)} v_x^{(1)} + q^{(2)} v_x^{(2)}$$

$$\frac{\partial E_y}{\partial x} = -\mu_o \frac{\partial H_z}{\partial t} \tag{34}$$

$$-\frac{\partial E_z}{\partial x} + \frac{\partial E_x}{\partial z} = -\mu_o \frac{\partial H_y}{\partial t}$$

$$-\frac{\partial E_y}{\partial z} = -\mu_o \frac{\partial H_x}{\partial t}$$

To the transverse equations of motion (Eq. 7), properly corrected for oblique incidence, we now add the longitudinal equations of motion:

$$p_t v_z^{(1)} = -\frac{e}{m} E_z$$

$$\frac{\partial}{\partial t} v_z^{(2)} = -\frac{e}{m} E_z \tag{35}$$

We next introduce the longitudinal a-c convection current density $i_z^{(1)}$ $[= q_1 v_o + q^{(1)} v_z^{(1)}]$ of the electron stream. The equation of continuity then yields

$$p_t i_z^{(1)} = q^{(1)} \left(\frac{\partial v_z^{(1)}}{\partial t} - v_o \frac{\partial v_x^{(1)}}{\partial x} \right) \tag{36}$$

by which q_1 can be eliminated from Eq. 34.

If we introduce the wave operators

$$p_e^2 = \frac{\partial^2}{\partial x^2} + \frac{\partial^2}{\partial z^2} - \mu_o \varepsilon_o \frac{\partial^2}{\partial t^2} \tag{37}$$

which annihilates an electromagnetic wave in vacuum, and

$$p_{xz}^2 = \frac{\partial^2}{\partial x \partial z} \tag{38}$$

the transverse coupling operator, and drop the e subscripts of the cyclotron wave and cyclotron oscillation operators (Eqs. 5 and 6), Maxwell's equations can be transformed into the instructive coupled wave equations

$$\Psi_1 E_y = \Psi_3 E_x - \frac{\omega_p^{(1)^2}}{c_o^2} \omega_H p_c^2 v_o \frac{\partial E_z}{\partial x} \tag{39}$$

$$\left(\Psi_1 - p_g^2 p_c^2 \frac{\partial^2}{\partial x^2}\right) E_x = - \Psi_3 E_y + p_g^2 p_c^2 p_{xz} E_z - \frac{\omega_p^{(1)^2}}{c_o^2} p_t p_c^2 v_o \frac{\partial E_z}{\partial x} \tag{40}$$

where

$$\Psi_1 = p_g^2 p_c^2 p_e^2 - \mu_o \varepsilon_o \left(\omega_p^{(1)^2} p_c^2 p_t^2 + \omega_p^{(2)^2} p_g^2 \frac{\partial^2}{\partial t^2}\right) \tag{41}$$

and

$$\Psi_3 = \mu_o \varepsilon_o \omega_H \left(\omega_p^{(1)^2} p_c^2 p_t + \omega_p^{(2)^2} p_g^2 \frac{\partial}{\partial t}\right) \tag{42}$$

We immediately notice that for $\partial/\partial x = 0$,

$$\Psi_1 E_{y_x} = \pm \Psi_3 E_{x_y} \tag{43}$$

When the coupling is weak, the cyclotron waves and the magnetoionic waves are thus almost circularly polarized. It is readily apparent that Eq. 43 is equal to Eq. 8 and therefore contains the longitudinal magnetoionic modes and the cyclotron waves, a fact that is very important to note when analyzing the complete set (Eqs. 39 and 40).

Let us next introduce the operators

$$p_{p_2}^2 = \frac{\partial^2}{\partial t^2} + \omega_p^{(2)^2} \tag{44}$$

which annihilates a plasma oscillation in the stationary homogeneous medium, and

$$p_{p_L}^4 = p_t^2 p_{p_2}^2 + \omega_p^{(1)^2} \frac{\partial^2}{\partial t^2} \tag{45}$$

which annihilates the unperturbed space-charge waves and the plasma oscillations of the system if $v_o = 0$.

E_z can now be eliminated from Eq. 40 after some transformations. We find that

$$p_{p_L}^4 (\Psi_1^2+\Psi_3^2) E_x = \left[\chi\Psi_1 + p_t^2\left(\frac{\Psi_3^2}{\mu_o \varepsilon_o} + \Lambda\right)\right] \frac{\partial^2 E_x}{\partial x^2} \tag{46}$$

where

$$p_d = v_o \frac{\partial}{\partial z} \tag{47}$$

is a drift operator, and

$$\chi = \omega_p^{(1)^2} p_c^2 \left(p_g^2 \frac{\partial^2}{\partial t^2} - p_t^4\right) + \omega_p^{(2)^2} \omega_H^2 p_t^2 p_g^2 \tag{48}$$

$$\Lambda = \omega_p^{(1)^2} \left(2p_c^2 (p_t\Psi_1 - \omega_H \Psi_3) p_d + \beta^2 \left\{ p_c^2 \left[\Psi_1 \left(\frac{1}{\mu_o \varepsilon_o} \frac{\partial^2}{\partial x^2} + \omega_p^{(1)^2} \frac{\omega_H^2 - p_t^2}{p_g^2} \right) + 2\Psi_3 \omega_p^{(1)^2} \frac{\omega_H p_t}{p_g^2} \right] - \frac{\Psi_1^2+\Psi_3^2}{\mu_o \varepsilon_o p_g^2} - \omega_p^{(1)^2} \omega_H^2 p_c^4 \frac{\partial^2}{\partial x^2} \right\} \right) \tag{48a}$$

If we introduce the combined transverse and drift coupling term

$$K = \chi\Psi_1 + p_t\left(\frac{1}{\mu_o \varepsilon_o} \Psi_3^2 + \Lambda\right) \tag{49}$$

then Eq. 46 assumes the form

$$p_{p_L}^4 (\Psi_1+j\Psi_3)(\Psi_1-j\Psi_3)\underset{(z)}{E_x} = K\frac{\partial^2}{\partial x^2}\underset{(z)}{E_x} \tag{50}$$

Since $\partial^2/\partial x^2 = -\gamma^2 \sin^2\theta$ for the homogeneous medium, we see from Eq. 49 that the coupling vanishes when $\theta = 0$.

Let us put $\omega_p^{(2)^2} = 0$. We then obtain

$$(K)_{\omega_p^{(2)}=0} = \omega_p^{(1)^2} p_g^2 p_c^4 \frac{\partial^2}{\partial t^2}\left[\omega_H^2 p_e^2 - \beta^2 p_t^2\left(p_e^2 - \frac{\omega_p^{(1)^2}}{c^2}\right)\right]$$

$$= \omega_p^{(1)^2} p_g^2 p_c^4 \frac{\partial^2}{\partial t^2}\left[\omega_H(\omega_H\Psi_1+p_t\Psi_3)+\beta^2 p_t(p_t\Psi_1-\omega_H\Psi_3)\right] \tag{51}$$

If this relation is used in Eq. 50, remembering that $\omega_p^{(2)^2}$ should be zero in its left-hand part, we obtain the coupled wave equation for the drifting magnetoionic medium. When $v_o = 0$, this reduces to the Appleton-Hartree relation [if we put $(\partial/\partial t)^2 = -\omega^2$, $\partial^2/\partial z^2 = -\gamma^2\cos^2\theta$, and $\partial^2/\partial x^2 = -\gamma^2\sin^2\theta$].

Since

$$\Psi_1^2 + \Psi_3^2 = p_g^4 p_c^4\left[p_e^2 - \mu_o\varepsilon_o\left(\omega_p^{(1)^2}\frac{p_t}{p_g} + \omega_p^{(2)^2}\frac{\partial/\partial t}{p_c}\right)\right]$$

$$\cdot\left[p_e^2 - \mu_o\varepsilon_o\left(\omega_p^{(1)^2}\frac{p_t}{p_g^*} + \omega_p^{(2)^2}\frac{\partial/\partial t}{p_c^*}\right)\right] \tag{52}$$

we notice that uncoupled cyclotron oscillations

$$p_c^2 E_x = 0 \tag{53}$$

are possible only when the medium does not drift ($p_g^2 = p_c^2$).

The form of Eq. 50 is very interesting, since it shows that the fast cyclotron wave and whistler mode interaction discussed in Section 2 will

be very strong even for moderate angles θ, and actually varies only slightly with the angle. This will be demonstrated by graphical presentations in Section 4. Note also that the drift coupling term in Eq. 50 is proportional to $\cos\theta \sin^2\theta$ when the β^2 terms are neglected, and consequently disappears for longitudinal as well as transverse propagation in this case.

Whenever any of the roots of $(\psi_1^2 + \psi_3^2)E_y = 0$ and $p_{p_L}^4 E_y = 0$ come close to each other, one should expect traveling-wave interactions of some kind to take place, to first order, for moderate θ values. This will be discussed in the following sections on the basis of graphical presentations of the roots of Eq. 50, which is an eighth order wave equation, for various θ values.

If we replace $\partial^2/\partial z^2$ by $-\gamma^2 \cos^2\theta$ and $\partial^2/\partial x^2$ by $-\gamma^2 \sin^2\theta$, we find from Eq. 50 that

$$\gamma = 0 \quad \text{if} \quad (1-X_1-X_2)[Y^2-(1-X_1-X_2)^2](1-Y^2)/(1-Y^2-X_2)=0 \qquad (54)$$

and

$$1/\gamma^2 = 0 \quad \text{if} \quad X_2/(1-Y^2) - 1/(1-Y^2\cos^2\theta) = 0 \qquad (54a)$$

(The corresponding Y value is denoted Y_R in what follows.) We thus note that the familiar magnetoionic zeros, $X_1 + X_2 = X_{12} = 1$, and $X_1 + X_2 = X_{12} = 1 \pm Y$, are drift-invariant. When the medium drifts, however, only a closer examination reveals what type or types of waves will experience γ zero. In that case, $\gamma = 0$ does not necessarily correspond to total or almost total reflection of the wave in question, as will be shown in the following sections (see also Fig. 2). Furthermore, $\gamma = 0$ for $Y^2 = 1$ if $X_2 \neq 0$. When part of the medium is stationary ($X_2 \neq 0$), we therefore have a fast cyclotron wave with $\gamma = 0$, that is, with infinite phase velocity, at the cyclotron resonance frequency. This zero disappears when the entire medium drifts, which means, as will be shown later, that the fast cyclotron wave transforms into a different kind of wave for $Y < 1$.

It is also very interesting to note from Eq. 54a, which is the fourth reflection level, that the zero disappears if the entire medium drifts (i.e., if $X_2 = 0$). Furthermore, the space-charge wave γ values approach infinity at this level only, which for $\theta = 0$ reduces to the familiar $X_2 = 1$.

Since not all waves interact, but when some waves do interact this takes place for different Y values, the operator presentation (Eq. 50)

of the wave equation is very useful for an approximate study of the various interaction regions. This applies where Eq. 50 can approximately be reduced to an equation of comfortably low order, about as was done in the Γ_1-Γ_3 interaction range in Section 2. This is almost impossible if one writes down the complete dispersion relation in γ (to be shown in Section 6). Furthermore, an operator analysis of the interaction mechanism yields a much deeper insight into the physical nature of the problem.

4. VARIOUS Γ VALUES AS FUNCTIONS OF θ AND Y

On the basis of Eq. 50, where $\partial^2/\partial z^2$ has been replaced throughout by $-\gamma^2 \cos^2 \theta$ and $\partial^2/\partial x^2$ by $-\gamma^2 \sin^2 \theta$, we have plotted Γ_q as a function Y for various θ values. The following notation has been used. Curves representing Γ_q are marked q. Curve 1 indicates the perturbed fast cyclotron wave, curves 2 and 3 the perturbed forward and backward extraordinary magnetoionic modes (where the terms forward and backward refer to the propagating range), curve 4 the perturbed slow cyclotron wave, curves 5 and 6 the perturbed forward and backward ordinary magnetoionic modes, and curves 7 and 8 the perturbed slow and fast space-charge waves. The unperturbed modes, which the perturbed modes will approach asymptotically in various regions of the Γ-Y plane, have been marked 10, 20, and so on. The $-n_x$ branch is marked 30; the $+n_o$ branch, 50; $(1/\beta_L)(1 \pm Y)$, 10 and 40; $(1/\beta_L)(1 \pm \sqrt{X_1/(1 - X_2)})$, 70 and 80. In these expressions,

$$\beta_L = \beta \cos\theta \tag{55}$$

and as before, $\beta = 1/3$, $X_1 = 2/3$, and $X_2 = 9$. Real components are marked by solid lines, imaginary components by dashed lines.

Figure 4 shows that the main interaction between waves Γ_3 and Γ_1 remains practically unaltered, as expected. The space-charge waves do not interact (they are practically unperturbed), and the same is true of the ordinary magnetoionic waves, which never propagate in this region. Notice, however, that the slow cyclotron wave and the forward extraordinary wave (the forward whistler mode) interact in a narrow Y range, from Y_3 to Y_4 (coupling levels C and D). This is due to the fact that these waves now have E-field components in the direction of the wave normal, as is clearly brought out by Fig. 5, which demonstrates the situation for $\theta = 30°$. In Fig. 5 all waves are more perturbed, but the change in the nonpropagating ordinary waves is very small.

The interaction in range C-D is interesting from a theoretical point of view, since it may lead to whistler mode traveling-wave amplification. Assume that a forward whistler mode (curve 2) approaches the coupling level C and there interacts with the electron stream, which for the mo-

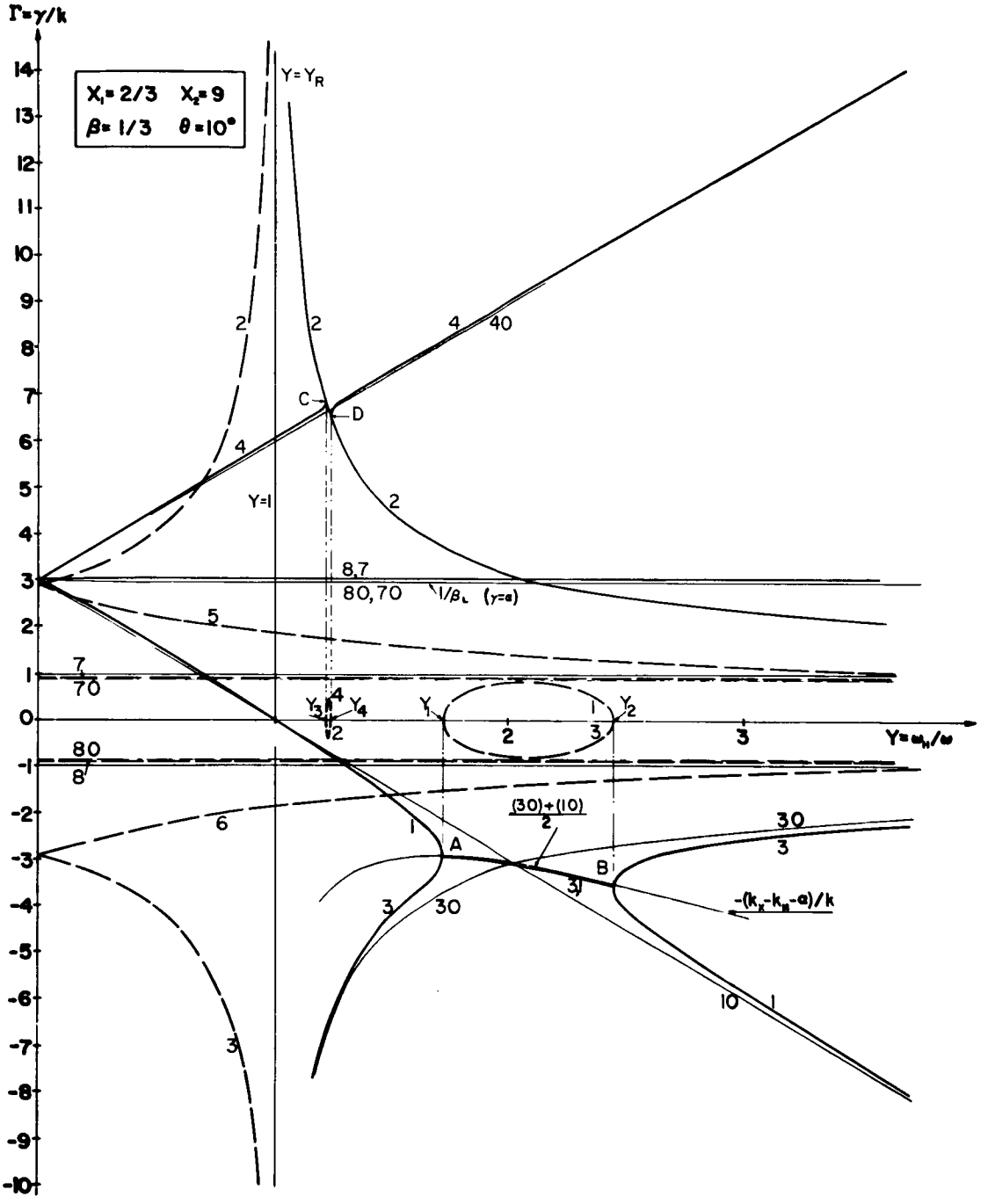

FIG. 4. Γ_q as a function of Y for $\theta = 10°$.

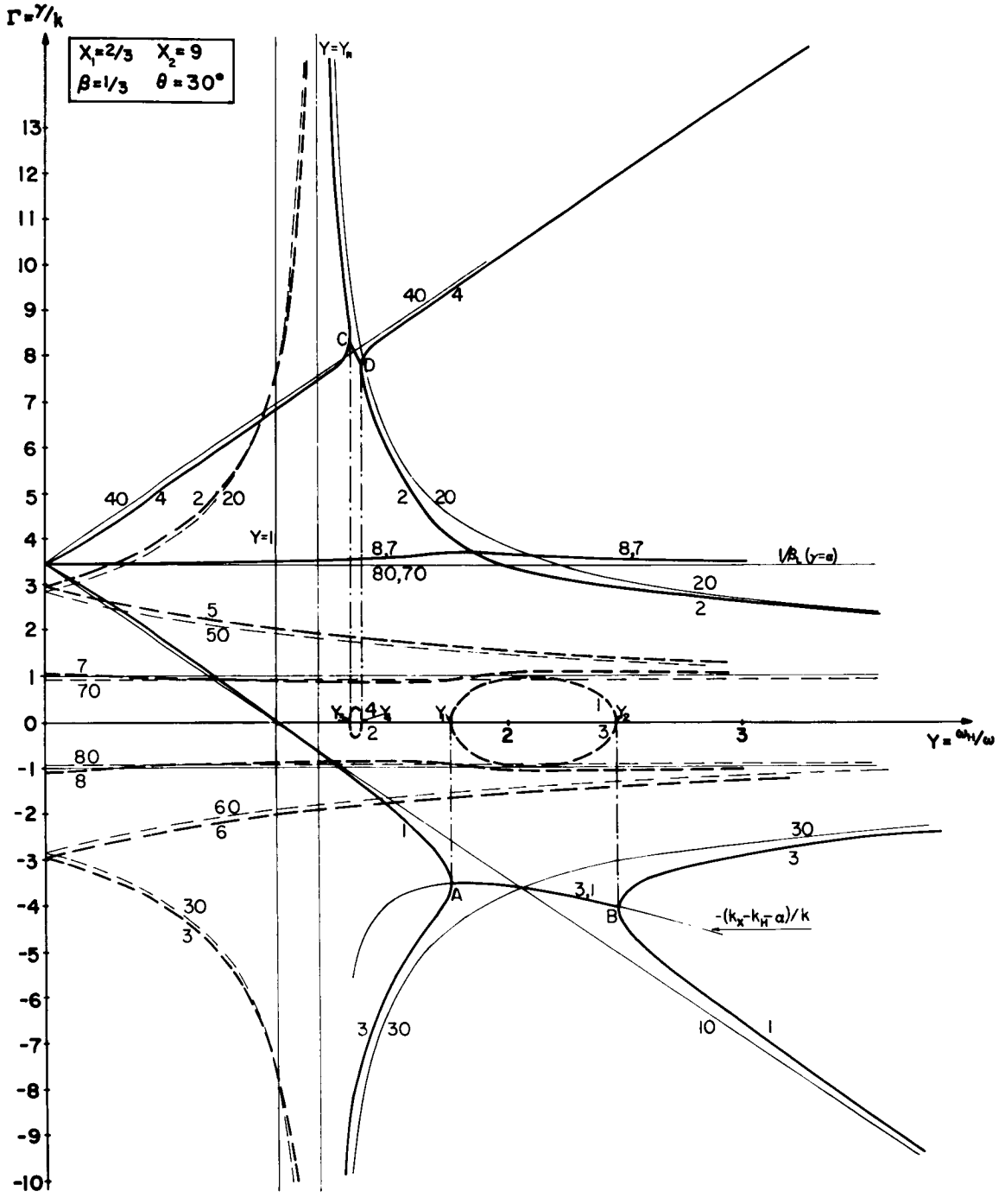

FIG. 5. Γ_q as a function of Y for $\theta = 30°$.

ment is considered to have no slow cyclotron-wave modulation. In the course of the interaction, the whistler mode becomes amplified and leaves level D along branch 2, with increased amplitude. The electron stream leaves the coupling region at D, carrying a slow cyclotron wave, which propagates along branch 4 in the positive z direction. This wave has a negative a-c kinetic power flow, and the energy provided to amplify the whistler mode is supplied, as it should be, by the electron stream.

If the input whistler power is $P_2^{(i)}$, the output whistler power $P_2^{(o)}$ becomes approximately

$$P_2^{(o)} \cong P_2^{(i)} e^{k[\mathrm{Im}(\Gamma_4)]_{max}\pi(z_4-z_1)/2} \tag{56}$$

where $z_4 - z_1$ is the length of the interaction range. [The detailed relation between $\mathrm{Im}(\Gamma_4)$ and the medium parameters will be discussed on the basis of the coupled wave equations in a later publication.]

Next let us look at Fig. 6, which depicts the Γ situation for $\theta = 40°$. We notice that the Γ_3-Γ_1 interaction remains about the same, as predicted from the coupled wave equations. The Γ_4-Γ_2 interaction has increased in strength and magnetic bandwidth, although the latter is still much smaller than the Γ_3-Γ_1 interaction band. The space-charge waves are now beginning to show some interesting features. They become strongly perturbed when $\mathrm{Re}(\Gamma_8)$ [$= \mathrm{Re}(\Gamma_7)$] $\cong \Gamma_2$, that is, when the phase velocity of the space-charge waves roughly equals the phase velocity of the forward extraordinary magnetoionic mode. Furthermore, it is of interest to note that the ordinary magnetoionic modes remain practically unperturbed by the electron stream.

The space-charge wave interaction situation changes drastically when we go to a θ value of 50°, as depicted in Fig. 7. Between the levels E and F (range Y_5 to Y_6) the space-charge waves are no longer evanescent and growing, a property they resume when $Y > Y_6$. The major part of the space-charge wave kinetic energy flow, assumed to be positive, will be converted to a very perturbed forward extraordinary magnetoionic mode at level E, and will travel in the positive z direction along branch 2. An amplified forward whistler mode (we still use this concept in spite of the fact that $\theta = 50°$), which may leave the Γ_4-Γ_1 range at D, may transform to space-charge waves at F, a matter that will be dealt with in more detail in a later publication.

At $\theta = 60°$ the space-charge wave interaction shows essentially the same features as at 50°, though more pronounced. Discussion of this is outside the scope of the present communication.

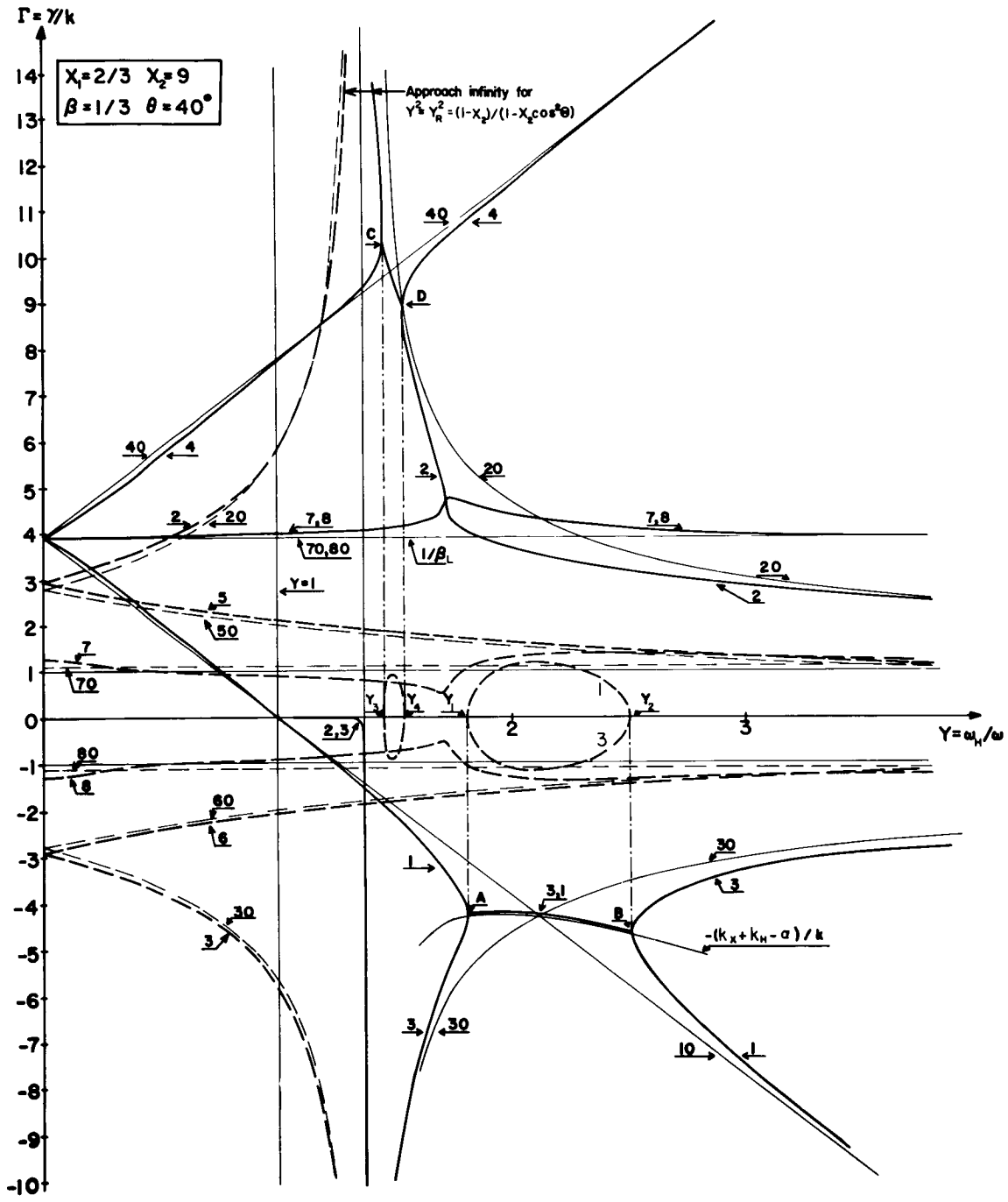

FIG. 6. Γ_q as a function of Y for $\theta = 40°$.

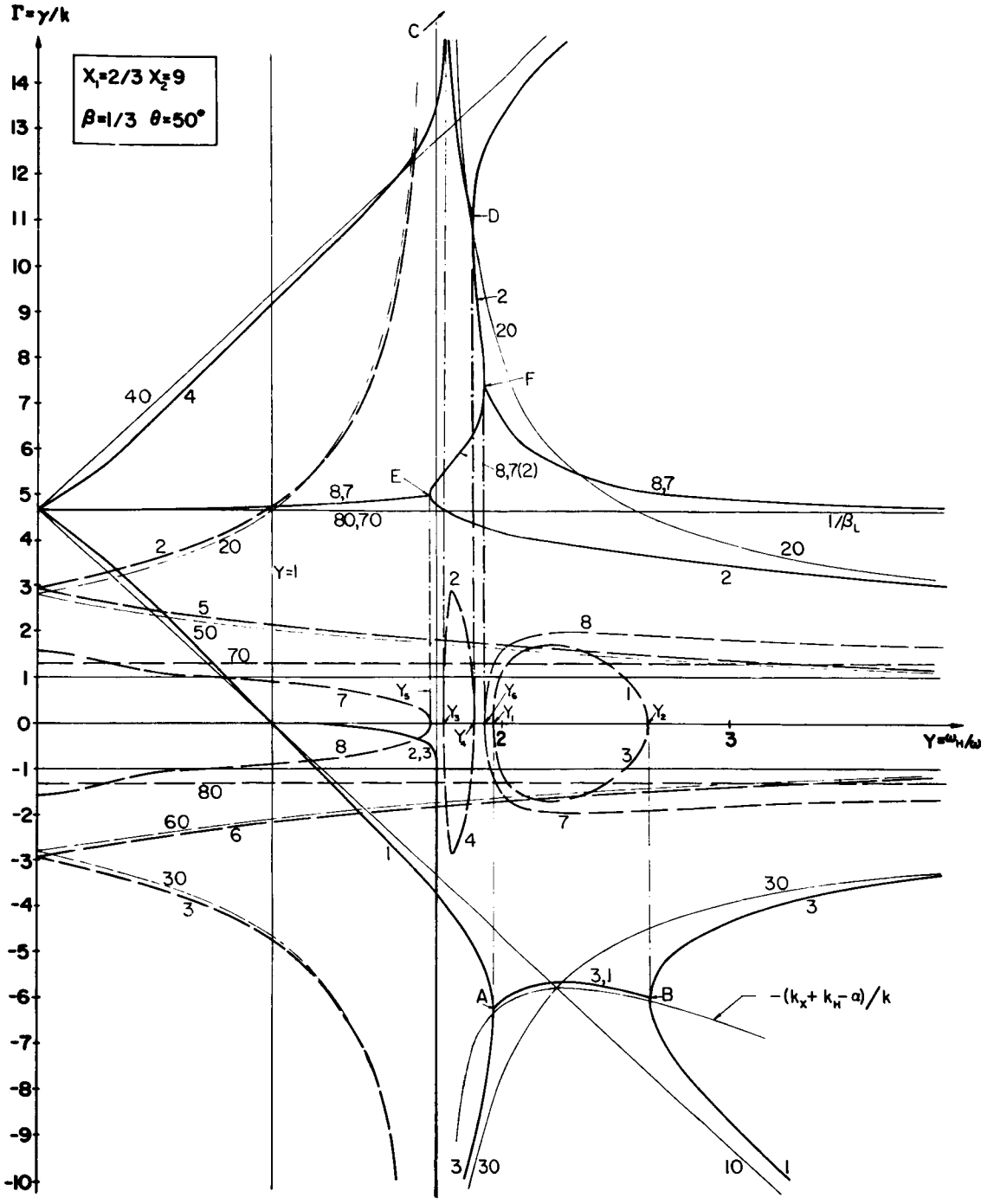

FIG. 7. Γ_q as a function of Y for $\theta = 50°$.

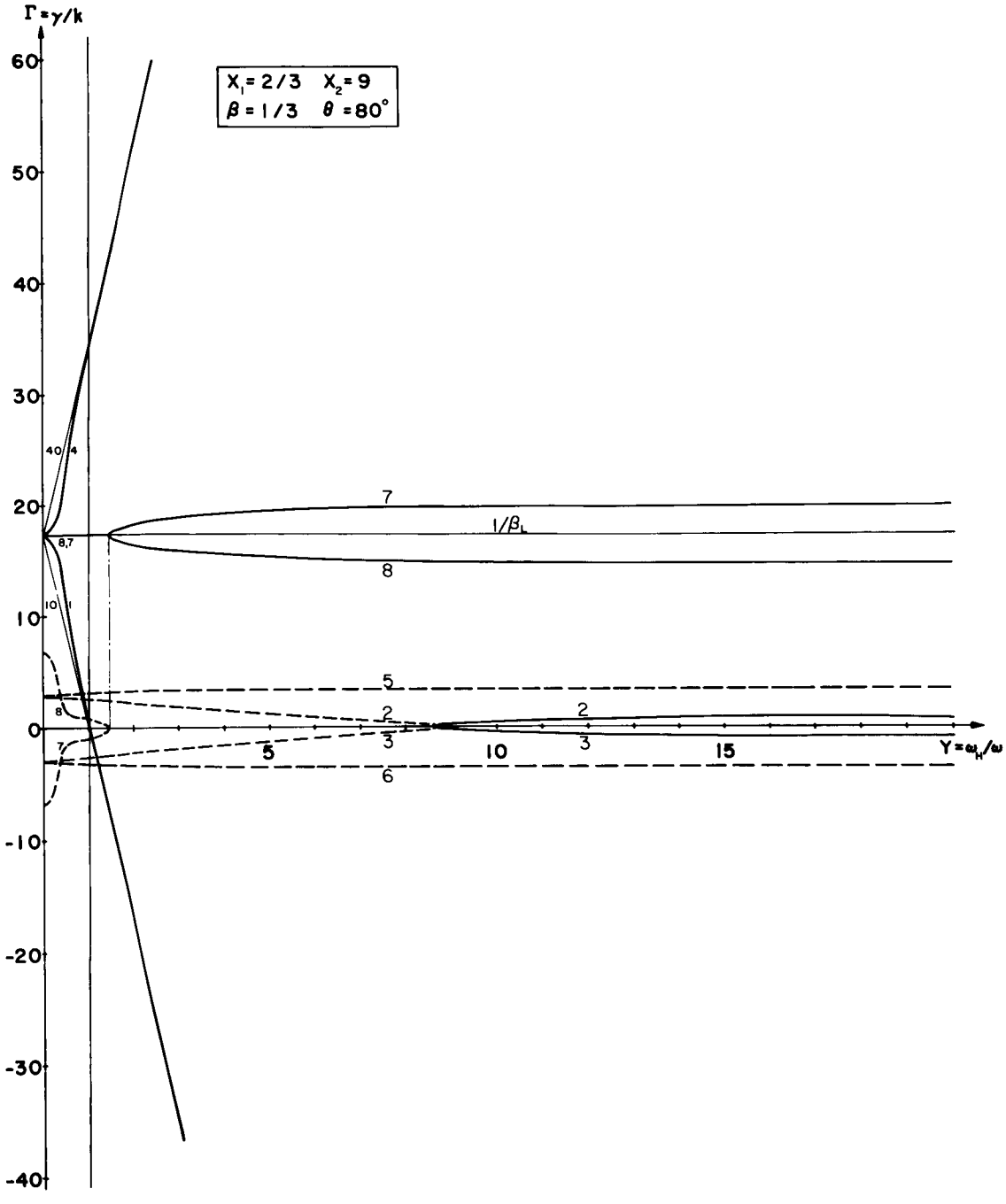

FIG. 8. Γ_q as a function of Y for $\theta = 80°$.

When $\cos^2 \theta < 1/X_2 = 1/9 = \cos^2 \theta_R$ ($\theta_R \cong \pm 70.5°$ in the present case), the fourth reflection level disappears and no wave interactions or couplings take place, as shown by Fig. 8. Thus no interesting things happen when $\theta^2 > \theta_R^2$, which illustrates the importance of the fourth reflection level in this and so many other magnetoionic interaction problems (3).

To demonstrate the angular dependence of cyclotron wave and whistler mode interactions, we have plotted in Fig. 9 the magnetic bandwidths as functions of θ. It is extremely interesting to note that the $\Gamma_3 - \Gamma_1$ interactions (fast cyclotron waves being reflected as whistler modes) remain very uniform and broad through a wide angular range. The $\Gamma_4 - \Gamma_2$ interactions, which lead to amplification of the forward whistler mode, have a narrow bandwidth and are easily "smeared" out by velocity distribution effects in the stream. Interaction $\Gamma_3 - \Gamma_1$ is a very probable phenomenon in the exosphere. Direct whistler amplification should occur only when the stream has a very narrow velocity spectrum, and under such circumstances it will take place in an annular cone of, say, $10° < \theta < \theta_R$.

In Fig. 10, $[\mathrm{Im}(\Gamma_{\frac{3}{1}})]_{\max}$ and $[\mathrm{Im}(\Gamma_{\frac{4}{2}})]_{\max}$ are depicted as functions of θ. The imaginary parts tend to great values when θ approaches θ_R, which corresponds to an infinitely strong static magnetic field, a case that may be approached in plasma amplifying devices. It is important to note that in the θ range for normal whistler mode operation (θ less than about 35°, Y less than 2.5) both the gyromagnetic bandwidth and $[\mathrm{Im}(\Gamma_{\frac{3}{1}})]_{\max}$ vary only slightly with θ. This must make the transformation from fast cyclotron wave to backward whistler mode very efficient, provided the velocity spread of the stream is small enough.

To demonstrate what happens when $N^{(z)}$ varies with z, as it actually does in the exosphere, Γ_q is plotted in Fig. 11 as a function of Y when $X_2 = 9Y$, which means that the ratio $N^{(z)}/H_o$ is assumed to be constant throughout the medium. If we compare this plot with Fig. 5, we note that there are no significant changes as far as the $\Gamma_3 - \Gamma_1$ interaction is concerned. The magnetoionic waves are reflected at the levels $X_{12} = X_1 + X_2 = 1$ and $1 - Y$, and the fast space-charge wave (curve 8) has $\gamma = 0$ for $X_{12} = 1 + Y$ (see Eq. 54). Furthermore, the space-charge waves transform into evanescent and growing waves when $Y_R = Y_{R_1}$ (the "first" fourth reflection level), which in this case corresponds to $X_2 \cong 1$ (see Eq. 54a). The fourth reflection level thus has a twofold meaning for the partly drifting and partly stationary medium ($X_1 \neq 0$, $X_2 \neq 0$).

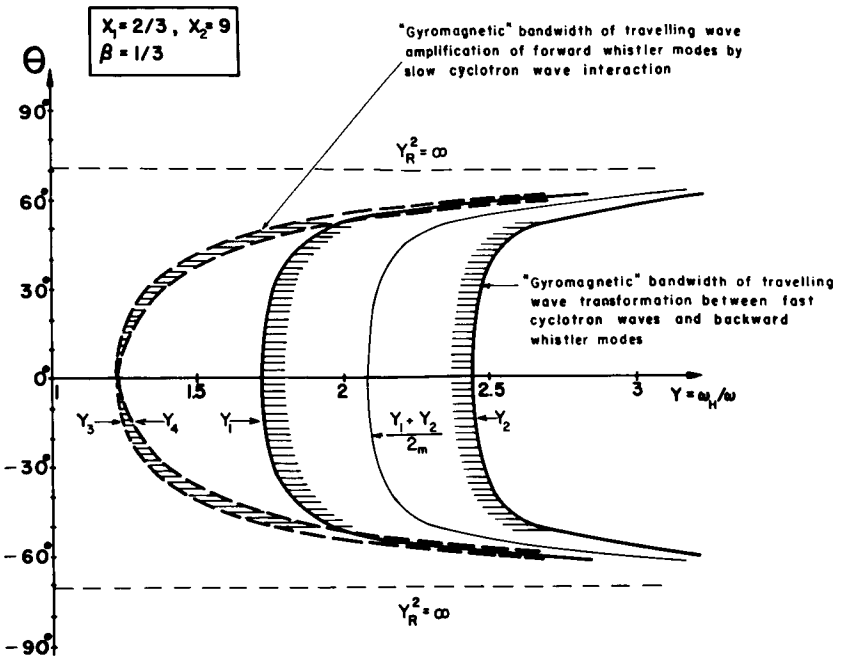

FIG. 9. Gyromagnetic interaction bandwidths as functions of θ.

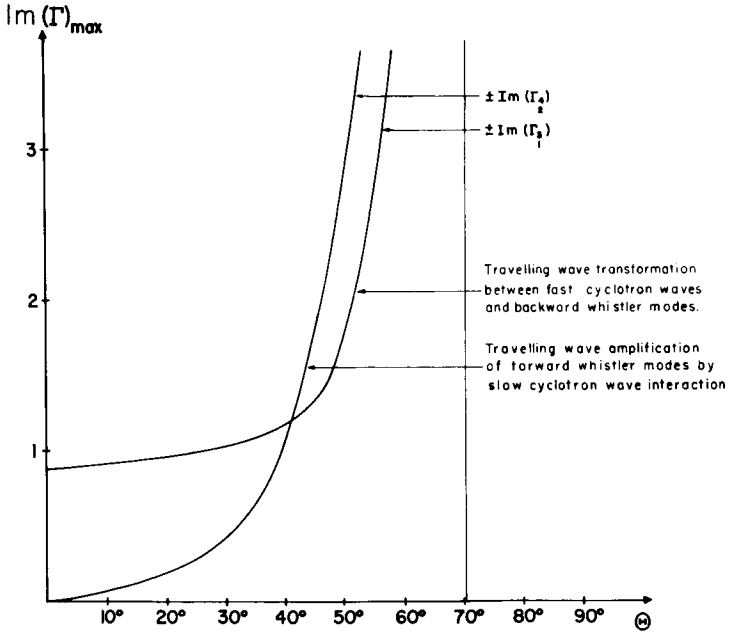

FIG. 10. $[I_m(\Gamma_{\frac{3}{1}})]_{max}$ and $[I_m(\Gamma_{\frac{4}{2}})]_{max}$ as functions of θ.

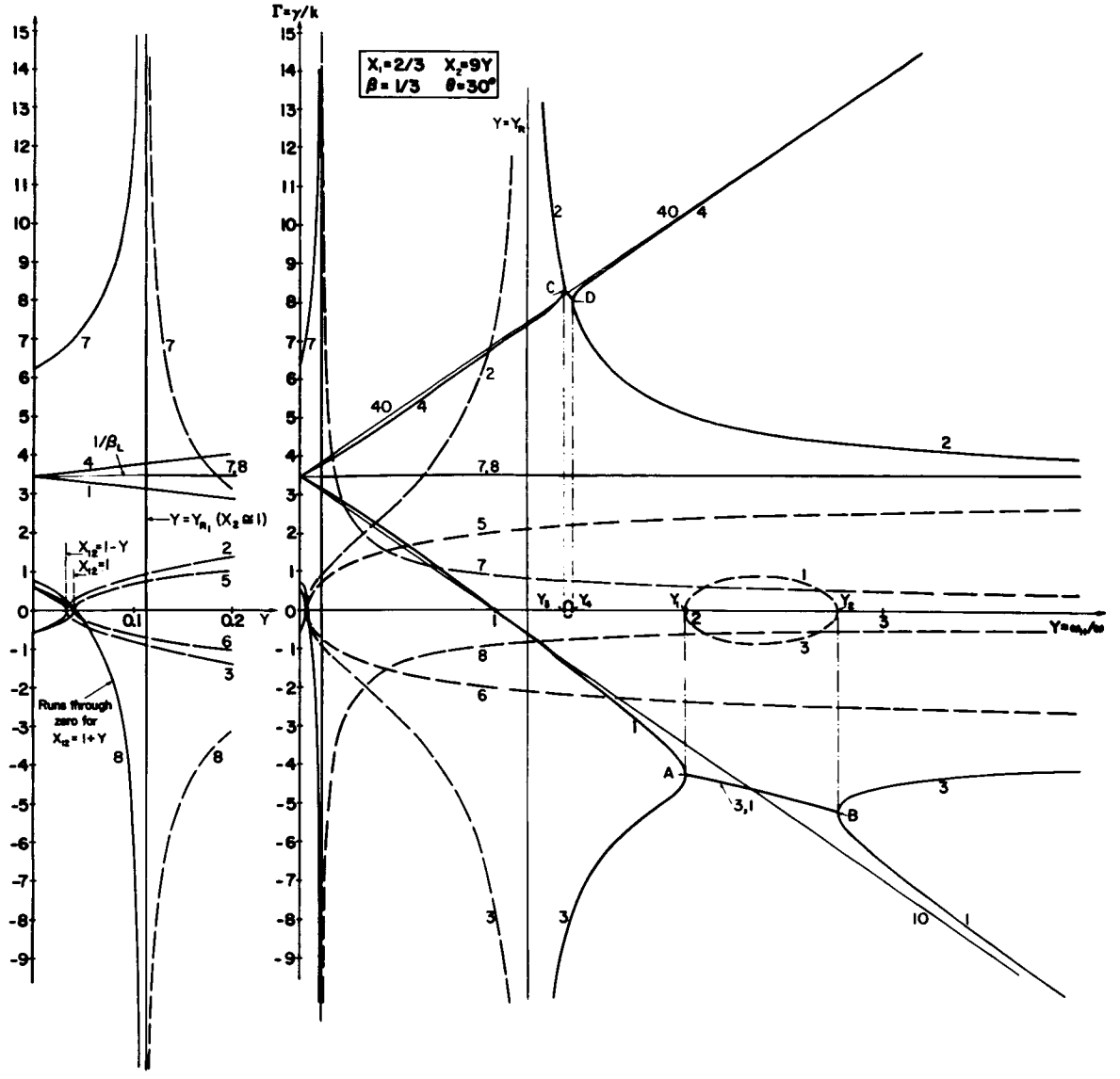

FIG. 11. Γ_q as a function of Y when $X_2/Y = 9$ and $\theta = 30°$.

To demonstrate how the cyclotron wave and whistler mode interactions vary with the wave frequency, Γ_q is plotted in Fig. 12 as a function of $1/Y = \omega/\omega_H$ for $\theta = 40°$, assuming $\omega_p^{(2)^2}/\omega_H^2 = 9$ and $X_1 = 2/3$. Actually $\omega_p^{(1)^2}$ should have been constant, but the general picture would not change much if this change were made. The reflection and amplification interactions now appear in reversed order. The backward Γ_6 mode interacts with the fast space-charge wave in the Y_7-Y_8 region, where the latter has a negative phase velocity. In this coupling region, therefore, the fast space-charge wave is partly or wholly converted into a backward z wave, a transformation that in principle is very similar to the Γ_3-Γ_1 interaction. The fast space-charge wave has $\gamma = 0$ for $X_{12} = 1$ (see Eq. 54). It will interact with the forward Γ_2 mode, of extraordinary type with $\gamma = 0$ for $X_{12} = 1 - Y$, when X_{12} is somewhat smaller than $1 - Y$ (not seen in Fig. 12). Since these interactions take place for $X_2 < 1$, they are of limited interest in the whistler case. Finally, it should be noted that the space-charge waves transform to a regular pair at the "second" fourth reflection level $Y_R = Y_{R_2}$.

It appears from Fig. 12 that, as expected, additional interactions occur when the ordinary magnetoionic modes also propagate. To illuminate the complexities of these interactions, Γ_q is plotted in Fig. 13 as a function of Y when $X_1 = 0.1$, $X_2 = 0.6$ (i.e., $X_{12} < 1$), for $\theta = 40°$. Although this choice of parameters applies mainly to plasma amplifier theory, it is nevertheless of great practical interest in connection with the present interaction studies.

We immediately notice the following interesting and somewhat different properties of the underdense system ($X_{12} < 1$). The slow cyclotron wave is perturbed near the fourth reflection level, but it does <u>not</u> directly interact with any of the other waves. The fast cyclotron wave smoothly transforms to a forward extraordinary magnetoionic wave and never acquires a negative phase velocity. The fast space-charge wave similarly transforms to a forward ordinary magnetoionic wave. The slow space-charge wave (branch 7) and the forward, really nonpropagating, extraordinary magnetoionic wave transform into growing and evanescent space-charge waves at the fourth reflection level. At the N level these waves transform into a normal slow and fast space-charge wave pair. The nature of this complicated transformation has not been analyzed in detail.

The forward extraordinary magnetoionic wave (curve 2) is reflected in a perfectly normal fashion at the level $X_{12} = 1 - Y$. The ordinary wave, on the other hand, reveals some very peculiar interaction properties. It is partly reflected at the M level, that is, at $Y = Y_9$.

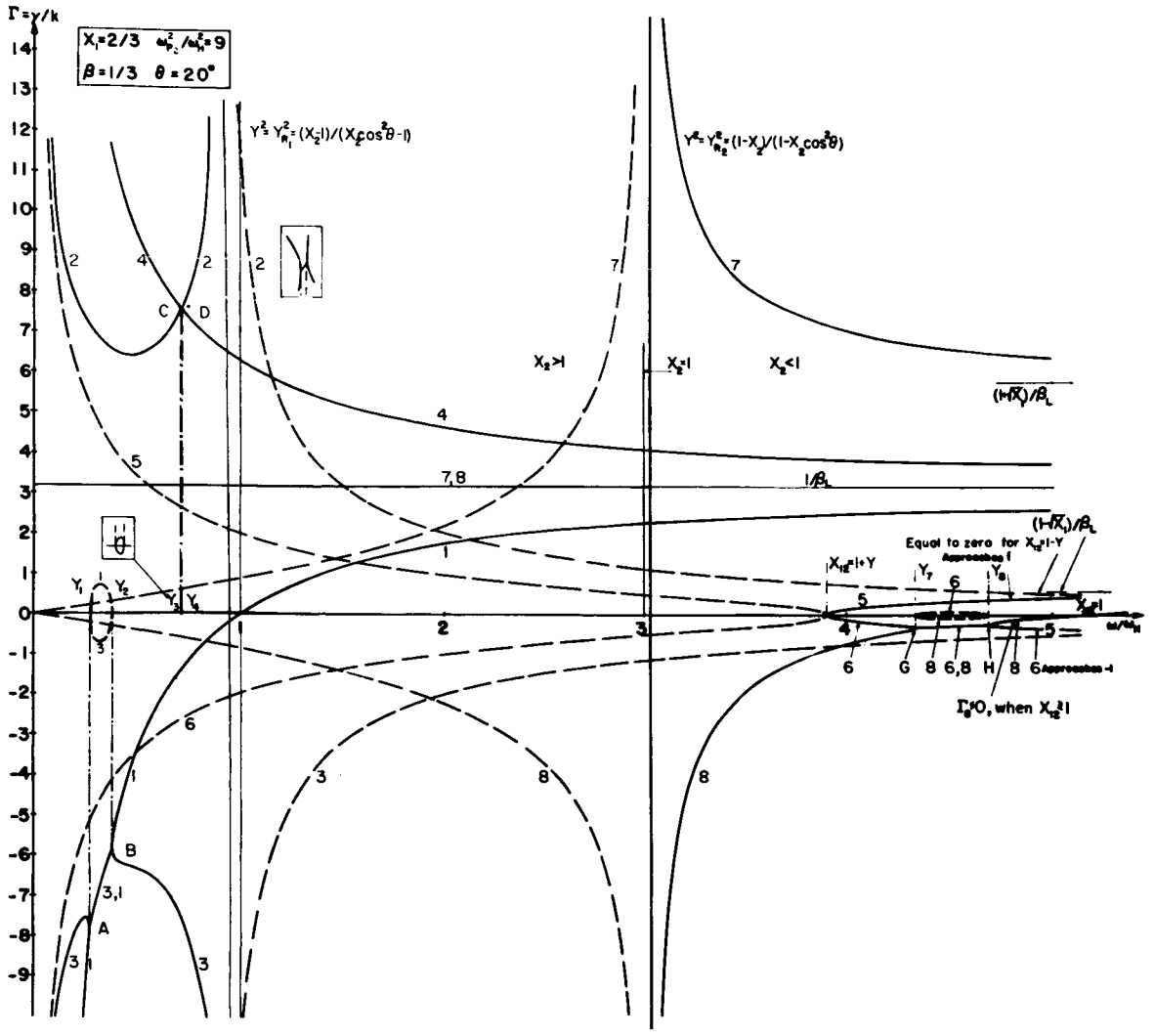

FIG. 12. Γ_q as a function of ω/ω_H for $\theta = 40°$ and $\omega_p^2/\omega_H^2 = 9$.

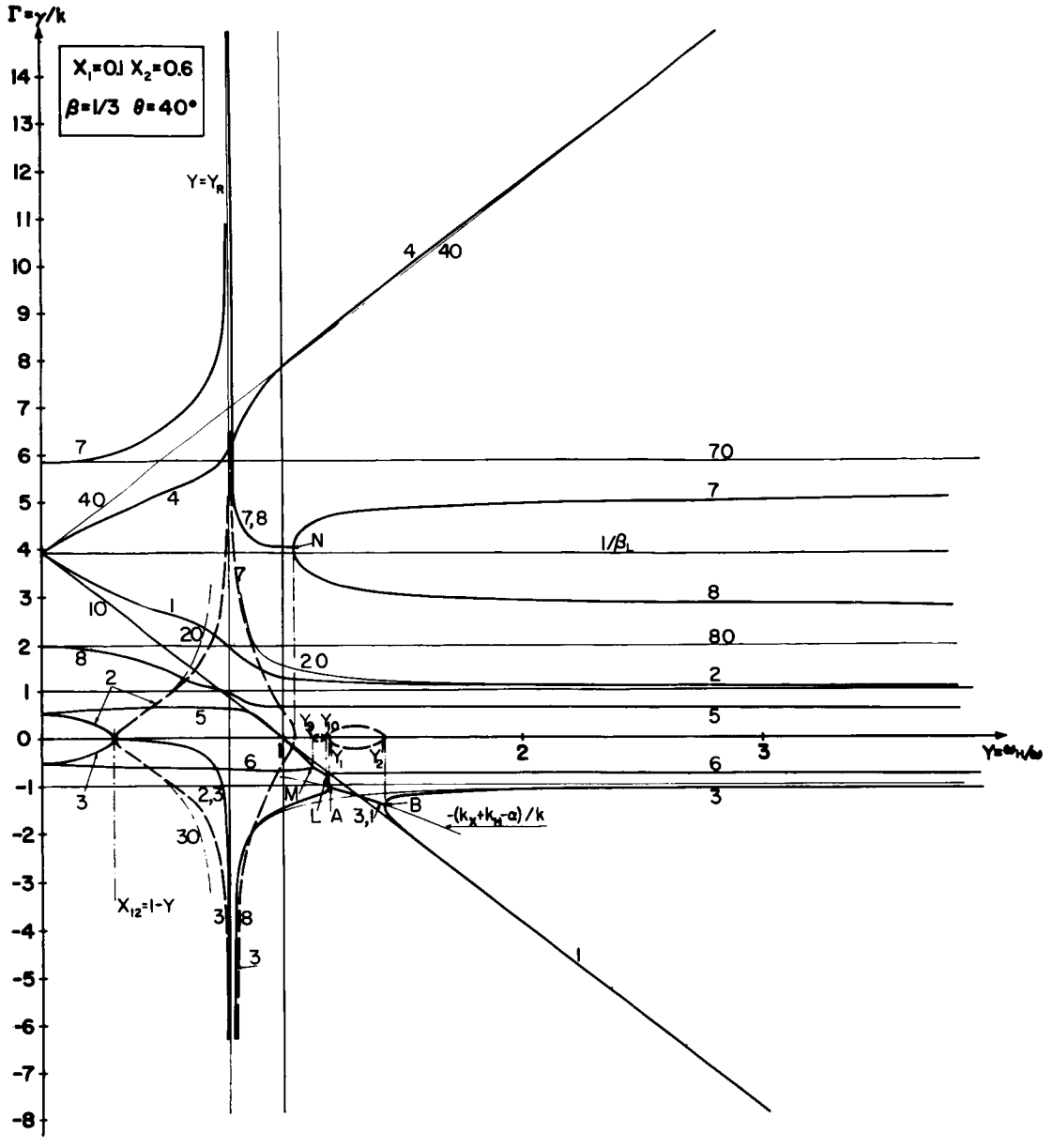

FIG. 13. Γ_q as a function of Y for $X_1 = 0.1$, $X_2 = 0.6$, and $\theta = 40°$.

(In the absence of the streaming medium it would proceed, without any reflections, in the positive z direction.) And it is partly transmitted as a hybrid wave from levels L to A, whence it again splits into a backward extraordinary magnetoionic mode and a fast cyclotron wave, along branch 1. The forward ordinary magnetoionic wave is thus split into no less than three different types of waves, but no wave amplification takes place.

5. WAVE PROPAGATION PROPERTIES OF A MOVING MAGNETOIONIC MEDIUM

The wave propagation properties of a moving magnetoionic medium are also of interest here, especially if one has in mind their application to the solar corona. To study them, we have "simply" to put $\omega_p^{(2)^2}$ in Eq. 50 equal to zero.

Let us first look at the basic case of purely longitudinal transmission, $\theta = 0$. If we let $\partial/\partial t = j\omega$ and allow ω_H to vary with z, we obtain the following wave equations for $\theta = 0$:

$$\underbrace{\left[k_H \mp (\alpha - j\frac{\partial}{\partial z})\right]}_{\substack{\text{Slow or fast}\\ \text{cyclotron wave}\\ \text{operator}}} \left\{ \underbrace{\left[k_H \mp (\alpha - j\frac{\partial}{\partial z})\right]}_{\substack{\text{Fast or slow}\\ \text{cyclotron wave}\\ \text{operator}}} \underbrace{\left[\frac{\partial^2}{\partial z^2} + k^2(1-X_1)\right]}_{\substack{\text{Isotropic wave}\\ \text{operator}}} + k_H k^2 X_1 \right\} E_x$$

$$= j\frac{\partial k_H}{\partial z}\left\{\frac{1}{k_H}\left(\alpha - j\frac{\partial}{\partial z}\right)\left[\frac{\partial^2}{\partial z^2} + k_o^2(1-X_1)\right] \mp \left(\frac{\partial^2}{\partial z^2} + k_o^2\right)\right\} E_x \qquad (57)$$

We see that a static magnetic field gradient now brings about a coupling of waves with different senses of polarization. Similar results would be obtained if Eq. 57 were extended to include also the stationary medium $(\omega_p^{(2)^2} > 0)$.

Neglecting the gradient coupling effects, in Fig. 14 we have plotted Γ_1, Γ_2, Γ_3, Γ_4, Γ_5, and Γ_6, plus the uncoupled space-charge waves Γ_7 and Γ_8, as functions of Y. The plane isotropic electromagnetic wave, assumed to travel in positive z direction (increasing Y), soon splits up into an ordinary and an extraordinary wave. The ordinary wave travels without any perturbations and is not affected by the motion of the medium. The extraordinary wave, however, is reflected not at the $X_1 = 1 - Y$ level as it would in a stationary medium, but at the A level, where reflection is almost total. The remaining wave energy is transmitted through the coupling barrier A-B, whence it emerges as a fast cyclotron wave following branch 1.

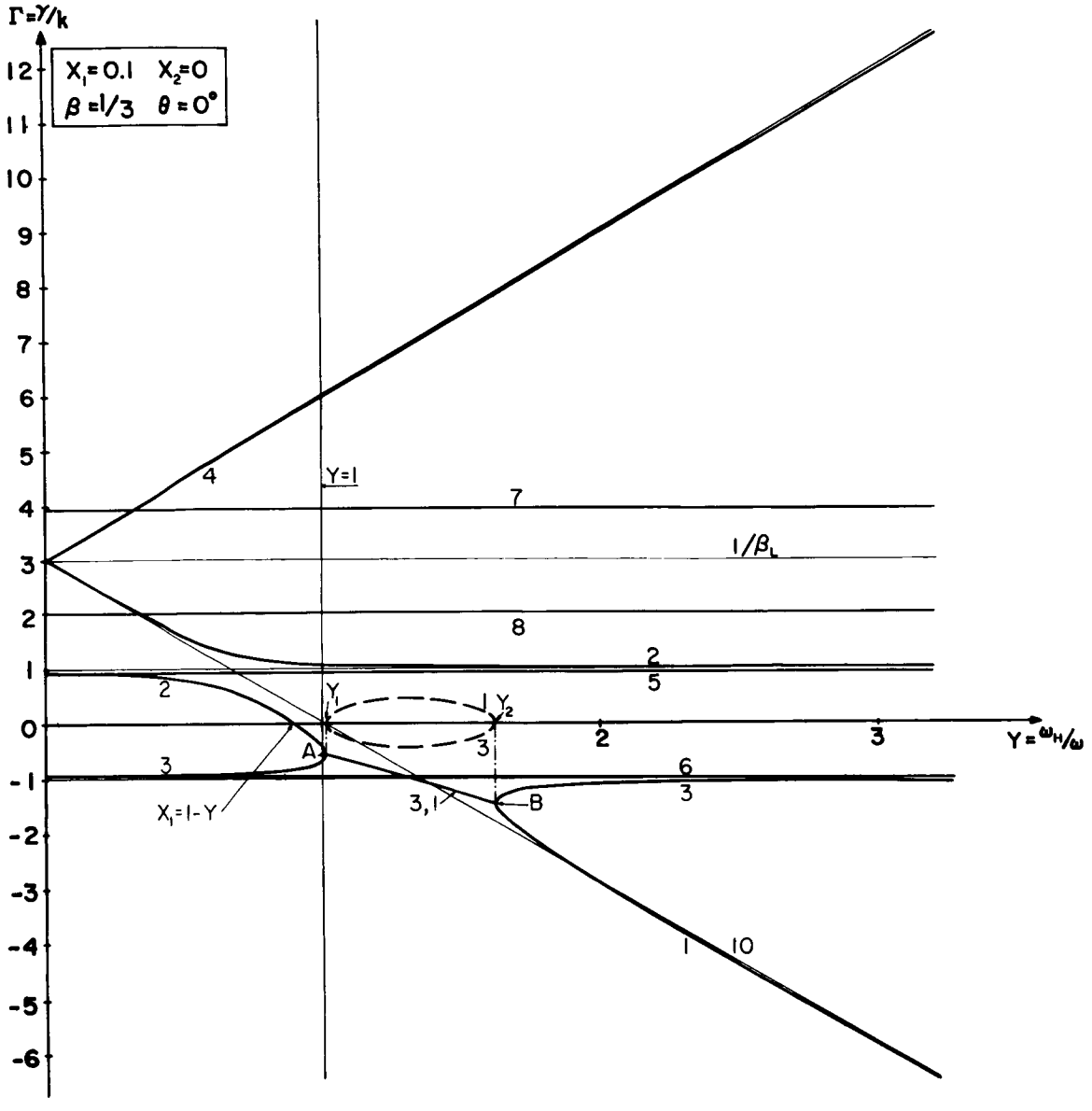

FIG. 14. Γ_q as a function of Y for a streaming magnetoionic medium when $\theta = 0°$.

The slow cyclotron wave, if it is excited in the streaming medium, proceeds in the positive z direction without any interactions. But note that the fast cyclotron wave transforms smoothly to a forward extraordinary magnetoionic wave. For large Y values the pair 2 and 5, if of equal amplitude, would form an almost plane polarized wave, with $k_{2,5} \rightarrow k$. The fourth reflection level, which in this case would be $Y_R = 1$, <u>disappears</u> for the streaming magnetoionic medium (see Eq. 54a).

In Fig. 15 we have plotted Γ_q versus Y for $\theta = 30°$. The electromagnetic wave interaction remains practically unchanged, but the two cyclotron waves now gradually transform to a symmetric space-charge wave pair. The slow space-charge wave smoothly transforms to a slow cyclotron wave. The fast space-charge wave transforms to an extraordinary magnetoionic wave, which proceeds "undisturbed" in the positive z direction.

We see that the traditional fourth reflection level, where $|\Gamma| \rightarrow \infty$, is again absent. In this respect the moving magnetoionic medium differs greatly from the stationary medium. When the medium does not move, the phase velocities of the extraordinary magnetoionic waves tend to zero at the fourth reflection level and thus become smaller than the drift velocity. This, as a matter of fact, is demonstrated by the drift-Doppler shift terms in Eqs. 16a and 16b, and also by the following Appleton-Hartree-type relation for the <u>moving</u> magnetoionic medium, obtained from Eqs. 50 and 51:

$$n^2 = \Gamma^2 = 1 - \frac{X_1 d}{b \pm \sqrt{b^2 - ad}} \tag{58}$$

where

$$d = 1+\mu\omega^2/p_{p_1}^2 \qquad \mu = -\beta^2 \Gamma^2 \sin^2\theta \qquad p_{p_1}^2 = p_t^2+\omega_p^{(1)^2}$$

$$b = 1-\frac{1}{2}Y^2\sin^2\theta \frac{\omega^4}{p_t^2 p_{p_1}^2} + \frac{1}{2}\frac{\omega^2}{p_{p_1}^2}\mu \tag{59}$$

$$a = 1+Y^2\frac{\omega^2}{p_t^2}\left(1-\frac{\omega_p^{(1)^2}}{p_{p_1}^2}\sin^2\theta\right)$$

Relation 58 is presented for the sole purpose of demonstrating what happens to the Appleton-Hartree equation when the magnetoionic medium

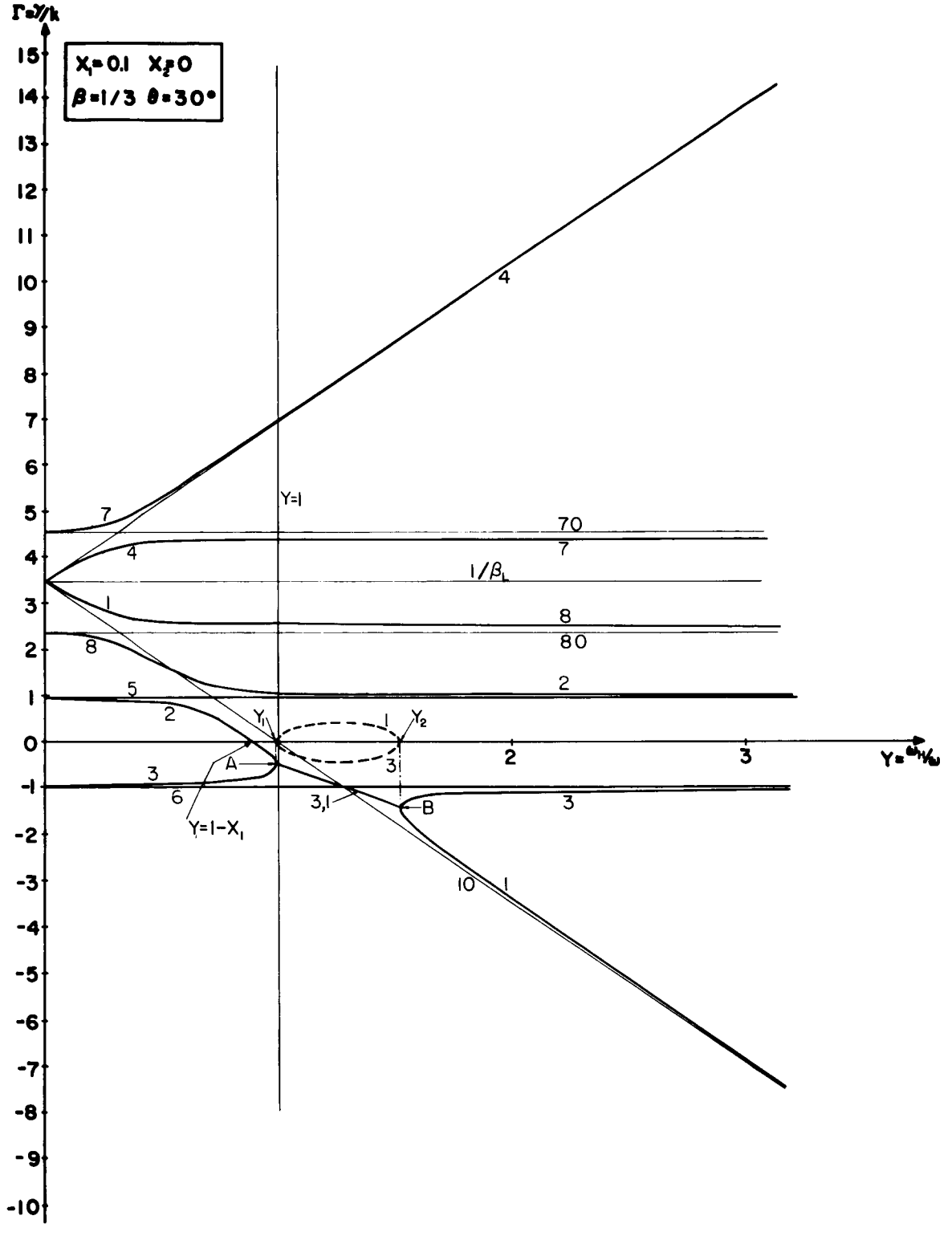

FIG. 15. Γ_q as a function of Y for a streaming magnetoionic medium when $\theta = 30°$.

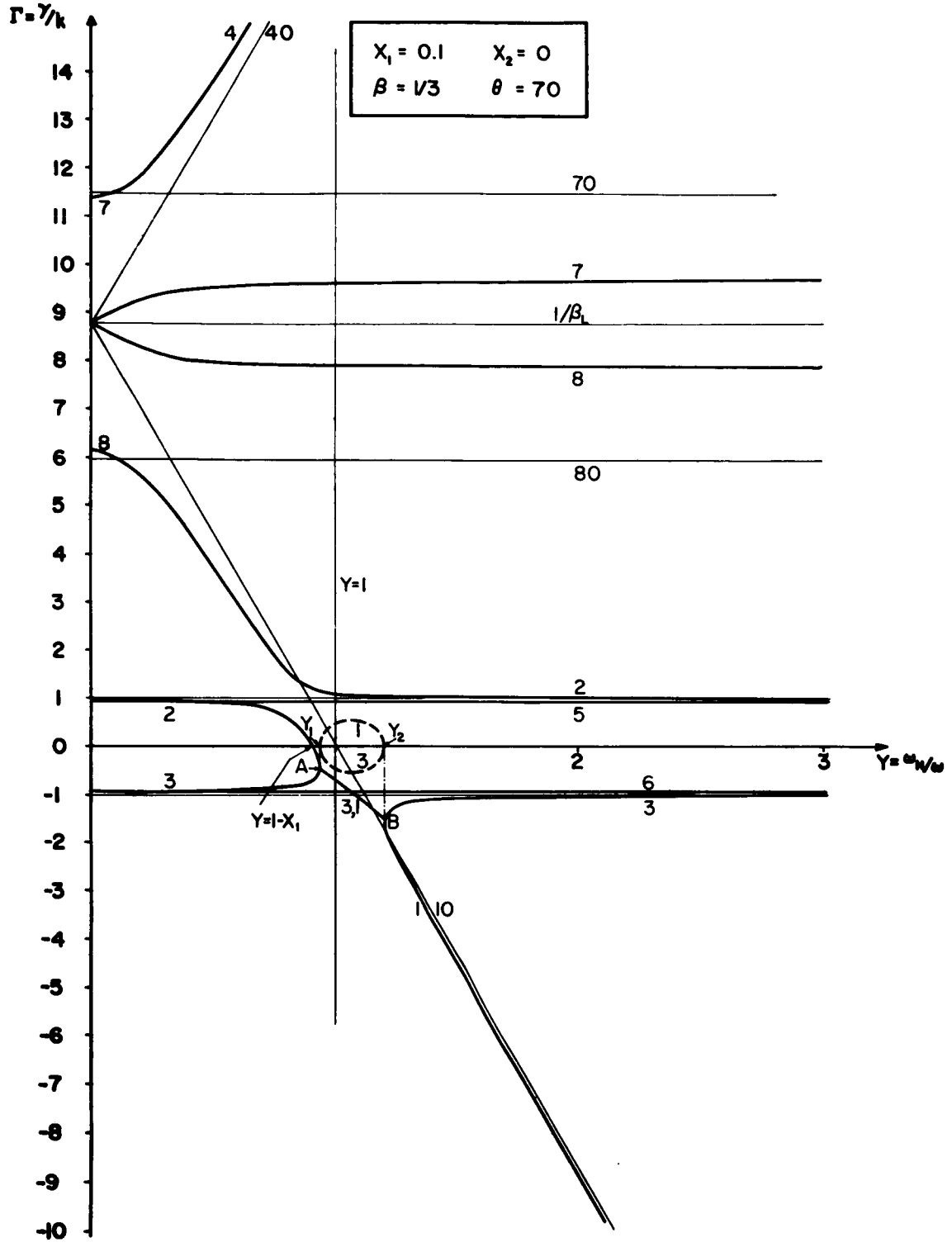

FIG. 16. Γ_q as a function of Y for a streaming magnetoionic medium when $\theta = 70°$.

[Figure 17 deleted in press by authors.]

moves. It is completely useless for numerical computations, since γ enters in all the operators when $v_o \neq 0$.

That the general situation does not change very much for larger θ values is borne out by Fig. 16. The wave transformations and couplings are essentially the same as for $\theta = 30°$. In relation to wave propagation the moving magnetoionic medium is almost simpler than the stationary medium, in spite of the fact that eight different waves can propagate in the moving medium.

Obviously, a more careful analysis should be made of the transition from a moving to a stationary magnetoionic medium ($v_o \approx c_o/n$). It is clear that $|n|$ can never be larger than c_o/v_o for the drifting medium. As $v_o \longrightarrow 0$ (i.e., k_H and $\alpha \longrightarrow \infty$), the Γ_q plot rapidly transforms into the familiar Appleton-Hartree form.

6. STATIC MAGNETIC FIELD AT ANGLE θ TO WAVE NORMAL, IONIZED STREAM AT ANGLE θ_s

It is of prime interest to investigate what happens when the stream makes some angle $\theta-\theta_s$ with the static magnetic field, assuming electrostatic field conditions that would make this possible (for example in a laboratory device).

If we introduce the drift velocity and cyclotron frequency components

$$v_T = v_o \sin\theta_s = \beta_T c_o \qquad v_L = v_o \cos\theta_s = \beta_L c_o$$

$$\omega_T = \omega_H \sin\theta \qquad \omega_L = \omega_H \cos\theta \qquad (Y_L = Y\cos\theta;\ Y_T = Y\sin\theta) \tag{60}$$

the dispersion relation corresponding to Eq. 50 can be written as follows, assuming the stream direction, the magnetic field direction, and the wave normal to lie in the x-z plane:

$$[(\Gamma^2-\varepsilon_{yy})\varepsilon_{zz}-\varepsilon_{zy}^2][(\Gamma^2-\varepsilon_{xx})\varepsilon_{zz}+\varepsilon_{zx}^2] = -(\varepsilon_{zz}\varepsilon_{yx}+\varepsilon_{zy}\varepsilon_{zx})^2 \tag{61}$$

where the ε_{pq} are the proper components of the dielectric tensor for the homogeneous medium. We find that

$$\varepsilon_{zz} = 1 - \frac{X_1}{(1-\beta_L\Gamma)^2}\left[1+\frac{Y_T^2}{(1-\beta_L\Gamma)^2-Y^2}\right] - X_2\left(1+\frac{Y_T^2}{1-Y^2}\right) \tag{62}$$

$$\varepsilon_{zy} = -jY_T\left[\frac{X_1}{(1-\beta_L\Gamma)^2-Y^2}+\frac{X_2}{1-Y^2}\right] \tag{63}$$

$$\varepsilon_{zx} = \frac{X_1}{(1-\beta_L\Gamma)^2}\left[\frac{Y_T(Y_L - Y\beta\cos(\theta-\theta_s)\Gamma}{(1-\beta_L\Gamma)^2 - Y^2} - \beta_T\Gamma\right]$$

$$+ X_2 \frac{Y_T Y_L}{1-Y^2} \tag{64}$$

$$\varepsilon_{yy} = 1 - \frac{X_1}{(1-\beta_L\Gamma)^2 - Y^2}(1-\beta_L\Gamma)^2 - \frac{X_2}{1-Y^2} \tag{65}$$

$$\varepsilon_{yx} = -j\left\{\frac{X_1}{(1-\beta_L\Gamma)^2 - Y^2}[Y_L - Y\beta\cos(\theta-\theta_s)\Gamma]\right.$$

$$\left. + \frac{X_2}{1-Y^2} Y_L\right\} \tag{66}$$

$$\varepsilon_{xx} = 1 - X_1\left\{1 + \frac{1}{(1-\beta_L\Gamma)^2}\left[\frac{[Y_L - Y\beta\cos(\theta-\theta_s)\Gamma]^2}{(1-\beta_L\Gamma)^2 - Y^2} + \beta_T^2\Gamma^2\right]\right\}$$

$$- X_2\left(1 + \frac{Y_L^2}{1-Y^2}\right) \tag{67}$$

Closer inspection of Eq. 61 reveals that we still obtain an eighth degree equation in γ. Synchronous-type waves ($p_t E_x \approx 0$) do not couple even to this more general system.

From Eqs. 62 to 67 it appears that the original eighth order equation is only perturbed slightly when $|\theta - \theta_s| \neq 0$. We find that the general nature of the interaction between the whistler mode and the stream does not change appreciably when $|\theta - \theta_s|$ has moderate values.

ACKNOWLEDGMENT

The authors are very indebted to Dr. Donald T. Laird, director of the Penn State Computation Center, for most generous computer advice and assistance without which none of the complicated graphical presentations of this communication would have been possible.

REFERENCES

1. R. M. Gallet and R. A. Helliwell, Origin of "Very-Low-Frequency Emissions," J. Research Natl. Bur. Standards, 63D(1):21-27 (1959).

2. O. E. H. Rydbeck, Research in the Field of Propagation and Interaction of Electromagnetic Waves and Space Charge Waves in Homogeneous and Inhomogeneous Media, Research Rept. No. 21, Research Laboratory of Electronics, Chalmers Univ. Technol., Gothenburg, 1960.

3. O. E. H. Rydbeck, Dynamic Non-linear Wave Propagation in Ionized Media: 4, Non-linear Electromagnetic Wave Propagation and Harmonic Radiation in Magneto-ionic Media, Research Rept. No. 30, Research Laboratory of Electronics, Chalmers Univ. Technol., 1963. See also paper II herein.

4. O. E. H. Rydbeck, The Propagation and Coupling of Waves in Inhomogeneous Media, Research Rept. No. 7, Research Laboratory of Electronics, Chalmers Univ. Technol., 1960.

5. O. E. H. Rydbeck and H. Wilhelmsson, The Influence of Electron Velocity Distribution on Space Charge Waves, Research Rept. No. 1, Research Laboratory of Electronics, Chalmers Univ. Technol., 1959.

NOTE

The following abstracts and papers are arranged in the order in which their titles appeared on the conference program.

NONLINEAR WAVE PHENOMENA IN PLASMAS

P. A. Sturrock
W. W. Hansen Laboratories of Physics
Stanford University, Stanford, California

[Dr. Sturrock's contribution condensed a series of lectures he presented at the Advanced Plasma Theory Course of the International School of Physics 'Enrico Fermi,' Varenna, Italy, July 1962. The Varenna lectures are normally published as a supplement to the Nuovo cimento. The informing study was supported by the U.S. Air Force Office of Scientific Research, under grant No. AFOSR 62-326.]

ABSTRACT

This lecture treats the nonlinear theory of waves in plasmas, being concerned principally with electrostatic waves (plasma oscillations) in homogeneous plasmas free from magnetic fields, but including discussion of the coupling of plasma oscillations to electromagnetic waves.

It is recalled that a one-dimensional disturbance of a cold plasma oscillates indefinitely at the plasma frequency, provided the amplitude is below the critical value that leads to crossover. It is also recalled that a plasma of nonzero temperature can support an arbitrary traveling-wave pattern, provided the velocity distribution is chosen appropriately.

The more general theory of electrostatic waves in plasmas is developed, with the restrictions that the temperature is taken to be zero and nonlinearity is treated by a perturbation procedure. This "fairly small amplitude" approximation is analyzed by the "derivative expansion" technique. The wave interaction kernel, to which this calculation leads, is investigated, and it is shown that a certain group of terms leads to modification of the dispersion relation of plasma oscillations, the form of this relation being similar to that derived in the linear theory of a thermal plasma, although the effect is substantially smaller and independent. The wave interaction process also leads to the exchange of energy between waves, and hence to the damping of a test wave due to interaction with an assembly of weak background waves. The decay time is estimated, and it is found that for sufficiently long wavelengths, damping due to nonlinear interaction would be more important than Landau damping.

The nonlinear theory of interaction between plasma oscillations and electromagnetic waves is developed by a similar perturbation approximation. In this analysis, the derivative-expansion technique is extended to allow for slow spatial variations of amplitudes as well as slow time variations. This theory demonstrates that, owing to the nonlinear character of the equations, there is electromagnetic radiation from plasma oscillations, the radiation occurring dominantly at the second harmonic $2\omega_p$.

The problem of radiation from plasma oscillation is also treated by Green-function integration of the approximate wave equation, treating the plasma oscillations as unperturbed by the presence of the electromagnetic waves. Formulas for the radiation power and damping time of the plasma oscillations are derived in this way.

THE QUASI-LINEAR THEORY OF PLASMA OSCILLATIONS AND INSTABILITIES

S. E. Bodner and E. A. Frieman
Plasma Physics Laboratory, Princeton University
Princeton, New Jersey

[Mr. Bodner spoke from the contribution of the authors, under this title, to the Seventh Lockheed Symposium on Magnetohydrodynamics (to be published). Their work was accomplished under the auspices of the U.S. Atomic Energy Commission.]

ABSTRACT

The quasi-linear theory, first discussed by Drummond and Pines (1) and Vedenov, Velikhov, and Sagdeev (2), is designed to treat the long-time behavior of weakly unstable plasma oscillations. The usual linearized theory keeps the spatially averaged distribution function time independent and determines the growth rate of the unstable waves. The quasi-linear theory considers the time dependent interaction between the particles and the waves.

Recently (3) the theory has been extended to include the nonlinear interactions between different modes of oscillation. The goal of the theory is then two coupled equations. The first describes the time rate of change of the spatially averaged distribution function; the second, the time rate of change of the spectral energy density. The theory has already shown that weakly unstable electron plasma oscillations tend to stabilize. The asymptotic behavior can be derived.

REFERENCES

1. W. Drummond and D. Pines, Paper CN-10/134, Conference on Plasma Physics and Controlled Nuclear Fusion Research, Salzburg, 1961.

2. A. Vedenov, E. Velikhov, and A. Sagdeev, Paper CN-10/199, Conference on Plasma Physics and Controlled Nuclear Fusion Research, Salzburg, 1961.

3. E. Frieman, S. Bodner, and P. Rutherford, Princeton Plasma Physics Laboratory Report, Matt-169 (to be published).

RADIO BURSTS FROM THE SUN

M. H. Cohen
Center for Radiophysics and Space Research
Cornell University, Ithaca, New York

ABSTRACT

Type II and Type III meter wavelength bursts from the sun drift downward in frequency with time. It is commonly accepted that this drifting results from an agency which moves out through the solar atmosphere, exciting the local plasma frequency as it goes (1,2). The details of the generation of the radio waves, and of their subsequent propagation through the solar atmosphere to the earth, are not at all clear, but nonlinear and particle-wave interaction phenomena are certainly involved.

The drifting rate of Type III bursts corresponds to an upward velocity of 1/4 to 1/2 c, where c is the velocity of light (2). The primary agency with this velocity must surely be a stream of charged particles. A two-step process (3,4,5,6,7,8) is regarded as generating the radio waves: (a) The particles excite longitudinal plasma waves by Cerenkov radiation; (b) the plasma waves are partially converted into transverse waves, which can propagate freely to the earth, by scattering on inhomogeneities in electron density.

Type III bursts often have a second harmonic. The Cerenkov spectrum (5), however, is concentrated just above the local plasma frequency, so the second harmonic is not generated directly, but rather comes from the second step, the scattering process. The density inhomogeneities responsible for this frequency doubling must themselves be plasma waves (6). This is also called combination scattering (3). Thermal fluctuations excite plasma waves, but it is very difficult to obtain the required intensity of second harmonic (as intense as the fundamental) by thermal excitation alone. It appears as though this scattering and generation of the second harmonic results when the Cerenkov plasma waves scatter off their cousins, the waves which have been generated a moment before by some preceding particles. There will be a continual overtaking and scattering of one wave by another because the Cerenkov spectrum is distributed both in angle and in frequency, and each component has its own group velocity.

The fundamental of a Type III burst may be obtained by scattering of the Cerenkov plasma waves on the ion component of thermal density fluctuations (3,6). This component consists of damped ion waves and has a spectrum of its own, so that the Type III spectrum is the convolution of the Cerenkov spectrum and the fluctuation spectrum (6).

A rough estimate shows that about 10^{31} particles are required to produce a medium-intensity Type III burst. This assumes that all particles radiate independently, that is, incoherently. If a volume of 10^{30} cm^3 is assumed for the source region, this gives about 10 particles per cubic centimeter or several hundred per Debye sphere. But if there are

many particles per Debye sphere, they must radiate partly coherently. This idea drastically reduces the required number of particles, so there might be a few per Debye sphere, radiating partly coherently. The theory of this situation has not been worked out, although the extreme cases are well known. Very many particles per Debye sphere is the two-fluid situation, with the plasma waves generated by a two-stream instability limited by nonlinearities (3,4); one particle per many Debye spheres is the independent particle situation, with the plasma waves generated by incoherent Cerenkov emission (5).

The drifting rate of Type II bursts corresponds to an upward velocity of 1000 to 1500 km per sec (9,10). It is thought that the primary agency with this velocity is a shock wave. Because the theory of the shock wave and its interaction with the plasma is very involved and incomplete, the theory of Type II bursts is less developed than that for Type III.

It is possible that electrons running through the shock front directly generate the transverse electromagnetic waves that we see as the Type II burst (11). But the shock wave may act in some way to accelerate particles until they radiate Cerenkov plasma waves that scatter off density irregularities (possibly the shock front itself). In this view the Type II is a superposition of many small Type III's. This idea is reinforced by the apparent clean bursts, like Type III's, that are sometimes superimposed (herringbone structure) on the slower drifting Type II background (9), and by the observation that the second harmonic appears to come from lower in the corona than the fundamental (6,8). A likely situation is that both of these processes are going on; the smooth background of the Type II is somehow generated by the shock wave, and the sharp superimposed structure comes from particles accelerated by the shock (12). Laboratory experiments on shock waves in plasma might well help in selecting the right mechanism for the Type II.

Most Type II bursts have a second harmonic, but not a third. This is readily explained by the two-step process, as for the Type III bursts (3,4). A different possibility (11) is that the density ratio across the fast shock wave is 4, and therefore the plasma frequencies just ahead of and just behind the shock wave differ by a factor of 2. These two plasma frequencies could be excited essentially simultaneously by fast particles.

Many Type II bursts show a split structure; that is, both fundamental and second harmonic bands are split into two bands each, with separation of the order of 10 Mc/s. This splitting has been thought due to a magnetic field, and various attempts to explain the splitting have been made, generally based on positions of zeros and singularites of the magnetoionic dispersion equation. The most plausible suggestion (13) is that the two frequencies correspond to the extraordinary mode singularity for $\theta = 0$ and $\theta = \pi/2$. Waves are generated near these singularities by Cerenkov radiation. The waves correspond closely to plasma waves, and they might be converted into the magnetoionic modes that can escape to the earth by scattering on the ion component of thermal density fluctuations.

Polarization observations (14) show that Type II bursts are always unpolarized, both fundamental and second harmonic, split and not split. This observation by itself cannot be used to rule on any of the foregoing ideas concerning Type II's. For lack of genuine knowledge, one can always assume that the magnetic field is sufficiently disordered in the vicinity of the shock wave that the integrated effect over the whole source is an unpolarized radio wave, regardless of the mechanism.

Type III bursts, on the other hand, are often in part circularly polarized (14), and more rarely show weak linear polarization (15). It is not clear whether these polarizations result from something intrinsic in the source or from some effect of the propagation through the long plasma path to the earth.

REFERENCES

1. J. P. Wild, K. V. Sheridan, and G. H. Trent, in Paris Symposium on Radio Astronomy, Stanford University Press, Stanford, Calif., 1959, p. 176.

2. J. P. Wild, K. V. Sheridan, and A. A. Neylan, Australian J. Phys., 12:369 (1959).

3. V. L. Ginzburg and V. V. Zhelezniakov, Soviet Astron.-AJ, 2:653 (1958).

4. V. L. Ginzburg and V. V. Zhelezniakov, Soviet Astron.-AJ, 5:1 (1961).

5. M. H. Cohen, Phys. Rev., 123:711 (1961).

6. M. H. Cohen, J. Geophys. Research, 67:2729 (1962).

7. J. M. Malville, Astrophys. J., 136:266 (1962).

8. S. F. Smerd, J. P. Wild, and K. V. Sheridan, Australian J. Phys., 15:180 (1962).

9. J. A. Roberts, Australian J. Phys., 12:327 (1959).

10. A. Maxwell and A. R. Thompson, Astrophys. J., 135:138 (1962).

11. D. A. Tidman, Phys. Fluids, 5:1104 (1962).

12. M. R. Kundu, Astrophys. J. (in press).

13. P. Sturrock, Nature, 192:58 (1961).

14. M. Komesaroff, Australian J. Phys., 11:201 (1958).

15. K. Akabane and M. H. Cohen, Astrophys. J., 133:258 (1961).

SOME INVESTIGATIONS OF INSTABILITIES IN ONE-DIMENSIONAL PLASMAS

John Dawson
Plasma Physics Laboratory
Princeton University, Princeton, New Jersey

[Dr. Dawson's contribution was based on a paper, titled the same, which he presented at the University of Paris, September 1962. The text has been published in Service de Physique des Plasmas, vol. III, Laboratoire des hautes energies, Universite de Paris. The work reported was accomplished under the auspices of the U.S. Atomic Energy Commission.]

ABSTRACT

One-dimentional plasma models (1,2) are used to investigate the nonlinear behavior of a number of plasma instabilities. Three unstable situations are investigated: case I, double stream instability; cases II and III, current instabilities.

In case I, two cold streams of electrons pass through each other and through a fixed neutralizing background (3). The growth of the unstable waves is accurately given by the linearized theory until the density perturbation becomes comparable to the mean density. At this time the streams rapidly break up, the velocity distribution becomes roughly Maxwellian, and the instability ceases.

When an electron current is passed through a plasma composed of electrons and cold, heavy, but movable ions, the plasma is unstable (2). In case II, the streaming velocity of the electrons is less than their thermal velocity, but greater than the velocity of ion waves $(kT_e/M_i)^{1/2}$, resulting in unstable ion waves. In case III, electron streaming velocity is greater than electron thermal velocity. For both cases, the current is maintained constant by an external electric field.

The high current problem exhibits violent instabilities, which result in an anomalously large resistance and rapid heating of the electrons. The instability turns itself off when the random electron velocity becomes equal to the streaming velocity.

For the low current case, the plasma quickly stabilizes itself by flattening out the velocity distribution in the vicinity of the phase velocity of the ion waves, and there is little indication that the plasma is unstable.

REFERENCES

1. J. Dawson, Phys. Fluids, 5:445 (1962).

2. C. Smith and J. Dawson, Princeton Plasma Physics Laboratory Report, Matt-151, January 1963.

3. J. Dawson, Princeton Plasma Physics Laboratory Report, Matt-83, November 1962.

SURVEY OF PROPAGATION PHENOMENA, LINEAR AND NONLINEAR, IN AN INFINITELY CONDUCTING COMPRESSIBLE FLUID

J. Bazer
Courant Institute of Mathematical Sciences
New York University, New York City

ABSTRACT

The propagation of weak hydromagnetic discontinuities (for example, weak shocks) is discussed in Ref. 1. The medium is assumed to be a nonviscous infinitely conducting compressible fluid. The undisturbed medium is not required to be homogeneous, so that in particular the density, fluid velocity, and magnetic field intensity may vary from point to point. An initial discontinuity is assumed given on an arbitrary initial surface. The wave fronts that evolve out of this surface -- there will be six of them, in general -- are obtained as solutions of first order partial differential equations.

These "eikonal" equations are solved, as in geometrical optics, by means of rays that are shown to satisfy Hamilton's equations and Fermat's principle. The hydromagnetic analog of Huygens' wave front construction is described. To complete the geometrical solution, the variation of the disturbance strengths along the rays is determined in terms of the disturbance strengths on the initial surface. A noteworthy feature of this solution is that the fundamental modes of propagation -- the slow, Alfven, and fast modes -- are uncoupled as long as the medium is free of diffracting objects and surfaces of discontinuity.

The theory described in Ref. 1 is closely related to the time-harmonic small wavelength type of geometrical solution, a detailed study of which is given in Ref. 2. The two theories may in fact be subsumed under one general formalism (2, page 154). As an illustration of the general theory, Ref. 2 (pages 160-163) gives the complete geometrical solution for the propagation of Alfven disturbances in a dipole field, with the aid of explicit formulas. Fast wave propagation in various types of inhomogeneous magnetic fields is also briefly discussed.

The problem of reflection and refraction of slow, Alfven, and fast disturbances at surfaces of discontinuity, possibly curved, is treated in Refs. 2 and 3. The hydromagnetic analogs of "Snell's" law are derived, and their relation to Huygens' wavelet construction is elucidated. It is shown that the introduction of an appropriate set of direction angles for the unperturbed magnetic field, on each side of the discontinuity, (a) reveals the symmetries of "Snell's" laws, (b) leads immediately to a simplification of V. C. A. Ferraro's laws relating to the reflection and refraction of Alfven waves, and (c) makes possible a simple graphical method for determining the angles and speeds at which the various reflected and refracted waves emerge.

The nonlinear hydromagnetic piston problem is treated in Ref. 4, with the aid of the methods and results developed in Refs. 5 and 6.

The linearized piston problem is discussed in Ref. 1. The geometric setup is as follows. An infinitely conducting rigid magnet fills the half-space $x < 0$; the half-space $x > 0$ is filled with a nonviscous infinitely conducting compressible fluid. It is assumed that the magnetic field is perpendicular to the interface, and that the fluid is at rest and everywhere uniform. The magnet is set in motion with a uniform velocity transverse to the direction of the magnetic field. This motion causes both a longitudinal motion and a transverse motion, specifically a fast hydromagnetic shock followed by a slow centered rarefaction wave. The effect of this pair of waves is to adjust the motion of the medium to the transverse motion of the magnet.

In the final steady state, which is achieved after the waves have propagated out to infinity, the fluid has everywhere the same transverse velocity as the wall, and a transverse magnetic field is present although none existed initially. A striking and basically nonlinear aspect of this motion is that a region of cavitation (a vacuum between the magnet and the fluid) can be created if the transverse velocity of the magnet is sufficiently large compared with the sound speed in the initially undisturbed medium.

REFERENCES

1. J. Bazer and O. Fleischman, Propagation of Weak Hydromagnetic Discontinuities, Phys. Fluids, 2:366 (1959).

2. J. Bazer and J. Hurley, Geometrical Hydromagnetics, J. Geophys. Research, 68:147 (1963).

3. J. Bazer, Reflection and Refraction of Weak Hydromagnetic Discontinuities, Research Report No. MH-11, Div. Electromagnetic Research, Courant Institute of Math. Sci., N. Y. University, 1961.

4. J. Bazer, Resolution of an Initial Shear Flow Discontinuity in One-Dimensional Hydromagnetic Flow, Astrophys. J., 128:686 (1958).

5. K. O. Friedrichs, Nonlinear Wave Motion in Magnetohydrodynamics, Los Alamos Report No. 2105 (written 1954, distributed 1957). See also later version by K. O. Friedrichs and H. Kranzer, Report No. MH-8, AEC Computing and Applied Math. Center, Courant Institute of Math. Sci., N. Y. University, 1958.

6. J. Bazer and W. B. Ericson, Hydromagnetic Shocks, Astrophys. J., 129:758 (1959).

ON THE NONLINEAR THEORY OF MULTISTREAM ELECTRONIC DEVICES

C. L. Dolph and R. J. Lomax
Electron Physics Laboratory
The University of Michigan, Ann Arbor, Michigan

INTRODUCTION

Most nonlinear theories of multistream devices such as the klystron, traveling-wave tube, and backward-wave oscillator are based upon a cold plasma approximation in which a ballistic theory is developed from the equations of continuity and force in Lagrangian form. The problem of overtaking electrons, and the multiple streaming which then occurs, can be overcome instead by introducing a velocity distribution. The density function thereby defined is always single-valued in phase space. This offers the possibility of using the velocity distribution as an artifice to solve problems in which its effect is expected to be small and to attack problems where its effect is expected to be significant.

The density method has frequently been used in the study of neutron transport problems as they occur in the design of nuclear reactors, and considerable effort has been directed toward the development of numerical methods appropriate for high speed digital computers. This paper presents a procedure similar to the so-called spherical harmonic method of neutron transport theory, in a form suitable for a wide variety of microwave and plasma devices. The expansions in terms of spherical harmonics of neutron transport theory are replaced by expansions in terms of Hermite functions, utilizing the systematic development of such expansions described by Korevaar (1) under the name pansions.

Other methods developed for neutron transport theory can also be adapted to microwave devices. In particular, the usefulness of the method of invariant imbedding as developed by Bellman (2) and Wing (3) should certainly be investigated.

The use of expansions in Hermite functions, or equivalently the associated Hermite polynomials, is not new in transport theory. The well-known paper by Grad (4) in which the thirteen-moment approximation to the Boltzmann equation is developed, is based on a similar expansion in terms of generalized Hermite polynomials. Many of the properties of these functions, defined by Grad in Ref. 5, will undoubtedly prove useful in later extensions of the one-dimensional problem to which the present discussion is limited.

To gain experience and insight into the advantages and disadvantages of the Hermite expansion method, the authors have so far concentrated on the one-dimensional traveling-wave tube problem as determined by the transmission-line approximation used by Brillouin (6), for example, and the transport equation now known as that of Landau and Vlasov. The corresponding linearized problem has been treated by Rynn and Watkins (7). At this writing, the detailed work on numerical procedures and programming has caused some delay, and it is not yet possible to present results

that can be compared with the existing nonlinear ballistic theory for the traveling-wave tube. Because of this, attention will be concentrated on the Landau-Vlasov transport equation, which is common to all similar problems.

Specifically then, the method will be developed for the equation

$$\frac{\partial f}{\partial t} + v\frac{\partial f}{\partial x} + \eta\frac{\partial e}{\partial x}\frac{\partial f}{\partial v} = 0 \qquad (\eta = e/m) \tag{1}$$

subject to the normalized boundary conditions for a tube of unit length

$$f(0,v,t) = f^{(1)}(v,t) \qquad (v > 0) \tag{2}$$

$$f(1,v,t) = 0 \qquad (v < 0) \tag{3}$$

$$f(x,v,0) = f^{(0)}(x,v) \qquad (-1 \leq x \leq 1) \tag{4}$$

under the assumption that $\partial e/\partial x$ is known. In an actual problem, $\partial e/\partial x$ would represent the sum of several voltage gradients and could include not only the transmission-line contribution but also a space-charge contribution and a d-c contribution. Because at least part of this gradient is affected by Eq. 1, realistic problems would involve a natural iteration process superimposed on the discussion to be given here. Full details necessary for this in the traveling-wave tube problem, as well as detailed proofs of the development to be sketched here, will be published elsewhere after numerical solutions have been obtained.

BASIC EXPANSION RELATIONS

In contrast to the neutron transport theory, it will be assumed that the distribution function $f(x,v,t)$ can be represented as

$$f(x,v,t) = \sum_{k=o}^{\infty} p_k(x,t)\,\phi_k(v) \tag{5}$$

where the Hermite functions $\phi_k(v)$ are defined by the equation

$$\phi_k(v) = \frac{e^{-v^2/2}H_k(v)}{\pi^{1/4}2^{k/2}(k!)^{1/2}} \tag{6}$$

The Hermite functions are readily seen to be orthonormal over the real velocity line, and as demonstrated by Korevaar (1) they form a complete set for even a class of generalized functions wide enough for most applications. Specifically, as shown by Widlund (8), this class includes the generalized functions considered by Lighthill (9). The "good" functions of Lighthill, considered as functions of velocity, are precisely those functions $g(v)$ admitting the expansion

$$g(v) = \sum_{o}^{\infty} g_k\phi_k(v) \tag{7}$$

where the coefficients g_k have the property that there exists a number M(n) such that the inequality

$$|g_k| < M(n)/(k + 1)^n$$

holds for arbitrary n. Moreover, if the symbol (u,v) is defined by the relation

$$(u,v) = \int_{-\infty}^{\infty} u(x)\bar{v}(x)\, dx \tag{8}$$

the class of generalized functions of Lighthill is precisely those functions G(v) for which the series of numbers

$$\sum_{k=o}^{\infty} (G,\phi_k)(\phi_k,g) \tag{9}$$

converges for all g in the class of good functions. Finally, the series will converge only if there exist positive constants A and n, independent of k, such that the inequality is

$$|(G,\phi_k)| \leq A(k + 1)^n \tag{10}$$

Delta function singularities do not usually occur in velocity space, but their occurrence would cause no difficulty since it is readily verified that $\delta(v)$ admits the representation

$$\delta(v) \sim \sum_{k=o}^{\infty} (-1)^k[(2k)!]^{1/2} \frac{\pi^{1/4}}{2^k k!} \phi_{2k}(v) \tag{11}$$

in which the last criterion is satisfied.

Further desirable properties follow from the fact that if the Fourier transform of a function u(v) is defined by

$$F(u) = \frac{1}{\sqrt{2\pi}} \int_{-\infty}^{\infty} u(v)e^{-i\sigma v}\, dv \tag{12}$$

then it is readily verified that

$$F(\phi_k) = (-i)^k \phi_k(\sigma) \tag{13}$$

In particular, this implies that all generalized functions in the sense of Lighthill have Fourier transforms that lie in the same class. In addition this property permits a partial realization of an idea enunciated earlier by Dolph (10), in that it permits the evaluation of

quantities such as density and current without knowledge of the full distribution function. For example, the density is defined by

$$\rho = \int_{-\infty}^{\infty} f(x,v,t)\, dv \tag{14}$$

and this is readily seen to be given by

$$\rho = \sqrt{2\pi}\, F(f)\Big|_{\sigma=o} = \sqrt{2\pi} \sum_{k=o}^{\infty} p_{2k}(x,v)\phi_{2k}(0)(-i)^{2k} \tag{15}$$

wherever f(x,v,t) admits the expansion Eq. 5, since

$$\phi_{2k+1}(0) = 0 \tag{16}$$

In the application of this method to the transport equation it will also be necessary to make use of the relations, proved for the example in Ref. 1, that if f(x,v,t) admits the expansion Eq. 5 then

$$vf(x,v,t) = \sum_{o}^{\infty} \left[\left(\frac{k}{2} + \frac{1}{2}\right)^{\frac{1}{2}} p_{k+1} + \left(\frac{k}{2}\right)^{\frac{1}{2}} p_{k-1}\right]\phi_k(v) \tag{17}$$

and

$$\frac{\partial f(x,v,t)}{\partial v} = \sum_{o}^{\infty} \left[\left(\frac{k}{2} + \frac{1}{2}\right)^{\frac{1}{2}} p_{k+1} - \left(\frac{k}{2}\right)^{\frac{1}{2}} p_{k-1}\right]\phi_k(v) \tag{18}$$

REDUCTION OF TRANSPORT EQUATION TO A SYMMETRIC HYPERBOLIC SYSTEM

For reasons which will be explained, it is more advantageous to apply the machinery of the previous paragraph to Eq. 1 after a transformation of the form

$$f = ge^{-v^2/2} \tag{19}$$

Under this transformation, Eq. 1 yields

$$\frac{\partial g}{\partial t} + v\frac{\partial g}{\partial x} = -\eta\left(\frac{\partial e}{\partial x}\ \frac{\partial g}{\partial v} - vg\right) \tag{20}$$

If the pansion expansion

$$g(x,v,t) = \sum_{o}^{\infty} g_k(x,t)\phi_k(v) \tag{21}$$

is now introduced into Eq. 20 and the orthogonal properties of the Hermite functions are used, the following infinite set of coupled equations results:

$$\frac{\partial g_k}{\partial t} + \left(\frac{k}{2} + \frac{1}{2}\right)^{\frac{1}{2}} \frac{\partial g_{k+1}}{\partial x} + \left(\frac{k}{2}\right)^{\frac{1}{2}} \frac{\partial g_{k-1}}{\partial x}$$

$$= \eta \frac{\partial e}{\partial x} 2\left(\frac{k}{2}\right)^{\frac{1}{2}} g_{k-1} \qquad (k = 0,1,2, \ldots) \tag{22}$$

If the one-parameter family of infinite Jacobi matrices is defined by the relations

$$A(\theta) = \{a_{mn}(\theta)\}$$

and

$$a_{mn}(\theta) = e^{i\theta} \left(\frac{n}{2}\right)^{\frac{1}{2}} \delta_{m+1,n} + e^{-i\theta} \left(\frac{n}{2} + \frac{1}{2}\right)^{\frac{1}{2}} \delta_{m-1,n} \tag{23}$$

and the infinite-dimensional vector $g = (g_1, g_2, \ldots)$ is introduced, this infinite system can be written in the formally self-adjoint form

$$i \frac{\partial \underline{g}}{\partial t} + i \frac{\partial}{\partial x} [A(0)\underline{g}] = - \eta \frac{\partial e}{\partial x} [A(\pi/2) - A(0)]\underline{g} \tag{24}$$

under the assumption that $\partial e/\partial x$ is a known function. That the system is formally self-adjoint follows from the readily established identity in which the superscript T refers to the transpose of the indicated quantity:

$$\iint \Big[\underline{h}^* \Big\{ i \frac{\partial \underline{g}}{\partial t} + i \frac{\partial}{\partial x} [A(0)\underline{g}] + \eta \frac{\partial e}{\partial x} [A(\pi/2) - A(0)]\underline{g} \Big\}$$

$$- \underline{g}^T \Big\{ i \frac{\partial \underline{h}^T}{\partial t} + i \frac{\partial}{\partial x} [A(0)\underline{h}^T] + \eta \frac{\partial e}{\partial x} [A(\pi/2) - A(0)]\underline{h}^T \Big\}^* \Big] \, dx \, dt$$

$$= \oint i \, [\underline{h}^* \underline{g} \, dx - \underline{h}^* i \, A(0)\underline{g} \, dt] \tag{25}$$

For any actual computation it is necessary to truncate the system Eq. 22. If one sets

$$g_k = 0$$

$$a_{mn}(\theta) = 0 \qquad (k, m, n \geq N) \tag{26}$$

the resulting system is an $N \times N$ determined system. However, as in the spherical harmonic method [compare the discussion in Weinberg and Wigner (11) or Kofink (12)], such a truncation has the effect of introducing a fictitious source term in either Eq. 1 or Eq. 20. This follows from the

fact that the first neglected equation

$$\left(\frac{N}{2}+\frac{1}{2}\right)^{\frac{1}{2}}\left(\frac{\partial g_{N+1}}{\partial x}+\eta\,\frac{\partial e}{\partial x}\,g_{N+1}\right)+\left(\frac{N}{2}\right)^{\frac{1}{2}}\left(\frac{\partial g_{N-1}}{\partial x}-\eta\,\frac{\partial e}{\partial x}\,g_{N-1}\right)=0 \qquad (27)$$

leads to an inconsistency unless the term

$$\left(\frac{N}{2}\right)^{\frac{1}{2}}\left(\frac{\partial g_{N-1}}{\partial x}-\eta\,\frac{\partial e}{\partial x}\,g_{N-1}\right) \qquad (28)$$

is added to the right-hand side of it. Reversing the process that led from Eq. 20 to the truncated system yields, instead of Eq. 20, the equation for an approximate g, say g_a of the form

$$\frac{\partial g_a}{\partial t}+v\,\frac{\partial g_a}{\partial x}+\eta\,\frac{\partial e}{\partial x}\left(\frac{\partial g_a}{\partial v}-v g_a\right)$$

$$=\left(\frac{N}{2}\right)^{\frac{1}{2}}\left(\frac{\partial g_{N-1}}{\partial x}-\eta\,\frac{\partial e}{\partial x}\,g_{N-1}\right)\phi_N(v) \qquad (29)$$

This in turn implies that the corresponding approximate distribution function f_a satisfies not Eq. 1 but

$$\frac{\partial f_a}{\partial t}+v\,\frac{\partial f_a}{\partial x}+\eta\,\frac{\partial e}{\partial x}\,\frac{\partial f_a}{\partial v}$$

$$=\left(\frac{N}{2}\right)^{\frac{1}{2}}\left(\frac{\partial g_{N-1}}{\partial x}-\eta\,\frac{\partial e}{\partial x}\,g_{N-1}\right)e^{-v^2/2}\phi_N(v) \qquad (30)$$

Therefore, in general, the truncation introduces a source except for those velocities corresponding to the zeros of $\phi_N(v)$. These are just the zeros of the Nth Hermite polynomial. But since

$$\int_{-\infty}^{\infty} v^k e^{-v^2/2}\phi_N(v)\,dv=0 \qquad (k=0,1,\ldots N-1) \qquad (31)$$

it follows from Eq. 30 that the first N moments of the approximate distribution function f_a are governed by the same differential equations as those which determine f, and that in particular they are unaffected to this order by the fictitious source term. Moreover, since

$$\int_{-\infty}^{\infty} e^{-v^2/2}\phi_N(v)\,dv=\pi^{1/4}\int_{-\infty}^{\infty}\phi_o(v)\phi_N(v)\,dv=0 \qquad (32)$$

the fictitious source term contributes approximately equal amounts of positive and negative error on the average, so that its over-all effect on the approximate distribution function is less than would otherwise be the case.

The substitution of g for f has one other advantage. From the representation Eq. 21 it follows that the coefficients are given by

$$g_k = \int_{-\infty}^{\infty} f e^{v^2/2} \frac{H_k(v) e^{-v^2/2}}{\pi^{1/4}(2^k k!)^{1/2}} dv = \int_{-\infty}^{\infty} \frac{f(v) H_k(v)\, dv}{\pi^{1/4}(2^k k!)^{1/2}} \tag{33}$$

so that the density is given directly by

$$\rho = \pi^{1/4} g_o \tag{34}$$

while the current is given by

$$j = \frac{\pi^{1/4}}{2^{1/2}} g_1 \tag{35}$$

This remark, coupled with the foregoing discussion of the agreement of the moments up to order N, fully justifies the use of Eq. 20 in place of Eq. 1.

To reduce the truncated system Eq. 22 to symmetric hyperbolic form, it is convenient to use the following theorems, which will be stated here without proofs since these are quite lengthy and involved and are given elsewhere (13).

Theorem 1. The N × N Jacobi matrix

$$A_N(0) = \{a_{ij}(0)\} \qquad (i, j = 0,1,\ldots N-1)$$

$$a_{ij} = \left(\frac{j}{2}\right)^{\frac{1}{2}} \delta_{i+1,j} + \left(\frac{j}{2} + \frac{1}{2}\right)^{\frac{1}{2}} \delta_{i-1,j}$$

has the following properties:

(a) The determinant $|A_N - \lambda I| = (-1)^N H_N(\lambda)/2^N$; hence the eigenvalues of A_N are the roots of $H_N(\lambda) = 0$.

(b) The orthonormal eigenvector $\underline{Q}_k$ associated with the eigenvalue λ_k has the components

$$Q_k^{\alpha} = \left(\frac{C_k}{2^{\alpha}\alpha!}\right)^{\frac{1}{2}} H_{\alpha}(\lambda_k) \qquad (\alpha = 0,1,\ldots N-1)$$

where C_k is a normalization constant given by

$$C_k = \frac{2^{N+1} N!}{[H_{N+1}(\lambda_k)]^2}$$

Theorem 2. Let U_N be the orthogonal matrix, whose elements are given by

$$U_{ij} = \left(\frac{2^{N+1}N!}{2^i i!}\right)^{\frac{1}{2}} \frac{H_i(\lambda_j)}{H_{N+1}(\lambda_j)}$$

while those of its inverse $U_N - 1$ are given by

$$(U_{ij})^{-1} = U_{ji} = (U_{ij})^T$$

and let $iB_N = A_N\,(\pi/2)$. Then

$$U_N^{-1} A_N U_N = D_N$$

where D_N is the matrix with elements (d_{ij}), $d_{ij} = \lambda_i\,\delta_{ij}$; and

$$U_N^{-1} B_N U_N = C_N$$

where C_N is the matrix with elements (c_{ij}):

$$c_{ij} = 1/(\lambda_i - \lambda_j) \qquad (i \neq j)$$

$$= 0 \qquad (i = j)$$

If the transformation of this last theorem is now applied to define the vector $\underline{w}_N$ by means of the relations

$$\underline{g}_N = U_N \underline{w}_N$$

$$\underline{w}_N = U_N^{-1} \underline{g}_N$$

the truncated system Eq. 22 takes the form

$$\frac{\partial w_k}{\partial t} + \lambda_k \frac{\partial w_k}{\partial x} = \eta\left(\frac{\partial e}{\partial x}\ \lambda_k w_k - \sum_{\substack{\ell=o \\ \ell \neq k}}^{N-1} \frac{1}{\lambda_k - \lambda_\ell}\ w_\ell\right) \tag{37}$$

which, under the assumption that $\partial e/\partial x$ is known, is in the standard or canonical form for a system of partial differential equations of hyperbolic type in two independent variables. The N distinct characteristics of this system satisfy the equations

$$\frac{dt}{ds} = 1 \qquad \frac{dx}{ds} = \lambda_k \tag{38}$$

where

$$H_N(\lambda_k) = 0 \qquad (k = 0,1,\ldots N-1) \tag{39}$$

BOUNDARY AND INITIAL CONDITIONS

A typical well-set boundary value problem, appropriate as an example for the traveling-wave tube, requires that the following quantities be specified:

$$\begin{aligned} f(x,v,0) &= f^{(o)}(x,v) && (0 \leq x \leq 1) \\ f(0,v,t) &= f^{(1)}(v,t) && (v > 0) \\ f(1,v,t) &= 0 && (v < 0) \end{aligned} \tag{40}$$

In these expressions it is assumed that $f^{(o)}$ and $f^{(1)}$ are known functions. From this information it is necessary to deduce appropriate initial and boundary values for the $w_k(x,t)$ functions that occur in Eq. 37. Since the boundary values cannot be satisfied exactly for all values of v, as in the spherical harmonic method it is convenient to take an even truncation of the system Eq. 22 so that an even number of roots are involved in the characteristic direction of the hyperbolic system. Thus if the roots of $H_{2N}(\lambda) = 0$ are divided into positive and negative roots and the positive roots are denoted by $\lambda_o,\ldots \lambda_{N-1}$ and the negative by $\lambda_N,\ldots \lambda_{2N-1}$ where

$$\lambda_{N+\ell} = -\lambda_\ell \qquad (\ell = 0,1,\ldots N-1)$$

it is convenient to satisfy the condition at x = 0 for all velocities $v = \lambda_k$, k = 0,1,... (N - 1), and to satisfy the condition at x = 1 for all velocities $v = \lambda_k$, k = N, N+1,... (2N - 1). If $g^{(o)}$ and $g^{(1)}$ are defined by the relations

$$\begin{aligned} g^{(o)} &= f_o e^{v^2/2} \\ g^{(1)} &= f_1 e^{v^2/2} \end{aligned} \tag{41}$$

it may be shown with the aid of the transformation of Theorem 2 that

$$g(x,v,t) = \sum_{j=o}^{2N-1} \frac{\phi_{2N}(v)}{\sqrt{2}} \frac{w_j(x,t)}{\lambda_j - v} \tag{42}$$

and that

$$w_k(x,t) = \frac{g(x,\lambda_k,t)}{\sqrt{2N+1}\ \phi_{2N+1}(\lambda_k)} \tag{43}$$

Equation 42 is exact for all values of the velocity only if $g(x,v,t)$ can be represented by a finite series of the form Eq. 21. For an arbitrary distribution function, however, it can be satisfied at the 2N distinct zeros of $H_{2N}(\lambda)$. Imposing this requirement leads to the following boundary and initial conditions for $w_k(x,t)$:

$$w_k(x,0) = \frac{g^{(0)}(x,\lambda_k)}{\sqrt{2N+1}\ \phi_{2N+1}(\lambda_k)} \qquad (k = 0,1,\ldots\ 2N-1) \qquad (44)$$

$$w_k(0,t) = \frac{g^{(1)}(\lambda_k,t)}{\sqrt{2N+1}\ \phi_{2N+1}(\lambda_k)} \qquad (k = 0,1,\ldots\ N-1) \qquad (45)$$

$$w_k(1,t) = 0 \qquad (k = N,N+1,\ldots\ 2N-1) \qquad (46)$$

since $\phi_{2N+1}(\lambda_k)$ is nonzero when λ_k is a root of $H_{2N}(\lambda) = 0$.

METHOD OF CALCULATION AND CONVERGENCE CRITERIA

The hyperbolic system Eq. 37, subject to the boundary and initial conditions Eqs. 44, 45, and 46, has been programmed for an IBM 7090 computer by use of a difference scheme essentially the same as that developed by Keller and Wendroff (14) for the neutron transport equation. Some simplifications are possible for the class of problems under consideration here, but the details are still involved and will be given elsewhere. The same situation prevails for the proof that the difference approximation really does converge to the hyperbolic system provided that certain relations are maintained on the mesh ratios.

The situation concerning the convergence of the solutions of the hyperbolic system to the corresponding solution of the transport equation is less satisfactory. Even for the extensively exploited spherical harmonic method, no general convergence proof seems to have been established. Such a proof has, however, been carried through by Kofink (12) at least semirigorously for the case of the Milne problem in neutron transport theory. The appearance of the fictitious source term results in a nonuniform convergent process, and much care must be taken in this exactly soluble problem to ensure that the spherical harmonic method will yield in the limit the well-known Wiener-Hopf solution. The situation is much better as far as convergence of the moments is concerned, and the exact treatment of the problem, as well as the experience gained from use of the method, seems to indicate that the method is eminently satisfactory for them.

Though we do not yet have a complete convergence proof, we have been able to use the theory of Jacobi matrices, as developed in Stone (15) and Smirnow (16), to prove that the truncated Jacobi matrices introduced earlier are in fact approximating operators to one and the same essentially self-adjoint operator in Hilbert space; and moreover, that the

Jacobi matrices $A(\theta)$ are all unitary equivalent C matrices in the sense of Von Neumann (compare Smirnow). The resulting operator has a simple continuous spectrum covering the entire λ axis. Hopefully, these results will eventually permit a rigorous proof of the convergence of the solutions of Eq. 37 to those of the transport equation in a Hilbert space context, at least for the case where it is assumed that $\partial e/\partial x$ is known.

GENERAL OBSERVATIONS ON THE METHOD

Although our actual numerical experience with the described method is still much too limited to permit firm conclusions, it tends to support the over-all conclusions reached by Weinberg and Wigner (11) for the case of the spherical harmonic method. The weakness of their method is also present here. It consists essentially of the appearance of the Gibbs phenomenon, or the nonuniform convergence of expansions of the form Eq. 21, in the neighborhood of an interface separating two media -- in our case at $x = 0$ and $x = 1$. This phenomenon causes the calculated approximate distribution function to become negative in some regions where it is supposed to vanish identically. The effect on the moments calculated by this means is much smaller, since the resulting oscillation from positive to negative values contributes much less to any moment integral than would the negative values alone. To any problem where this might prove serious the modifications devised by Yvon (17) for the neutron case could be adapted, but not without a considerable increase in computational complexity.

Nothing in our experience as yet would seem to contradict the following general statement of Weinberg and Wigner (11):

> At present, with so much of the practical work on reactor design being done with large digital computers, the arguments in favor of one method of approximation rather than another tend to center around the question of how well suited the method is for digital computers. Actually as the computers become larger the choice between methods becomes less and less clear; any method which converges will do if the computer is large enough. This viewpoint certainly has practical merit; however, convenience for a digital computer is hardly a substitute for intrinsic mathematical beauty or physical relevance. In this respect the spherical method is most satisfying; its first order is identical with diffusion theory, and its higher order shows the deviations from diffusion theory very clearly.

Finally, as we gain experience, we confidently expect that the method developed here will eventually play the same role in a wide variety of electron-plasma problems as the spherical harmonic method does in neutron transport theory.

REFERENCES

1. Korevaar, J., Pansions and the Theory of Fourier Transforms, Trans. Am. Math. Soc., 91:53 (1959).

2. Bellman, R., Applied Dynamic Programming, Princeton University Press, Princeton, N. J., 1962.

3. Wing, G. Milton, An Introduction to Transport Theory, John Wiley, New York, 1962.

4. Grad, H., On Kinetic Theory of Rarefied Gases, Communs. Pure and Appl. Math., 2:331 (1949).

5. Grad, H., Note on N-Dimensional Hermite Polynomials, Communs. Pure and Appl. Math., 2:325 (1949).

6. Brillouin, L., The Traveling-Wave Tube (Discussion of Waves of Large Amplitude), J. Appl. Phys., 20:1196 (1949).

7. Rynn, D., and Watkins, D., Effects of Velocity Distribution on Traveling-Wave Tube Gain, J. Appl. Phys., 25:1375 (1954).

8. Widlund, O., On the Expansion of Generalized Functions in Series of Hermite Functions, Kgl. Tek. Högskol. Handl. (Trans. Roy. Inst. Technol. Stockholm), No. 173, 1961.

9. Lighthill, M. J., An Introduction to Fourier Analysis and Generalized Functions, Cambridge University Press, New York, 1958.

10. Dolph, C. L., The Extant Nonlinear Mathematical Theory of Plasma Oscillations, Army Research Symposium on Nonlinear Mathematics, University of Wisconsin Press, Madison, 1963.

11. Weinberg, A., and Wigner, E., The Physical Theory of Reactors, University of Chicago Press, Chicago, 1958, Ch. IX.

12. Kofink, W., Studies of the Spherical Harmonic Method in Neutron Transport Theory, Suppl. Nuovo cimento, IX (Ser. X):497 (1958).

13. Dolph, C. L., and Lomax, R. J., The Nonlinear Theory of Multistream Devices, EPL Memo 62-5-05003, The University of Michigan, Ann Arbor, August, 1962, 21 pp.

14. Keller, H. B., and Wendroff, B., On the Formulation and Analysis of Numerical Methods for Time Dependent Transport Equations, Communs. Pure and Appl. Math., 10:567 (1957).

15. Stone, M. H., Linear Transformations in Hilbert Space and Their Application to Analysis, Colloquium Pub. 15, American Mathematical Society, New York, 1932.

16. Smirnow, W., Lehrgang der höheren Mathematik, Berichtigte Aufl. Hochschulbücher für Mathematik, vol. 5, Deutscher Verlag der Wissenschaften, Berlin, 1961.

17. Yvon, J., La Diffusion Macroscopique des Neutrons une Methode d'Approximation, J. Nuclear Energy, 4:305 (1957).

BEAM-PLASMA AMPLIFIER EXPERIMENTS

Paul Chorney
Microwave Associates, Inc.
Burlington, Massachusetts

ABSTRACT

Experimental work is described that is directed toward demonstrating the feasibility of using the beam-plasma interaction to amplify millimeter waves. Discharges with plasma frequencies near 60,000 Mc were generated by means of a dual hot-cathode Penning discharge at low pressures. The densities were measured by Langmuir probe techniques. Extensive amplification experiments performed at 10,680 Mc produced net gains as high as 25 db and electronic gains as high as 60 db. The original study vehicle was redesigned, and preliminary results show substantial net gains.

Several research programs are in progress at Microwave Associates to determine the feasibility of using the beam-plasma interaction to amplify microwaves. Most of the work has been concerned with the amplification of millimeter waves. Toward this goal, interaction experiments have been conducted in X band, and densities have been generated with corresponding plasma frequencies in the millimeter wave region. Some of this work is described here.

PRINCIPLE OF BEAM-PLASMA INTERACTION AND AMPLIFICATION

Shown in Fig. 1 is a block diagram of a beam-plasma amplifier. It is similar to any linear beam amplifier, except that the interaction region is replaced by a plasma. In this amplifier an electron gun delivers an electron beam to an input coupler, an interaction space, an output coupler, and finally to a collector. The couplers usually are cavities, helices, or other conventional tube couplers.

The operation of the amplifier is as follows. A signal is introduced into the input coupler, and the input coupler transduces the signal to a density modulation of the electron beam, or a bunching of the electron beam. The modulated beam drifts into the plasma interaction region, where the modulation of the beam grows exponentially because of the beam-plasma interaction. (The beam-plasma interaction we speak of here is commonly known as the two-stream instability.) The modulated beam emerges from the plasma with enhanced modulation and passes through the output coupler, where the modulation of the beam is transduced to microwave energy. If the couplers and the plasma are properly designed, the output signal will be greater than the input, resulting in amplification.

The very elementary one-dimensional theory for an electron beam drifting through a cold, collisionless plasma predicts the propagation constant

$$k = \frac{\omega}{v_o} \pm \frac{\omega_{pb}}{v_o} \left(1 - \frac{\omega_{pp}^2}{\omega^2}\right)^{-\frac{1}{2}} \qquad (1)$$

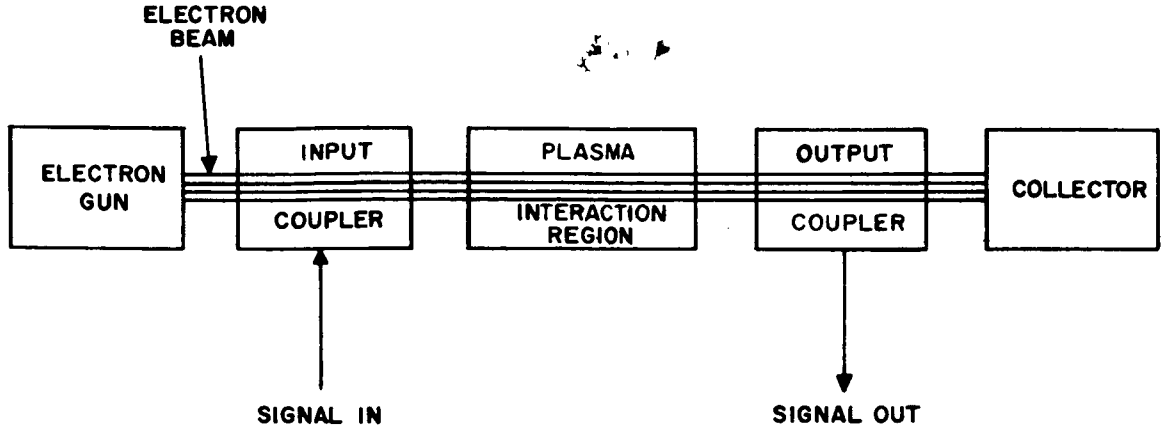

FIG. 1. Block diagram of beam-plasma amplifier.

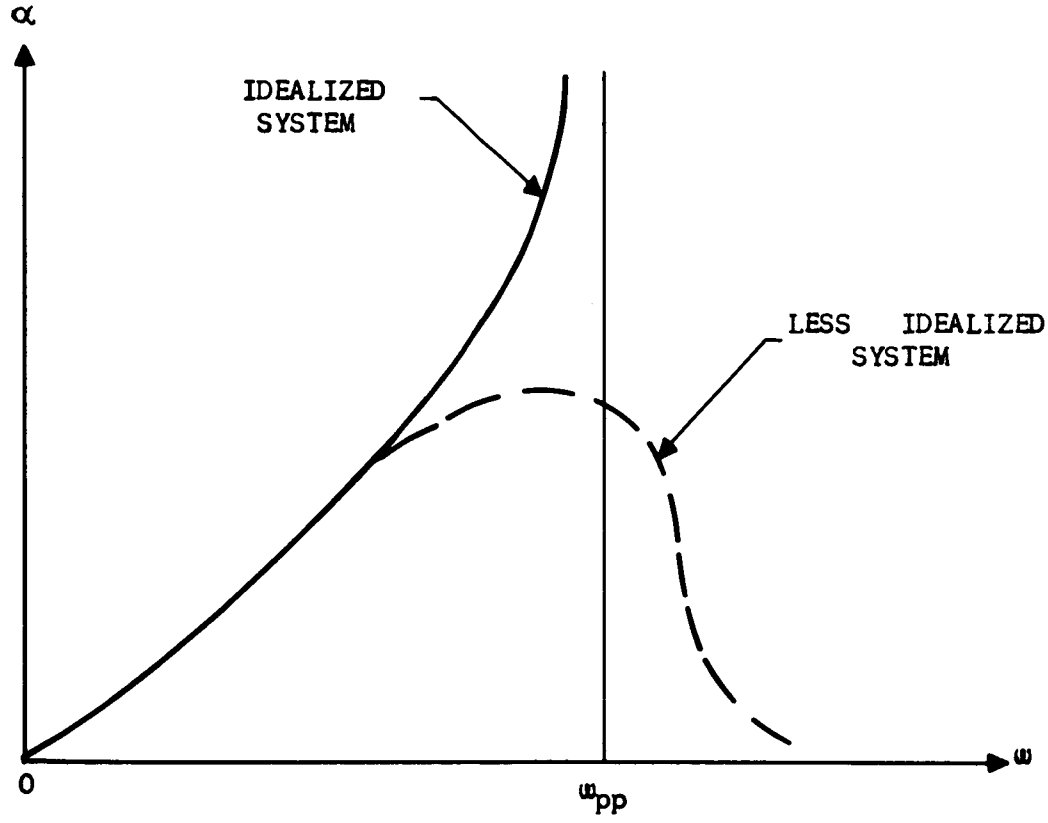

FIG. 2. Theoretical frequency behavior of growth constant.

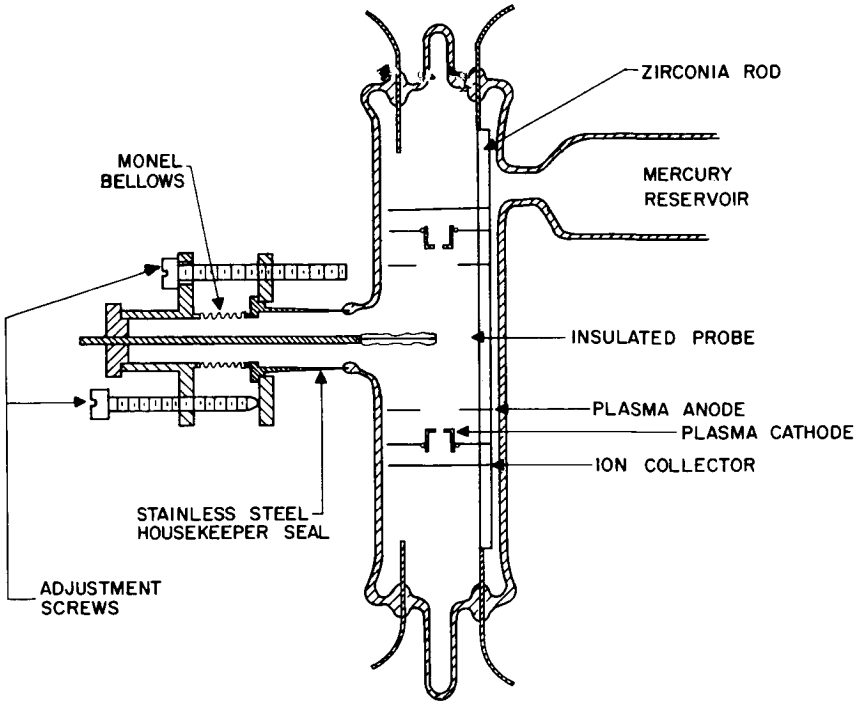

FIG. 3. Langmuir-probe plasma tester.

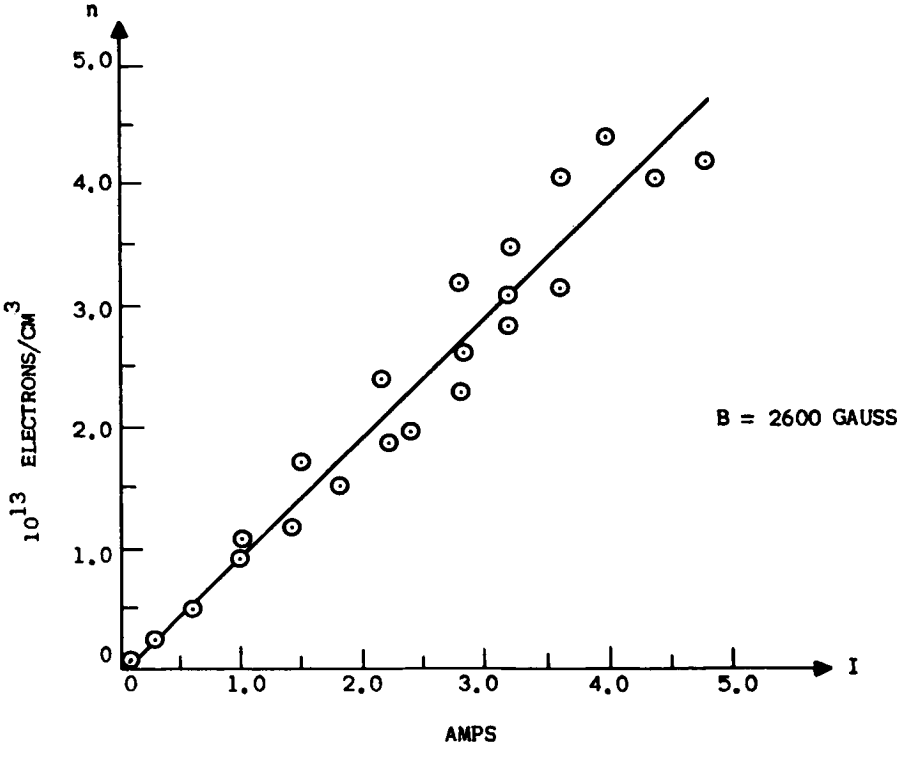

FIG. 4. Plasma density versus discharge current.

when the dependence exponent ($j\omega t - jkz$) is assumed. In Eq. 1, ω is the radian frequency, v_o is the drift velocity of the beam, ω_{pp} is the plasma frequency of the plasma, and ω_{pb} is the plasma frequency of the beam. For frequencies below the plasma frequency, k is complex, the imaginary part being given by

$$\alpha = \frac{\omega_{pb}}{v_o}\left(\frac{\omega_{pp}^2}{\omega^2} - 1\right)^{-\frac{1}{2}} \qquad (2)$$

Equation 2 is sketched in Fig. 2, where it is seen that the gain becomes infinite at the plasma frequency. This is the result of a very idealized model. Figure 2 also shows qualitative results for a less idealized model, that is, one which accounts for finite plasma temperature, collisions, finite geometry, and magnetic fields. The infinite gain at the plasma frequency becomes finite, but the gain per unit length is very large compared with that of interaction mechanisms normally used in microwave tubes. Gains of 15 to 20 db/cm are typical.

Besides the very high unit-length gains, the beam-plasma interaction offers other attractions. High powers can be handled at high frequencies (millimeter waves), since delicate mechanical structures are replaced by the gaseous plasma. In conventional microwave and millimeter-wave devices, beam interception and rf dissipation on delicate interaction structures limit power-handling capability. Employing the plasma as an interaction structure also eliminates the difficult problem of fabricating mechanical structures with dimensions necessarily much smaller than the wavelength of interest.

PLASMA GENERATION EXPERIMENTS

Several methods of generating high plasma densities were considered. The method found to be the most practical and most efficient was the dual hot-cathode Penning discharge. The experimental tube constructed to study this discharge (Fig. 3) contains a Langmuir probe mounted on a movable metal bellows that allows the probe to be positioned across the diameter of the column. The spacing between cathodes is 1.5 in., and the cathode diameter is 0.250 in. The cathodes are normally run at about 900° C. The gas atmosphere is mercury vapor, and the discharge tube is operated in an axial magnetic field.

Some typical data from this discharge tube are shown in Fig. 4, where plasma density is plotted against discharge current. Note that the density seems to be linear with the discharge current. The spread in the points is due to heating of the probe while the curves were being recorded. The electron density and the plasma temperature are obtained from the Langmuir probe curves. The plasma temperature was about 2 ev. The magnetic field was 2600 gauss, and the background pressure was about 2×10^{-3} Torr. The highest densities shown in Fig. 4 correspond to plasma frequencies of about 60,000 Mc. The voltage drop across the tube in producing these plasma densities is about 15 v. The power expenditure is therefore quite modest, about 75 w.

The percentage of ionization is very high. At the pressure of 2×10^{-3} Torr. the neutral density is about 6×10^{13} cm^3. Low pressures are necessary in beam-plasma amplifiers, because the mean free path of the electron beam must be long so that the beam passes through the tube without being scattered appreciably.

AMPLIFICATION EXPERIMENTS

Several vehicles have been constructed to study beam-plasma amplification. In one of these tubes, shown in Fig. 5, the cavities are coupled by means of loops to miniature coaxial lines. The cavity resonators are of the common klystron variety, being re-entrant so that very strong electric fields appear on the axis in the vicinity of the beam. The plasma is generated by a Penning configuration. The distance between cathodes is 1.5 in., and their diameter is 0.250 in. as in the plasma testers. A hole in the center of each cathode allows the passage of the electron beam, which is 0.040 in. in diameter and can be adjusted to deliver several milliamperes at a few thousand volts. A detail of the construction is shown in Fig. 6.

Extensive amplifier data was gathered from such a study vehicle. The experiments were conducted at a frequency of 10,680 Mc, and the magnetic focusing field was 1400 gauss. Table 1 gives some typical amplifier data. In this table, I_b is the beam current, V_b the beam voltage, and I_p the plasma discharge current. For each setting two gains are given, net gain and electronic gain. Net gain is defined as the decibel equivalent of the ratio of output power to input power in the presence of the plasma. Electronic gain is the decibel equivalent of the ratio of output power in the presence of the plasma to output power in the absence of the plasma, the conditions on the beam being identical. The difference between the net gain and the electronic gain is attributed to loss in the couplers. The electronic gain may be regarded as the amplification due to the beam-plasma interaction.

TABLE 1. Typical Amplifier Data

I_b, ma	V_p, volts	I_p, ma	Net Gain, db	Electronic Gain, db
1.05	715	28	10	45
1.50	960	35	13	52
1.31	715	32	18	61
1.77	755	33	22	66
3.30	880	33	25	61

More amplifier data are shown in Fig. 7, where both electronic gain and net gain are plotted as a function of the perveance of the beam. The perveance K is defined by $K = I_b/V_b^{3/2}$, which is directly proportional to ω_{pb}^2/v_o^2.

FIG. 5. Beam-Plasma amplifier study vehicle.

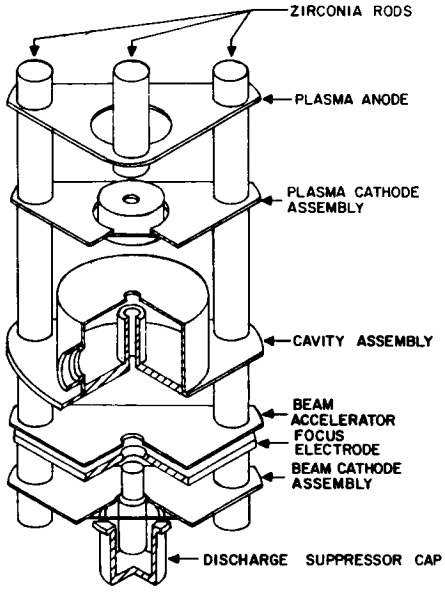

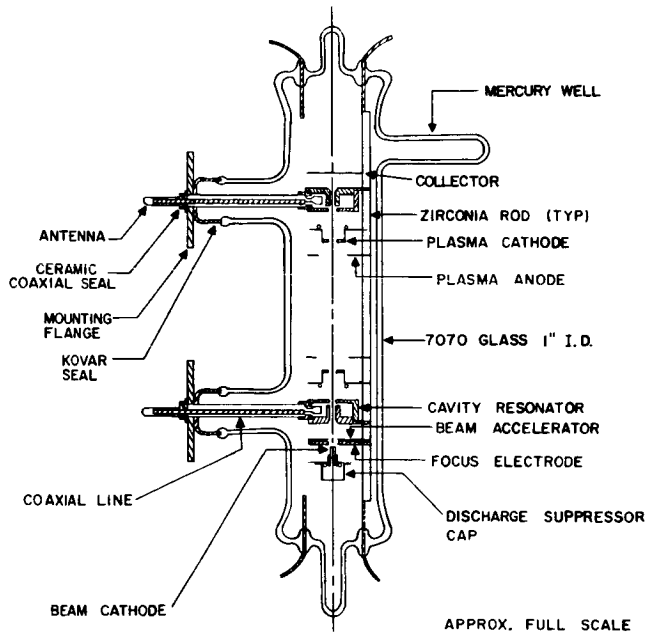

FIG.6. Construction detail, beam-plasma amplifier.

FIG. 7. Gain versus perveance.

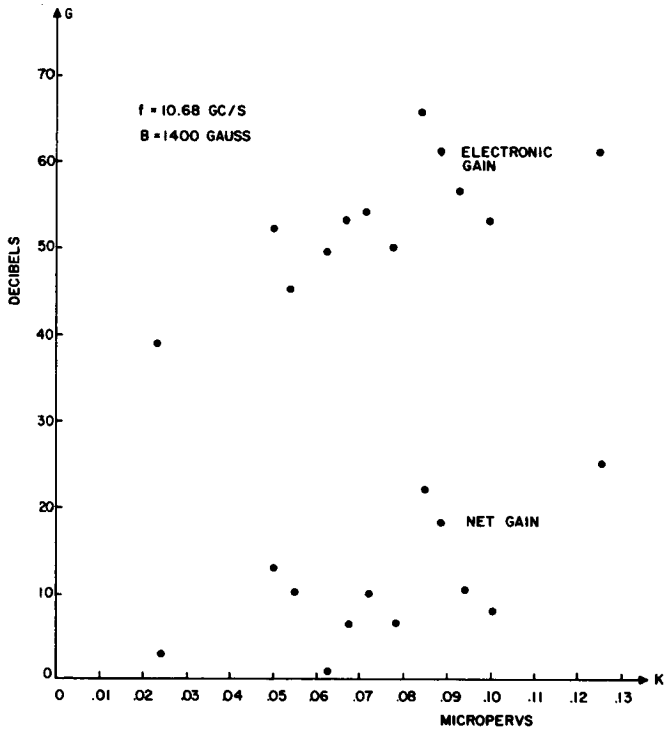

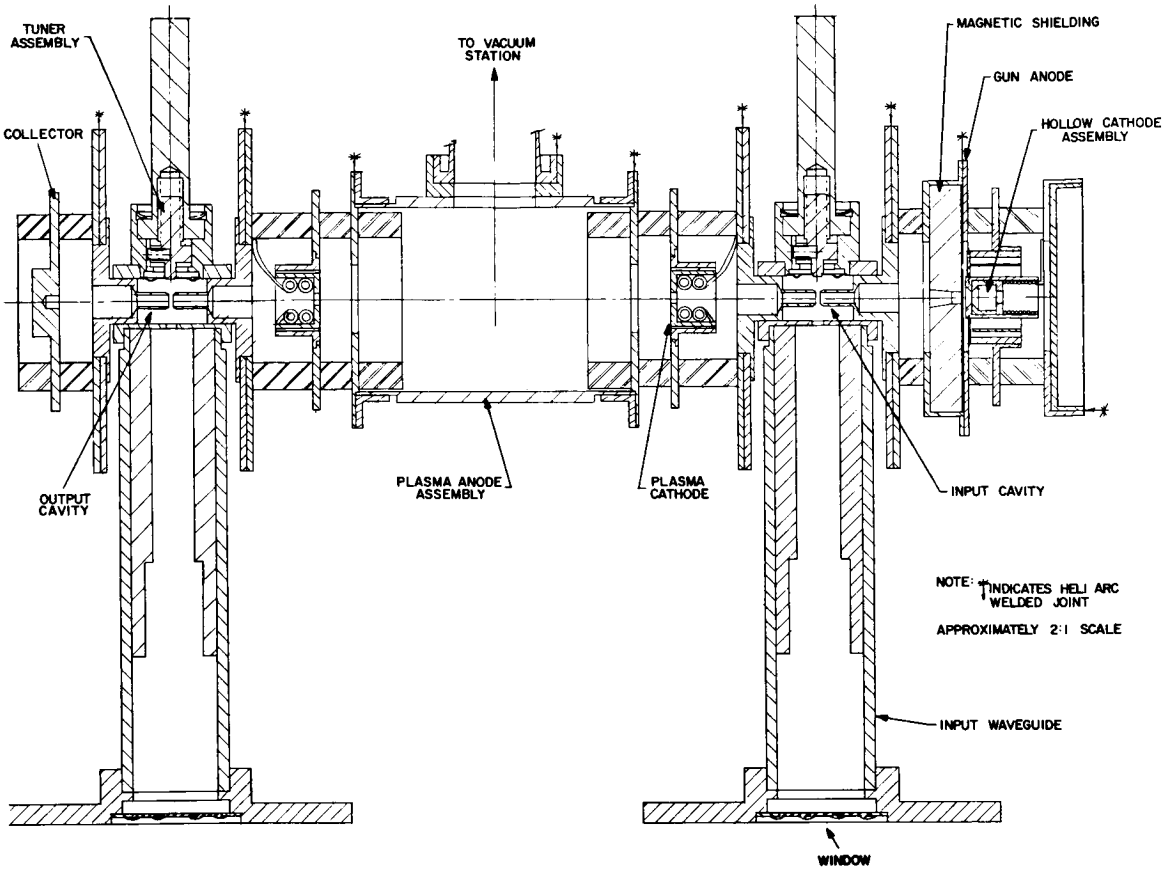

FIG. 8. Metal and ceramic beam-plasma amplifier study vehicle.

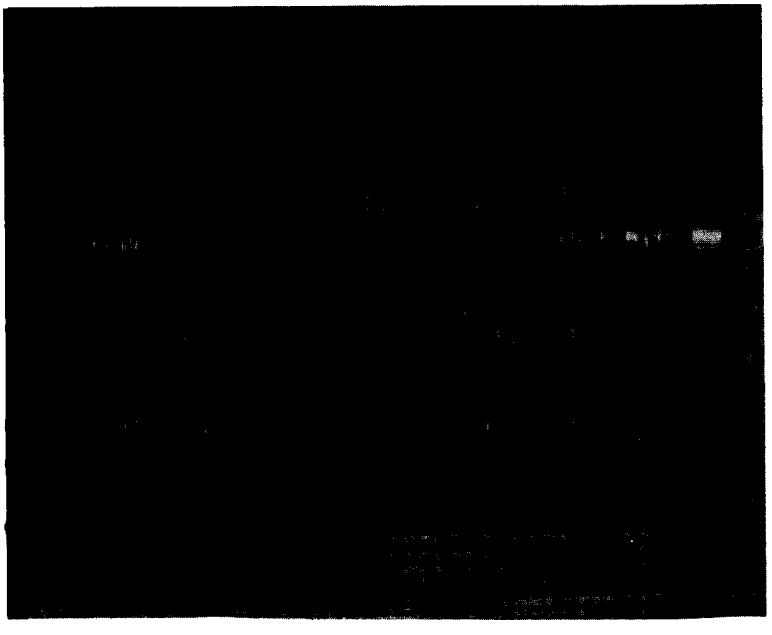

FIG. 9. Modified study vehicle.

A more refined study vehicle, recently completed, is shown in Figs. 8 and 9. The essential dimensions of the tube are identical to those of the tube described earlier. The new vehicle is constructed entirely of metal and ceramic disks, a type of construction offering many advantages. For instance, the cavities can be tuned, whereas the tuning of cavities in the previous tube was fixed. Incorporated into this vehicle is an improved gun, which employs a hollow cathode. Only preliminary experimental data are available at this time. A net gain of 30 db has been observed with an electron beam of 1 ma at 1100 v, a frequency of 11,000 Mc, and a focusing magnetic field of 1300 gauss.

CONCLUSIONS

Experiments with the equipment here described have demonstrated that substantial net gains can be obtained from the beam-plasma interaction. These experiments have been conducted at relatively long wavelengths as compared to our ultimate goals. Three-centimeter wavelengths have been studied, whereas 4 mm wavelengths and shorter are of interest. The plasma densities necessary for the amplification of 4 mm wavelengths have been produced quite conveniently. The feasibility of amplifying millimeter waves by means of the beam-plasma interaction has yet to be proved, but present results are encouraging.

ACKNOWLEDGMENT

The author wishes to express his appreciation to O. L. Cunningham, D. J. Fitzgerald, and J. Valun for their help in the construction and testing of the experimental tubes. This work is sponsored by the Department of the Navy, Bureau of Ships, under Contract No. NObsr 81206.

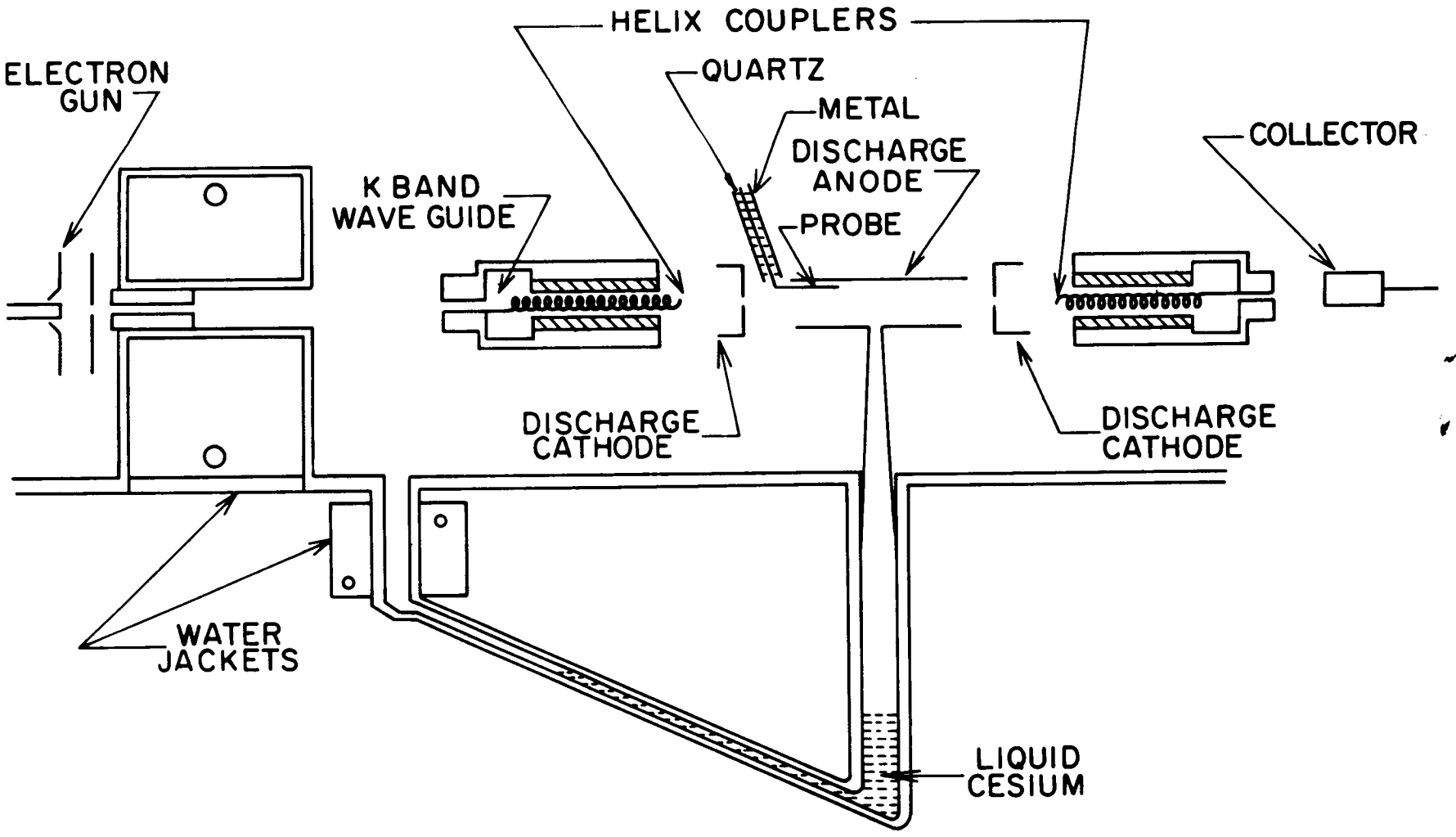

FIG. 1. Schematic of electron beam-plasma amplifier.

EFFECT OF NONUNIFORM PLASMA DENSITY ON ELECTRON BEAM-PLASMA INTERACTION

G. A. Swartz and L. S. Napoli
RCA Laboratories
Princeton, New Jersey

ABSTRACT

A 23 kMc microwave amplifier that utilizes the two-stream instability as a gain mechanism was constructed. The two-stream instability is generated by passing a 1400 v electron beam through a cesium plasma 3 cm long, with a density that can be varied in a range up to 10^{13} ions/cm^3. The plasma is generated by a Penning discharge. Microwave power is coupled on and off the beam with helices. The electronic gain shows a maximum at one or more measured plasma densities. The number of maxima depends on the magnetic field, percent ionization of the plasma, electron temperature of the plasma, and the input power level. The maximum electronic gain is 40 db, and the net gain for the tube is 8 db. A probe placed in the plasma 1.5 mm from the beam indicated an increase in the saturated ion current to the probe as the microwave power was increased above 1 mw.

Author

Numerous theoretical and experimental investigations of the two-stream plasma instability have been carried out in recent years (1-8). In our investigation of an electron beam interaction with a high density cesium plasma, some interesting effects were observed that are believed related to the plasma nonuniformity.

Observation of the rf signal gain as a function of plasma density showed a maximum at one or more plasma densities. The number of maxima and their relationship to the measured density depended on such factors as magnetic field, percent ionization of the plasma, electron temperature, and power level of the input signal. The observations indicate that a plasma density variation along the electron beam radius is responsible for the occurrence of multiple maxima.

EXPERIMENTAL TUBE

A 23 kMc microwave amplifier that utilizes the two-stream instability as a gain mechanism was constructed. A schematic of the tube is shown in Fig. 1. Electrons from a Phillips "L" cathode are accelerated to 1350 v, and the electron beam is sent through an input helix coupler, a cesium plasma 3 cm long, and an output helix coupler, to a collector. The diameter of the beam is determined by a 0.035 in. ID drift tube in front of the gun. A Penning discharge is used to generate the plasma. The plasma density can be increased to above 10^{13} ions/cm^3. A cylindrical probe 0.025 cm in diameter and 0.5 cm long is placed in the plasma, 0.5 mm from the anode wall and parallel to the beam axis. The probe lead is shielded from the plasma region back to the glass envelope.

Holes 0.050 in. in diameter in the faces of the Penning discharge cathodes allow the electron beam to pass through the plasma. A magnetic field parallel to the beam axis serves to confine the electron beam and the plasma electrons in the discharge.

Cesium vapor is supplied to the discharge through a conical feed tube extending from a cesium well beneath the discharge to a hole in the discharge anode. The cesium well temperature is kept near 180° C. A water jacket is placed around the drift tube of the electron gun to cool the drift tube and the glass walls separating the electron gun region from the rest of the tube. Cesium condenses on the glass walls and drift tube. Thus the amount of cesium vapor that gets into the electron gun region is minimized, and the vapor pressure in the gun region is kept below 10^{-5} mm Hg. This allows operation of the gun at voltages up to 2000 v. The cesium is recycled via a tube connecting the cesium well to a second water-cooled condenser. The remaining walls of the tube section that houses the helices and plasma are kept at a temperature above 100° C to ensure that all the vapor will condense on the water jacket walls.

The input and output helices are installed perpendicular to the broad face of a K-band waveguide, with triple stub tuners in the waveguide to provide a proper match between the waveguide and helix. One end of the waveguide is shorted, and the other end is open and butted against the glass envelope. Another section of waveguide is butted against the outside of the glass envelope, and microwave power is transmitted through the glass envelope. It is expected that the system would be improved if the waveguides passed through the envelope, but it proved to be adequate for the experimental investigations described.

OPERATION

The tube is capable of operating as an amplifier, or with the addition of a feedback loop, as an oscillator. Microwave power fed through the input waveguide to the input helix induces a space-charge wave on the electron beam passing through the input helix. The wave is amplified as the beam penetrates the plasma. Microwave power is extracted from the space-charge wave as the beam passes through the output helix. The microwave circuit is shown in Fig. 2.

The circuitry for the operation of the tube is shown in Fig. 3. The electron beam current to the collector is about 1 ma. The anode of the electron gun is raised to a potential several hundred volts positive with respect to the drift tube, to form an ion trap and protect the gun cathode from ion bombardment. The collector is biased positive with respect to ground to prevent secondary electrons from traveling back along the beam.

Power for the discharge is supplied from a constant voltage source, and the discharge voltage is kept between 10 and 15 v. The most stable plasma, as indicated by the probe, is produced with an 11 v discharge. If the discharge voltage is less than 10 v, the probe indicates a 50 percent density fluctuation at a frequency of 100 kc. In an 11 v discharge, the density fluctuation is reduced to 10 to 15 percent a frequency of about 1 Mc.

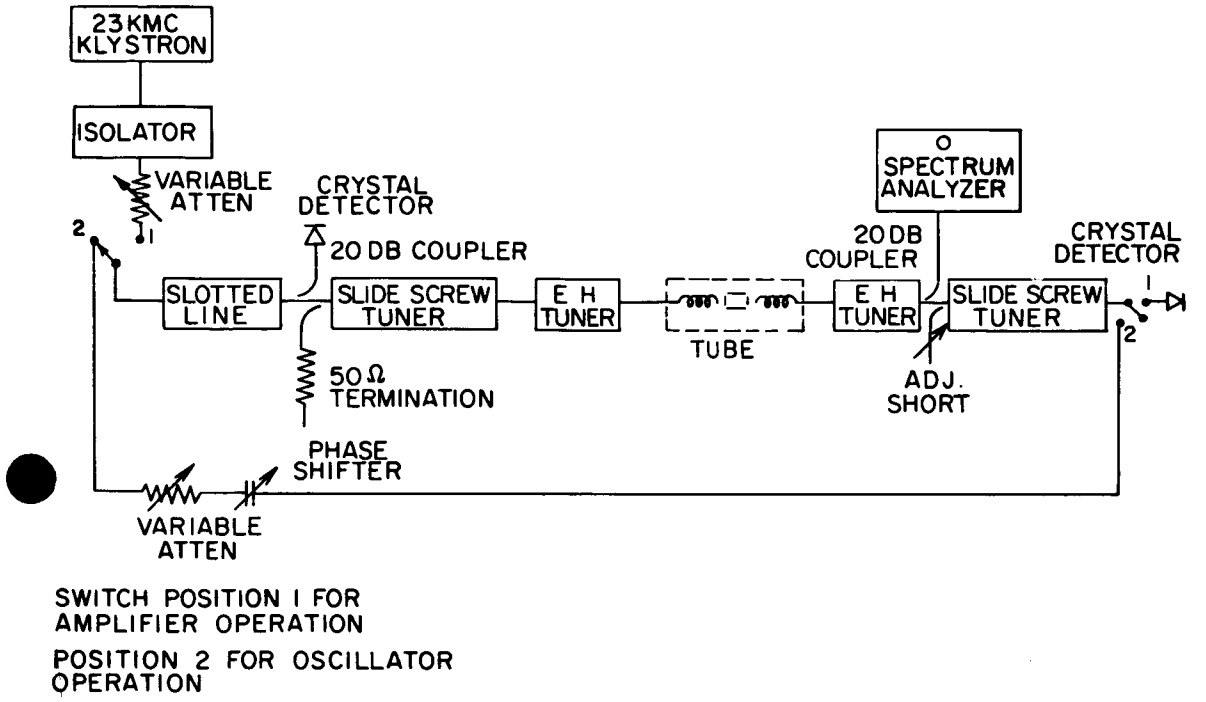

FIG. 2. Microwave circuit for electron beam-plasma tube.

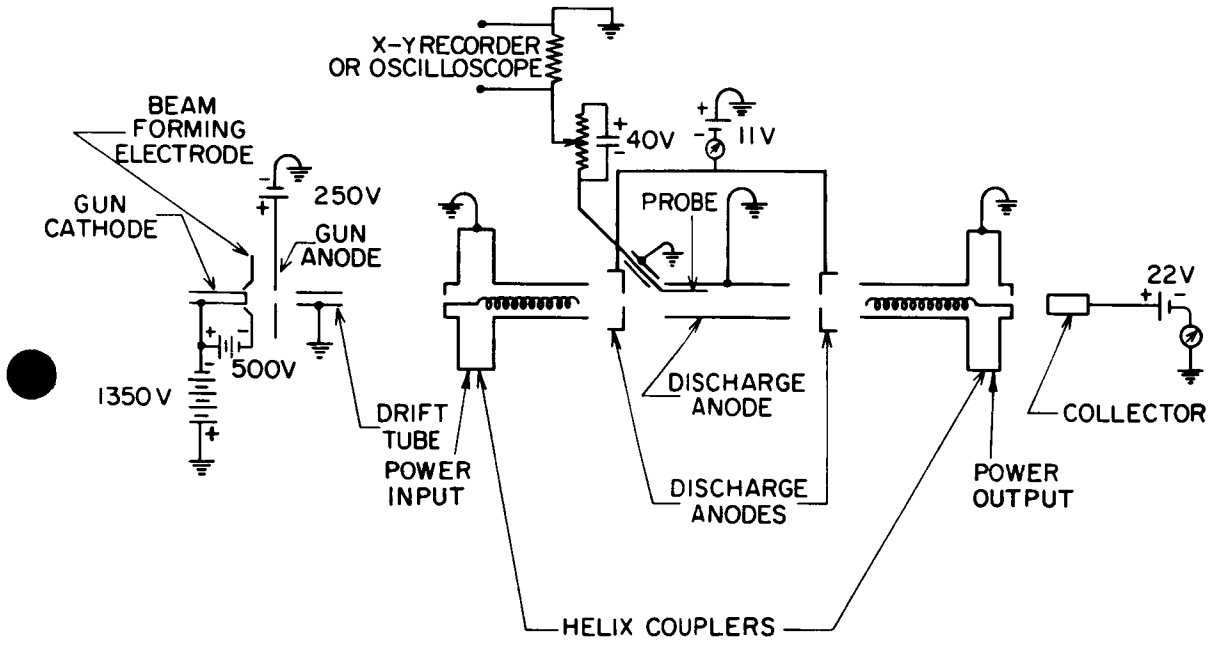

FIG. 3. Electron gun, discharge and probe circuits.

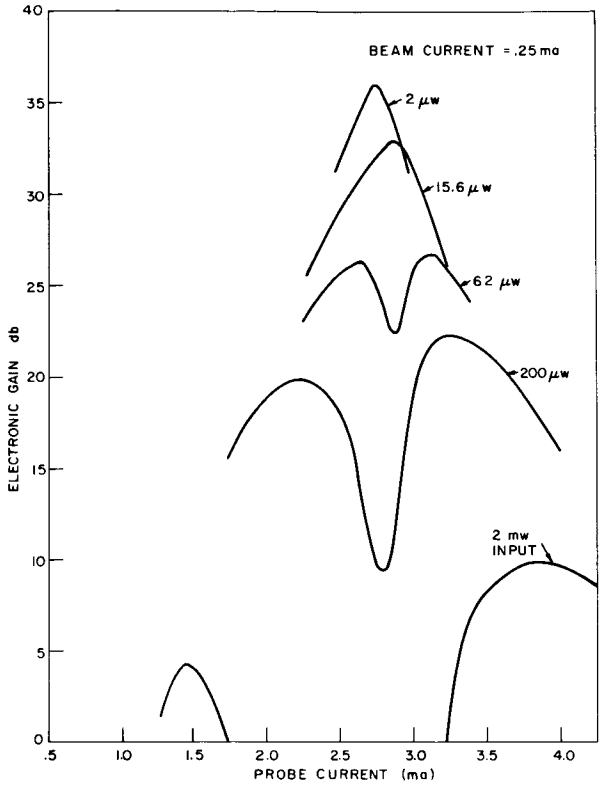

FIG. 4. Electronic gain versus probe current for various input power levels.

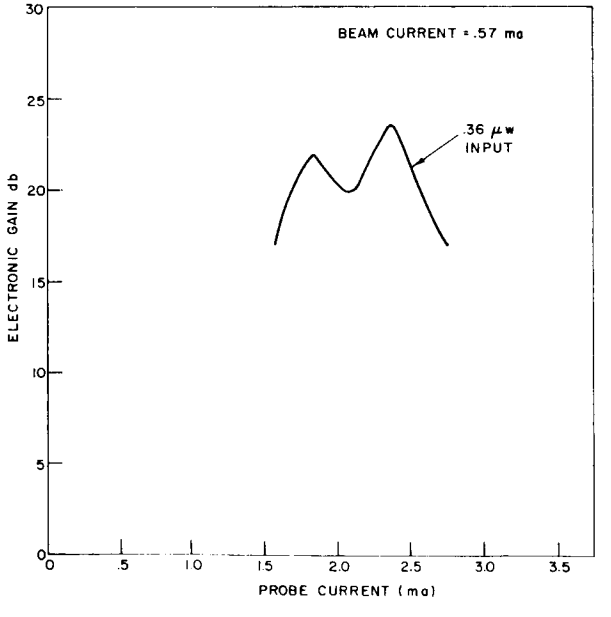

FIG. 5. Electronic gain versus probe current at low input power after some deterioration of tube.

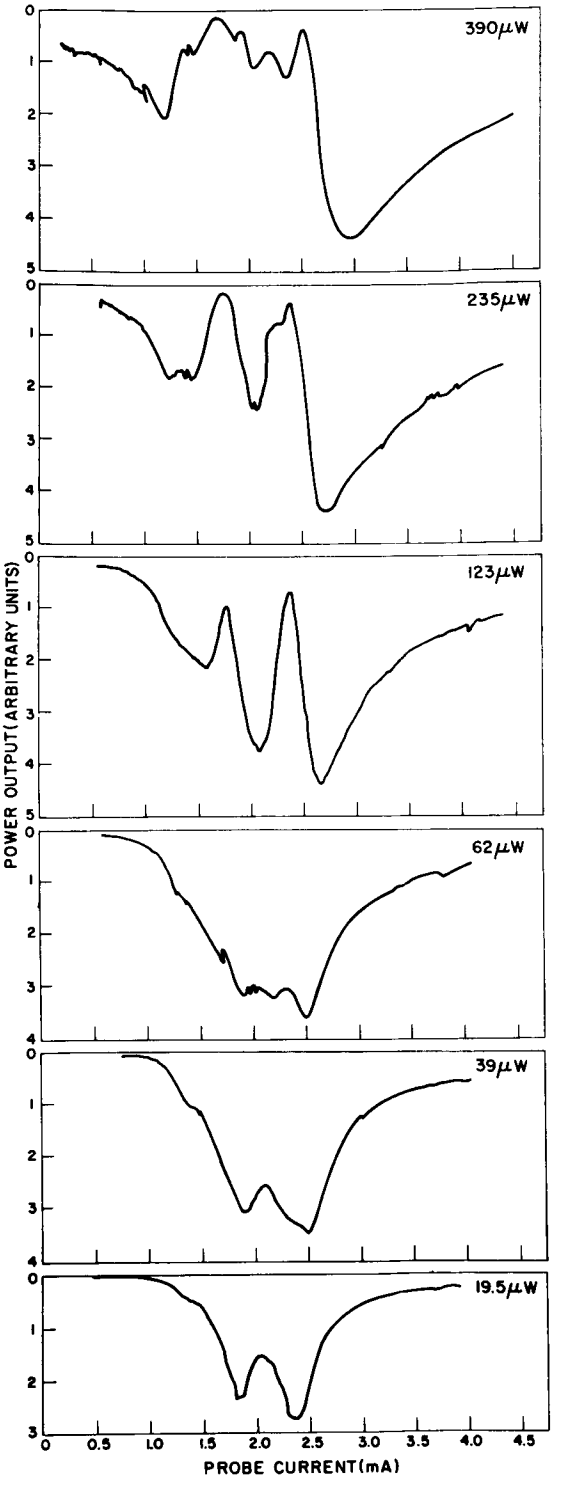

FIG. 6. Electronic gain versus probe current at intermediate input power levels.

RESULTS

The variation of output power with plasma density was measured in two different ways. In the first method, the discharge voltage is maintained at 11 v and the vapor pressure in the cesium well is slowly increased. The rectified rf output (detecting-crystal current) is measured on an x-y recorder and plotted as a function of the ion current to the probe. In the second method, the discharge power is supplied by a constant current source. The discharge current and the cesium vapor pressure are maintained high enough to ensure a plasma frequency in the discharge greater than the applied frequency. The discharge anode and cathode are then shorted together, and the plasma is allowed to decay. During the plasma decay, the ion current to the probe and the output power are observed as a function of time on an oscilloscope.

Measurement by the first method of the electronic gain as a function of the probe current is shown in Fig. 4 for various input powers. The electronic gain in decibels is defined here as the log of the ratio of the output power with plasma present to that without plasma present. As the input power is increased, power saturation occurs, the gain decreases, and two gain maxima appear. The separation of the maxima increases with input power.

After much use of the tube, two gain peaks instead of one occurred at very low input powers, as shown in Fig. 5. The electronic gain decreased by 10 to 15 db. At intermediate input power three gain peaks were observed. Presumably, some of the plasma properties may have been altered by some deterioration of the plasma cathodes. Figure 6 shows the output power in arbitrary units as a function of the probe current for various intermediate input powers. At 390 μw input there are two obvious widely separated maxima and some additional structure. At 235 and 123 μw input there are three maxima, whereas at 19.5 μw input there are again two maxima. Note that the two "low power" maxima appear at the same probe current as the two minima that occur for input powers of 235 and 123 μw.

When the output power was measured in the decaying plasma, the results were in some ways different from the results previously described. At high input power, the results were the same. Two maxima occurred and separated as the input power increased. At low input power, however, the number of maxima is dependent on the magnetic field strength, the percent ionization, and the electron temperature. Figure 7 shows simultaneous oscilloscope traces of the output power and probe current for magnetic field strengths of 1900 gauss and 1200 gauss. At 1900 gauss there are two widely separated maxima, while at 1200 gauss the two maxima have almost emerged into one. Figure 8 shows output power and probe current traces with a magnetic field of 1700 gauss. The cesium well pressure in (b) of Fig. 8 is 0.07 mm Hg and there are two maxima, whereas in (a) the well pressure is 0.12 mm Hg and there is only one maximum.

In another experiment the magnetic field and cesium vapor pressure were kept constant, but the electron temperature was varied. The discharge power was decreased, and thus the initial plasma density before

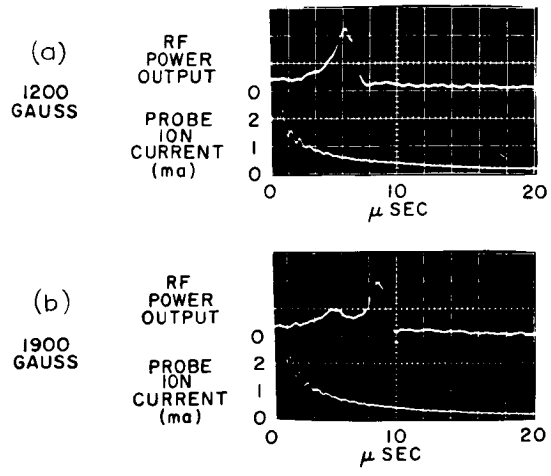

FIG. 7. Output power and probe ion current in afterglow at two magnetic field strengths.

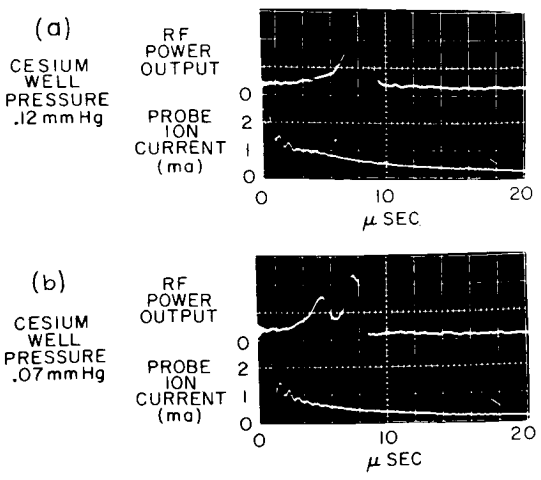

FIG. 8. Output power and probe ion current in afterglow at two vapor pressures.

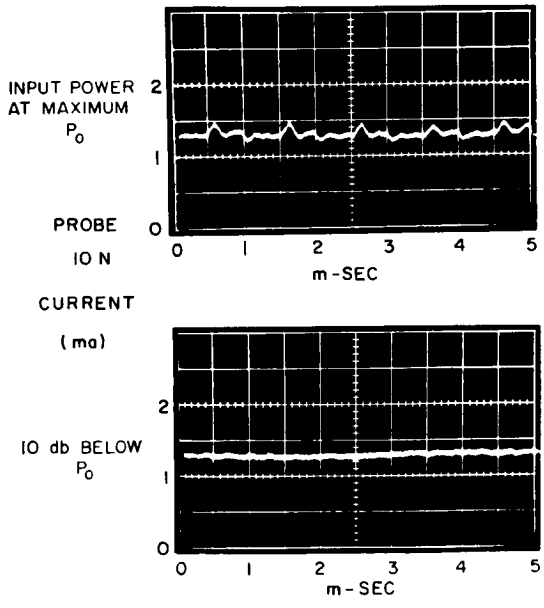

FIG. 9. Effect of high input power on saturation ion current to probe, input power modulated at 1 kc/sec.

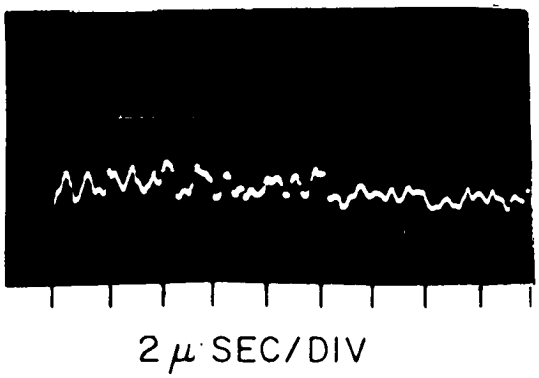

FIG. 10. One Mc fluctuation of output power.

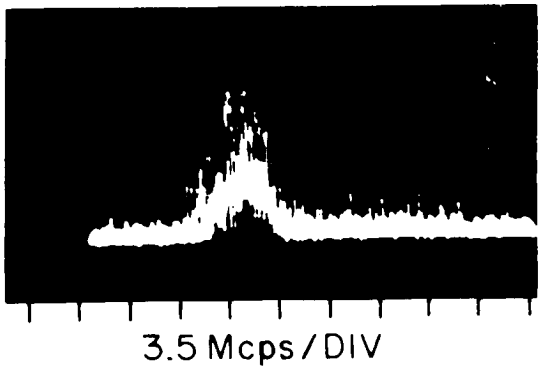

FIG. 11. Frequency spectrum during oscillation.

decay was decreased. The time from initiation of the plasma decay to the time at which $\omega_p = \omega$ is thus reduced. The electron temperature is correspondingly higher, because the electrons have had less time to lose their energy. With high energy electrons present in the plasma, a double peak was observed; with more of the lower energy electrons present, a single peak was observed.

As the 23 kMc input power was increased above 1 mw, the ion current to the probe and the plasma electron current that reached the collector increased noticeably. Figure 9 shows the probe current for two input power levels. The input was modulated at 1 kc.

At input powers below 1 μw and 1 ma beam current, the maximum electronic gain under single-peak conditions is 40 db and the net gain for the tube is 8 db. The output power, measured by the crystal detector, is shown in Fig. 10. The power output fluctuated at approximately the same frequency as the plasma density, that is, 1 Mc. The tube could be made to oscillate by inserting the feedback loop shown in Fig. 2. Figure 11 shows the oscillation power in arbitrary units as a function of frequency. The bandwidth is about 3 Mc.

DISCUSSION

With a low power input, the double-peaked gain curves can be transformed to single-peaked curves by decreasing the magnetic field, increasing the density of neutral cesium, which increases the electron-neutral collision frequency, or decreasing the electron temperature. These changes tend to alter the plasma density profile along the radius of the beam.

The plasma density variation is dependent on the ratio of the axial diffusion rate to the radial diffusion rate. This ratio is proportional to the ratio of the ambipolar diffusion constant D_a to the magnet diffusion constant D_B.

$$D_a = \frac{D_- \mu_+ + D_+ \mu_-}{\mu_+ + \mu_-} \tag{1}$$

where D_- and D_+ are the diffusion coefficients of the electrons and ions respectively, and μ_+ and μ_- are the ion and electron mobilities (9). With the Einstein relationship

$$D/\mu = kT/e \tag{2}$$

and μ_+ much less than μ_-, D_a can be expressed as

$$D_a = D_+ \left(1 + \frac{T_-}{T_+}\right) = \frac{1}{3} v_+ \ell_+ \left(1 + \frac{T_-}{T_+}\right) \tag{3}$$

where v_+ = ion thermal velocity
ℓ_+ = ion mean free path
T_- = electron temperature
T_+ = ion temperature

With the ion gyro radius less than the cylinder diameter, the magnetic diffusion constant is (10)

$$D_B = \frac{1}{3} v_- \frac{r_c^2}{\ell_-} = \frac{1}{3} v_-^2 \frac{\nu}{\omega_c^2} \tag{4}$$

where v_- = electron thermal velocity
r_c = electron cyclotron radius
ℓ_- = electron mean free path
ω_c = electron cyclotron frequency
ν = electron collision frequency

The ratio

$$\frac{D_a}{D_B} = \left(1 + \frac{T_-}{T_+}\right) \sqrt{\frac{T_+}{T_-} \frac{m}{M}} \frac{\ell^2}{r_c^2}$$

$$= \left(1 + \frac{T_-}{T_+}\right) \sqrt{\frac{T_+}{T_-} \frac{m}{M}} \frac{\omega_c^2}{\nu^2} \tag{5}$$

where $\ell_+ = \ell_- = \ell$, and m and M are the masses of the electron and ion respectively.

As D_a/D_B increases, the plasma density variation along the radius increases and the plasma becomes partially hollow. A decrease in magnetic field tends to reduce the hollowness of the plasma. Calculations indicate that for the discharge used in these experiments the electron-ion collision frequency ν_i is the same order of magnitude as the electron-neutral collision frequency ν_m. For ion-electron collisions alone, $\nu^2 \propto T^{-3}$ and

$$\frac{D_a}{D_B} \propto \left(1 + \frac{T_-}{T_+}\right) T_-^{2.5} \tag{6}$$

Thus a decrease in temperature or an increase in neutral particles will increase ν and decrease D_a/D_B, thereby reducing the hollowness of the plasma.

For a high power input the effective electron temperature is increased, as evidenced by the current measurements at the probe and collector. The increased electron temperature is the result of the

resonance phenomenon in the plasma. The additional electron energy will increase D_a/D_B and thus also result in a partially hollow plasma.

Two of the mechanisms that may be involved in generating the observed multiple peaks due to the partially hollow plasma are under investigation. (a) The center and edge of the electron beam are in resonance with the plasma only when $\omega = \omega_p$ at the center or edge, and (b) the power in the space-charge wave on the beam is fed into a backward wave mode that exists in a hollow plasma.

For the first mechanism, consider the following qualitative argument. A cylindrical electron beam of uniform current density j passes through a plasma with a radially varying density. The plasma density can change by Δn_c over a resonance bandwidth at an applied frequency ω. Since Δn_c depends on the plasma electron collision frequency ν, it can be expressed in the form

$$\Delta n_c = \int_{r_{c1}}^{r_{c2}} \frac{dn}{dA}\, dA \tag{7}$$

where r_{c1} and r_{c2} are the radii where $1 - \omega_p^2/\omega^2 = \nu^2/\omega^2$. The power output P is a function of the beam current that passes through the resonant section of plasma. In integral form

$$P \propto \int_{r_{c1}}^{r_{c2}} j\, dA \tag{8}$$

Because Δn_c is fixed by ν, the integral is maximized by minimizing dn/dA. For a plasma density function that is uniform at r = 0 and increases at large r and is of arbitrary form, such as

$$n = n_o\left(1 + \frac{Kr^3}{1+r^2/a^2}\right) \tag{9}$$

where K and a are constants, there are two minima for dn/dA, at r = 0 and r = ∞. Since only the region inside the beam is considered, the second minimum is at r = b, the beam radius. Hence two power maxima will occur as the plasma density at the probe is increased from zero.

The twin maxima could also result from absorption of power by the backward wave mode when conditions in the plasma are such that the electron beam velocity is in synchronism with the phase velocity of the backward wave.

It is possible that at low power input the first mechanism is responsible, and at high power input the backward wave mode is responsible.

At intermediate power inputs, such as those shown in Fig. 6, both mechanisms may be at work to give three maxima.

CONCLUSIONS

With a low power input, the double-peaked gain curves can be transformed to single-peaked curves by decreasing the magnetic field, increasing the density of neutral cesium, or decreasing the electron temperature. All these changes tend to change the plasma density contour along the beam radius from a hollow contour to a flat contour. For a high power input, where multiple gain peaks are observed, the effective electron temperature is increased, as evidenced by current measurements at the probe and collector. The increased temperature decreases the diffusion across the magnetic field, and the plasma density contour tends to become hollow. The hollow plasma is apparently associated with the multiple gain peaks. The possible mechanisms involved in generating the observed multiple peaks are currently under investigation.

ACKNOWLEDGMENTS

The authors wish to thank M. Glicksman for many helpful suggestions during the course of the work. We wish to express our graditude to L. E. Norton for construction of the helix couplers, and to R. Chamberlain for his flawless assembly of the tube.

REFERENCES

1. D. Bohm and E. Gross, Phys. Rev., 75:1851 (1949).
2. M. Lampert, J. Appl. Phys., 27:5 (1956).
3. G. D. Boyd, R. W. Gould, and L. M. Field, Proc. IRE, 49:1906 (1961).
4. E. V. Bogdanov, V. J. Kislov, and Z. S. Tchernov, in Proceedings of the Symposium on Millimeter Waves, Polytechnic Press, New York, 1960, p. 57.
5. I. F. Kharchenoko and others, Soviet Phys.-JETP, 38:685 (1960).
6. M. Allen and G. Kino, Phys. Rev. Letters, 6:163 (1961).
7. Ya. B. Fainberg, V. I. Kurilko, and V. D. Shapiro, Soviet Phys.-Tech. Phys., 6:459 (1961).
8. V. S. Imshennik and Yu. I. Morozov, Soviet Phys.-Tech. Phys., 6:464 (1961).
9. S. C. Brown, Basic Data of Plasma Physics, John Wiley & Sons, New York, 1959, Ch. 3, p. 91.
10. A. Guthrie and R. K. Wakerling, The Characteristics of Electrical Discharges in Magnetic Fields, McGraw-Hill Book Co., New York, 1949, Ch. 2, p. 59.
11. L. S. Napoli and G. A. Swartz, Wave Propagation in a Tubular Plasma, presented at Plasma Physics Division of A.P.S. meeting, November, 1962.

NONPLANAR PHENOMENA IN SINGLE AND MULTIPLE ELECTRON BEAMS

Theodore G. Mihran
General Electric Research Laboratory
Schenectady, New York

ABSTRACT

Attention is directed toward nonlinear phenomena that occur in one or more electron beams of finite radius drifting in a region free from external fields after receiving density or velocity modulation at an input plane.

The one-dimensional single-beam bunching theory of Webster is reviewed, and its modification in the case of finite diameter beams at small signal levels as given by Hahn and Ramo is discussed. The need for a large-signal finite beam theory leads to the disk-electron model of Tien and co-workers. In calculations made by Webber this model correctly predicts the phenomenon of harmonic growth, which subsequently was verified experimentally by Mihran.

Paschke and Olving have recently developed a closed-form analytic theory for this effect. New computer calculations are reported that point up a basic disagreement with the Paschke-Olving theory in that signal level is found to affect profoundly the functional dependence of harmonic current with distance. Plots of phase shift versus distance for the fundamental and the first two harmonic currents of a space-charge wave are shown to give an excellent picture of the loss mechanism that is inherent at medium signal levels in the propagation of space-charge waves along finite diameter beams.

The extension by Yu and Mihran of the nonlinear disk-electron analysis to the case of multiple electron streams of finite diameter is discussed. Two applications of this analysis are given: (a) calculation of the saturation characteristics of double-stream amplification, in which the harmonic levels are found to exceed the fundamental level; and (b) damping of a space-charge wave in multiple (four and eight) stream flow, which again is found to be accompanied by pronounced harmonic growth. One possible interpretation of this phenomenon is that it represents spatial Landau damping.

An electron beam is, by itself, a particularly interesting and useful member of the class of plasmas. I use the word "plasma" here in its most general sense, for electron beams do not meet the two requirements most often encountered in the definition of a plasma, which are charge neutrality and behavior independent of the plasma boundary. Nonetheless, in electron beam problems we do deal with the dynamic characteristics of a charged moving gas, and I welcome this opportunity to attempt to correlate the large body of organized and verified knowledge that has developed within the microwave beam tube art during the past twenty-five years with related phenomena in the plasma and propagation fields.

In particular, some important insights into the nonlinear behavior of electron beams have been gained recently as a result of the use of a so-called "disk-electron" calculation scheme. Much of what we shall be considering in the latter half of this talk stems from the results of such disk-electron calculations in both single and multiple electron streams of finite diameter.

In many ways the electron beam as it is utilized in microwave tubes constitutes a very simple plasma. It is very nearly collisionless, in regard to both electron-neutral collisions and short-range electron-electron interactions. It is a single-constituent plasma. Furthermore, it normally has a very simple velocity distribution, a delta function at the velocity corresponding to the beam voltage. All of these statements are approximations, but they have proved to be useful in that they simplify consideration of the dynamic problems of beams without altering many of the basic wave phenomena of interest to us here.

In the mathematical consideration of electron beams two more assumptions are commonly added to this list. One is the assumption of a stationary positive ion core, and the other is the assumption of one-dimensional motion. We will retain the first of these, but the second will be relaxed to some extent and as a result there will emerge a new class of nonlinear phenomena not present in the one-dimensional case. The positive ion assumption can be shown not to alter the rf behavior of the electrons in any way significant to our present interests, because of the large mass of the ions compared to the electrons.

In Fig. 1 the specific medium and boundaries of the system with which we will be concerned are shown. An electron beam is produced by an electron gun to the left (not shown). The beam passes through an input plane consisting of a pair of closely spaced parallel planes across which a sinusoidally varying signal voltage appears. The electrons then pass through a drift tube, which constitutes a region free from external electric fields. To keep the electrons from spreading laterally in this region due to their mutual repulsion, a very strong magnetic field is assumed to exist in the axial direction. Thus, in truth, the electrons describe tight spiral trajectories as they travel forward. The frequency of this cyclotron motion will be assumed to be much higher than the operating frequency. This situation, referred to as "confined" flow, is one of the two methods most commonly used in beam-type tubes to counteract the radial repulsion forces of the electrons.

After traversing the drift tube the electrons pass through another set of grids, and then are collected. That completes the picture as far as direct current is concerned. It is the <u>waves</u> that can exist in such a system that interest us, particularly the waves in the drift space. This setup is essentially that of a two-cavity klystron; the input grids constitute the capacitance of the first resonator or buncher cavity, and the second grids constitute the gap of the catcher cavity. It is important to note that electromagnetic energy flows into the beam at the buncher and electromagnetic energy is extracted at the output grids, but that in the drift tube the energy is principally transported <u>electromechanically</u>, not electromagnetically. The drift tube constitutes a

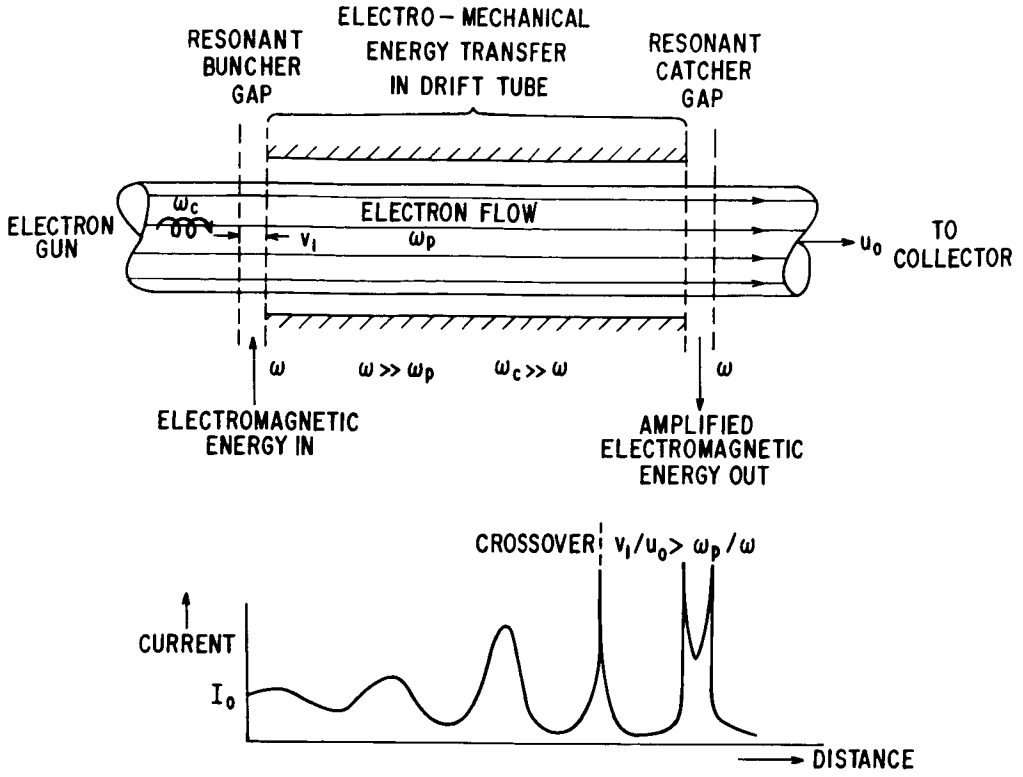

FIG. 1. Terrestrial klystron, confined flow.

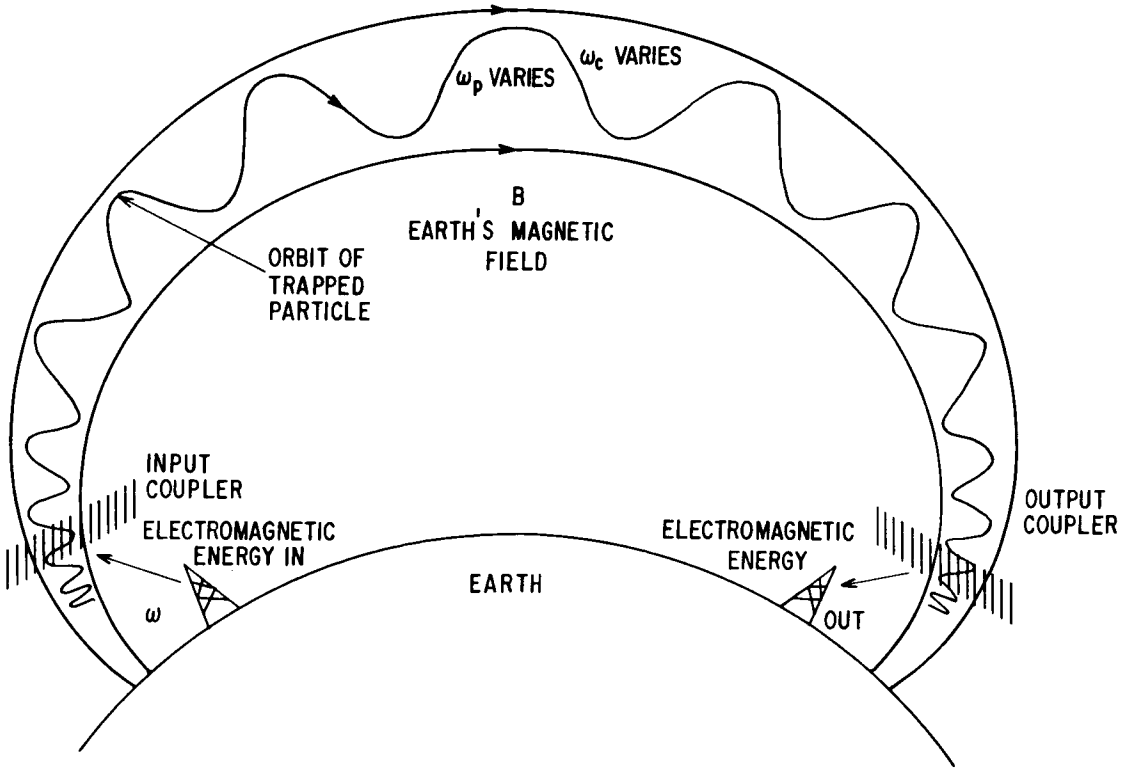

FIG. 2. Extraterrestrial klystron.

circular waveguide, which in practice is always arranged to be operated below its cutoff frequency so that electromagnetic waves cannot propagate through it.

Let us note two other conditions. The cyclotron frequency ω_c is much greater than the operating frequency ω in idealized confined flow, and in general the operating frequency ω is much greater than the plasma frequency. We will see shortly why the latter inequality holds, even at extremely low signal frequencies.

The lower portion of Fig. 1 depicts a typical bunching pattern in a high power klystron. For high efficiency performance the velocity index -- the ratio of peak a-c bunching velocity v_1 to d-c beam voltage u_o -- is made larger than ω_p/ω. This gives what is called "ballistic bunching" because space-charge forces have a negligible effect on the electron trajectories. In this case some of the electrons actually overtake one another, as evidenced by the infinite current spike that develops along the drift tube, and optimum fundamental current occurs when an interesting double-spiked current waveshape is developed. These current waveforms are obviously rich in harmonic content, and the behavior shown here is highly nonlinear. For two reasons, however, we will not further consider this kind of nonlinear behavior. It is well known and has been described clearly in the older literature (1), and since it does not represent the flow of energy back and forth between two types of energy storage, it is not a wave phenomenon in the strict sense of the word. When we reduce the signal level considerably below ω_p/ω, space-charge forces do enter and promote wavelike behavior.

Before going into a detailed discussion of space-charge waves that result when v_1/v_o is small compared to ω_p/ω, let me attempt to put this phenomenon in terms more familiar to workers in the propagation and plasma fields. In Fig. 2 we see that many of the elements of a klystron are present in the region above the earth. Here again we have trapped charged particles following B lines. If we visualize an input coupling system by which electromagnetic energy from the earth is somehow made to modulate the velocity or density of the charged particles, then in situations where the signal frequency is higher than the effective plasma frequency, these particles could conceivably carry energy electromechanically to an output coupling region, as in a klystron. Whether or not this behavior actually takes place in the exosphere is a question best left to those of you who are specialists in such far-out phenomena.

Let us now take a look at what strikes me as an extremely neat method of classifying plasma behavior. Shown in Fig. 3 is the so-called "plasma pond," a name given by Stix (2) to a diagram proposed by Allis (3) and others. I am grateful to Professor Holt and Mr. Haskell of R.P.I. for calling this type of presentation to my attention. In Fig. 3 the square of cyclotron frequency over signal frequency is plotted as the ordinate, and the square of plasma frequency over signal frequency is plotted horizontally. The cutoffs and resonances characteristic of plasma behavior divide the pond up into several subponds in which the wave behavior differs rather fundamentally. Two basic boundaries of the subponds are the lines $\omega_c = \omega$ and $\omega_p = \omega$. Other boundaries are defined by the straight line joining 1-0 and 0-1, as well as a parabola passing through the same

two points. Finite plasma temperature adds another line at $(\omega_c/\omega)^2 = 1/4$. Ion effects have been neglected in the present problem.

It is interesting to see where space-charge waves on confined-flow beams fit into the plasma pond of Fig. 3. First of all, we have assumed a magnetic field strength approaching infinity. The cyclotron frequency, which is proportional to B, is therefore very large, and we are in one of the upper three regions, 11, 12, or 13. As mentioned before, another characteristic of space-charge waves is that the signal frequency is always higher than the effective plasma frequency. This puts us near the vertical axis in region 11, shown by the shaded area.

The utility of this diagram is greatly enhanced by the sketches of the wave normal surfaces that appear in each of the thirteen regions. Dr. Bazer has given us excellent insight into the meaning of such plots earlier in this conference. Only two of these surfaces are shown here, but Papa (4) has calculated them for each of the regions, for the case of a warm electron plasma. The dashed line represents the wave front of a wave traveling with the velocity of light; this is merely for reference. The solid surfaces represent the wave fronts of waves that are characteristic of the entire region. If one dropped a pebble into each subpond, waves would move outward in these shapes. These diagrams preserve their topological properties as one moves within the confines of any given region, although they are distorted elastically as one moves about, especially approaching the boundaries.

The vertical direction on these diagrams represents propagation in the direction of the magnetic field, and the horizontal direction is that perpendicular to B. In region 11, the region of immediate concern to us, we see that three waves are possible. The outer two are electromagnetic waves; it can be shown that they are present for zero temperature beams (3). The inner wave appears as a direct result of the electron temperature. It is the longitudinal plasma electron wave, and it is generically related to the one we are concerned with in electron beams, for the other electromagnetic waves are cut off in the drift tube.

Note the striking resemblance between the wave normal surface of this wave and those of the slower waves to the right of the $\omega_p = \omega$ line. The latter are found even in zero temperature plasmas and are therefore electromagnetic waves, contrasted to the slow electromechanical wave we are dealing with. In fact, the slow wave in regions 12 and 13 represents the "whistler" mode, which has come in for a great deal of attention during this conference. Thus in regions 11, 12, and 13 we can have a wave whose velocity is directed along the B lines and is slower than the velocity of light. It may be helpful to remember that the waves we shall be discussing in the rest of this talk occur when $\omega_p \ll \omega$, and are the electromechanical counterpart of the familiar "whistler" modes.

So much for orientation. Now let us describe the linear properties of space-charge waves on electron beams as a preliminary to moving on to their nonlinear behavior. The simplest way to think of a space-charge wave is to think of a moving beam of electrons neutralized by a fixed core of positive ions, such as that shown in the top sketch in Fig. 4.

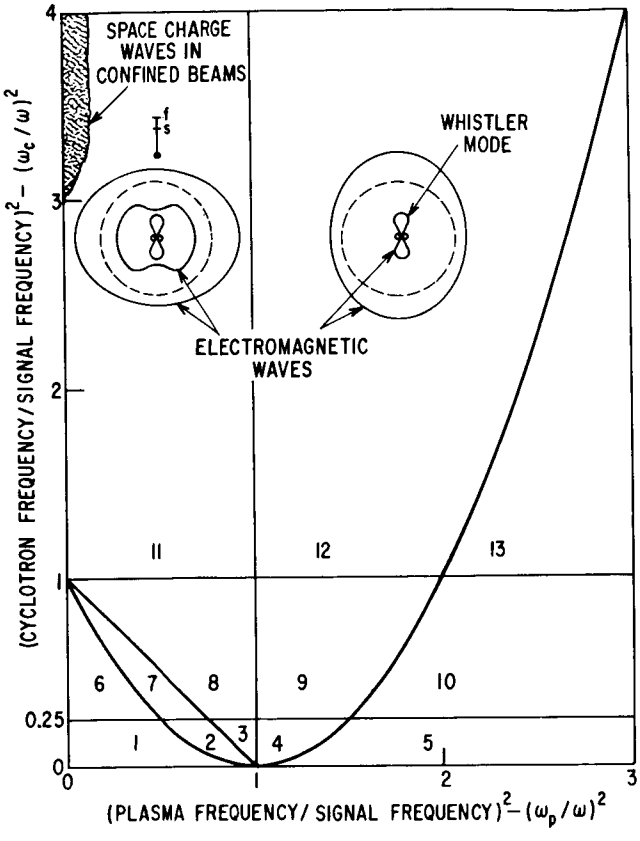

FIG. 3. Some normal wave surfaces in a warm plasma with magnetic field (from Refs. 3 and 4).

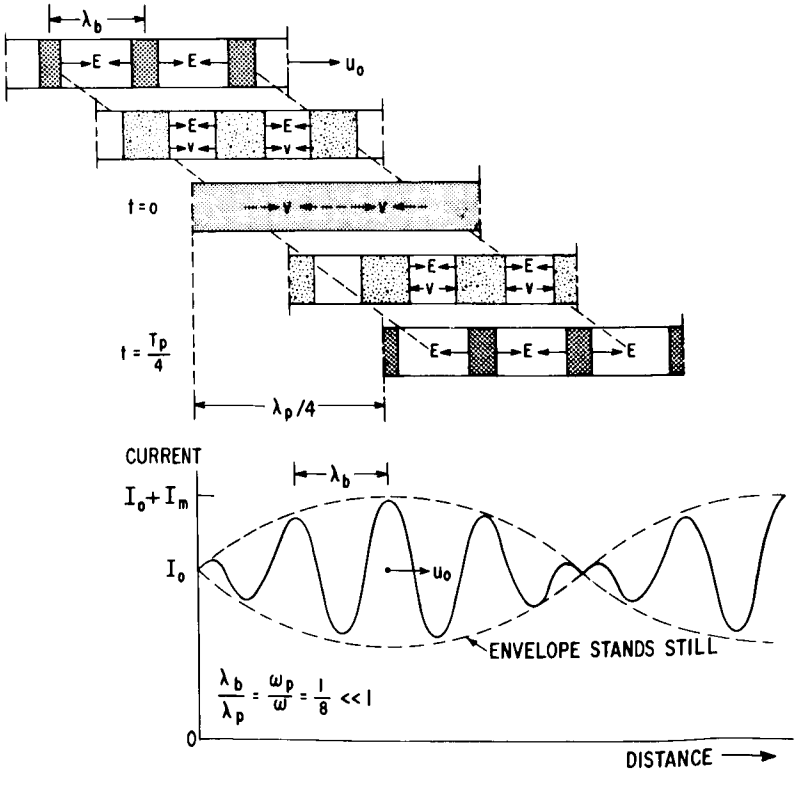

FIG. 4. Space-charge wave on an electron beam.

Let us somehow reach into the beam and bunch the electrons periodically with spacing λ_b, a distance whose significance will become clear shortly. Longitudinal electric field lines will emerge from each bunch, as shown, and this will lead with time to an axial spreading out of the bunches.

Sometime later, when the whole beam has moved forward as shown in the second line of Fig. 4, the bunches will have partially spread out. The electrons have acquired outward velocities as a result of the action of the electric fields, and the electric fields are reduced because each bunch now encompasses more positive ions. Later the bunches will spread out completely to form a beam of uniform density, as shown in the third line of Fig. 4. The process does not stop here, however, because the a-c potential energy of the bunch represented by the E field in the first sketch has been converted into a-c kinetic energy in the form of periodic velocity modulation of the electrons, as shown in the third line. These velocities institute a rebunching process which leads, sometime later, to a density modulation equal to the initial density modulation but of the opposite phase.

You may recognize that this series of five sketches depicts a half period of an electron plasma oscillation in a moving beam; the process would go on indefinitely if there were no losses. The distance the beam travels in this period is one-half a plasma wavelength, $\pi u_o/\omega_p$.

In a situation as in a klystron where the beam is velocity modulated at an input plane, as in Fig. 1, the behavior is very similar to that shown in the third line of Fig. 4. The periodic spacing is set by the signal frequency ω and the forward velocity of the beam, and is simply $2\pi u_o/\omega$. As the beam travels subsequently in the drift tube, electron bunches are formed which increase in density until the space-charge forces wipe out the velocity modulation, as shown in lines 4 and 5 of Fig. 4. This is followed by a quarter plasma cycle of debunching, then rebunching in the opposite phase, and so on. This behavior is sketched in the lower portion of Fig. 4. Here we have a standing wave whose period is set by the plasma frequency, with electron bunches rising and falling as they move through it. This behavior is very closely related to the behavior shown in the sketch above in Fig. 4, provided the rate of growth is small; that is, $\lambda_b \ll \lambda_p$, which means $\omega_p/\omega \ll 1$. The case shown in Fig. 4 is drawn for $\lambda_b/\lambda_p = 1/8$.

The sketch at the bottom of Fig. 4 represents the space-charge wave regime of operation of a klystron. This is how all klystrons would operate if driven at low signal level. If a sliding cavity were moved along the beam to sample the rf current developed in the beam, it would measure a current proportional to the envelope of this curve. Actual experimental measurements (5) of this phenomenon are shown in Fig. 5. These were made using an experimental setup in which the drift length could be varied continuously from 1 to 21 cm. In Fig. 5 the square of output current is plotted versus distance for various drive levels. At the lower drive levels, note that the variation of current with distance is fairly sinusoidal, as space-charge wave theory predicts. As the drive level is increased, we continue to get space-charge wave behavior until, at the largest drive levels, we finally encounter a saturation phenomenon. This is due to the crossover phenomenon mentioned in connection with

Fig. 1. This phenomenon enters at an output signal level about 3 db below the ultimate saturation value, which has a theoretical value of $I_1/I_o = 1.16$.

Let us return again to the space-charge wave regime of operation depicted by the lower curves in Fig. 5, for it is the nonlinear aspect of this current behavior that interests us here. The equations for the current variation in this case are given at the top of Fig. 6. Since the current envelope is a standing wave, it can be written in terms of two waves, one going slightly faster than the d-c velocity and one going slightly slower. These are sketched in the upper diagram in Fig. 6. Note that the spacing of the two waves from the d-c velocity is about equal to ω_p/ω times u_o. (This is correct to the first order, but since some of our later curves will show a slight phase shift, let me point out here that to second-order, both waves are shifted upward by $(\omega_p/\omega)^2$ in relative velocity because only the first term in the expansion has been retained in going from the first equation to the second. The lower sketch in Fig. 6 is a more accurate representation of what the velocities actually are.)

Let me make another point in passing. Later we will be interested in double-stream amplification in which two beams mutually interact. It can be shown that if we arrange to have the slow space-charge wave of the faster stream travel at the same velocity as the fast space-charge wave of the slower beam, as shown in Fig. 6, we will achieve very nearly the optimum condition for double-stream gain. Later we will see the results of a nonlinear calculation of such double-stream amplification carried to saturation.

We will now consider the behavior, still linear, of space-charge waves in single streams but now of finite diameter, and we will contrast this behavior with that found in beams of infinite radial extent. Space-charge wave behavior of finite diameter electron beams can be calculated by two basically different methods. The oldest method treats it as a linearized boundary-value problem. This was first done by Hahn (6) in 1939, using a linearized analysis based on seven equations: Maxwell's four equations, the force equation, the equation of continuity, and the definition of current. An entire book has been devoted to this approach and its ramifications (7). Hahn gives us only linear behavior, but we will look into it briefly for it gives us an extremely important concept, reduction of the effective plasma frequency due to finite beam diameter.

How this reduction in effective plasma frequency comes about is evident from the sketches in Fig. 7. In an infinite beam the E lines are purely longitudinal and the beam is fairly "stiff," corresponding to a natural oscillation frequency at the finite-beam plasma frequency ω_p. Consider, however, what happens when a finite diameter core is removed from that picture and placed in a drift tube, as in the central sketch in Fig. 7. This situation is no longer describable by a one-dimensional or planar theory, for the E lines now fringe outside the beam; some may even terminate on the walls of the drift tube. This leads to a reduction of the stiffness of the beam, hence to a reduction of the effective plasma frequency. Plasma oscillations will take place at a lower frequency in this finite diameter beam than in the infinite beam.

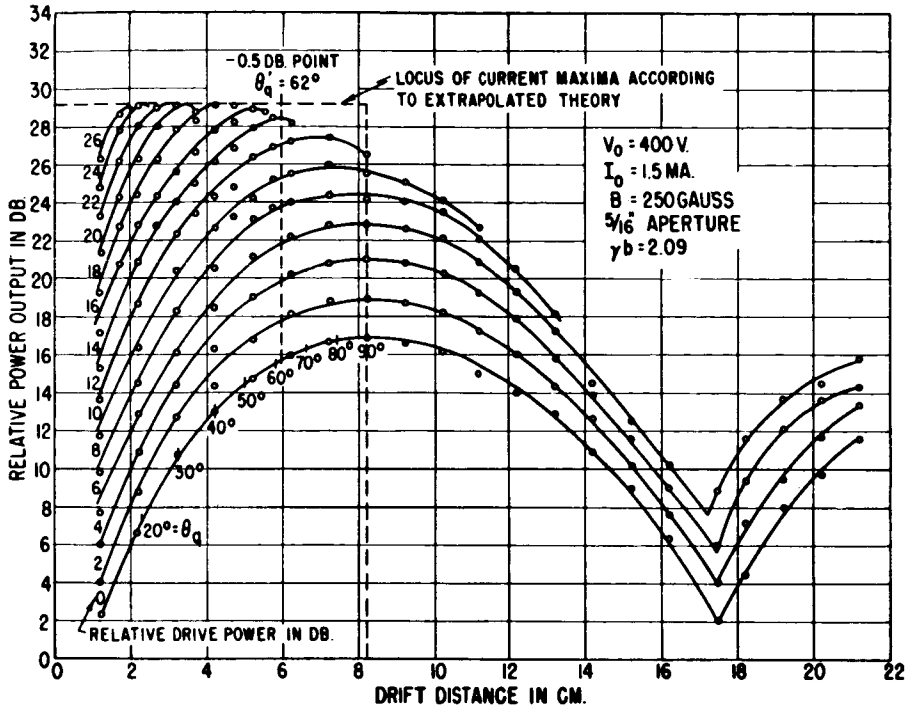

FIG. 5. Experimental data showing transition from space-charge wave behavior to ballistic behavior, with drive power as a parameter.

$$\frac{I_1}{I_0} = \frac{I_m}{2}\cos\omega\left[t - \frac{z(1-\frac{\omega_p}{\omega})}{u_0}\right] - \frac{I_m}{2}\cos\omega\left[t - \frac{z(1+\frac{\omega_p}{\omega})}{u_0}\right]$$

$$\frac{I_1}{I_0} \approx \frac{I_m}{2}\cos\omega\left[t - \frac{z}{u_0(1+\frac{\omega_p}{\omega})}\right] - \frac{I_m}{2}\cos\omega\left[t - \frac{z}{u_0(1-\frac{\omega_p}{\omega})}\right]$$

FAST WAVE SLOW WAVE

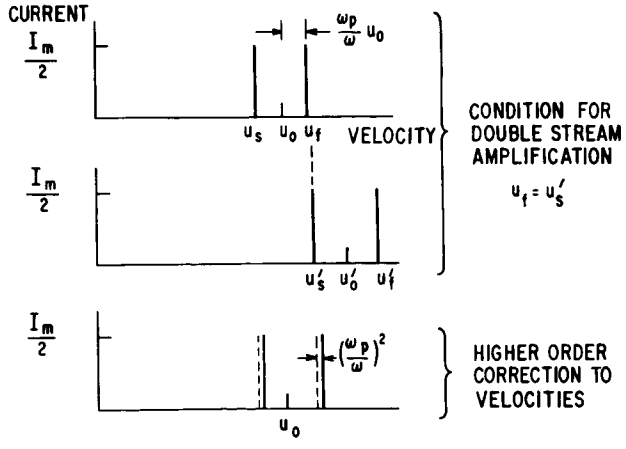

FIG. 6. Some results of space-charge wave theory.

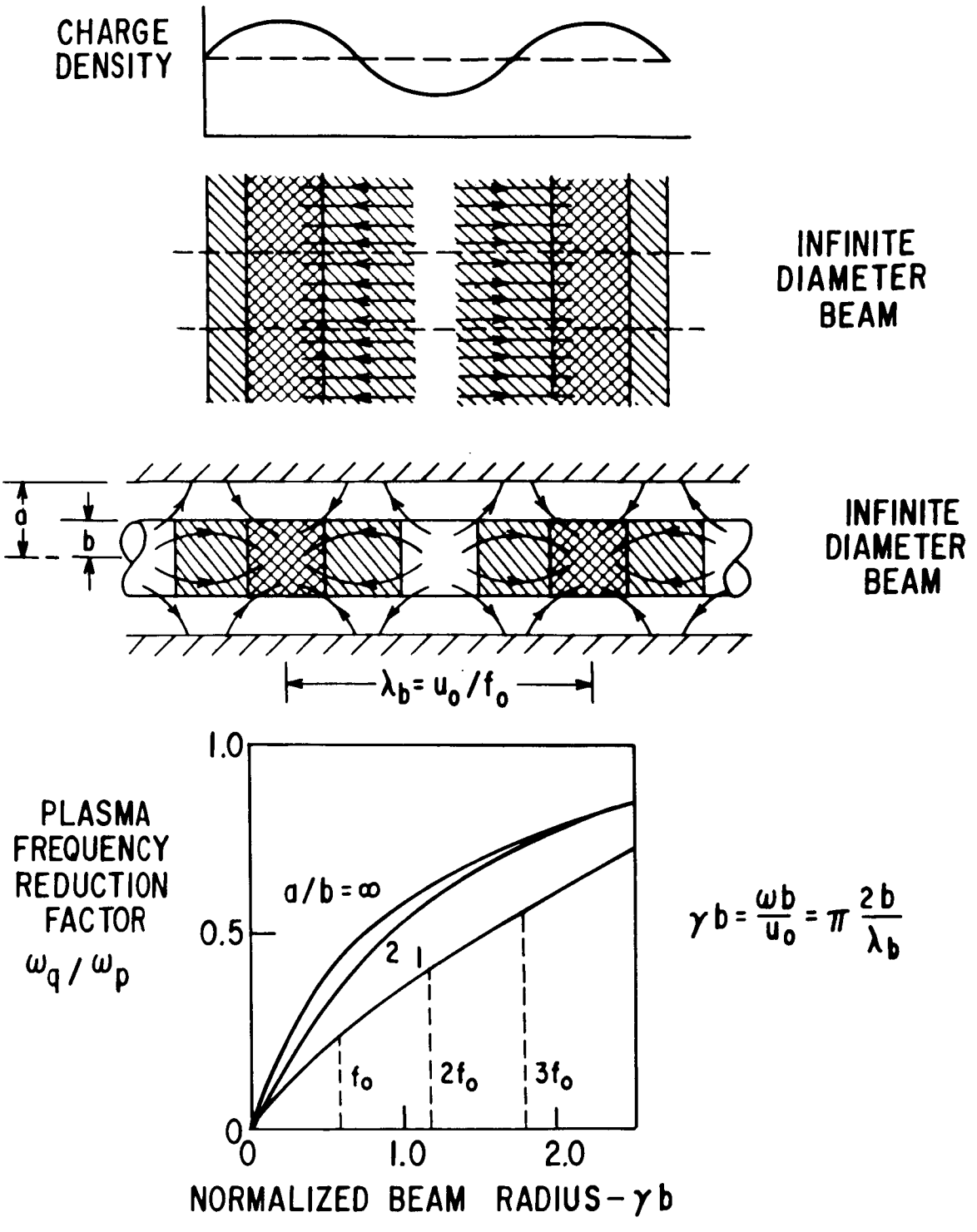

FIG. 7. Effect of finite-beam diameter on electric field and plasma frequency.

Hahn's space-charge wave theory enables us to calculate the reduced plasma frequency, called ω_q, and plots of ω_q/ω_p have been made by Branch and Mihran (8) for a variety of beam geometries. These have proved to be extremely useful in the microwave tube art. For a pencil beam the ratio ω_q/ω_p is shown at the bottom of Fig. 7. The abscissa here is γb. Note that γb is proportional to frequency. Another way to look at this variable is to note that it is π times the ratio of beam diameter to bunch spacing. It is evident that as beam diameter is reduced below bunch spacing -- that is, if γb is less than 3 -- we begin to get a significant reduction of the plasma frequency.

This phenomenon is responsible for a curious restriction found in practical microwave tubes. An electron beam can never be modulated with a signal whose frequency is below the effective plasma frequency of the beam. If you try to reduce the signal frequency below the plasma frequency, the bunch spacing increases and the finite-beam effect reduces the effective plasma frequency lower still. Try as you will, you can never operate a tube so that ω_q/ω is greater than unity. I wonder if it is possible that the finite lateral extent of the charged regions above the earth leads to similar reduction factors at the extremely low radio frequencies that are involved in some extraterrestrial propagation phenomena. Again I must leave the answer to that question to specialists in the propagation field.

Since we are interested primarily in nonlinear effects at this conference, let us move on to a consideration of the harmonics that accompany a space-charge wave in a finite diameter beam. On this subject linear theory is silent, of course, so we must go to a completely different type of analysis. Before we do, one bit of harmonic information can be gleaned from the one-dimensional plasma oscillation model set up by Webster in the second part of his classic paper dealing with klystron behavior (9).

Webster's theory predicts that the harmonic currents accompanying a space-charge wave will nestle within the fundamental current, as shown at the top of Fig. 8. This seems reasonable, but now let us ask what happens in a finite diameter beam. We know that the plasma frequency of the fundamental current is reduced, so the effective wavelength of the fundamental component of current is increased, as shown in the lower sketch of Fig. 8. But what do the harmonics do? Do they exhibit an equal increase of plasma wavelength? This seems unlikely because, if you recall from Fig. 7, the plasma frequency reduction factor is a function of frequency. From this we might expect the plasma period of the harmonics to lie somewhere between the unreduced and reduced plasma frequencies of the fundamental. For what actually happens, let us look at the experimental data (10) in Fig. 9. We see the fundamental displaying fairly conventional behavior with distance, but here is a surprise: the second harmonic is found to grow with distance!

Can we calculate such behavior? The answer turns out to be yes. To do this we need a nonlinear theory valid for finite diameter beams. Of several such theories that exist, one called the disk-electron analysis (11-15) has been used with great success by workers in the microwave tube field since 1955. This method of analysis is based on the model

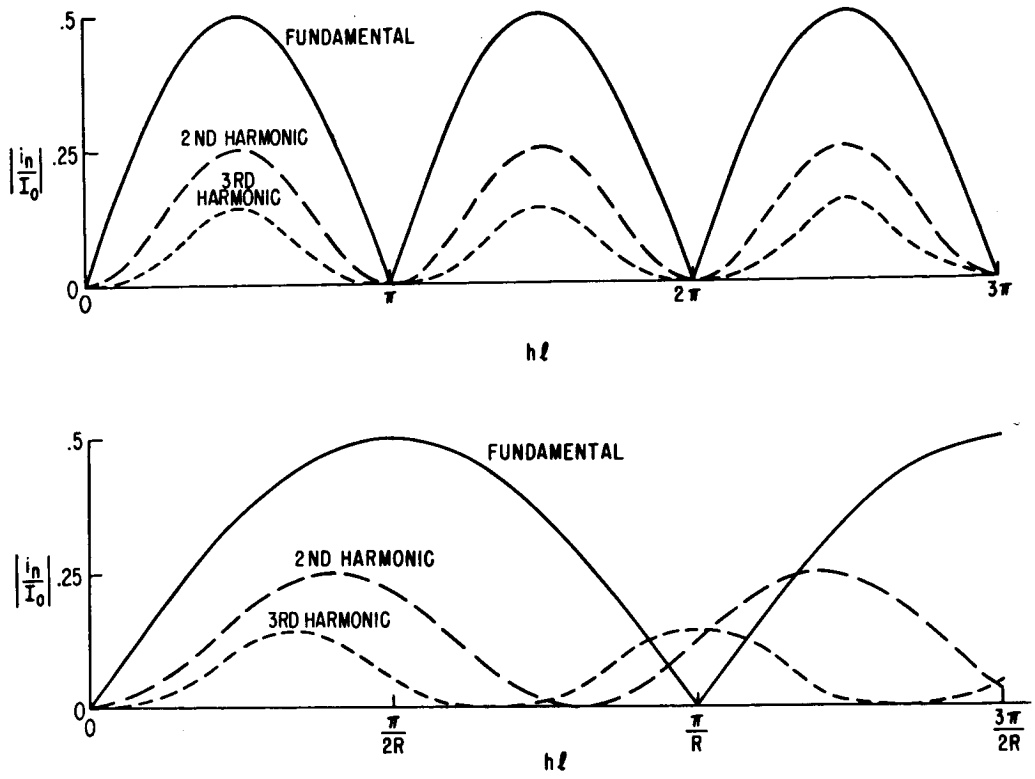

FIG. 8. Fundamental and projected harmonic current behavior in electron beams with infinite diameter (top) and finite diameter (bottom). Behavior suggested for finite-diameter beam is incorrect.

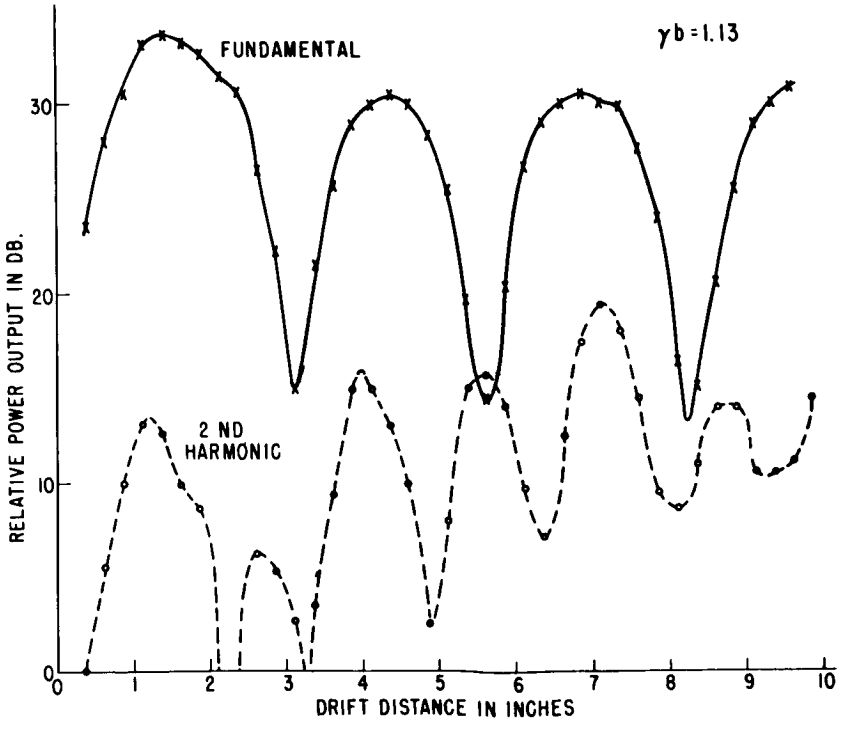

FIG. 9. Experimental data showing growth of second harmonic maxima.

shown in Fig. 10. Here we see a beam of electrons in which a current wave is growing. If the rate of growth per rf cycle is small, we may calculate rf behavior by considering just one cycle's worth of electrons, assuming this to be preceded and followed by identical cycles. This assumption increases in validity as the ratio ω_q/ω is made smaller. We then break the cycle's worth of electrons into N cylinders, and replace these by N disks. This has been found to be a valid procedure if $\gamma b < 1$.

The behavior of these disks as a function of distance is then calculated as a function of (a) their initial modulation and (b) the space-charge forces that they exert upon one another as they travel. External electric fields may also be taken into account in the drift tube, but these are zero in our case. The calculation of the actual trajectories is an arduous but straightforward task and calls for a computer, usually the biggest and fastest one you can find. In our case we used an IBM 7090. With no modulation, if we plot time versus distance we will have a series of straight lines for the trajectories of the disks, as shown at lower left in Fig. 10. It is convenient to subtract out the average slope of these lines, as shown at lower right in Fig. 10. We then have just a series of horizontal lines for the case of no modulation.

In Fig. 11 we see what happens when a small initial velocity modulation is imposed on the beam at Y = 0. These trajectories are the result of a computer run in which N = 16. Distance increases vertically in this plot; horizontally, we plot the phases of the electrons at various distances from the starting plane. We see at the quarter-space charge point that electrons, on the average, lose their inward velocity and start debunching. To make the computation more revealing, we ask the computer to perform a Fourier series at each increment of distance and to calculate the first three harmonics of current. A typical result for the fundamental and second harmonic (14) is shown in Fig. 12. Here we see that the fundamental current is varying nearly sinusoidally, and that the harmonic current is growing! This gives us great confidence in our computational model, since the same behavior has been observed experimentally (Fig. 9).

What is the physical reason for this unexpected harmonic growth? I call it the "staggered turn-around" effect. If we carefully examine the calculated trajectories in Fig. 11, we find that the electrons do not all reverse their motion at the same distance from the input plane as they would do in an infinite beam. This is shown in simpler fashion in Fig. 13; the electrons closest to bunch center encounter strong repulsive forces characteristic of the full plasma frequency ω_p, and therefore turn around sooner than those electrons at the outposts of the bunch, like 6 and -6. These latter electrons meet reduced repulsive forces due to the fringing of the E lines, hence they turn around later than the inner ones. This staggering of the turn-around points leads to a beam at the half plasma wavelength point that has a pronounced second harmonic content instead of being uniform in charge density. The second harmonic perturbation forms the starting point for the second half-cycle of plasma oscillation, which in the same fashion contributes still more second harmonic current. This effect piles up for some distance before other consideration overcome the tendency to build up second harmonic current.

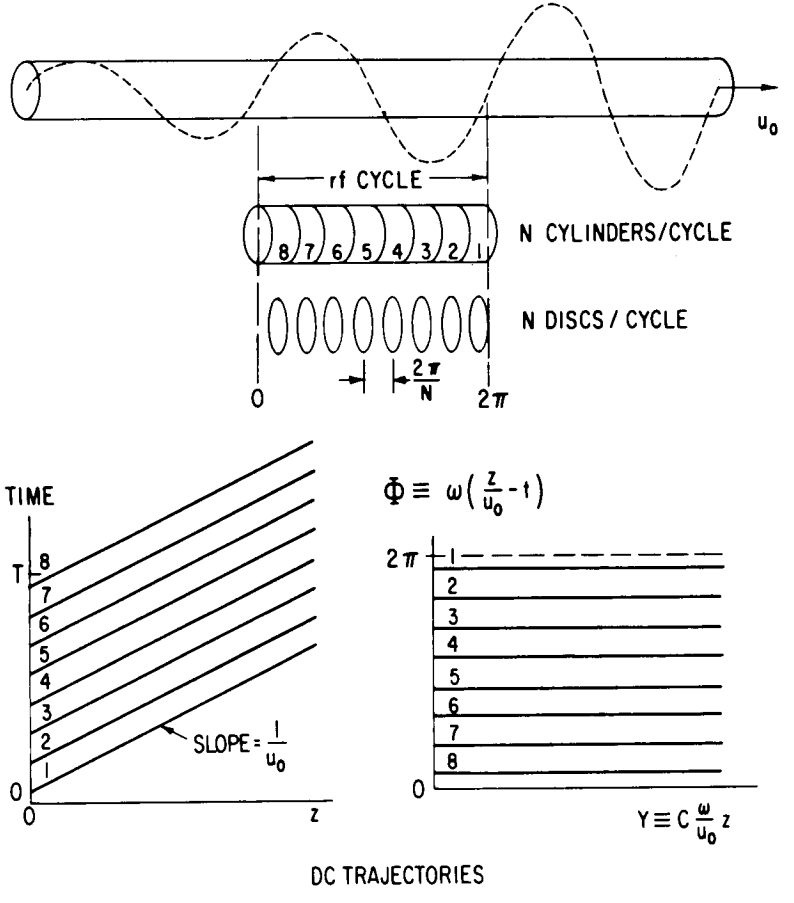

FIG. 10. Disk model of single-velocity electron beam.

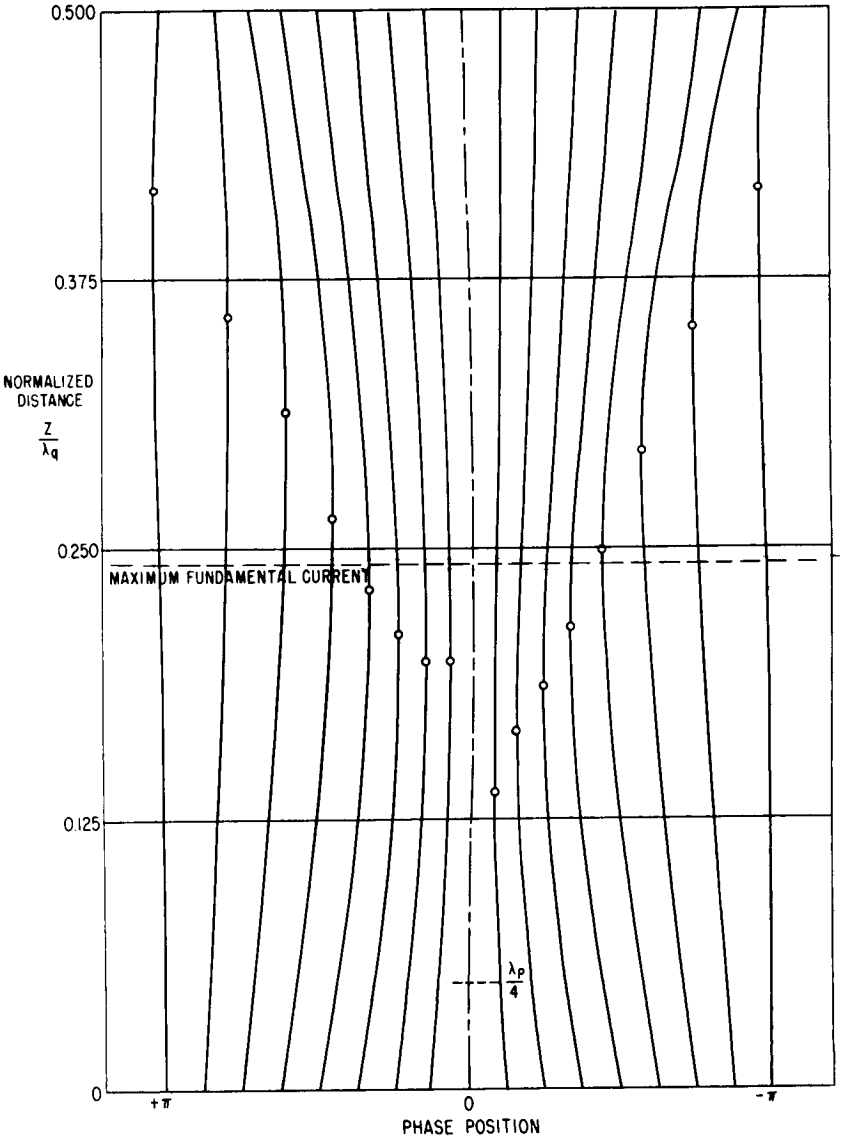

FIG. 11. Electron trajectories, showing staggered turn-around points.

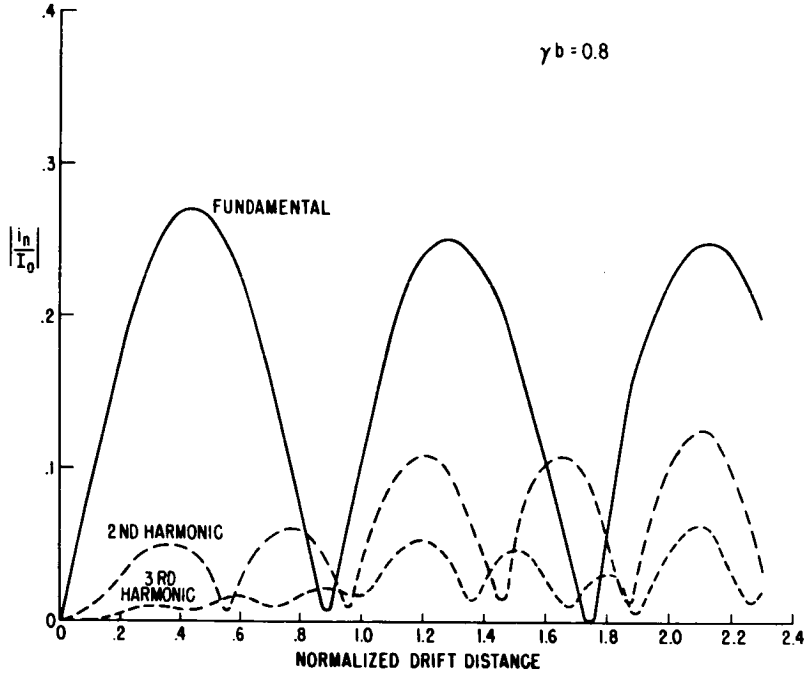

FIG. 12. Calculated harmonic growth using disk model (from Ref. 14).

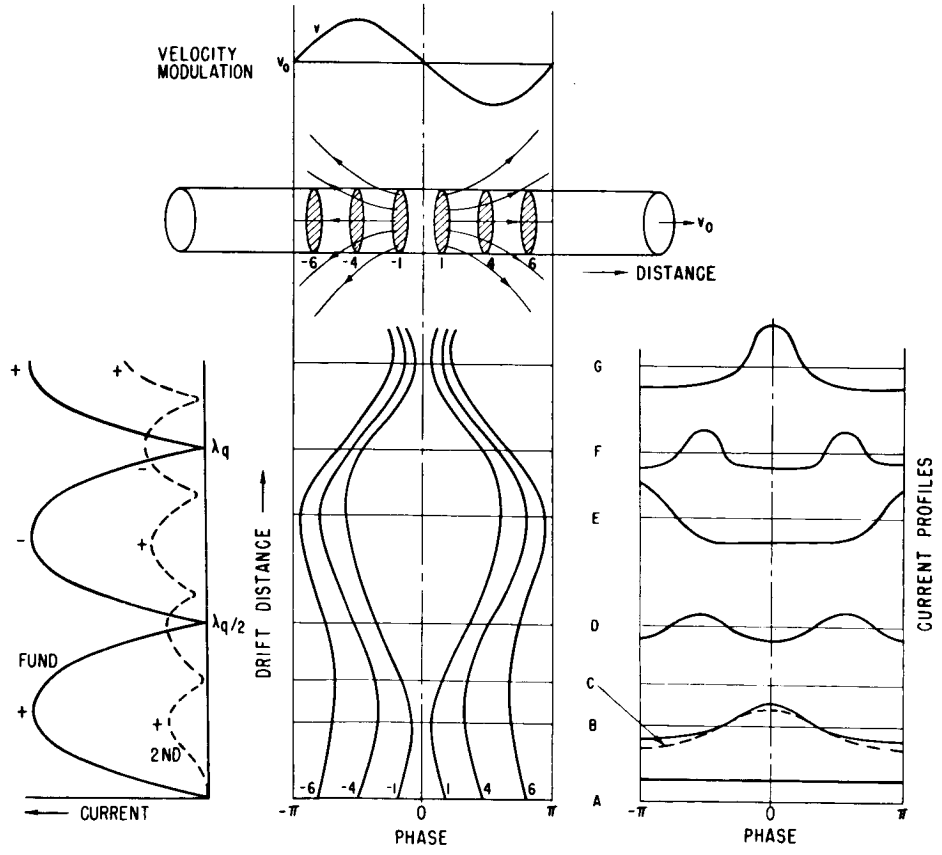

FIG. 13. Typical phase trajectories and current profiles in a finite beam.

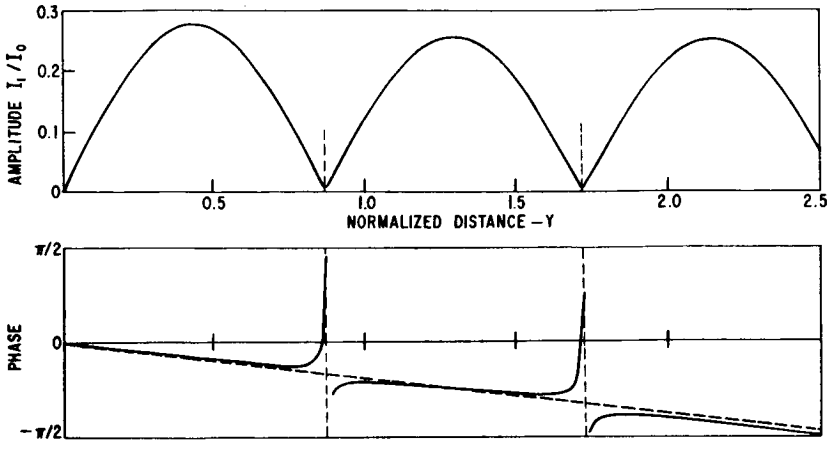

FIG. 14. Calculated amplitude and phase shift of fundamental current.

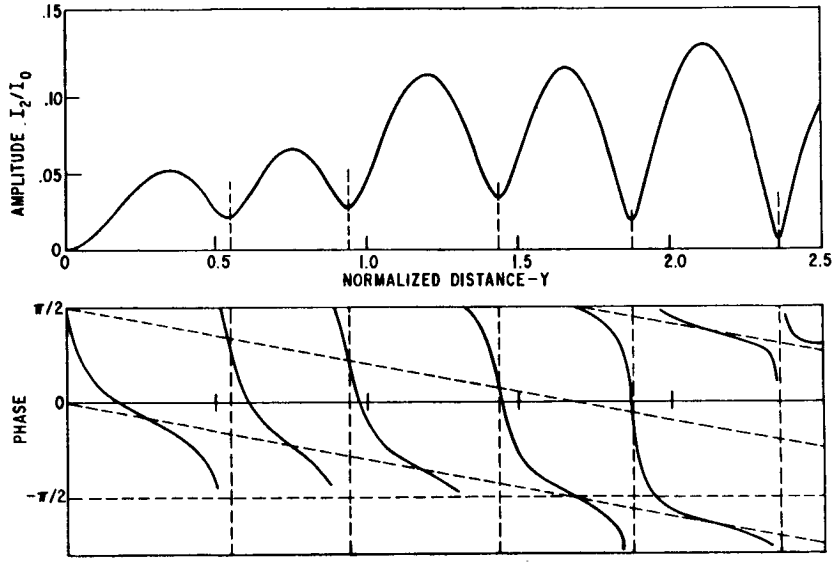

FIG. 15. Calculated amplitude and phase shift of second harmonic current.

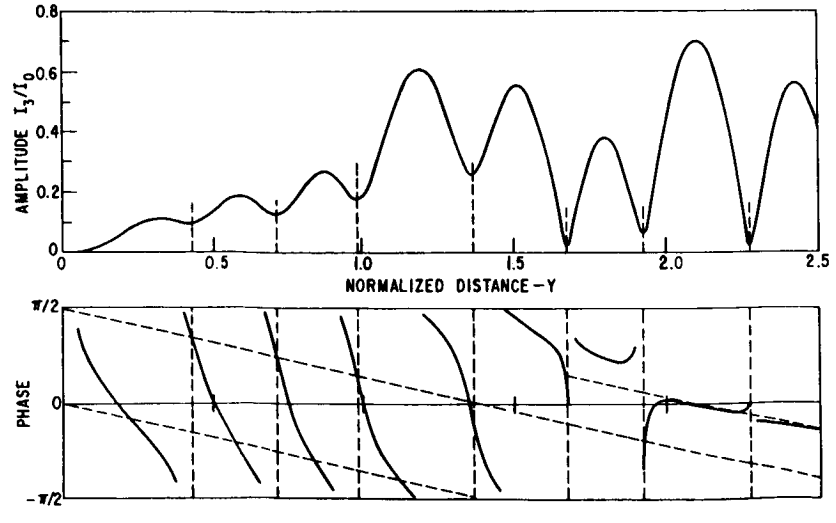

FIG. 16. Calculated amplitude and phase shift of third harmonic current.

Figures 14, 15, and 16 show detailed calculated results for the variation of the fundamental and the first two harmonics with distance in a typical case. The interesting point to notice is the phase shift curves, for they give the most revealing clue as to whether the wave is damping or growing. Figure 14 shows the fundamental current and its phase. The magnitude is behaving as expected, but the phase shift shows two characteristics we would not expect on the basis of linear space-charge wave theory -- which, incidentally, is very much akin to lossless transmission line theory (16). The first is the slope; the wave is not moving along at quite the beam velocity, but is moving ahead of it at a constant rate. It has been found that this tilt in the phase shift curve is proportional to $(\omega_q/\omega)^2$ and is described by the second order correction for velocity mentioned in connection with Fig. 6. The tilt appears in all the curves, and we shall speak of it no more. I should also point out that the middle cycle of phase should be displaced upwards by π. As you remember, in a standing wave adjacent nodes are 180 deg out of phase with each other. This phase shift has been removed in this and the following plots for convenience of discussion.

The really interesting aspect of the phase shift curve is the rounding that shows up in the vicinity of the current nulls. Taking our cue from lossy transmission line theory, this slope indicates that a loss mechanism is at work which extracts energy from the fundamental component of current. Where does this energy go? Remembering that a positive slope of phase shift is energy loss, let us look at the second harmonic in Fig. 15. Ignoring the tilt, we see that the phase shift now has a negative slope. Obviously, the second harmonic is gaining energy, and it is reasonable to expect that this energy is coming from the fundamental space-charge wave, which is undergoing a loss. That the second harmonic is gaining energy is evident in the growth of its magnitude.

The phase of the third harmonic, Fig. 16, displays even more interesting behavior. It starts out with a negative slope, which reverses itself and becomes positive. This wave evidently receives energy for a while and then starts giving it up. The magnitude displays this behavior, too, but not nearly as cryptically as does the phase data.

With these recently calculated phase curves, I believe that we are for the first time in a good position to understand the true nature of the interchange of energy between the fundamental and harmonic space-charge wave currents propagating in a finite diameter electron beam.

To complete this part of the talk, let me say that upon seeing the experimental harmonic growth data of Fig. 9, Paschke (17,18) and later Olving (19) developed a second order theory that predicts this phenomenon analytically in closed form. Let me show, however, a final set of curves computed by the disk-electron method, which disagrees with the results of Paschke and Olving.

The curves in Fig. 17 show calculated fundamental and harmonic current at three different signal levels. To obtain these curves the signal level was halved and then halved again; all other parameters were maintained constant. It is evident that the harmonic growth phenomenon

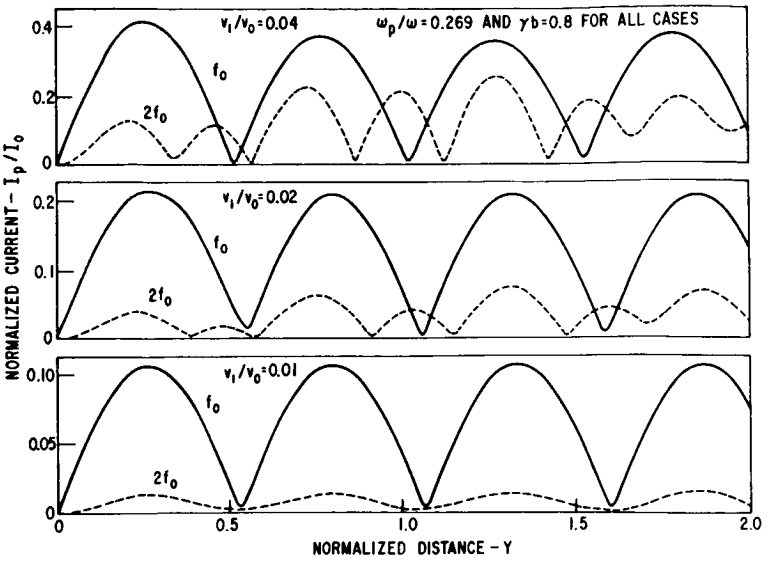

FIG. 17. Calculated curves showing variation of harmonic current growth with drive level.

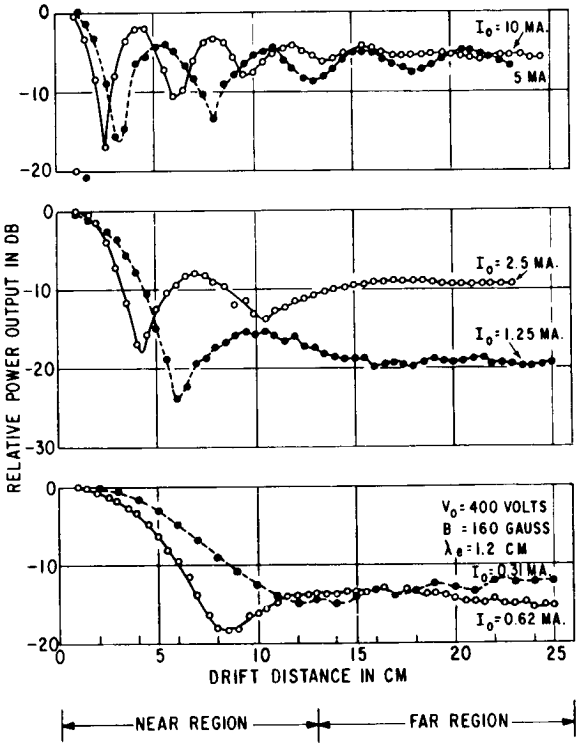

FIG. 18. Experimental rf current versus distance, with d-c beam current as a parameter.

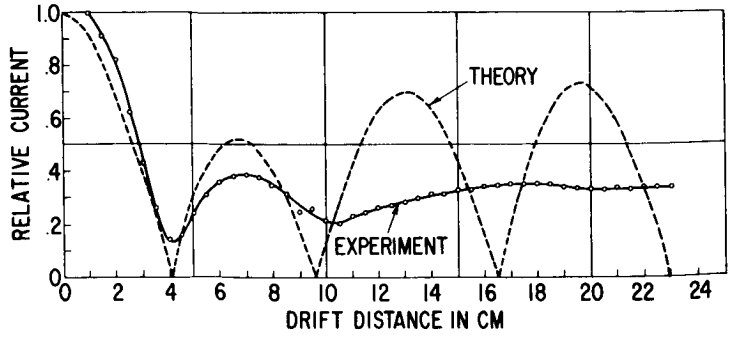

FIG. 19. Comparison of experimental current and current calculated by linearized one-dimensional distribution function analysis.

appears only at the higher signal levels. At the lowest level we have behavior very similar to that in an infinite beam (Fig. 8). But the prediction of the Paschke-Olving theory is that the functional dependence of current with distance is independent of signal level. In their work, signal level appears merely as a scaling factor. Such is definitely not the case according to our calculations. Here is an interesting discrepancy, which must be looked into further.

As our final topic, let us discuss some facets of space-charge wave behavior in multiple beams. Here we approach one step closer to the situation in a plasma, for we now introduce velocity distribution into the problem. Several years ago I took some interesting data on the propagation of space-charge waves along the electron beam, which possessed, among other things, a longitudinal velocity distribution. These data (20) are shown in Fig. 18. The space-charge wave does not maintain its magnitude at successive peaks, as we are used to seeing, but rather, the peaks decrease monotonically. Furthermore, the standing wave nature of the wave disappears, particularly at small d-c levels.

To try to explain this interesting behavior, we first applied linearized distribution function theory. This method allows us to take into account both space-charge and velocity distribution. In the experimental setup there is reason to believe we are getting a fairly straight-sided, flat-topped d-c velocity distribution function, whose width is about 10 percent of the forward beam velocity. When linearized distribution function analysis is applied in a typical case with this form of velocity distribution, we get the variation of current shown in Fig. 19. We see that distribution function theory predicts the reduction of the first current maximum in agreement with experiment, but for distances greater than a half plasma wavelength the agreement is poor.

Because I once suspected that the linearization of the distribution function theory was the basis of this disagreement, Se Puan Yu of our laboratory and I set about devising a nonlinear theory that would allow for a distribution of velocities. Before discussing this theory let me point out that it is possible, choosing a special type of velocity distribution function, to make the linearized one-dimensional distribution function theory give a result that agrees most strikingly with the experimental result (21).

The special distribution consists of a half Maxwellian approximately 10 percent in width to the 1/e point, extending upward from the d-c beam velocity. This causes the fast space-charge wave to be damped by Landau damping because it is in the middle of a downward-tilting velocity distribution. The slow space-charge wave is undamped, since it appears below the edge of the velocity distribution function. If this interpretation is correct, the experimental data of Fig. 18 may be interpreted as spatial Landau damping, a phenomenon hitherto unobserved. Much as I would like to think that it is Landau damping, I personally have a most difficult time accepting the physical reality of the velocity distribution function that must be postulated for this explanation to be valid. Since the velocity distribution has not yet been measured experimentally, we cannot exclude this interpretation. But though I am quite sure that

velocity distribution effects are the source of the present phenomenon, I feel that one-dimensional theory cannot describe what to me appears to require a multidimensional treatment of the velocity distribution.

Let us now consider the nonlinear multiple beam analysis. Since the disk-electron analysis had proved so successful in predicting the nonlinear behavior of single electron beams, it seemed reasonable to try to extend it to the case of multiple beams. The validity of using discrete beams to simulate a continuous velocity distribution may be questioned, but the consistent results we have obtained give us considerable confidence in this method.

The theory of the disk-electron calculation for beams with velocity distribution, as worked out by Se Puan Yu and me (22,23), is summarized in Fig. 20. The variables are normalized distance y and normalized time at fixed distance ϕ. The instantaneous velocity is treated in terms of a normalized deviation from the average velocity u_o, which is defined in the usual fashion. As in the single-stream analysis, the method of Lagrangian hydrodynamics is used in that the force equation is applied to each disk individually. The key to the modification of the analysis to allow velocity distribution is the introduction of a third variable v_o that designates the initial velocity of each disk. The equation for the approximate force between two disks is an exponential function of the spacing between two disks, as suggested by Tien and co-workers (11), except that it now is extended to allow velocity distribution by introducing the factor $\rho(z',v_o,t)\,dv_o$. The continuity equation is used to refer ρ back to the input plane as usual.

So far we have allowed a continuous velocity distribution, but for computer use we must replace the continuous distribution function $f(v_o)$ with a set of discrete beams, as shown in Fig. 21. In most cases, four or eight beams were used to simulate a rectangular distribution. When this is done, the integro-difference equations ready for programming on the computer take the form shown in Fig. 22. These equations are the counterparts of the equations in Fig. 20. Equation 2 is the force equation.

I would like to call your attention to the new term $T_{j,n}^{m}$ that appears here, which I call the force-taper term. It is unity for most force calculations, but when two disks approach so close to one another that there is an overlap of the charge cylinders they represent, the term scales the force linearly to zero proportional to the degree of overlap. It can be shown (23) that this is a much closer approximation to the true force than simply letting the force reverse instantaneously as two disks pass through one another as is done by Tien and co-workers. The presence of this force-taper term has a calming effect on the trajectories, as we shall see.

The computer is asked to calculate the Fourier coefficients (Fig. 22), both magnitude and phase, at each y position. The "fallout" and "surrounding cycles" corrections are essential, since we focus our attention on only one cycle's worth of electrons. We allow the initial conditions to consist of either velocity modulation or density modulation, or both.

FIG. 20. Basic equations for multiple d-c velocity disk-electron calculation.

MULTI-DC-VELOCITY DISC ELECTRON CALCULATION

$$Y \equiv C\frac{\omega}{u_0} z \qquad \text{- DISTANCE}$$

NORMALIZED VARIABLES

$$\Phi(Y, \Phi_0, v_0) \equiv \omega\left(\frac{z}{u_0} - t\right) \qquad \text{- TIME, AT FIXED Y}$$

$$q(Y, \Phi_0, v_0) \equiv \frac{v - u_0}{u_0} \qquad \text{- VELOCITY DEVIATION}$$

where $u_0 = \int_{v_1}^{v_2} v_0 F(v_0)\, dv_0 \qquad F(v_0) = \frac{f(v_0)}{\int_{v_1}^{v_2} f(v_0) dv_0}$

FUNDAMENTAL EQUATIONS (LAGRANGIAN HYDRODYNAMICS)

FORCE EQN. $$m\frac{\partial^2 z}{\partial t^2} = -eE_s$$

FORCE BETWEEN TWO DISCS $$E(z-z') = -\frac{1}{2\pi b^2 \epsilon_0 M_r^3} e^{-2|z-z'|/b} \cdot \text{Sign}(z'-z) \cdot \rho(z', v_0, t)\, dv_0\, dz'$$

CONTINUITY $$\rho(z', v_0, t)\, dz' = \rho(z_0', v_0, t)\, dz_0' = -e' f(v_0)\, dz_0'$$

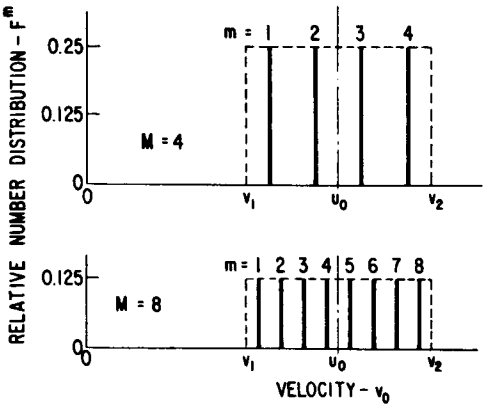

FIG. 21. Simulation of continuous velocity distribution by discrete velocity classes.

1. $$\left(\frac{\Delta\Phi_i}{\Delta Y}\right)_j^k = \frac{q_{j,i}^k}{C(1+q_{j,i}^k)}$$

2. $$\left(1+q_{j,i}^k\right)\left(\frac{\Delta q_i^k}{\Delta Y}\right)_j = \frac{-\pi(\omega_p/\omega)^2}{NCM_r^3} \sum_{m=1}^{M}\sum_{n=1}^{N} T_{j,n}^m \cdot F^m \epsilon^{-2|P_{j,n}^m|/R} \cdot \text{Sign}\, P_{j,n}^m$$

where $$P_{j,n}^m = \left(1+q_{j,n}^m\right)\left(\Phi_{j,n}^m - \Phi_{j,i}^k\right)\left[1 + \frac{C}{2}\left(\Phi_{j,n}^m - \Phi_{j,i}^k\right)\left(\frac{\Delta q_n^m}{\Delta Y}\right)_j + \cdots\right]$$

and $$T_{j,n}^m = \begin{cases} \dfrac{|P_{j,n}^m|}{2\pi/N} & \text{if } T_{j,n}^m < 1 \\ 1 & \text{if } T_{j,n}^m > 1 \end{cases}$$

FIG. 22. Integro-difference equations for IBM 7090.

FOURIER COEFFICIENTS

$$\left.\begin{matrix} A_p^j/I_0 \\ B_p^j/I_0 \end{matrix}\right\} = -\frac{2}{N}\sum_{m=1}^{M}\sum_{n=1}^{N}\left(1+q_0^m\right) F^m \left\{\begin{matrix}\sin\\ \cos\end{matrix}\right\} p\,\Phi_{j,n}^m$$

CORRECTIONS

1. FALLOUT
2. SURROUNDING CYCLES

INITIAL CONDITIONS

EITHER VELOCITY OR DENSITY MODULATION

ADAPTATION TO M VELOCITY CLASSES
(M=4)

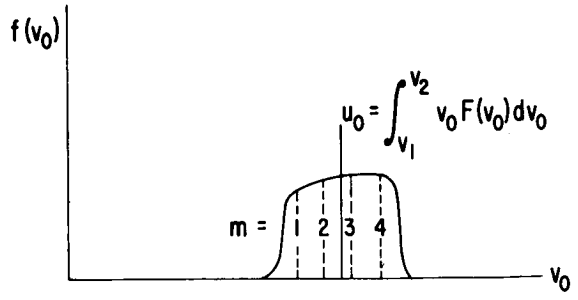

$$F(v_0) = \frac{f(v_0)}{\int_{v_1}^{v_2} f(v_0)\,dv_0}$$

$$\sum_{m=1}^{M} F^m = 1$$

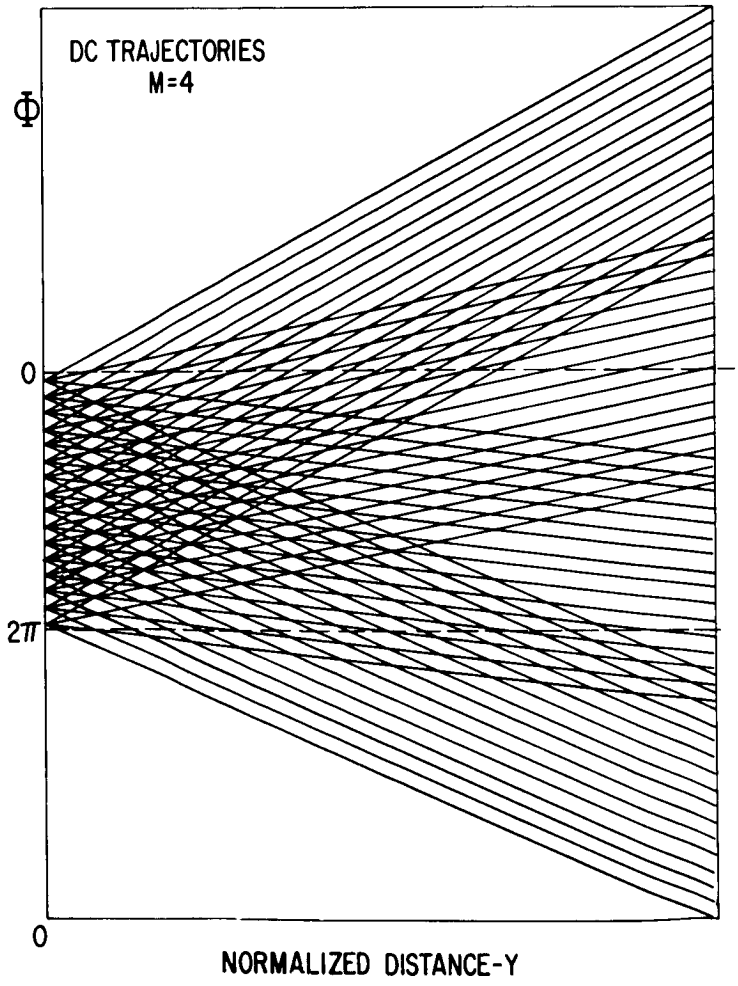

FIG. 23. Direct-current trajectories with four velocity classes.

To make the meaning of the calculated results clearer, let us look at the curves in Fig. 23. Here a velocity distribution has been simulated by four velocity classes. With no modulation we would expect four overlapping sets of trajectories, as shown to the left in Fig. 23. There are 16 particles in each of the four velocity classes, for a total of 64 particles. With 10 percent density modulation imposed on all velocity classes, we get the trajectories shown in Fig. 24. These have been separated here for convenience; in the actual calculation they are superimposed.

Before we look at the details of the trajectories and the results of their Fourier analysis, let me give you a glimpse of the effect the force-taper factor has. Notice the fairly laminar nature of the electrons in the second velocity class in Fig. 24. In Fig. 25 this class is shown for the same case but with the force-taper factor removed. It is evident that the force-taper factor adds considerable stability to the calculation.

Let us now look at the current behavior that our nonlinear analysis predicts for space-charge wave propagation in a beam with a rectangular velocity distribution. In Fig. 26 the results of a 128-particle calculation are plotted, starting with 10 percent density modulation. Only four of the eight trajectory classes are shown. The fundamental current is given in Fig. 27.

Does it look familiar? It should, for it is almost identical with the result obtained from linear distribution function analysis, as is evident from the direct comparison in Fig. 28. Obviously, nonlinear terms do not affect the small-signal behavior of beams with a spread of d-c velocities. This restores our confidence in linearized analysis, and suggests that we must look elsewhere for the reason for the disagreement in Fig. 19. We may also consider the agreement in Fig. 28 as a check on the correctness of our newly developed multivelocity program.

Let us now return to Fig. 27 and look at the new information we have obtained. Notice the behavior of the magnitude of the third harmonic. It reaches a value higher than the initial value of the fundamental! I think it is significant to note that this takes place at about the same distance that we first observe crossover within a velocity class, about two space-charge wavelengths down the beam. This crossover behavior is quite unexpected, especially in a beam of such low initial modulation.

One might be suspicious that this growth is artificial and merely depends upon the number of particles used. We could check this by increasing the number of particles per velocity class from 16 to 32. Unfortunately, this is too expensive, but let us look at the results for current when the number of particles per cycle is reduced from 16 to 8, as shown in Fig. 29. Qualitatively, we have substantially the same behavior as we had before, although things are a little lumpier, as we might expect. The qualitative agreement between the currents in Figs. 29 and 27 suggests that the harmonic growth is a real phenomenon and would persist regardless of the number of disks used. The plots in Fig. 30 show what happens when we return to N = 16 but use only four velocity

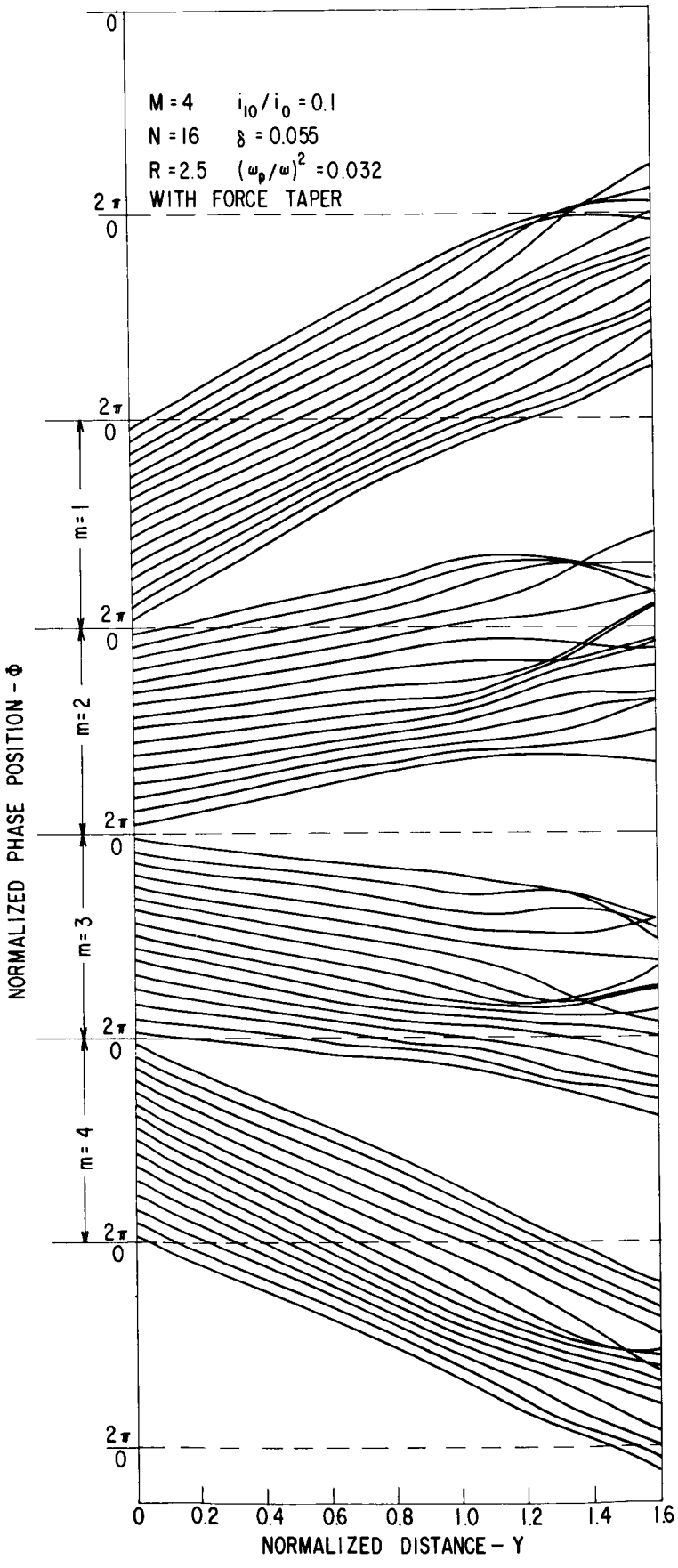

FIG. 24. Radio-frequency trajectories with four velocity classes, 10 percent modulation on all classes. (See Fig. 30 for current behavior.)

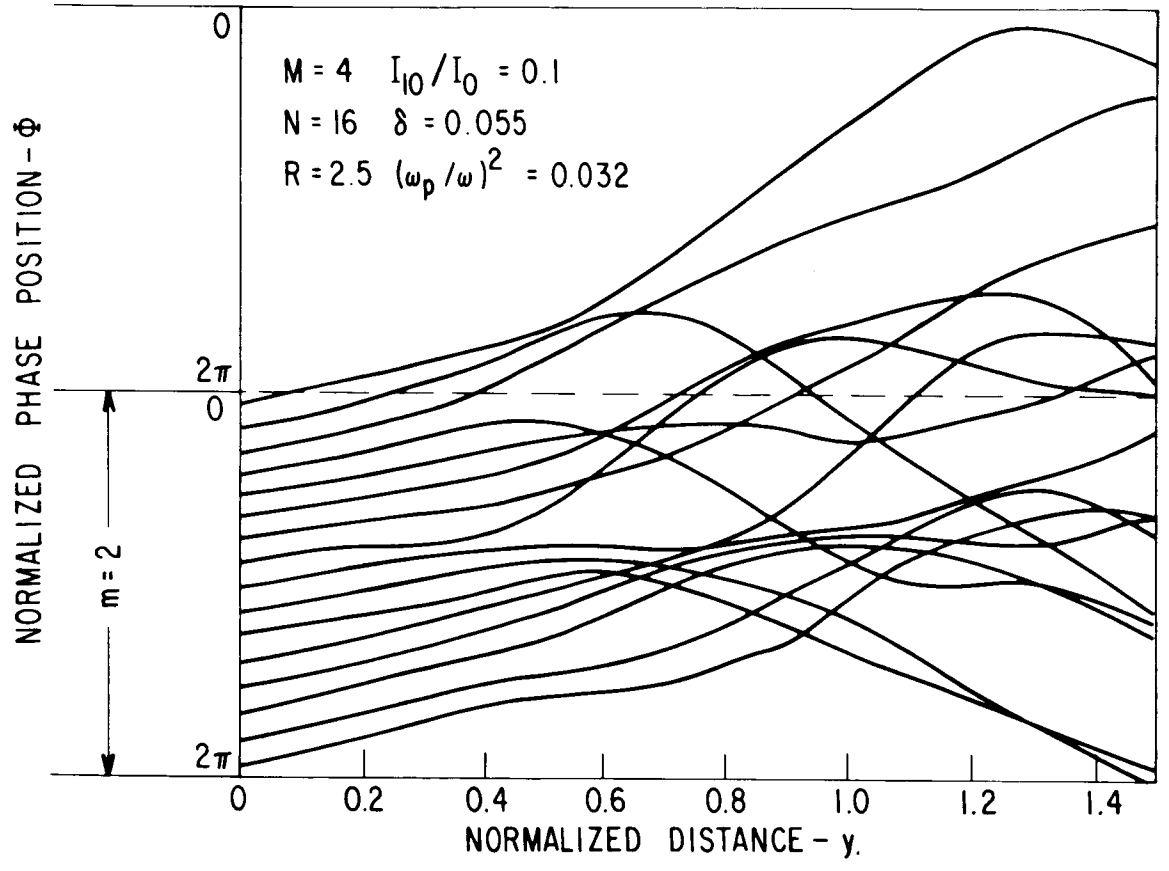

FIG. 25. Class 2 electron trajectories without force taper (compare with Fig. 24).

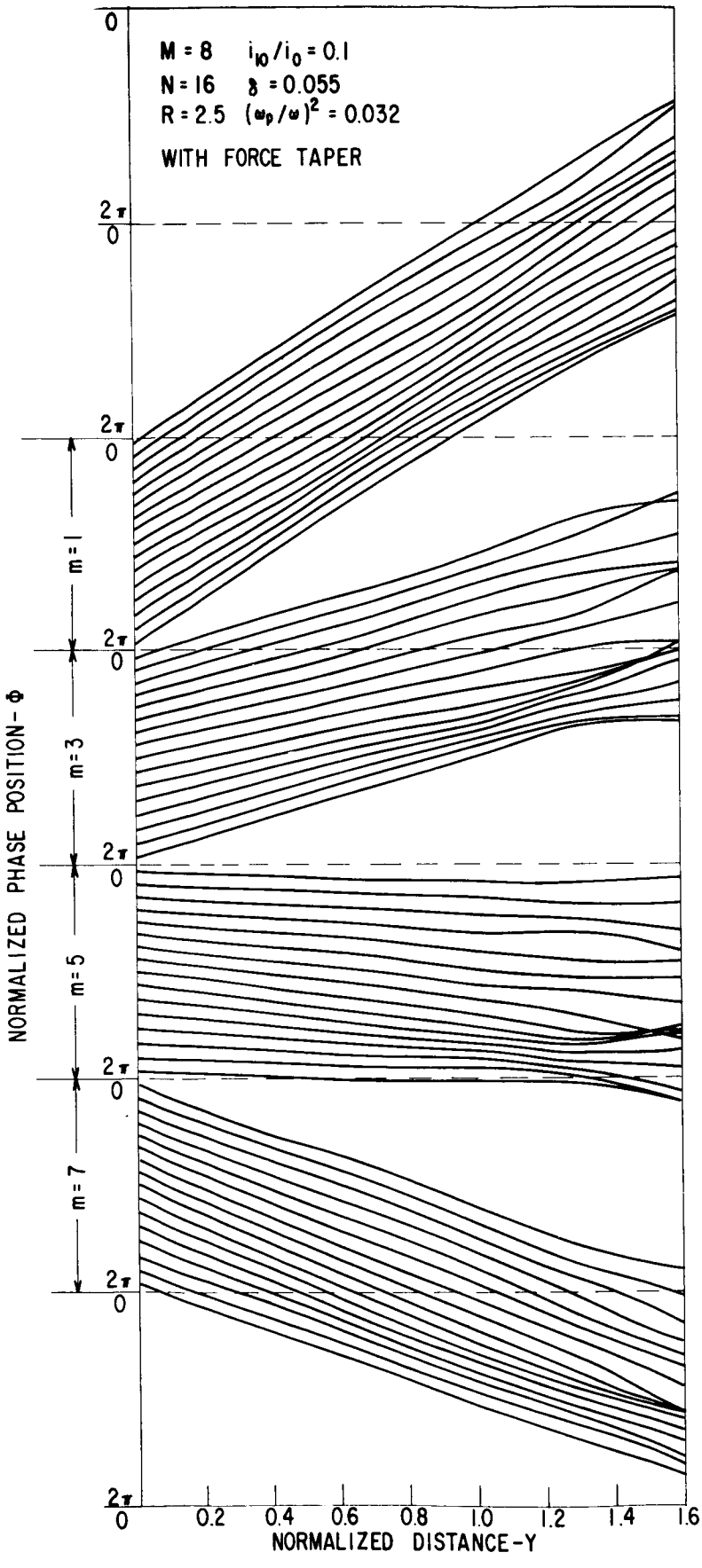

FIG. 26. Calculated electron trajectories for sixteen electrons in each of eight velocity classes (four shown).

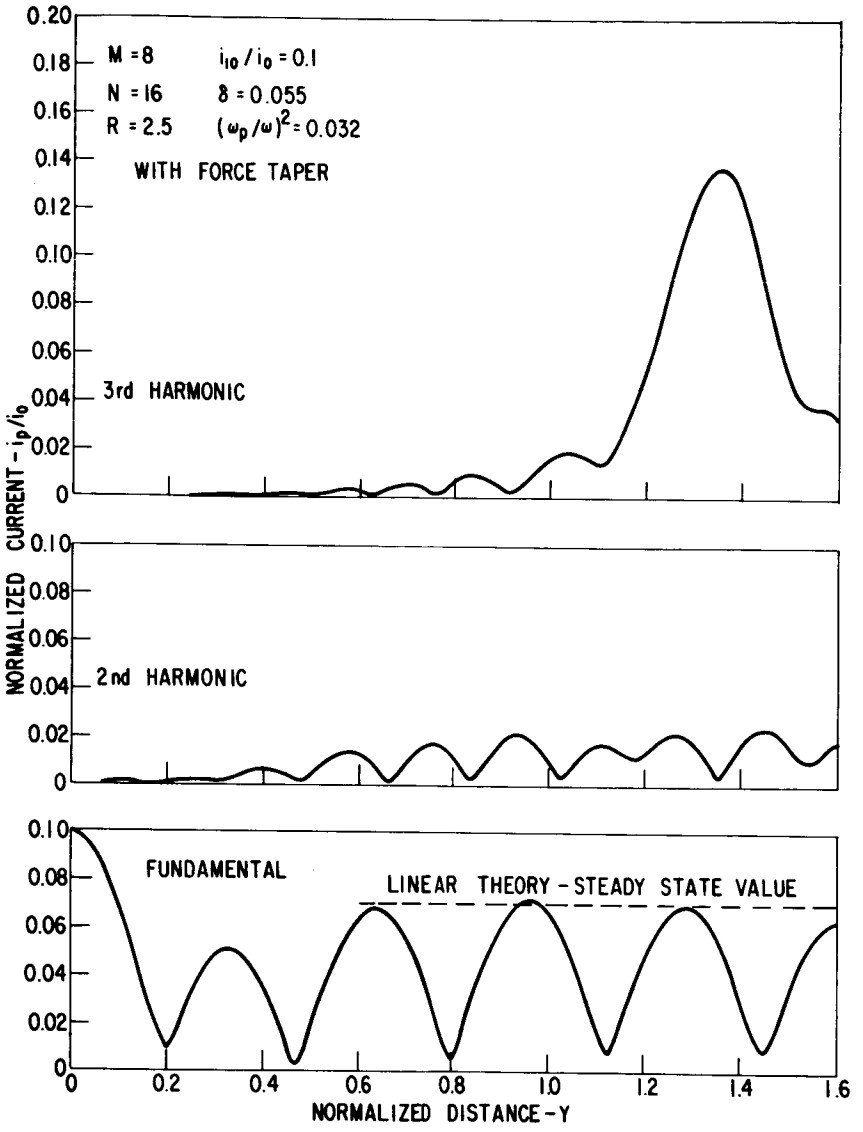

FIG. 27. Fundamental and harmonic currents for the case of Fig. 26.

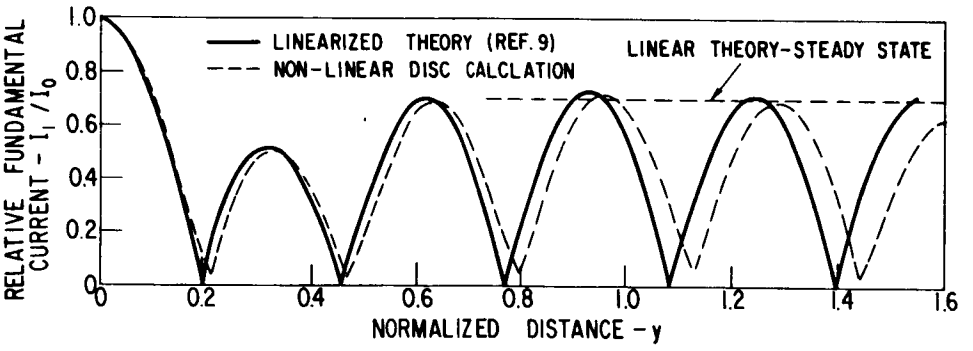

FIG. 28. Comparison of fundamental current as calculated by linearized distribution function analysis and by nonlinear disk-electron analysis.

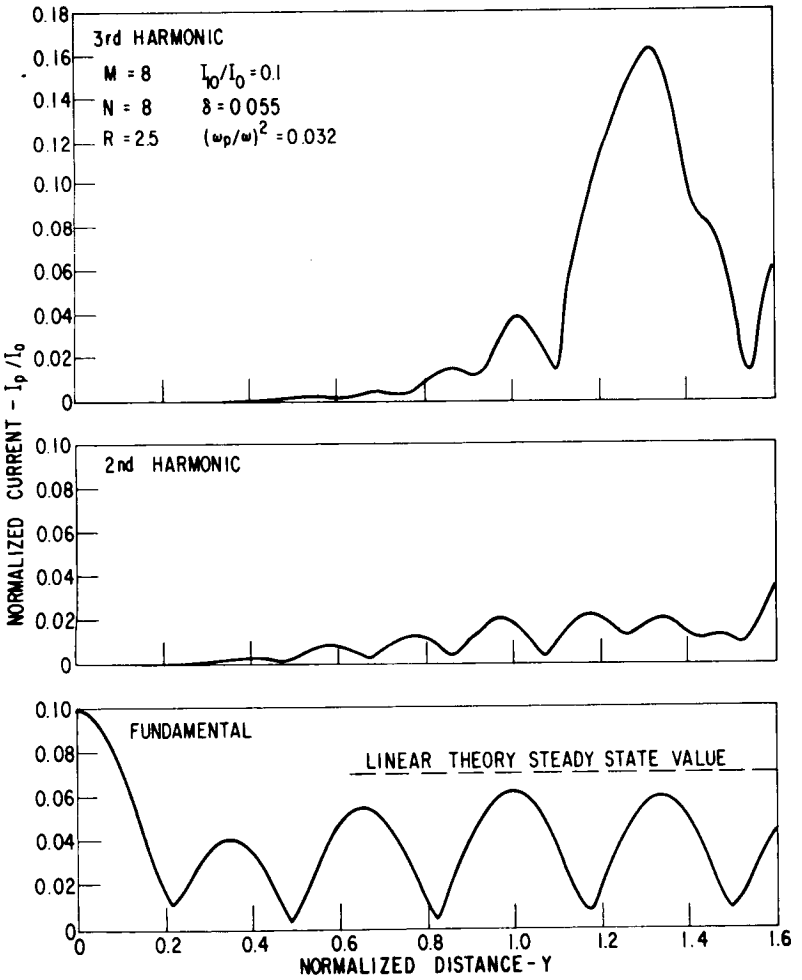

FIG. 29. Calculated currents for eight electrons in each of eight velocity classes.

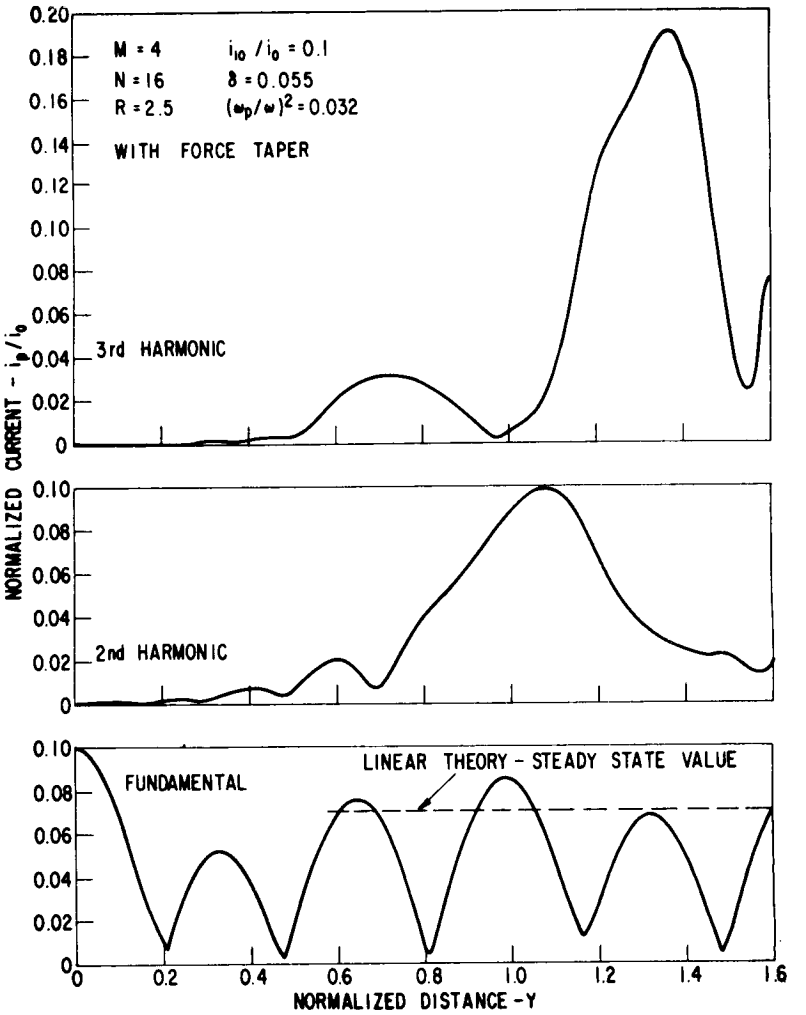

FIG. 30. Fundamental and harmonic currents for the case of Fig. 24.

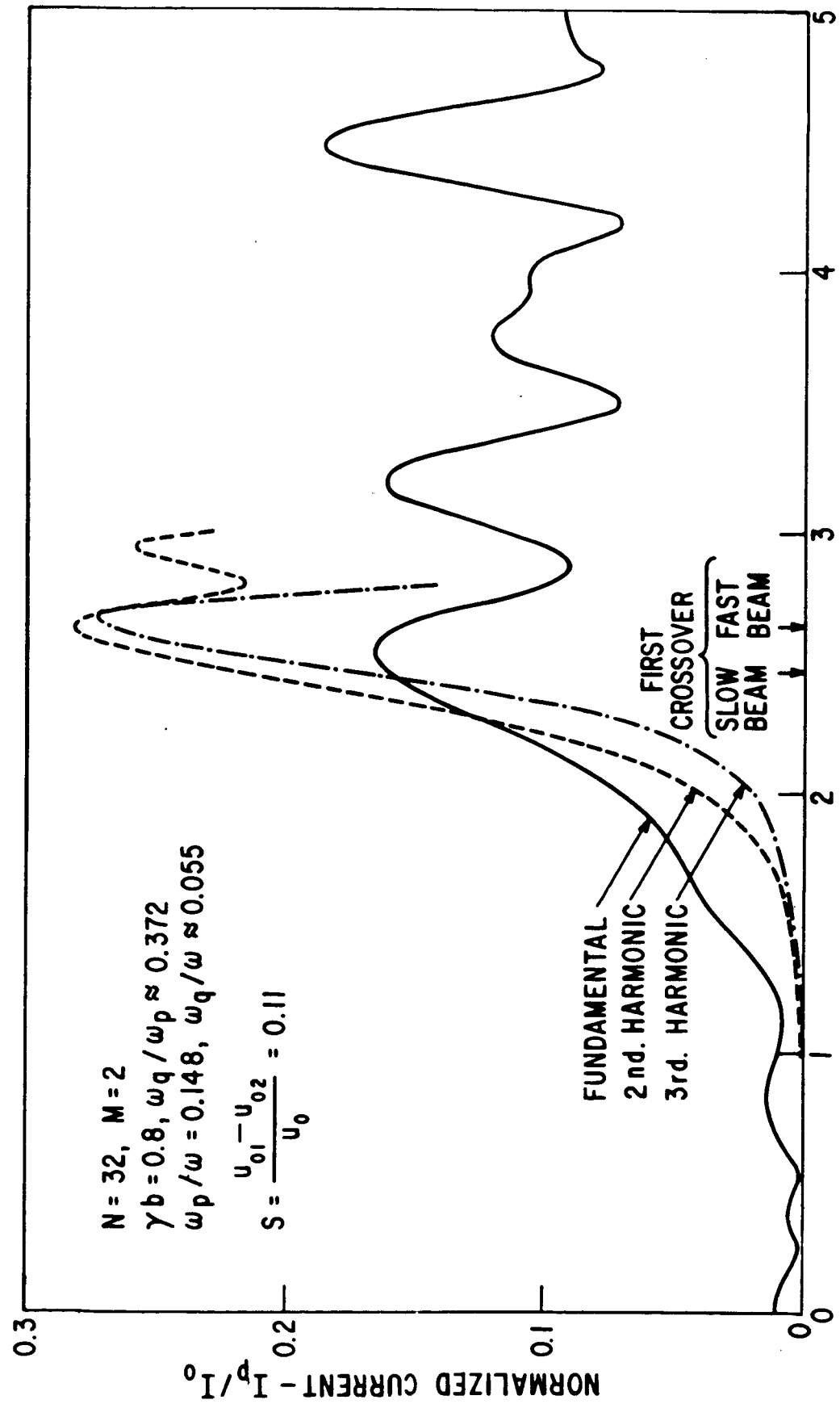

FIG. 31. Calculated current variation for the case of double-stream amplification.

classes. Again the crossover phenomenon is present (see Fig. 24), this time accompanied by a large second harmonic as well as third.

As a practical application of our nonlinear analysis, I thought it would be interesting to calculate the simplest multiple beam case, double-stream amplification (24,25). To my knowledge, only linear analyses exist for this phenomenon, and these are unable to predict the saturation of the phenomenon. Our analysis can do this, so let us look at results for the case of two beams, the fast wave of one coinciding with the slow wave of the other as in Fig. 6. With a 1 percent density modulation on both beams, the calculated result is shown in Fig. 31. The fundamental current shows a gain with distance of more than 20 db before it levels off at about 0.15 of the direct current. Note that the harmonics come up fast and actually overtake the fundamental at the leveling-off point.

It is undoubtedly significant that this high harmonic content occurs at the same distance at which crossover first takes place within each beam, as shown by the arrows in Fig. 31. We are surprised to find saturation and crossover taking place at such a low signal level. This seems to be characteristic of the behavior of finite diameter multiple-velocity beams, and is probably a result of the counterpart of harmonic growth in single-velocity finite diameter beams, which we talked about earlier.

That about completes the story. Let me summarize what we have learned.

(1) We discussed the physical picture of linear space-charge waves in both infinite and finite diameter electron beams; this led to the important concept of the plasma frequency reduction factor.

(2) We saw how a harmonic growth mechanism exists for space-charge waves in finite diameter beams. This behavior is neatly charted by the phase shift characteristics of the waves as calculated by a disk-electron analysis.

(3) Finally, we discussed the extension of the nonlinear disk-electron analysis to the case of multiple electron beams, where we found the interesting phenomenon of harmonic growth, associated with crossover within a velocity class. Both of these effects are outside the regime of linear one-dimensional theory.

REFERENCES

1. D. R. Hamilton, J. K. Knipp, and J. B. H. Kuper, Klystrons and Microwave Triodes, McGraw-Hill Book Co., New York, 1948 (M.I.T. Radiation Laboratory Series, vol. 7).

2. T. H. Stix, The Theory of Plasma Waves, McGraw-Hill Book Co., New York, 1962.

3. W. P. Allis, Propagation of Waves in a Plasma in a Magnetic Field, IRE Trans. on Microwave Theory Tech., MTT-9:79-82, January 1961.

4. R. J. Papa, M.I.T. Quarterly Progress Report No. 55, October 1959.

5. T. G. Mihran, The Effect of Space Charge on Bunching in a Two-cavity Klystron, IRE Trans. on Electron Devices, ED-6:54-64, January 1959.

6. W. C. Hahn, Small Signal Theory of Velocity Modulated Electron Beams, Gen. Elec. Rev., 42:258-270, June 1939.

7. A. H. W. Beck, Space Charge Waves, Pergamon Press, New York, 1958.

8. G. M. Branch and T. G. Mihran, Plasma Frequency Reduction Factors in Electron Beams, IRE Trans. on Electron Devices, ED-2:3-11, April 1955.

9. D. L. Webster, Cathode Ray Bunching, J. Appl. Phys., 10:501-508, July 1939.

10. T. G. Mihran, Harmonic Current Growth in Velocity-Modulated Electron Beams, J. Appl. Phys., 30:1346-1350, September 1959.

11. P. K. Tien, L. R. Walker, and V. M. Wolontis, Large Signal Theory of Traveling-Wave Amplifiers, Proc. IRE, 43:269-276, March 1955.

12. J. E. Rowe, A Large-Signal Analysis of the Traveling-Wave Amplifier: Theory and General Results, IRE Trans. on Electron Devices, ED-3: 39-56, January 1956.

13. P. K. Tien, A Large Signal Theory of Traveling-Wave Amplifiers, Bell Sys. Tech. J., 35:349-374, March 1956.

14. S. E. Webber, Ballistic Analysis of a Two Cavity Finite Beam Klystron, IRE Trans. on Electron Devices, ED-5:98-108, April 1958.

15. J. E. Rowe, Relativistic Beam-Wave Interactions, Proc. IRE, 50:170-178, February 1962.

16. S. Bloom and R. W. Peter, Transmission Line Analog of a Modulated Electron Beam, R.C.A. Rev., 15:95-112, March 1954.

17. F. Paschke, Generation of Second Harmonic in a Velocity-Modulated Electron Beam of Finite Diameter, R.C.A. Rev., 19:617-627, December 1958.

18. F. Paschke, Non-Linear Theory of a Velocity Modulated Electron Beam with Finite Diameter, R.C.A. Rev., 21:53-74, March 1960.

19. S. Olving, Nonlinear Space-Charge-Wave Theory of the Radially Finite Electron Beam, Cornell University, School of Electrical Engineering, Research Report EE 497, June 1961.

20. T. G. Mihran, R-f Current Behavior in Electron Beams with D-c Velocity Spread, J. Appl. Phys., 33:1582-1590, April 1962.

21. S. Bloom, Space-Charge-Wave Decay Along a Signal-Current-Excited Multivelocity Beam, submitted to J. Appl. Phys, 1963.

22. S. P. Yu and T. G. Mihran, Non-Linear Behavior of Electron Beams with Velocity Distribution: I, General Analysis, submitted to J. Appl. Phys., 1963.

23. T. G. Mihran and S. P. Yu, Non-Linear Behavior of Electron Beams with Velocity Distribution: II, Application to Rectangular Velocity Distribution, submitted to J. Appl. Phys., 1963.

24. L. S. Nergaard, Analysis of a Single Model of a Two-Beam Growing-Wave Tube, R.C.A. Rev., 9:585-601, December 1948.

25. A. V. Hollenberg, Experimental Observation of Amplification by Interaction Between Two Electron Streams, Bell Sys. Tech. J., 28:52-58, January 1949.

MULTIDIMENSIONAL NONLINEAR THEORY OF MICROWAVE INTERACTION

J. E. Rowe
Department of Electrical Engineering
The University of Michigan, Ann Arbor, Michigan

ABSTRACT

The subject of nonlinear interactions between accelerated streams (ions and/or electrons) and electromagnetic waves is discussed in the framework of a Lagrangian analysis. One-, two-, and three-dimensional analyses are developed, including arbitrary magnetic fields as specified by ω_c/ω. The cold plasma approximation is generally used but can easily be removed. Digital computer solutions of the nonlinear equations yield information on the growth rate and phase of the electromagnetic wave, in addition to velocity, phase, and harmonic current values for the stream charges as functions of distance and rf signal amplitude. Finally it is shown that the nonlinear equations can be solved in closed form in the framework of a hard-kernel bunch description of the stream charge.

Author

INTRODUCTION

In recent years the subject of nonlinear beam-plasma phenomena has become of great interest in radio astronomy, ionospheric propagation, and short wavelength coherent power generation. To understand and exploit the essential features of beam-wave interactions in anisotropic media, a general nonlinear analysis is required in order to calculate energy transfer between system constituents. The many linear (small amplitude) analyses that have been made give detailed information on the wave propagation constants (eigenvalues), but do not shed any light on the energy exchange characteristics.

Some nonlinear analyses of wave propagation in plasmas have been made using a one-dimensional model and neglecting the effect of electron crossovers. Neglecting the crossing of particle trajectories permits the use of fluid flow equations (Eulerian analysis) and thereby considerably simplifies the problem. It is the purpose of this paper to outline the use of a Lagrangian method of analysis for the study of nonlinear wave propagation in plasmas and electron beams. This method has proved quite valuable in the study of microwave electron-beam tubes on the basis of a one-dimensional model.

The Lagrangian method allows for trajectory crossovers, and multidimensional effects are easily included. The basis of the formulation is the integration of the equations of motion along a dynamical trajectory, summing all forces acting on representative charge groups injected at some initial plane. The method is outlined here for both one- and two-dimensional systems. In general, solutions are obtained by digital computer methods, although under certain specialized conditions the nonlinear equations may be solved in closed form. The assumption of a cold plasma is made for simplicity, but this is not necessary.

The Lagrangian formulation can and has been applied to the following nonlinear wave interaction systems:

Electron beam, electromagnetic wave
- Klystron
- Traveling-wave amplifier
- Backward-wave oscillator
- Crossed-field amplifier
- Crossed-field backward-wave oscillator

Double-beam interaction with either cavity coupling or distributed wave interaction circuits

Electron beam-plasma interaction with either cavity coupling or distributed wave interaction circuits

The wave propagation is described using equivalent circuit methods, and interparticle forces are calculated with the aid of Green's-function techniques. All of these nonlinear systems are solved as initial-value problems. It is possible, however, with the penalty of greater computation expense, to solve them as boundary-value problems. The development of the one-dimensional Lagrangian analysis and its application has been given in detail in several articles (1,2,3,4); hence the details are omitted here.

LAGRANGIAN ANALYSIS

To simplify the development, only one system of nonlinear equations is given. An axially symmetric coordinate system is assumed, and an electromagnetic wave is considered to propagate in the axial direction along either a radio frequency circuit or a plasma column. The wave is coupled to an electron beam that drifts along the axis of the system. This beam-wave configuration is illustrated in Fig. 1.

The variation of rf voltage along the equivalent transmission line is given by

$$\frac{\partial^2 V(z,t)}{\partial t^2} - v_o^2 \frac{\partial^2 V(z,t)}{\partial z^2} + 2\omega C d \frac{\partial V(z,t)}{\partial t} = \pm v_o Z_o \left(\frac{\partial^2 \sigma}{\partial t^2} + 2\omega C d \frac{\partial \sigma}{\partial t} \right) \qquad (1)$$

where σ = linear charge density coupled to circuit

v_o, Z_o = characteristic velocity and impedance of transmission line

$C = (Z_o I_o / 4V_o)^{1/3}$

The upper of the two signs on the right-hand side of Eq. 1 is used for forward-wave interaction and the lower for backward-wave interaction.

For a cylindrical coordinate system in which the electron or ion stream does not fill the circuit, the radial wave equation governs propagation in the intermediate region. Thus

$$\nabla^2 V(r,z) - \frac{1}{c^2}\frac{\partial^2 V(r,z)}{\partial t^2} = 0 \tag{2}$$

It is convenient to introduce a normalized potential function of the following form into Eq. 2:

$$V(y,x,\Phi,\theta_y) \triangleq \mathrm{Re}\left[\frac{Z_o I_o}{C} A(y)\,\psi(x)\,e^{-j\Phi}\,e^{j\theta_x}\right] \tag{3}$$

where $y = C\omega z/u_o$, axial distance

$x = C\omega r/u_o$, radial distance

$x_o = C\omega r_o/u_o$, normalized initial radius

$\Phi_o = \omega t_o$

$\Phi(z,r_o,t) = (\omega z/u_o) - \omega t - \theta_y$

The radial propagation equation may now be written in two parts:

$$\psi\frac{d^2A}{dy^2} - A\psi\left(\frac{1}{C} - \frac{d\theta_y}{dy}\right)^2 + A\frac{d^2\psi}{dx^2} - \left(\frac{d\theta_x}{dx}\right)^2 A\psi + \frac{A}{x}\frac{d\psi}{dx} + A\psi\left(\frac{k_e}{C}\right)^2 = 0 \tag{4}$$

and

$$-2\psi\left(\frac{1}{C} - \frac{d\theta_y}{dy}\right)\frac{dA}{dy} + A\psi\frac{d^2\theta_y}{dy^2} + 2A\frac{d\psi}{dx}\frac{d\theta_x}{dx} + A\psi\frac{d^2\theta_x}{dx^2} + \frac{A\psi}{x}\frac{d\theta_x}{dx} = 0 \tag{5}$$

The radial coupling function is shown in Fig. 2.

The forcing function on the right of Eq. 1 is calculated from the conservation of charge, $\rho r\,dr dz = \rho_o r_o\,dr_o dz_o$, and is written as

$$\sigma = 2\pi\int_0^{b'} \rho_o r_o \left|\frac{\partial z_o}{\partial z}\right| dr_o \tag{6}$$

where $\rho_o = I_o/\pi b'^2 u_o$. In normalized coordinates Eq. 6 becomes

$$\sigma = \frac{2I_o}{x_{b'}^2 u_o}\int_0^{x_{b'}} \left|\frac{\partial\Phi_o}{\partial\Phi}\right| \frac{x_o}{1+2Cu_y}\,dx_o \tag{7}$$

After introduction of Lagrangian variables and considerable simplification, Eq. 1 may also be written in two parts:

$$\frac{d^2A(y)}{dy^2} + A(y)\left[\frac{(1+Cb)^2}{C^2} - \left(\frac{1}{C} - \frac{d\theta_y}{dy}\right)^2\right]$$

$$= \mp \frac{2(1+Cb)}{\pi C\, x_{b'}^2}\left\{\int_0^{x_{b'}}\left[\int_0^{2\pi} \frac{\psi(x)\cos\Phi'\, x'_o\, dx'_o\, d\Phi'_o}{1+2Cu_y(y,x'_o,\Phi'_o,\phi'_o)}\right.\right.$$

$$\left.\left. + 2Cd\int_0^{2\pi} \frac{\psi(x)\sin\Phi'\, x'_o\, dx'_o\, d\Phi'_o}{1+2Cu_y(y,x'_o,\Phi'_o,\phi'_o)}\right]\right\} \qquad (8)$$

and

$$A(y)\left[\frac{d^2\theta_y}{dy^2} - \frac{2d}{C}(1+Cb)^2\right] + \frac{2dA(y)}{dy}\left(\frac{d\theta_y}{dy} - \frac{1}{C}\right)$$

$$= \mp \frac{2(1+Cb)}{\pi C}\left\{\int_0^{x_{b'}}\left[\int_0^{2\pi} \frac{\psi(x)\sin\Phi'\, x'_o\, dx'_o\, d\Phi'_o}{1+2Cu_y(y,x'_o,\Phi'_o,\phi'_o)}\right.\right.$$

$$\left.\left. - 2Cd\int_0^{2\pi} \frac{\psi(x)\cos\Phi'\, x'_o\, dx'_o\, d\Phi'_o}{1+2Cu_y(y,x'_o,\Phi'_o,\phi'_o)}\right]\right\} \qquad (9)$$

where $dz/dt \triangleq u_o[1+2Cu_y(y,\Phi_o,x_o,\phi_o)]$, axial velocity

$dr/dt \triangleq 2Cu_o u_x(y,\Phi_o,x_o,\phi_o)$, radial velocity

$d\phi/dt \triangleq u_o[(2C/r)\, u_\phi(y,\Phi_o,x_o,\phi_o)]$, angular velocity

In a cylindrical coordinate system the components of the vector Lorentz equation are conveniently written as

$$\frac{d^2r}{dt^2} - r\left(\frac{d\phi}{dt}\right)^2 = |\eta|\left(E_{sc-r} - \frac{\partial V_c}{\partial r} + B_z r\frac{d\phi}{dt}\right) \qquad (10)$$

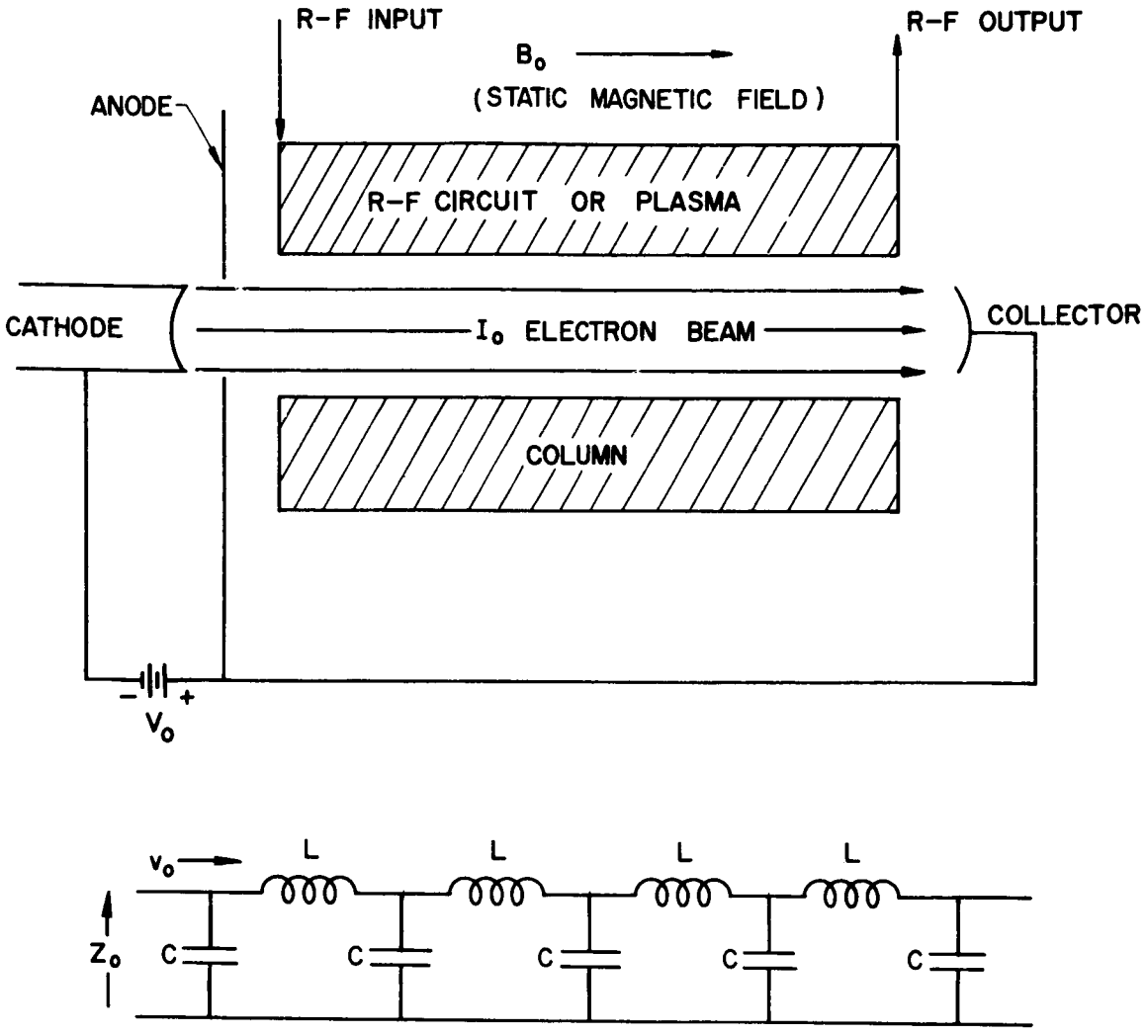

FIG. 1. Schematic and equivalent circuit for beam-plasma interaction.

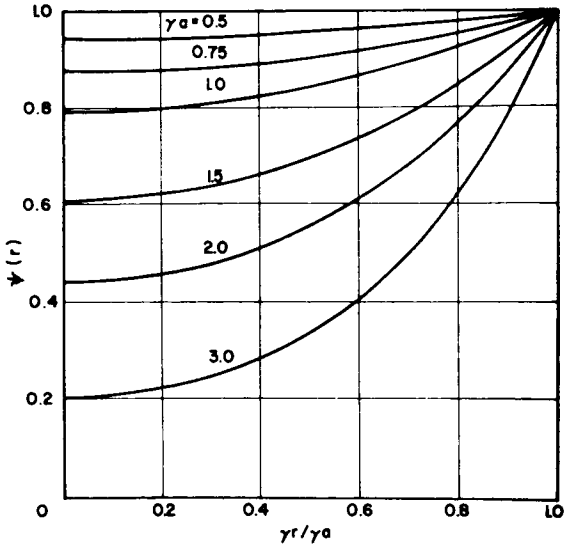

FIG. 2. Radial coupling function.

$\psi(r) = I_0(\gamma r)/I_0(\gamma a)$

$$\frac{1}{r}\frac{d}{dt}\,r^2\,\frac{d\phi}{dt} = |\eta|\left(E_{sc-\phi} - \frac{1}{r}\frac{\partial V_c}{\partial \phi} - B_z\frac{dr}{dt}\right) \tag{11}$$

and

$$\frac{d^2z}{dt^2} = |\eta|\left(E_{sc-z} - \frac{\partial V_c}{\partial z}\right) \tag{12}$$

where E_{sc-z}, E_{sc-r}, $E_{sc-\phi}$ are the components of the space-charge fields (coulomb interaction fields between particles), conveniently calculated using Green's function techniques for the geometry involved.

These equations are quite general, accounting for particle motion about the axis of symmetry. The magnetic field is assumed to be wholly axially directed. The general three-dimensional space-charge potential is given by

$$V_{sc} = \left(\frac{u_o}{C\omega}\right)^2 \iiint \frac{CI_o x_o' \, d\phi_o' \, dx_o' \, d\Phi_o'}{2\pi\epsilon\, a'^2 \pi b'^2 u_o} \sum_{\ell=1}^{\infty}\sum_{s=0}^{\infty} (2-\delta_s^o)\, e^{-\nu_{\ell s}|y-y'|}$$

$$\cdot \cos s(\phi - \phi') \frac{J_s(\nu_{\ell s}x')\, J_s(\nu_{\ell s}x)}{\nu_{\ell s}[J_{s+1}(\nu_{\ell s}x_{a'})]^2} \tag{13}$$

where a' = circuit radius
b' = stream radius
ϕ = angular position coordinate

After introduction of the previously defined normalized variables and some simplification, the force equations for three-dimensional flow take the form of Eqs. 14, 15, and 16. The magnetic field terms appear as the normalized cyclotron frequency, ω_c/ω. The weighting functions, which indicate the effect of interparticle coulomb forces, are shown in Figs. 3 through 6 for an axially symmetric stream that has been divided into six annular rings of charge.

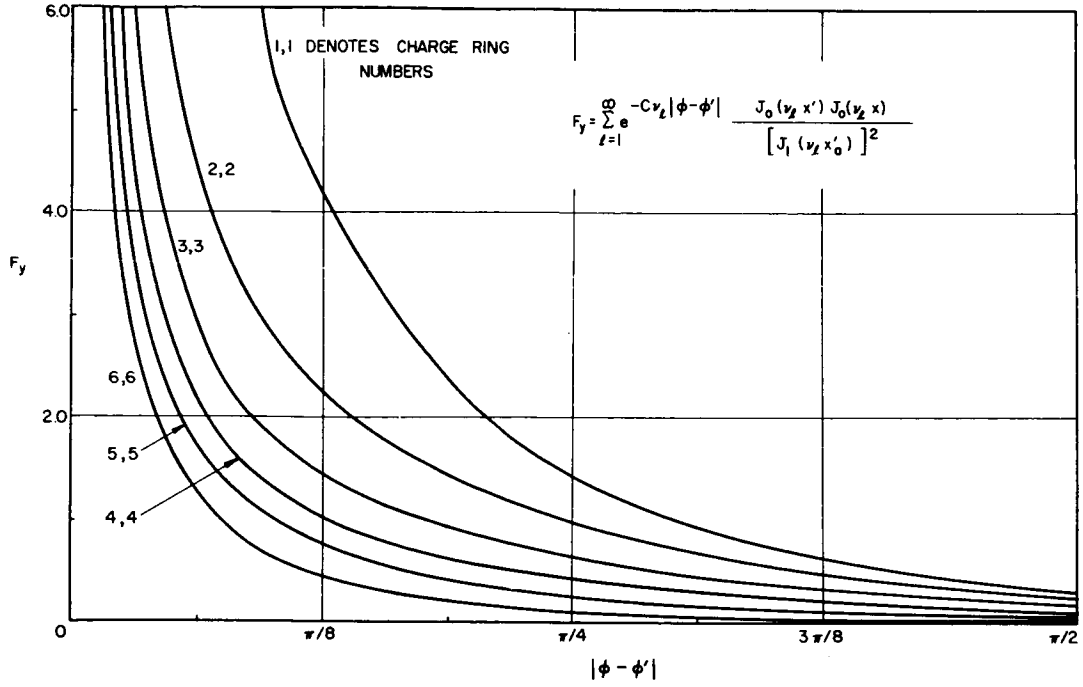

FIG. 3. Axial space-charge weighting function forces between particles in the same ring. b'/a' = 0.7

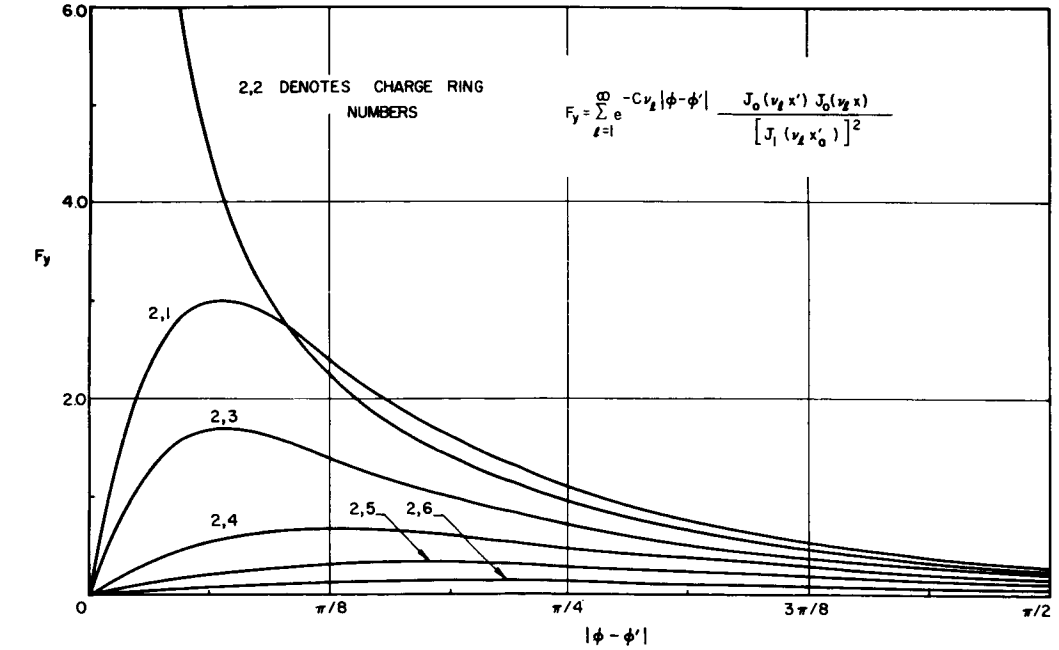

FIG. 4. Axial space-charge weighting function forces between particles in different rings. b'/a' = 0.7

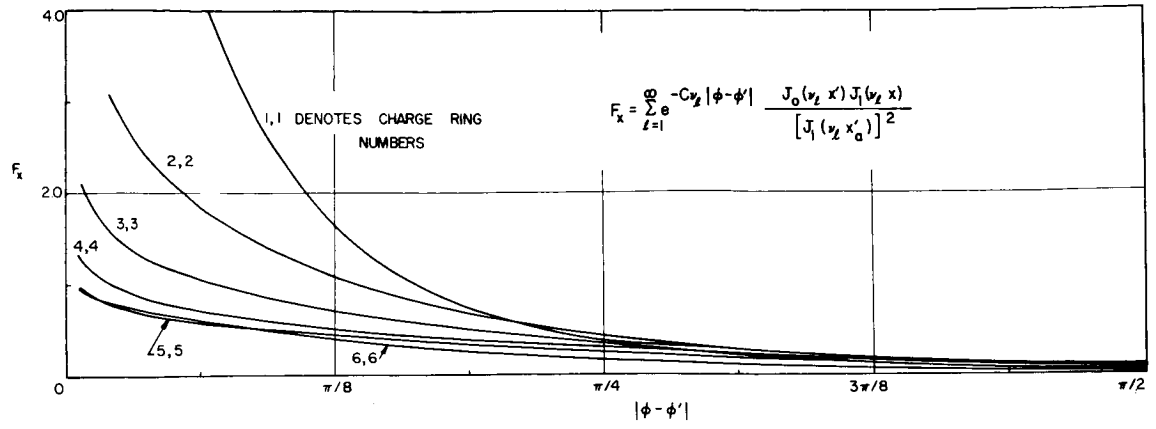

FIG. 5. Radial space-charge weighting function forces between particles in the same ring. b'/a' = 0.7

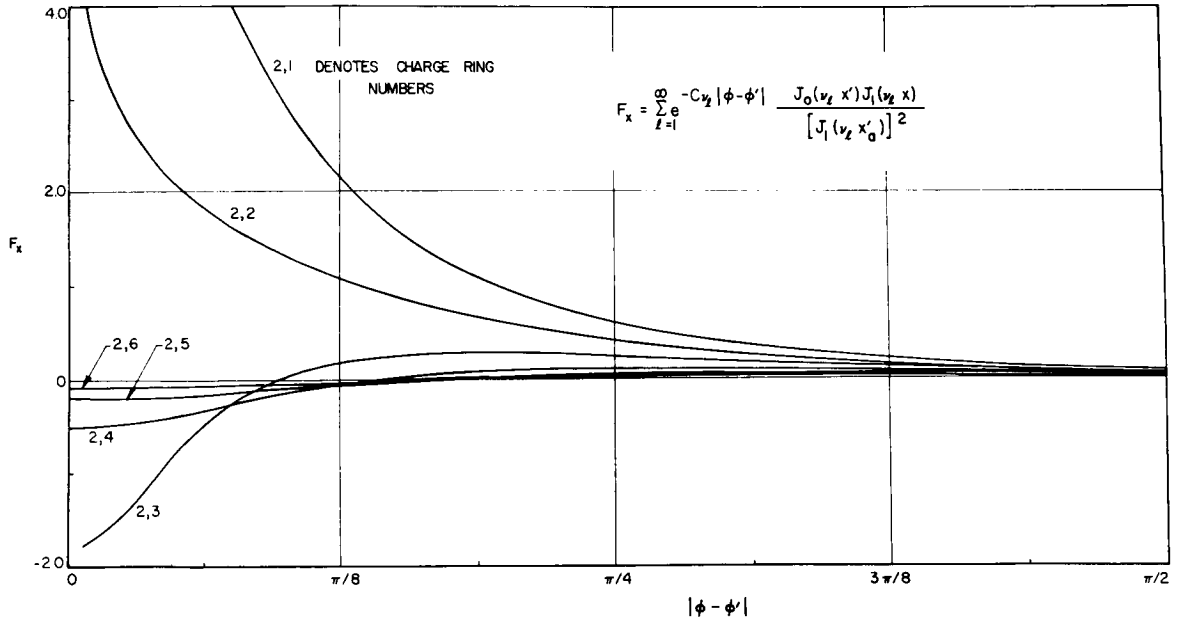

FIG. 6. Radial space-charge weighting function forces between particles in different rings. b'/a' = 0.7

$$\frac{\partial u_y(y,x_o,\Phi_o,\phi_o)}{\partial y}\left[1 + 2Cu_y(y,x_o,\Phi_o,\phi_o)\right]$$

$$= -\left[1 - C\frac{d\theta_y(y)}{dy}\right] A(y)\psi(x)\sin(\Phi - \theta_x)$$

$$+ C\frac{dA(y)}{dy}\psi(x)\cos(\Phi - \theta_x)$$

$$+ \left(\frac{\omega_p}{\omega C}\right)^2 \frac{1}{2x_{a'}^2}\int_0^{x_{b'}} \left\{\int_0^{2\pi} x'_o\, dx'_o \,\mathrm{sgn}(y - y')\, d\Phi'_o \right.$$

$$\left. \cdot \sum_{\ell=1}^{\infty} e^{-\nu_\ell |y-y'|} \frac{J_o(\nu_\ell x)J_o(\nu_\ell x')}{[J_1(\nu_\ell x_{a'})]^2}\right\} \tag{14}$$

and

$$\frac{\partial u_x(y,x_o,\Phi_o,\phi_o)}{\partial y}\left[1 + 2Cu_y(y,x_o,\Phi_o,\phi_o)\right]$$

$$= A(y)C\frac{d\psi(x)}{dx}\cos(\Phi - \theta_x) + A(y)C\psi(x)\frac{d\theta_x}{dx}\sin(\Phi - \theta_x)$$

$$+ \left(\frac{\omega_c}{\omega C}\right) u_\phi + \left(\frac{\omega_p}{\omega C}\right)^2 \frac{1}{2x_{a'}^2}\int_0^{x_{b'}} \left\{\int_0^{2\pi} x'_o\, dx'_o\, d\Phi'_o \right.$$

$$\left. \cdot \sum_{\ell=1}^{\infty} e^{-\nu_\ell |y-y'|} \frac{J_o(\nu_\ell x')J_1(\nu_\ell x)}{[J_1(\nu_\ell x_{a'})]^2}\right\} \tag{15}$$

and

$$\frac{\partial u_\phi(y,x_o,\Phi_o,\phi_o)}{\partial y}\left[1 + 2Cu_y(y,x_o,\Phi_o,\phi_o)\right] = -\left(\frac{\omega_c}{\omega C}\right) u_x \tag{16}$$

Since the normalized radial and angular position variables have been considered as dependent variables, the following additional equations are required to complete the system.

$$\frac{d\theta_y}{dy} + \frac{\partial\Phi(y,\Phi_o,x_o,\phi_o)}{\partial y} = \frac{2u_y(y,\Phi_o,x_o,\phi_o)}{1+2Cu_y(y,\Phi_o,x_o\phi_o)} \tag{17}$$

$$x(y,x_o,\Phi_o,\phi_o) = x_o + 2C\int_0^y \frac{u_x(y,x_o,\Phi_o,\phi_o)\,dy}{1+2Cu_y(y,x_o,\Phi_o,\phi_o)} \tag{18}$$

$$\phi(y,x_o,\Phi_o,\phi_o) = \phi_o + 2C\int_0^y \frac{u_\phi}{x}\,\frac{dy}{1+2Cu_y(y,x_o,\Phi_o,\phi_o)} \tag{19}$$

This system of equations describes a nonlinear traveling-wave interaction between a stream and an arbitrary type of wave propagating medium. Either forward-wave interaction (wave phase and group velocity in the same direction) or backward-wave interaction (oppositely directed phase and group velocities) may be investigated. Both problems are solved as initial-value problems in which the system parameters are selected and the dependent variables and their derivatives are given at the input plane, $z = 0$. The details of parameter selection and variable specification are not given here for reasons of brevity. (See Refs. 1, 3, and 4 for these details and for a discussion of the method of solution on a high-speed digital computer.)

The system may be simplified to a one-dimensional system for many problems, providing that the transverse dimensions of the beam and the plasma are not large. Beam-plasma equations have been derived on this basis, including the interaction with a propagating electromagnetic wave.

THEORETICAL RESULTS

The results from digital solution of the system described and other systems of nonlinear interaction equations may generally be considered in two categories, namely, those associated with the wave (amplitude and phase) and those associated with the stream (velocity, phase position, and rf harmonic current amplitudes). A typical set of results for a three-dimensional space-charge flow in an axially symmetric propagating circuit is shown in Fig. 7, where the gain of the rf wave is shown versus distance as a function of the strength of the beam confinement field as measured by ω_c/ω. These particular results have assumed very weak interparticle coulomb fields. The gain is also compared with the one-dimensional nonlinear results.

An interesting aspect of the charge flow is depicted in the dynamical trajectory plots for the injected charge groups shown in Fig. 8. Recall that axial symmetry persists, and hence each trajectory identifies a figure of revolution. Since in the case shown there is no confining Lorentz force, in the region of large amplitude rf fields the charges move radially to the circuit and eventually are intercepted there.

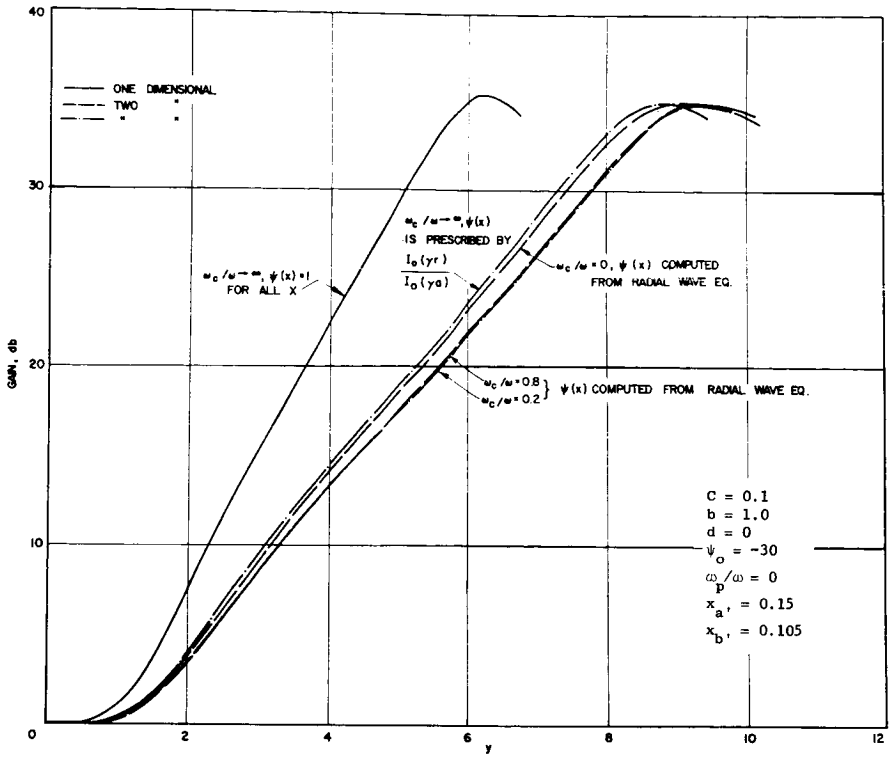

FIG. 7. Gain versus distance.

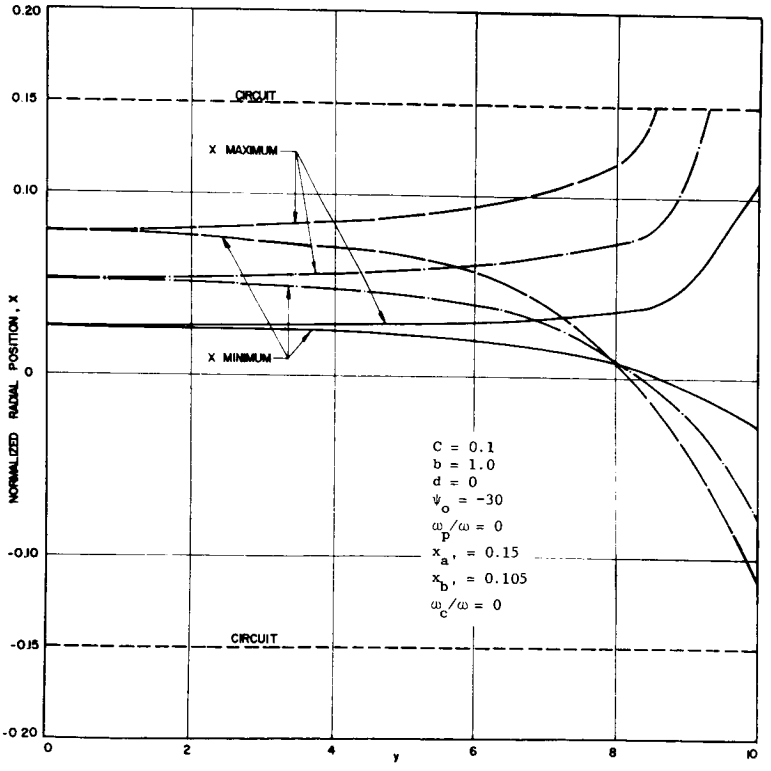

FIG. 8. Radial versus axial position.

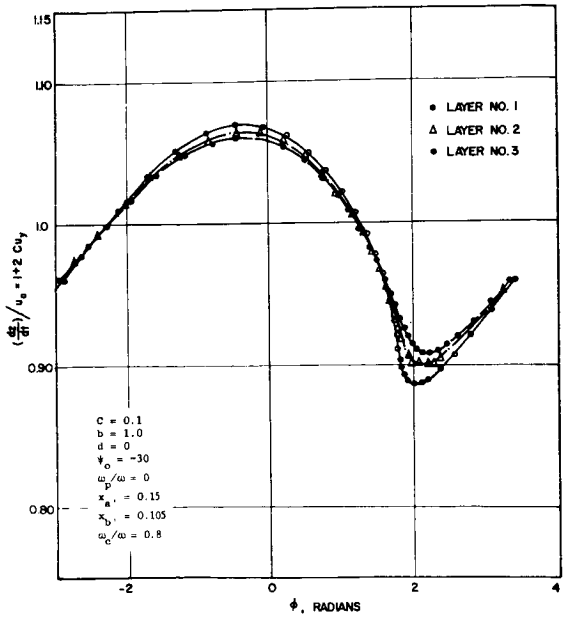

FIG. 9. Axial velocity versus phase, y = 7.2.

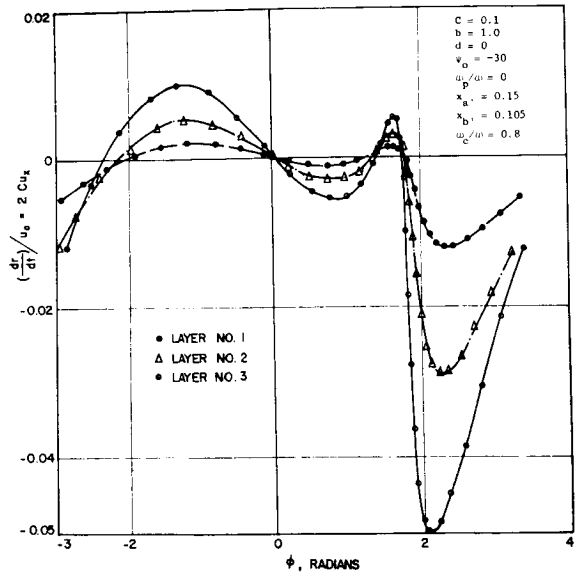

FIG. 10. Radial velocity versus phase, y = 7.2.

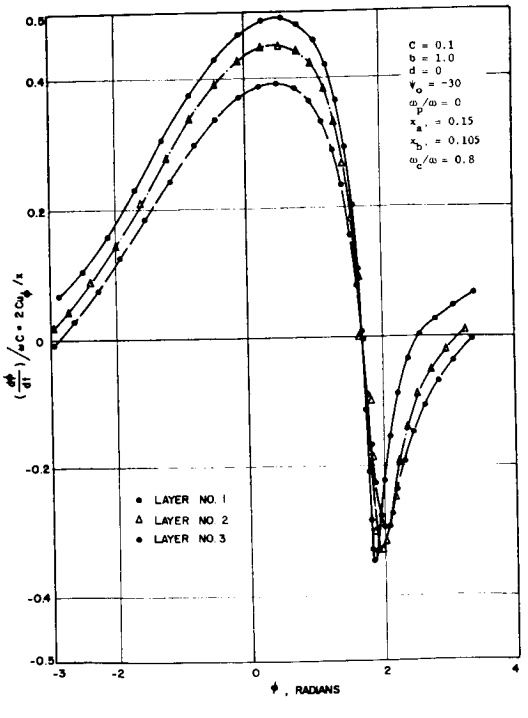

FIG. 11. Angular velocity versus phase, y = 7.2.

It is then necessary, of course, to modify the beam equations to account for a reduction in current.

The rf velocity versus phase relation for the stream charges indicates the strength of modulation and bunching in the beam, from which information on the amount of kinetic energy converted to rf can be obtained. A typical set of plots of the velocity functions defined following Eq. 9 is shown in Figs. 9, 10, and 11 for $\omega_c/\omega = 0.8$, which amounts to essentially confined flow. Notice that at a position of large rf signal strength along the structure, a vortex develops in the dz/dt versus Φ curve at a phase position of 1.5 to 2 radians (maximum decelerating rf field). A value of $1 + 2Cu_y$ greater than 1 indicates that those charge groups have taken energy from the wave and have been accelerated. But if $1 + 2Cu_y$ is less than 1, the charge group has given up energy to the wave and is decelerated. As expected, those charges in the strong decelerating field region are affected most by the wave and hence achieve the largest radial and angular velocities as measured by u_x and u_ϕ.

For all of these calculations the "cold plasma" approximation was used; that is, all charge-group velocities were assumed to be initially equal. It is relatively easy to remove this assumption by giving the injected charges and the plasma a distribution of velocities, following a Maxwell-Boltzmann distribution, for example, by specifying the velocity functions u_y, u_x, and u_ϕ at $y = 0$.

ANALYTIC SOLUTION OF NONLINEAR EQUATIONS

The solutions of the nonlinear interaction equations presented in the previous section were all obtained by digital computer methods. To obtain a complete understanding of the energy conversion process, one must accumulate a vast number of solutions and carefully analyze the data. This procedure is both costly and time-consuming and is therefore usually not completed. The question naturally arises as to whether the nonlinear equations can be solved in closed form. The answer is fortunately affirmative, providing that certain assumptions are made concerning the rf bunching in the stream.

At a position along the structure corresponding to a signal level of 6 to 10 db below the saturation level, the stream is well bunched and the predominance of charge is located in the decelerating phase of the rf wave, as illustrated in Fig. 12. The beam is treated as a single "hard-kernel" bunch. As the rf wave continues to grow, this bunch gives up kinetic energy and drops back in phase, thereby delivering less energy to the wave. To maximize the energy conversion process, it is desired to maintain ϕ_f invariant with distance. The one-dimensional nonlinear equations (5) describing the dynamics of this hard-kernel bunch have been derived as

$$\frac{dA(y)}{dy} = \frac{\sin \phi_f}{2\pi} \int_0^{2\pi} d\phi'_{oj} = \sin \phi_f \qquad (20)$$

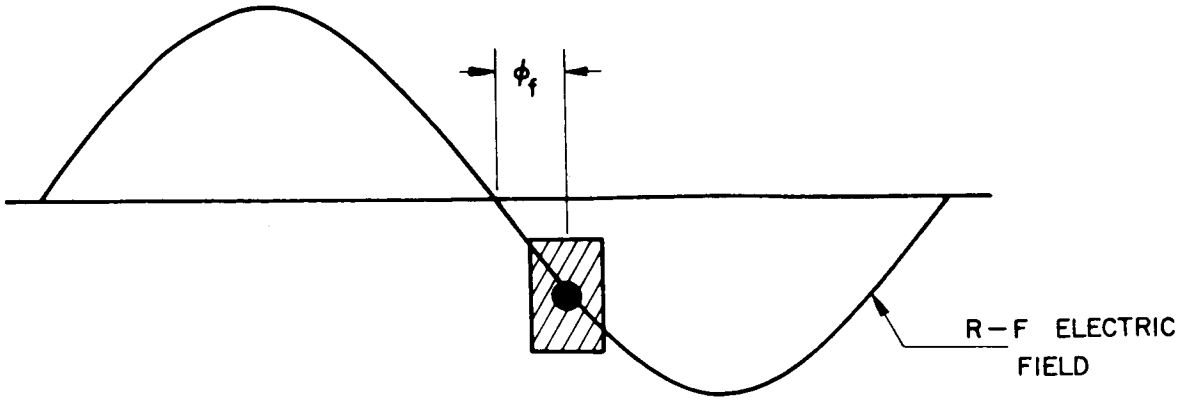

FIG. 12. Hard-kernel-bunch beam model.

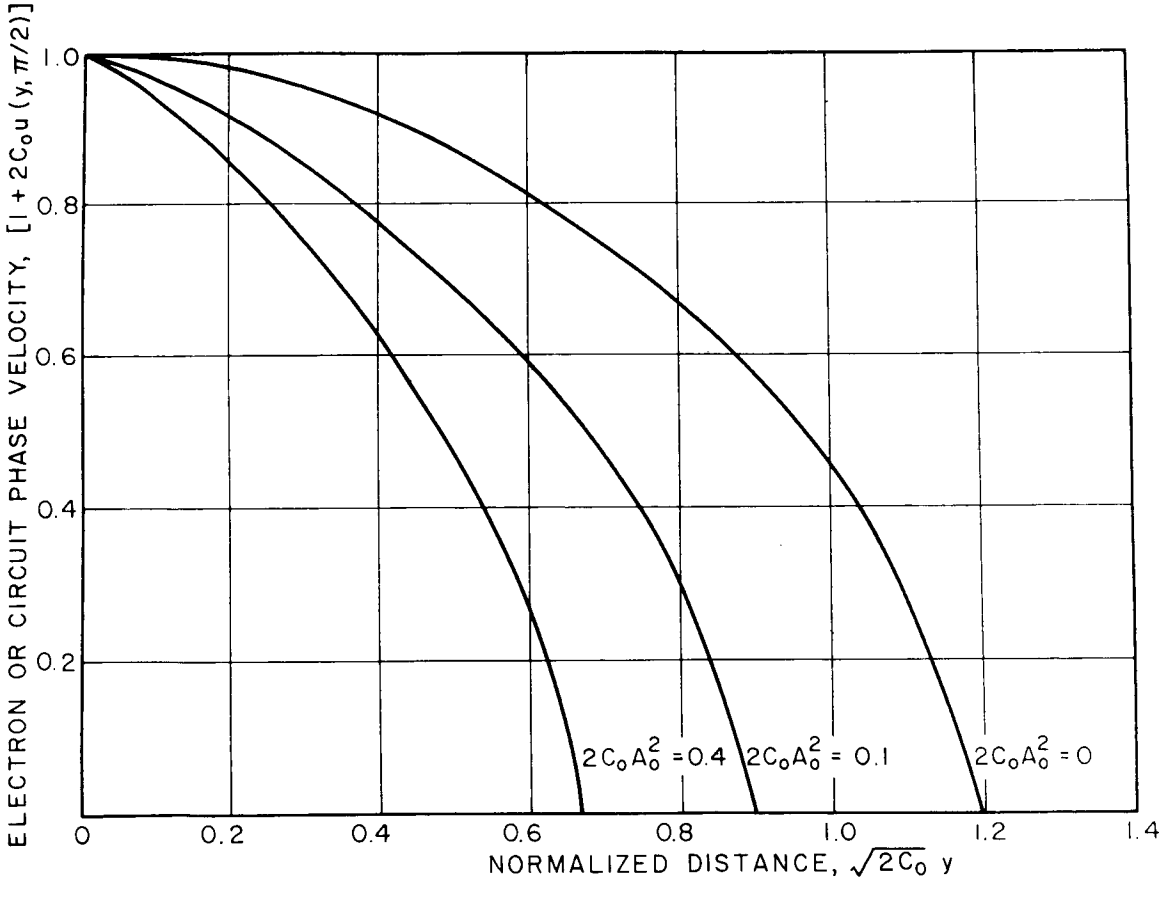

FIG. 13. Velocity profiles based upon hard-kernel-bunch approximation. Interaction impedance varies as $[1 + 2C_o u(y,\pi/2)]^{3/2}$.

$$\frac{d\theta(y)}{dy} + b = \frac{\cos \phi_f}{2\pi A(y)} \int_0^{2\pi} d\phi'_{oj} = - \frac{\cos \phi_f}{A(y)} \tag{21}$$

$$\frac{du(y,\phi_f)}{dy} = - A(y) \sin \phi_f \tag{22}$$

and

$$\frac{d\theta(y)}{dy} = 2u(y,\phi_f) \tag{23}$$

In order to maintain the phase position of the bunch ϕ_f invariant, the phase velocity of the propagating circuit must be varied in a prescribed manner. The necessary variation is given by

$$\frac{v_o(y)}{v_o} \approx 1 - C(y^2 + 2A_o y) \tag{24}$$

More exact closed-form solutions have been obtained, and are shown in Fig. 13. Experimental data indicate that through such a phase-focusing process the efficiency of energy conversion in a traveling-wave amplifier (kinetic energy conversion) has been increased from 30 percent to approximately 50 percent.

Using the hard-kernel bunch model similar calculations have been made for other interaction configurations, and it has been found that both potential and kinetic energy conversion systems may be analyzed in this manner. These closed-form analysis techniques have not yet been applied to beam-plasma interactions, but there seem to be no restrictions on their range of application. It should be possible to extend them to the study of many other nonlinear interaction phenomena.

CONCLUSIONS

A general method known as a Lagrangian analysis has been developed to study nonlinear beam-wave-plasma interactions. The method is readily adaptable to one-, two-, and three-dimensional systems and various rf and static field configurations. The equations for a three-dimensional space-charge flow in a traveling-wave interaction system were presented, and various typical solutions were given that indicate both beam and wave characteristics.

If the hard-kernel bunch model of the stream is used, the nonlinear equations for most types of interaction can be solved in closed form. This method has the advantage of simplicity and elegance, and its results yield detailed information on the energy conversion process.

REFERENCES

1. J. E. Rowe, A Large-Signal Analysis of the Traveling-Wave Amplifier: Theory and General Results, Trans. IRE-PGED, ED-3:39-57, January 1956.

2. P. K. Tien, A Large Signal Theory of Traveling-Wave Amplifiers, Bell Sys. Tech. J., 35:349-374, March 1956.

3. J. E. Rowe, One-Dimensional Traveling-Wave Tube Analyses and the Effect of Radial Electric Field Variations, Trans. IRE-PGED, ED-7: 16-21, January 1960.

4. O. P. Gandhi and J. E. Rowe, Nonlinear Theory of Injected-Beam Crossed-Field Devices, in Crossed-Field Microwave Devices, Academic Press, New York, 1961, vol. 1, pp. 439-495.

5. J. G. Meeker and J. E. Rowe, Phase Focusing in Linear-Beam Devices, Trans. IRE-PGED, ED-9:257-266, May 1962.

ON THE NONLINEAR THEORY OF THE PLANE TRAVELING-WAVE TUBE

S. Olving
Research Laboratory of Electronics
Chalmers University of Technology
Gothenburg, Sweden

ABSTRACT

This paper deals with the nonlinear theory of a plane TWT model. An infinitely wide electron beam interacts with an infinitely wide homogeneous slow wave structure whereby the difficulties associated with radial boundary conditions are avoided. The nonlinear wave equation is solved to the third order accuracy by the use of the method of successive approximations. The one-valued velocity assumption limits the analysis to the range well below the saturation level. Within this range, however, the results describe such effects as the dependence of fundamental frequency gain and output phase on drive power, and the production of the first two harmonics. Furthermore, it is shown that by the use of suitable approximations one can write the nonlinear plane TWT equation in a form very similar to the exact nonlinear plane klystron equation. From this point on, one can deal with the plane TWT by the methods that have already been successfully applied in the plane klystron case.

Author

1. DESCRIPTION OF THE PLANE TWT MODEL

The principles of space-charge wave devices, such as klystrons, double-stream amplifiers, velocity step amplifiers, resistive medium amplifiers, and microwave vacuum diodes, are most conveniently analyzed using plane models with infinitely wide beams. Such models lend themselves to comparatively convenient studies of the basic effects in the various devices. The price one has to pay is neglect of the important phenomena produced by the fringe fields in real tubes. Nevertheless, since the traveling-wave tube (TWT) is an extremely difficult object to study, especially in the nonlinear region, it should be of some interest to develop a nonlinear theory for the plane TWT model.

The linearized analysis of the plane TWT has been published elsewhere (1). The plane TWT consists of an infinitely wide confined electron beam moving with a constant d-c velocity v_o in an anisotropically conducting homogeneous medium (Fig. 1). The medium represents the slow wave structure. It has to be anisotropic, since an isotropic homogeneous medium would support plane TEM waves. The TWT mechanism depends, however, on the presence of an electric field component in the direction of the electron and wave motion, and thus requires a TM wave.

A simple TM slow wave medium can be thought of as consisting of closely placed straight parallel wires filling the whole three-dimensional space. The wires are parallel to the y-z plane, and they make an angle ξ with the x-y plane. The angle ξ corresponds directly to the

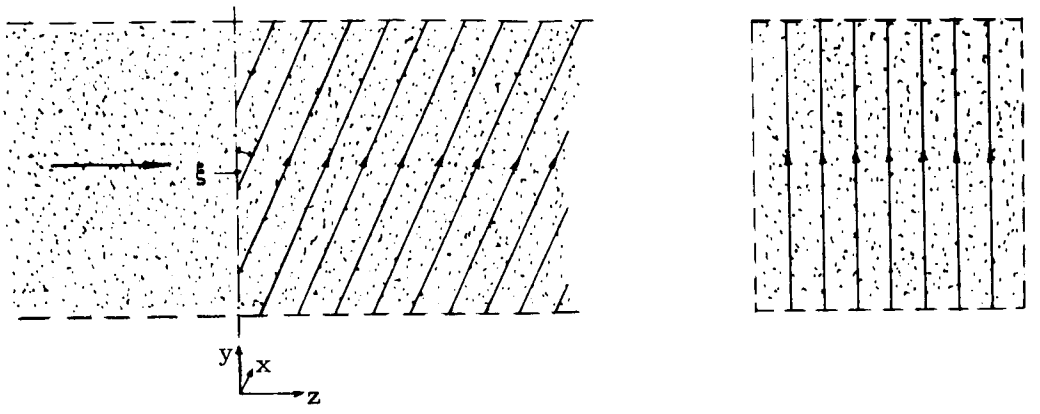

FIG. 1. Infinitely wide electron beam moving in the infinitely wide wire structure.

pitch angle of a helical slow wave structure. Mathematically we will take the presence of the wires into account by letting the conductivity of the whole space be infinity in the wire direction and zero in all other directions. The wire medium is supposed, of course, to be transparent with respect to the beam electrons, which move along the positive z direction. The beam is confined by a very strong d-c magnetic field.

In the absence of the electron beam the medium supports a plane TM wave with field components E_y, E_z, and H_x propagating in the positive (or negative) z direction with a phase velocity $v_{ph} = c \sin \xi$ (c = velocity of light). The constant phase and amplitude planes are assumed to be perpendicular to the z axis, that is, $\partial/\partial x = 0 = \partial/\partial y$. In the presence of the beam, interaction will take place, and the four characteristic TWT waves are easily found from Maxwell's equations.

2. THE NONLINEAR WAVE EQUATION

Let us define a quantity $z_1(z,t)$, the displacement of an electron from the position z_o it would have if a-c forces were not applied. If z is the actual position of the electron, one has the relation $z = z_o + z_1$. Similarly we denote the electron velocity by $v = v_o + v_1$, the convection current density by $i = i_o + i_1$, and the electronic charge density by $\rho = \rho_o + \rho_1$. The quantities indexed by o refer to undisturbed conditions; the quantities indexed by 1 denote the change produced by the signal.

From the relations

$$v_1 = \frac{dz_1}{dt} \tag{1}$$

$$i_1 = \rho_o v_1 + v_o \rho_1 + v_1 \rho_1 \tag{2}$$

and

$$\frac{\partial i_1}{\partial z} = - \frac{\partial \rho_1}{\partial t} \tag{3}$$

one easily obtains (2) the expressions

$$i_1 = \rho_o \frac{\partial z_1}{\partial t} \tag{4}$$

$$\rho_1 = - \rho_o \frac{\partial z_1}{\partial z} \tag{5}$$

The nonrelativistic equation of motion is

$$\frac{d^2 z_1}{dt^2} = - \frac{e}{m} E_z \tag{6}$$

Relations 4 and 6 will now be used in Maxwell's equations in order to obtain a nonlinear wave equation for z_1. Maxwell's equations yield for the TM case with $\partial/\partial x = 0 = \partial/\partial y$:

$$\frac{\partial E_y}{\partial z} = \mu_o \frac{\partial H_x}{\partial t}$$

$$\frac{\partial H_x}{\partial z} = I_y + \epsilon_o \frac{\partial E_y}{\partial t} \tag{7}$$

$$0 = I_z + \epsilon_o \frac{\partial E_z}{\partial t}$$

where μ_o and ϵ_o are the permeability and permittivity, respectively, of free space. I_y and I_z are the current density components:

$$I_y = I \cos \xi$$

$$I_z = I \sin \xi + i_1 \tag{8}$$

where I is the conduction current density along the direction of infinite conductivity. Since the electric field must be perpendicular to the direction of infinite conductivity, we also have the relation

$$E_y \cos \xi + E_z \sin \xi = 0 \tag{9}$$

By the use of Eqs. 4, 6, 8, and 9 in Eq. 7, one easily deduces the desired wave equation.

$$\frac{\partial^2}{\partial z^2}\frac{d^2 z_1}{dt^2} - \frac{1}{v_{ph}^2}\frac{\partial^2}{\partial t^2}\frac{d^2 z_1}{dt^2} - \frac{\omega_p^2}{v_{ph}^2}\cos^2\xi\,\frac{\partial^2 z_1}{\partial t^2} = 0 \tag{10}$$

where

$$v_{ph} = (\epsilon_o \mu_o)^{-\frac{1}{2}} \sin\xi = c \sin\xi$$

is the phase velocity of the TM wave in the absence of the electron beam and

$$\omega_p = \left(-\frac{e\rho_o}{m\epsilon_o}\right)^{\frac{1}{2}}$$

is the angular plasma frequency.

Equation 10 is the exact wave equation in the system under consideration. It is nonlinear on account of the quantity $d^2 z_1/dt^2$, as we will see in what follows. It should be pointed out that Eq. 10 is valid only in regions where overtaking does not occur, since it has been assumed that the total convection current density in a plane z is given by Eq. 4. If overtaking occurs, then z_1 is no longer a one-valued function of z and Eq. 4 does not give the total convection current density, which we need in Maxwell's first equation.

With $d/dt = \partial/\partial t + (v_o + v_1)\partial/\partial z$ we obtain, after some elementary calculations, the following nonlinear exact expression for $d^2 z_1/dt^2$:

$$\frac{d^2 z_1}{dt^2} = \frac{\ddot{z}_1}{(1-\partial z_1/\partial z)} + \frac{(\partial/\partial z)(\dot{z}_1)^2}{(1-\partial z_1/\partial z)^2} + \frac{(\dot{z}_1)^2(\partial^2 z_1/\partial z^2)}{(1-\partial z_1/\partial z)^3} \tag{11}$$

where

$$\dot{z}_1 \equiv \left(\frac{\partial}{\partial t} + v_o \frac{\partial}{\partial z}\right) z_1$$

and

$$\ddot{z}_1 \equiv \left(\frac{\partial^2}{\partial t^2} + 2v_o \frac{\partial^2}{\partial t\,\partial z} + v_o^2 \frac{\partial^2}{\partial z^2}\right) z_1$$

Thus the dot denotes the linearized time derivative. Note, however, that Eq. 11 is an exact expression for the electron acceleration. In the case of the linearized theory (see Section 3) one would approximate Eq. 11 by the expression $d^2 z_1/dt^2 \approx \ddot{z}_1$.

The excess velocity v_1 is related to z_1 by the exact expression

$$v_1 = \frac{dz_1}{dt} = \frac{\dot{z}_1}{(1-\partial z_1/\partial z)} \tag{12}$$

Upon the insertion of Eq. 11 into Eq. 10 one would obtain the complete nonlinear partial differential equation for z_1. Obviously this equation, in spite of the simplicity of the plane TWT model, is an extremely complicated one. There is no hope to find a proper exact solution. Nevertheless, it is interesting to note that the function $e^{j(\omega t-\gamma z_o)}$, where ω and γ are constants (γ is the same as in Eq. 16), is an exact solution to Eq. 10. This solution is physically meaningless, since its real and imaginary parts taken separately are not exact solutions to Eq. 10. But we will show in Section 6 that certain properties of the plane TWT can be studied by the use of this solution.

3. THE LINEARIZED SOLUTION

If we linearize our wave equation (Eq. 10), the result is

$$Da_1 = 0 \tag{13}$$

where D denotes the operator

$$D = \left(\frac{\partial^2}{\partial t^2} - \frac{1}{v_{ph}^2}\frac{\partial^2}{\partial t^2}\right)\left(\frac{\partial^2}{\partial t^2} + 2v_o\frac{\partial^2}{\partial t\,\partial z} + v_o^2\frac{\partial^2}{\partial z^2}\right) - \frac{\omega_p^2}{v_{ph}^2}\cos^2\xi\,\frac{\partial^2}{\partial t^2} \tag{14}$$

and a_1 is the linearized electron displacement z_1. An amplifying solution to Eq. 13 is

$$a_1 = Ae^{\alpha z}\cos(\omega t - \beta z) = A\mathrm{Re}\left[e^{j(\omega t-\gamma z)}\right] \tag{15}$$

where $\beta = \mathrm{Re}\gamma$ and $\alpha = \mathrm{Im}\gamma$ (α is supposed to be positive). The complex propagation constant γ obeys the dispersion equation

$$(\gamma^2 - \gamma_o^2)(\gamma - \beta_e)^2 + \beta_p^2\gamma_o^2\cos^2\xi = 0 \tag{16}$$

which is obtained by inserting Eq. 15 into Eq. 13. The notations are

$\gamma_o = \omega/v_{ph}$ propagation constant in absence of beam

$\beta_e = \omega/v_o$ mathematical beam propagation constant

$\beta_p = \omega_p/v_o$ plasma propagation constant

Equation 16 determines the real quantities α and β. For the amplifying wave, α is positive. We are interested in cases where v_o is very close to v_{ph} and where $\omega_p^2 \ll \omega^2$. Under these usual conditions γ will be very close to β_e and γ_o. Hence Eq. 16 can be approximated by

$$(\gamma - \beta_e)^2(\gamma - \gamma_o) + \frac{1}{2}\beta_p^2\beta_e \cos^2 \xi \approx 0 \tag{17}$$

Using the same assumptions in Pierce's (3) Eq. 7.10, we would get

$$(\gamma - \beta_e)^2(\gamma - \gamma_o) + (\beta_e C)^3\left(1 - 4Q\frac{\gamma-\gamma_o}{\beta_e}\right) \approx 0 \tag{18}$$

where C and Q are the well-known parameters defined by Pierce.

We observe that Eqs. 17 and 18 are equivalent if

$$C^3 = \frac{1}{2}\frac{\omega_p^2}{\omega^2}\cos^2 \xi \tag{19}$$

and if QC is a small number ($4QC \ll 1$). The latter requirement shows that the plane TWT bears a close resemblance to the small-Q helical TWT [strong coupling between beam and helix, beam radius equal to helix radius (4,5)].

Returning to Eq. 17, we introduce the notations originally used by Pierce:

$$\gamma = \beta_e + \beta_e C(jx - y)$$

$$\gamma_o = \beta_e + \beta_e Cb$$

and rewrite Eq. 17 in the form

$$(jx - y)^2(jx - y - b) + 1 = 0 \tag{20}$$

If $|b| \ll |jx - y|$ (that is, operating point near velocity synchronism, the region of maximum amplification), we have the approximate solution

$$x \approx \sqrt{3}/2$$

$$y \approx -\frac{1}{2} - \frac{1}{3}b \tag{21}$$

The parameter x is associated with the exponential growth of the wave (positive x corresponds to amplification), whereas y is related to the propagation constant of the wave (Fig. 2).

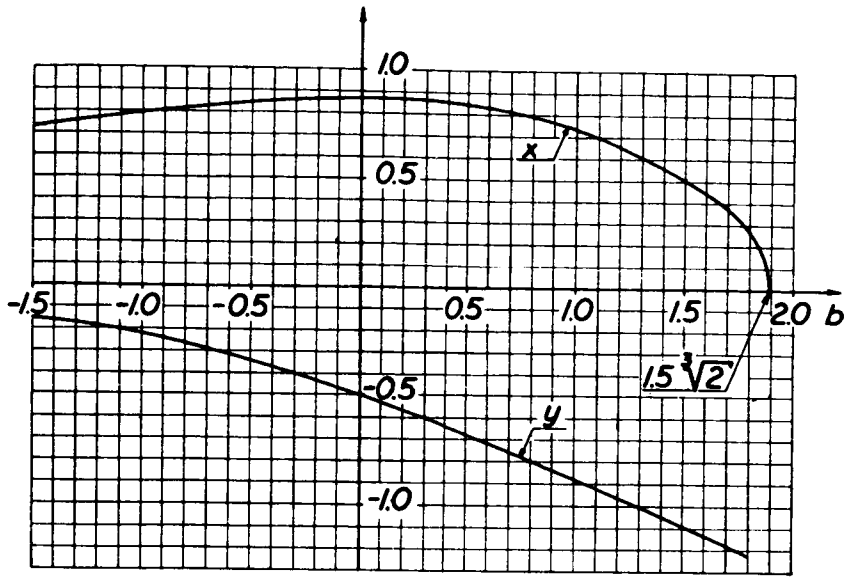

FIG. 2. Gain parameter x and phase parameter y versus electron velocity parameter b for the plane TWT. Parameters x, y, and b are those of Pierce (3).

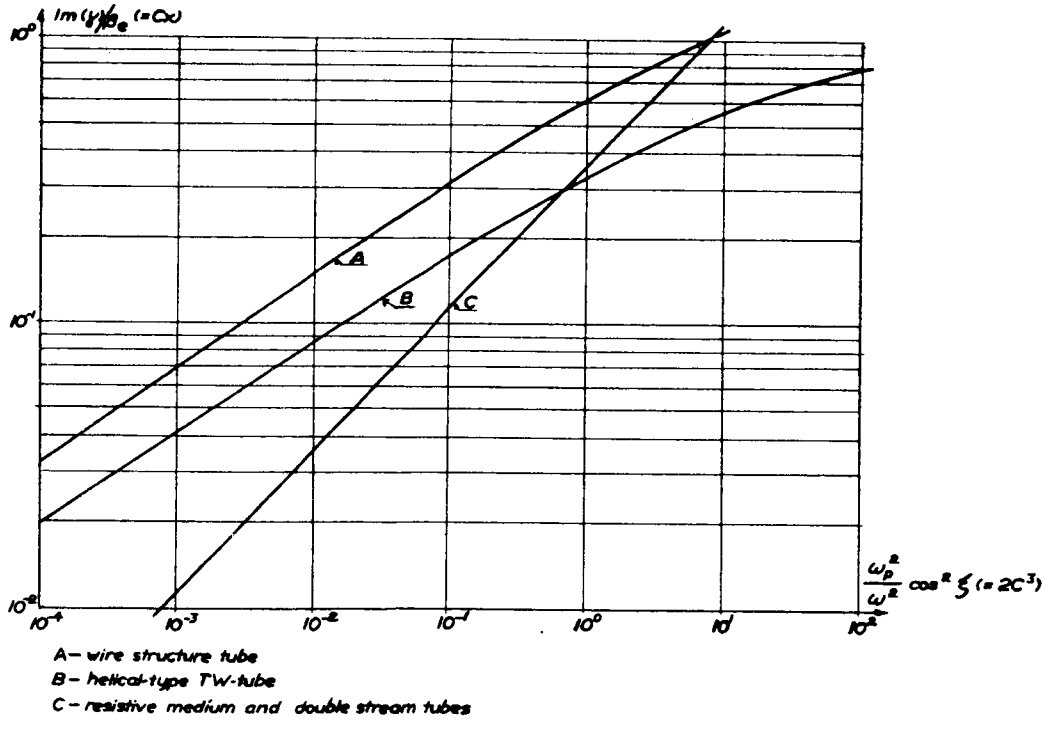

FIG. 3. Normalized exponential gain parameter versus normalized d-c density parameter for the principal continuous-interaction-type plane wave amplifiers.

In this connection it is interesting to compare the exponential linearized amplification of the principal continuous-interaction-type amplifiers. The electronic amplification is given by the factor $e^{2\mathrm{Im}(\gamma)z}$. In Fig. 3 $\mathrm{Im}(\gamma)/\beta_e$ is depicted versus ω_p^2/ω^2 (assuming, as usual, that $\cos^2 \xi \approx 1$) for the following amplifiers, all adjusted for maximum amplification: A, plane TWT (1a); B, sheath helix TWT, the radius of the solid electron beam equaling that of the helix (1b,4,5,); C, plane resistive medium tube (6) and plane double-stream tube (3). In the plane double-stream tube, $\omega_p^2 = 2\omega_{p_1}^2$ where ω_{p_1} is the angular plasma frequency of one beam alone.

4. THE NONLINEAR SOLUTION, METHOD OF SUCCESSIVE APPROXIMATIONS

It is well known that a set of three linear forward waves will be excited at the input of a TWT. One of these will be an amplifying wave. This is the wave described by Eq. 15. When the waves have traveled far enough, the amplifying wave will dominate the other two. Hence, at the distance where the propagation becomes nonlinear we need to consider only the amplifying wave and the nonlinear effects associated with this particular wave.

We want to make use of the method of successive approximations (7) to find a third order solution to Eq. 10. This means that we think of the solution in terms of a power series in $Ae^{\alpha z}$, the amplitude of the linearized displacement (see Eq. 15), and we want to find the first three terms in the series. The third term, which contains a nonlinear wave of the fundamental frequency, allows us to study the low-level nonlinear effects at the frequency ω, and also describes the excitation of the third harmonic 3ω. The second harmonic 2ω and a d-c correction constitute the second term in the power series.

The total electronic charge density can never be positive; therefore $\rho_o + \rho_1 \leq 0$. By the use of Eq. 4 one easily concludes now that $\partial z_1/\partial z < 1$. Assuming $|\partial z_1/\partial z| < 1$, we expand Eq. 11 as follows:

$$\frac{d^2 z_1}{dt^2} \approx \left[1 + \frac{\partial z_1}{\partial z} + \left(\frac{\partial z_1}{\partial z}\right)^2\right]\ddot{z}_1 + \left(1 + 2\frac{\partial z_1}{\partial z}\right)\frac{\partial(\dot{z}_1)^2}{\partial z} + \frac{\partial^2 z_1}{\partial z^2}(\dot{z}_1)^2 \qquad (22)$$

Relation 22 includes the nonlinear terms to the third order. Expanding Eq. 12 in the same manner yields

$$v_1 = \frac{dz_1}{dt} \approx \left[1 + \frac{\partial z_1}{\partial z} + \left(\frac{\partial z_1}{\partial z}\right)^2\right]\dot{z}_1 \qquad (23)$$

We will now assume that z_1 can be written in the form

$$z_1 = a_1 + a_2 + a_3 \qquad (24)$$

where $a_1 \propto Ae^{\alpha z}$, $a_2 \propto (Ae^{\alpha z})^2$ and $a_3 \propto (Ae^{\alpha z})^3$ are the three first terms of the power series. The linear term a_1 is already expressed in Eq. 15. By the use of Eqs. 24 and 22 in Eq. 10 one obtains, upon equating terms of equal powers in $Ae^{\alpha z}$, the following three equations:

$$Da_1 = 0 \tag{25}$$

$$Da_2 = -\left(\frac{\partial^2}{\partial z^2} - \frac{1}{v_{ph}^2}\frac{\partial^2}{\partial t^2}\right)\left[\frac{\partial a_1}{\partial z}\ddot{a}_1 + \frac{\partial}{\partial z}(\dot{a}_1)^2\right] \tag{26}$$

$$\begin{aligned} Da_3 = -\left(\frac{\partial^2}{\partial z^2} - \frac{1}{v_{ph}^2}\frac{\partial^2}{\partial t^2}\right)\Bigg[&\frac{\partial a_1}{\partial z}\ddot{a}_2 + \frac{\partial a_2}{\partial z}\ddot{a}_1 \\ &+ 2\frac{\partial}{\partial z}(\dot{a}_1\dot{a}_2) + \left(\frac{\partial a_1}{\partial z}\right)^2 \ddot{a}_1 \\ &+ 2\frac{\partial a_1}{\partial z}\frac{\partial}{\partial z}(\dot{a}_1)^2 + \frac{\partial^2 a_1}{\partial z^2}(a_1)^2\Bigg] \end{aligned} \tag{27}$$

The solution to Eq. 25 is known. Thus Eq. 26 is a linear nonhomogeneous wave equation. Its particular integral a_2 can be found by standard methods. Once a_1 and a_2 are known, one can attack Eq. 27 and find its particular integral a_3.[2] The results, written in complex notations, are

$$\beta_e a_1 = (A\beta_e e^{\alpha z})e^{j(\omega t - \beta z)} \tag{28}$$

$$\begin{aligned} \beta_e a_2 = (A\beta_e e^{\alpha z})^2\Big\{&\frac{1}{2}\,j[1 + C(-y + jx)]e^{2j(\omega t - \beta z)} \\ &+ \left[\frac{y}{4x} - \frac{3C}{8x}(x^2 + y^2)\right]\Big\} \end{aligned} \tag{29}$$

$$\begin{aligned} \beta_e a_3 \approx (A\beta_e e^{\alpha z})^3\Bigg[&-\frac{3}{8}\,e^{3j(\omega t - \beta z)} \\ &- \frac{(y+b-3jx)(x^2+y^2-2jxy)}{1-(y+b-3jx)(y-3jx)^2}\,e^{j(\omega t - \beta z)}\Bigg] \end{aligned} \tag{30}$$

Equations 28 and 29 are exact solutions to Eqs. 25 and 26 respectively, whereas Eq. 30 is deduced with the same approximations as Eq. 17.

Remembering that $E_z = -\frac{m}{e}\frac{d^2 z_1}{dt^2}$ we can write $E_z = E_{z1}+E_{z2}+E_{z3}$, where

$$\frac{E_{z1}}{2\beta_e V_o C^2(-y+jx)^3} = (A\beta_e e^{\alpha z})e^{j(\omega t-\beta z)} \tag{31}$$

$$\frac{E_{z2}}{2\beta_e V_o C^2(-y+jx)^2} = (A\beta_e e^{\alpha z})^2 \frac{1}{2} j[1 + C(-y + jx)]e^{2j(\omega t-\beta z)} \tag{32}$$

$$\frac{E_{z3}}{2\beta_e V_o C^2(-y+jx)^2} \approx (A\beta_e e^{\alpha z})^3\left[-\frac{3}{8} e^{3j(\omega t-\beta z)} - \frac{(x^2+y^2-2jxy)}{(-y+jx)^2}\frac{e^{j(\omega t-\beta z)}}{1-(y+b-3jx)(y-3jx)^2}\right] \tag{33}$$

in which V_o $(= \frac{mv_o^2}{2e})$ denotes the beam voltage.

We also express the velocity $v_1 = dz_1/dt$ by writing $v_1 = v_{11} + v_{12} + v_{13}$, where

$$\frac{v_{11}}{v_o}\frac{1}{C(-y+jx)} = -j(A\beta_e e^{\alpha z})e^{j(\omega t-\beta z)} \tag{34}$$

$$\frac{v_{12}}{v_o}\frac{1}{C(-y+jx)} = (A\beta_e e^{\alpha z})^2 \cdot \left\{\frac{1}{2}[1+C(-y+jx)]e^{2j(\omega t-\beta z)} + \frac{C}{4}(y+jx)\right\} \tag{35}$$

$$\frac{v_{13}}{v_o}\frac{1}{C(-y+jx)} \approx (A\beta_e e^{\alpha z})^3\left\{\frac{3}{8} je^{3j(\omega t-\beta z)} + j\left[\frac{(y+b-3jx)(x^2+y^2-2jxy)}{1-(y+b-3jx)(y-3jx)^2}\frac{(-y+3jx)}{(-y+jx)} - \frac{1}{4}\frac{(3y+jx)}{(-y+jx)}\right]e^{j(\omega t-\beta z)}\right\} \tag{36}$$

From the relation $i_1/i_o = \partial z_1/\partial(v_o t)$ we finally express the a-c current density, writing $i_1 = i_{11} + i_{12} + i_{13}$, where

$$\frac{i_{11}}{i_o} = (A\beta_e e^{\alpha z})je^{j(\omega t-\beta z)} \tag{37}$$

$$\frac{i_{12}}{i_o} = -(A\beta_e e^{\alpha z})^2[1 + C(-y + jx)]e^{2j(\omega t-\beta z)} \tag{38}$$

$$\frac{i_{13}}{i_o} \approx (A\beta_e e^{\alpha z})^3\left[-\frac{9}{8}je^{3j(\omega t-\beta z)} - j\frac{(y+b-3jx)(x^2+y^2-2jxy)}{1-(y+b-3jx)(y-3jx)^2}e^{j(\omega t-\beta z)}\right] \tag{39}$$

In the synchronous case (b = 0) these results can be written in the form

$$\beta_e z_1 \approx R\cos Z + R^2\left(\frac{1}{2}\sin 2Z - \frac{1}{4\sqrt{3}}\right) - R^3\left(\frac{3}{8}\cos 3Z + \frac{7}{72}\cos Z + \frac{7\sqrt{3}}{72}\sin Z\right) \tag{40}$$

$$\frac{E_z}{2\beta_e V_o C^2} \approx R\sin(Z - 30°) - \frac{1}{2}R^2\cos(2Z - 30°) - R^3\left[\frac{3}{8}\sin(3Z - 30°) + \frac{1}{18}\sin(Z - 30°) - \frac{\sqrt{3}}{36}\cos(Z - 30°)\right] \tag{41}$$

$$\frac{v_1}{v_o C} \approx R\cos(Z + 30°) + R^2\left[\frac{1}{2}\sin(2Z + 30°) - \frac{C}{4}\right] - R^3\left[\frac{3}{8}\cos(3Z + 30°) + \frac{7}{72}\cos(Z + 30°) + \frac{3\sqrt{3}}{72}\sin(Z + 30°)\right] \tag{42}$$

and

$$\frac{i_1}{i_o} \approx R\sin Z - R^2\cos 2Z - R^3\left(\frac{9}{8}\sin 3Z + \frac{7}{72}\sin Z - \frac{7\sqrt{3}}{72}\cos Z\right) \tag{43}$$

where $R = A\beta_e e^{\alpha z}$ and $Z = \beta z - \omega t$.

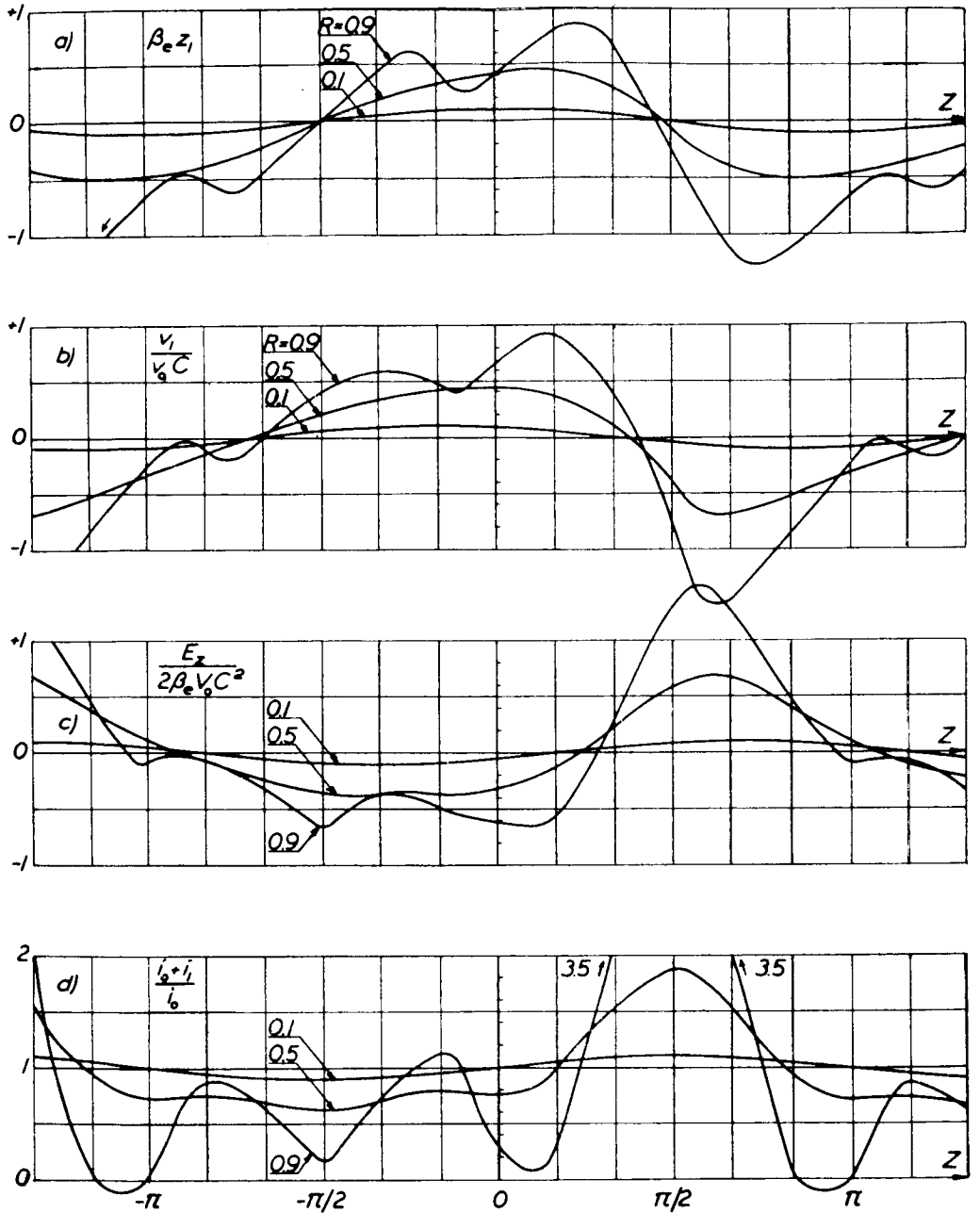

FIG. 4. For three values of amplitude parameter R (= $A\beta_e e^{\alpha z}$): (a) displacement z_1, (b) excess velocity v_1, (c) axial electric field strength E_z, and (d) total electron current density i (= $i_0 + i_1$), as functions of phase Z (= $\beta z - \omega t$).

In Fig. 4, Eqs. 40, 41, 42, and 43 have been plotted versus Z, the phase, for three values of the amplitude parameter R. Observe that the abscissa Z in these graphs can be interpreted as the normalized axial distance βz if time is kept constant and if R varies negligibly within a distance of one axial wavelength (this implies $2\pi\alpha/\beta \ll 1$).

At the small amplitude R = 0.1, all curves in Fig. 4 are practically sinusoidal. When R = 0.5, the nonlinearities clearly manifest their presence and the curves become nonsinusoidal. In the case of R = 0.9, one can see from Fig. 4 or from Eqs. 40, 41, 42, and 43 that the second and third order terms are comparable to the first order terms. The third order theory will not describe the situation very accurately for such large R. Note, for instance, that the total current density (d of Fig. 4) becomes negative for some values of Z when R = 0.9. This would correspond to a negative electron number density, which is unacceptable.

However, extrapolating (a) of Fig. 4 to even larger R, one would expect the situation $\partial(\beta_e z_1)/\partial Z = -\infty$, which is the electron overtaking condition, to occur at Z slightly less than $\pi/2$. This is in good agreement with the experimental findings of Cutler (8). Part (c) of Fig. 4 indicates that the Z range where the electric field is decelerating (E_z positive) narrows when R increases. In this useful Z range, according to (b) of Fig. 4, most electrons travel slower than the undisturbed electrons; that is, v_1 is negative. Observe finally, in (d) of Fig. 4, that for large R a strong electron bunch is built up somewhat to the left of the middle of the decelerating range, around $Z \approx \pi/2$.

5. NONLINEARITIES OF THE AMPLITUDE AND THE PHASE

The purpose of this section is to study how the low-level nonlinearities manifest themselves in the amplitude and phase of the fundamental frequency waves.

Denoting the fundamental frequency component of E_z by $E_{z\omega}$, one obtains from Eqs. 31 and 33

$$\frac{E_{z\omega}}{2\beta_e V_o C^2 R(-y+jx)^2} = [1 - R^2 f_E(x,y,b)]e^{j(\omega t-\beta z)} \tag{44}$$

where

$$f_E(x,y,b) = \frac{(x^2+y^2-2jxy)}{(-y+jx)^2[1-(y+b-3jx)(y-3jx)^2]} \tag{45}$$

Similarly, Eqs. 37 and 39 yield

$$\frac{i_{1\omega}}{i_o R j} = [1 - R^2 f_i(x,y,b)]e^{j(\omega t-\beta z)} \tag{46}$$

where

$$f_i(x,y,b) = \frac{(y+b-3jx)(x^2+y^2-2jxy)}{1-(y+b-3jx)(y-3jx)^2} \tag{47}$$

Since the theory presented here is based on the method of successive approximations, we must assume $|R^2 f_{E,i}| \ll 1$. We can therefore write for the right-hand sides of Eqs. 44 and 46.

$$(1 - R^2 f_{E,i})e^{j(\omega t-\beta z)} \approx (1 - S_{E,i})e^{j(\omega t-\beta z-\Phi_{E,i})} \tag{48}$$

where

$$S_{E,i} = R^2 \mathrm{Re}(f_{E,i}) \tag{49}$$

$$\Phi_{E,i} = R^2 \mathrm{Im}(f_{E,i}) \tag{50}$$

Obviously, S_E and S_i are the lowest order nonlinear amplitude corrections to the electric field and electron current density waves, respectively, at the fundamental frequency. Similarly Φ_E and Φ_i are the lowest order nonlinear phase corrections to these waves. Positive S indicates that the wave amplitude is less than the linearized theory would predict. Positive Φ indicates that the phase is delayed.

Thus we can write

$$E_{z\omega} = E_{z1}(1 - S_E)e^{-j\Phi_E} \tag{51}$$

$$i_{1\omega} = i_{11}(1 - S_i)e^{-j\Phi_i} \tag{52}$$

where the linearized waves E_{z1} and i_{11} are given by Eqs. 31 and 37.

For the electromagnetic power flow $P_{em\omega}$ one finds

$$\frac{P_{em\omega}}{P_{em1}} = \left|\frac{E_{z\omega}}{E_{z1}}\right|^2 \approx 1 - 2S_E$$

where P_{em1} is the electromagnetic power flow associated with the linearized solution. With $S_P = 2S_E$,

$$P_{em\omega} = P_{em1}(1 - S_P) \tag{53}$$

It is convenient, before we proceed, to express the parameter R ($= A\beta_e e^{\alpha z}$) in terms of physically more meaningful quantities. For

this purpose we make use of the nonrelativistic kinetic power theorem (9):

$$P_{k1} = -\frac{mv_o}{2e}\,\mathrm{Re}(v_{11}i_{11}^*) = -\frac{mi_o}{2e}\,\mathrm{Re}\left(\dot{a}_1\,\frac{\partial a_1^*}{\partial t}\right) \tag{54}$$

where P_{k1} is the time average kinetic power flow associated with the linearized waves. [The complete second order expression for the time average kinetic power flow is $P_k = P_{k1} + P_{k2}$, where P_{k1} is given by Eq. 54 and where $P_{k2} = -(mi_o/e)(1/4\, v_{11}v_{11}^* + v_o v_{12dc})$. The notation v_{12dc} stands for the d-c part of the velocity expressed by Eq. 35. The term P_{k2}, although of the same order as P_{k1}, is associated with the lowest order nonlinear waves (9). In the case treated here, one easily proves by the use of Eqs. 34 and 35 that $P_{k2} = 0$. This is as expected with respect to the fact that there is no electromagnetic power present that could balance out a nonzero P_{k2}.]

Now the total linearized power flow, which is the sum of P_{k1} and the corresponding electromagnetic power flow P_{em1}, must vanish for obvious reasons (see Ref. 5, p. 27). Hence $P_{em1} = -P_{k1}$. Denoting the undisturbed d-c kinetic power flow by P_o, one easily obtains by the use of Eqs. 34 and 37 in Eq. 54

$$\eta \equiv \frac{P_{em1}}{P_o} = -CyR^2 \tag{55}$$

where η may be called the efficiency at the distance z. Note that η is the efficiency corresponding to the linearized theory.

By the use of Eq. 55 in Eqs. 49 and 50 we can now write

$$\frac{S_{E,i}}{\eta/C} = -\frac{\mathrm{Re}(f_{E,i})}{y} \tag{56}$$

$$\frac{\Phi_{E,i}}{\eta/C} = -\frac{\mathrm{Im}(f_{E,i})}{y} \tag{57}$$

Equations 56 and 57 are plotted in Figs. 5 and 6 respectively. Note from Fig. 5 that the theory predicts negative S_p values for sufficiently high beam voltages ($b > 1$). The conclusions are that in this interesting beam velocity range the gain of a TWT initially increases when the drive increases, and that when $b \approx 1$ the gain is independent of the drive within the accuracy of the third order theory. From the practical standpoint this means that there exists, according to present theory, an optimum beam voltage which should be used in situations where a linear relationship is essential between the input and output powers up to high drive levels. Because this optimum beam voltage is higher ($b = 1$) than the voltage corresponding to maximum gain ($b = 0$), some gain has to be sacrificed in order to increase amplitude linearity.

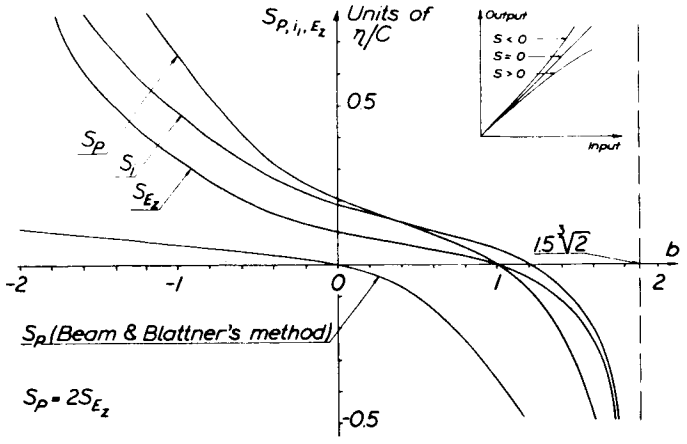

FIG. 5. Amplitude nonlinearity parameters S_E, S_i, and S_P versus electron velocity parameter b.

FIG. 6. Phase delay of a-c electric field Φ_E and of a-c density Φ_i versus electron velocity parameter b.

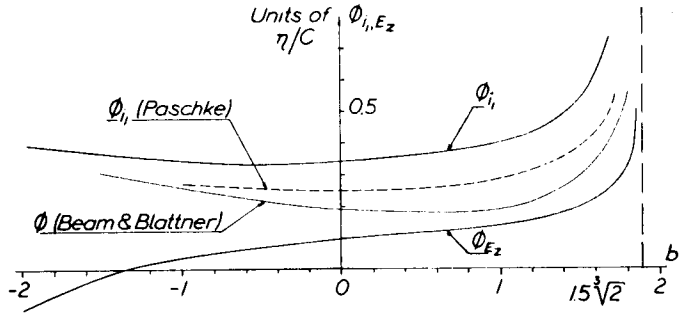

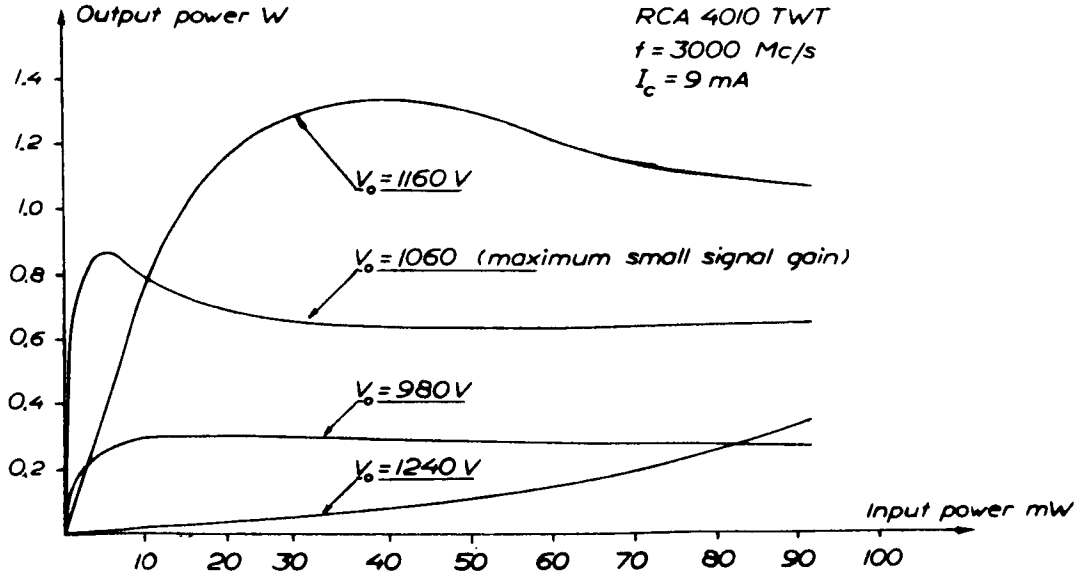

FIG. 7. Output power versus input power of an RCA 4010 traveling-wave tube for several values of beam/helix voltage.

Figure 7 shows some experimentmental results obtained with an RCA 4010 traveling-wave tube. The output power was measured as a function of the input power, with the beam/helix voltage as a parameter. The experimental results are in good qualitative agreement with the theoretical predictions. The beam voltage V_o = 1060V corresponds to maximum small signal gain. At this voltage, saturation is produced by 5 mw input power. When V_o = 1160V, then $S_p \approx 0$ and the initial phase of the curve is essentially linear. Gain is lower but the efficiency is higher than for V_o = 1060V. When V_o = 1240V we clearly have a negative S_p, as predicted by the theory. At the low voltage V_o = 980V we see that S_p is large and positive, also in good agreement with the theory.

Beam and Blattner (10) have considered nonlinear effects in traveling-wave tubes in an early paper. Their approach is based on the assumption that the energy delivered by the beam to the electromagnetic wave can be interpreted in terms of a continuous decrease of the average electron velocity v_o as the beam travels along. From a linearized theory one easily calculates the energy lost by the beam. How v_o (that is, b) varies with distance can then be calculated. Assuming that Eq. 20 remains valid, it is now possible to calculate the continuous change in the complex propagation constant, that is, the variation of x and y. A WKB-type phase integral has to be used, of course, to describe the waves. The results are, in our earlier notations,

$$\frac{S_p}{\eta/C} \approx \frac{dx/db}{2x} \tag{58}$$

$$\frac{\Phi_{E,i}}{\eta/C} \approx \frac{1+dy/db}{4x} \tag{59}$$

in which the quantities dx/db and dy/db can be obtained from Fig. 2.

Equation 58 is also plotted in Fig. 5, and Eq. 59 is plotted in Fig. 6. It is interesting to note that this rather unsophisticated method gives results the principal features of which are in acceptable qualitative agreement with our results. Beam and Blattner's method, which they have used for phase studies, is not entirely correct, but its physical basis is simple and the approach may be helpful in developing a physical understanding of the phenomena involved.

Figure 6 shows the phase delay versus b. For sufficiently slow beam velocities ($b < -1.4$), the electric field is accelerated rather than delayed by nonlinear phenomena (Φ_E negative).

The various nonlinear waves (E_z, i_1, v_1, etc.) are described by different axial wave functions rather than by one common wave function as are the linearized waves. Hence the amplitude corrections S are different for the E_z and i_1 waves, and the corresponding phase delays Φ also differ from each other (see Figs. 5 and 6). The method of Beam and Blattner gives one common wave function also in the nonlinear case. Consequently the parameters S and Φ obtained from their theory apply to all wave quantities involved (E_z, i_1, etc.).

The dashed curve in Fig. 6 was computed by Paschke (11), who, with some simplifying assumptions, developed a nonlinear successive approximation theory for the ordinary delay-line-type TWT, a radially finite device. The curve for QC = 0, taken from Paschke's Fig. 3, describes the phase delay of the fundamental frequency a-c wave (Φ_i). The qualitative agreement between Paschke's and our results is obviously good. Paschke assumes, however, without any further discussion, that his Φ_i is identical to the phase delay of the signal in the output terminal. But the output signal is the amplified electromagnetic wave. Its phase delay, as we have shown, is not the same as that of the electronic a-c wave.

The phase delay at the signal ouput also depends, of course, on the matching conditions at the output. The plane TWT model cannot be used realistically for detailed studies of the phenomena at the output (1b). Nevertheless, with reference to the Φ_E curve in Fig. 6, it might be possible to reduce the nonlinear output phase delay at the expense of gain if the beam/helix voltage were made less than that corresponding to maximum gain.

6. THE NONLINEAR SOLUTION, METHOD OF DOMINANT TERMS

This section will show that it is possible to develop a very elegant method for investigations of the dynamic nonlinearities in the plane TWT. The method yields the dominant part of all harmonic frequency waves (frequencies $n\omega$, n = 1, 2, 3, 4 ...) propagating in the system. The integer n will not be limited to 3 as it was in Sections 4 and 5. In addition the method offers a possibility of dealing with the plane TWT by use of the theory of the plane klystron tube (12,13).

Very cumbersome calculations would have been involved if we had tried to develop the successive approximation approach to higher order than the third. From the procedure used in the treatment of Eqs. 25, 26, and 27, it is easy to see that the dominating term of the frequency ω appears in the first order solution. The higher order solutions contain smaller terms of the frequency ω. These terms describe saturation and nonlinear phase shift effects. The dominating term of the frequency 2ω appears in the second order solution, the dominating term of the frequency 3ω in the third order solution, and so on. We ignore now the saturation and phase shift terms and attempt to find the dominating terms for all harmonic frequencies.

We start from the original wave equation (Eq. 10), which is written

$$\left(\frac{\partial}{\partial z^2} - \frac{1}{v_{ph}^2}\frac{\partial^2}{dt^2}\right)\frac{d^2 z_1}{dt^2} - \frac{\omega_p^2}{v_{ph}^2}\cos^2\xi\,\frac{\partial^2 z_1}{\partial t^2} = 0 \qquad (60)$$

Next we assume that z_1 can be written in the form

$$z_1 \approx \sum_{n=1}^{\infty} A_n e^{jn(\omega t - \gamma z)} \qquad (61)$$

where complex notations have been used for simplicity. The terms in the series are supposed to be the dominant terms just discussed. Saturation and phase shift terms are neglected. The quantity γ is, as before, a solution of Eq. 16.

The acceleration can be written in the form

$$\frac{d^2 z_1}{dt^2} = \ddot{z}_1 + \frac{d^2 g}{dt^2} \tag{62}$$

where the double dot is the linearized second order time derivative, $\partial^2/\partial t^2 + 2v_o \partial/\partial z + v_o^2 \partial^2/\partial z^2$. The quantity d^2g/dt^2, actually defined by Eq. 62, takes care of that part of the acceleration which is not included in the term $\ddot{z}_1$.

If the series from Eq. 61 is a solution to Eq. 60, then d^2g/dt^2 must be of the form

$$\frac{d^2 g}{dt^2} \approx \sum_{n=2}^{\infty} B_n e^{jn(\omega t - \gamma z)} \tag{63}$$

The frequency ω does not appear in the series from Eq. 63, since the term $\ddot{z}_1$ in Eq. 62 naturally contains the dominant term of the frequency ω (given by the first order or linearized solution) and the other terms of frequency ω are ignored.

By the use of Eq. 62 in Eq. 60, we obtain

$$\left(\frac{\partial^2}{\partial z^2} - \frac{1}{v_{ph}^2}\frac{\partial^2}{\partial t^2}\right)\ddot{z}_1 - \frac{\omega_p^2}{v_{ph}^2}\cos^2\xi\,\frac{\partial^2 z_1}{\partial t^2}$$

$$+\left(\frac{\partial^2}{\partial z^2} - \frac{1}{v_{ph}^2}\frac{\partial^2}{\partial t^2}\right)\frac{d^2 g}{dt^2} = 0 \tag{64}$$

Now the term $A_1 e^{j(\omega t - \gamma z)}$ is our linearized solution; that is, it is a solution to Eq. 64 with the term containing d^2g/dt^2 ignored. With this in mind one easily proves by using Eq. 61 in the first two terms of Eq. 64 that

$$\left(\frac{\partial^2}{\partial z^2} - \frac{1}{v_{ph}^2}\frac{\partial^2}{\partial t^2}\right)\ddot{z}_1 - \frac{\omega_p^2}{v_{ph}^2}\cos^2\xi\,\frac{\partial^2 z_1}{\partial t^2} = \left(\frac{\partial^2}{\partial z^2} - \frac{1}{v_{ph}^2}\frac{\partial^2}{\partial t^2}\right)$$

$$\sum_{n=1}^{\infty}\left(1 - \frac{1}{n^2}\right)(-n^2)(\omega - \gamma v_o)^2 A_n e^{jn(\omega t - \gamma z)}$$

$$= \left(\frac{\partial^2}{\partial z^2} - \frac{1}{v_{ph}^2}\frac{\partial^2}{\partial t^2}\right)\left[\ddot{z}_1 + (\omega - \gamma v_o)^2 z_1\right] \tag{65}$$

[To obtain this result one has to observe that

$$\frac{\omega_p^2}{v_{ph}^2}\cos^2\xi\frac{\partial^2}{\partial t^2}S_n = \left(\frac{\partial^2}{\partial z^2} - \frac{1}{v_{ph}^2}\frac{\partial^2}{\partial t^2}\right)\frac{1}{n^2}S_n$$

where $S_n = e^{jn(\omega t-\gamma z)}$.]

Note that it has been possible to eliminate the term

$$\frac{\omega_p^2}{v_{ph}^2}\cos^2\xi\frac{\partial^2 z_1}{\partial t^2}$$

Furthermore, Eq. 65 can be used in Eq. 64, which yields, after dropping the operator $\partial^2/\partial z^2 - (1/v_{ph}^2)\,\partial/\partial t^2$,

$$\ddot{z}_1 + \frac{d^2 f}{dt^2} + (\omega - \gamma v_o)z_1 = 0$$

or, with Eq. 62,

$$\boxed{\frac{d^2 z_1}{dt^2} + (\omega - \gamma v_o)^2 z_1 = 0} \qquad (66)$$

What has now been shown is that the dominant terms at the various frequencies in the solution to the complicated fourth order equation (Eq. 60) are identical to those in the solution to the much simpler second order equation (Eq. 66).

It is interesting to note that both Eq. 60 and Eq. 66 possess the exact solution

$$z_1 = Ae^{j(\omega t-\gamma z_o)}$$

As was pointed out in Section 2, however, the real and imaginary parts taken separately are not exact solutions to Eq. 60. As far as Eq. 66 is concerned, the real and imaginary parts are indeed exact solutions. This means that a reasonably good nonlinear solution to our problem is

$$z_1 = Ae^{\alpha z_o}\cos(\omega t - \beta z_o)$$

$$= Ae^{\alpha z}e^{-\alpha z_1}\cos(\omega t - \beta z + \beta z_1) \qquad (67)$$

Since $|\alpha z_1| \ll 1$, we can also write

$$\beta_e z_1 = R \cos (\omega t - \beta z_o) \tag{68}$$

or with $Z_o = \beta z_o - \omega t$,

$$\beta_e z_1 = R \cos Z_o \tag{69}$$

Equation 69 is plotted in (a) of Fig. 8 for R = 0.1, R = 0.5, and R = 1.0. If $\beta_e \approx \beta$ and if $2\pi\alpha/\beta \ll 1$, it is now easy to plot $\beta_e z_1$ versus Z (= $\beta z - \omega t$), the normalized axial distance. This is done in (b) of Fig. 8. Observe in this connection that $Z = Z_o + \beta z_1$ and that βz_1 is easily obtained from (a) of Fig. 8. One sees that electron overtaking is just about to occur at $Z = \pi/2$ when R = 1.0. The dashed curve in (b) of Fig. 8 is taken from (a) of Fig. 4 for R = 0.5. It is obvious that the agreement between the results obtained with the successive approximation method on the one hand and with the dominant term method on the other is good. The dominant term method is elegant and time saving, but the price one pays is the neglect of information about phase shift and saturation. (It should be remarked that Eq. 67 is not yet of the form of Eq. 61. We will return to this question and compute the dominant terms in the next section.)

If we write Eq. 67 in the form

$$z_1 = A \operatorname{Re}[e^{j(\omega t - \gamma z_o)}] = A \operatorname{Re}[e^{j(\omega t - \gamma z + \gamma z_1)}] \tag{70}$$

we find by the use of Eq. 1 that

$$\frac{v_1}{v_o C} = R \operatorname{Re}[(x - jy)e^{jZ_o}] \tag{71}$$

In the case b = 0 we now find, with $x = \sqrt{3}/2$ and $y = -(1/2)$, that

$$\frac{v_1}{v_o C} = R \cos (Z_o + 30°) \tag{72}$$

Equation 72 is plotted versus Z in (c) of Fig. 8, and graphs of Eq. 71 are shown in (a) and (b) of Fig. 9. From these curves one can see how the d-c velocity v_o (that is, the parameter b) influences the shape of the nonlinear a-c velocity v_1. Especially in (a) of Fig. 9 one notices that the faster the beam, the more the velocity wave falls back in phase.

By using Eq. 6, one obtains from Eq. 70

$$\frac{E_z}{2V_o\beta_e C^2} = R \operatorname{Re}[(jx + y)^2 e^{jZ_o}] \tag{73}$$

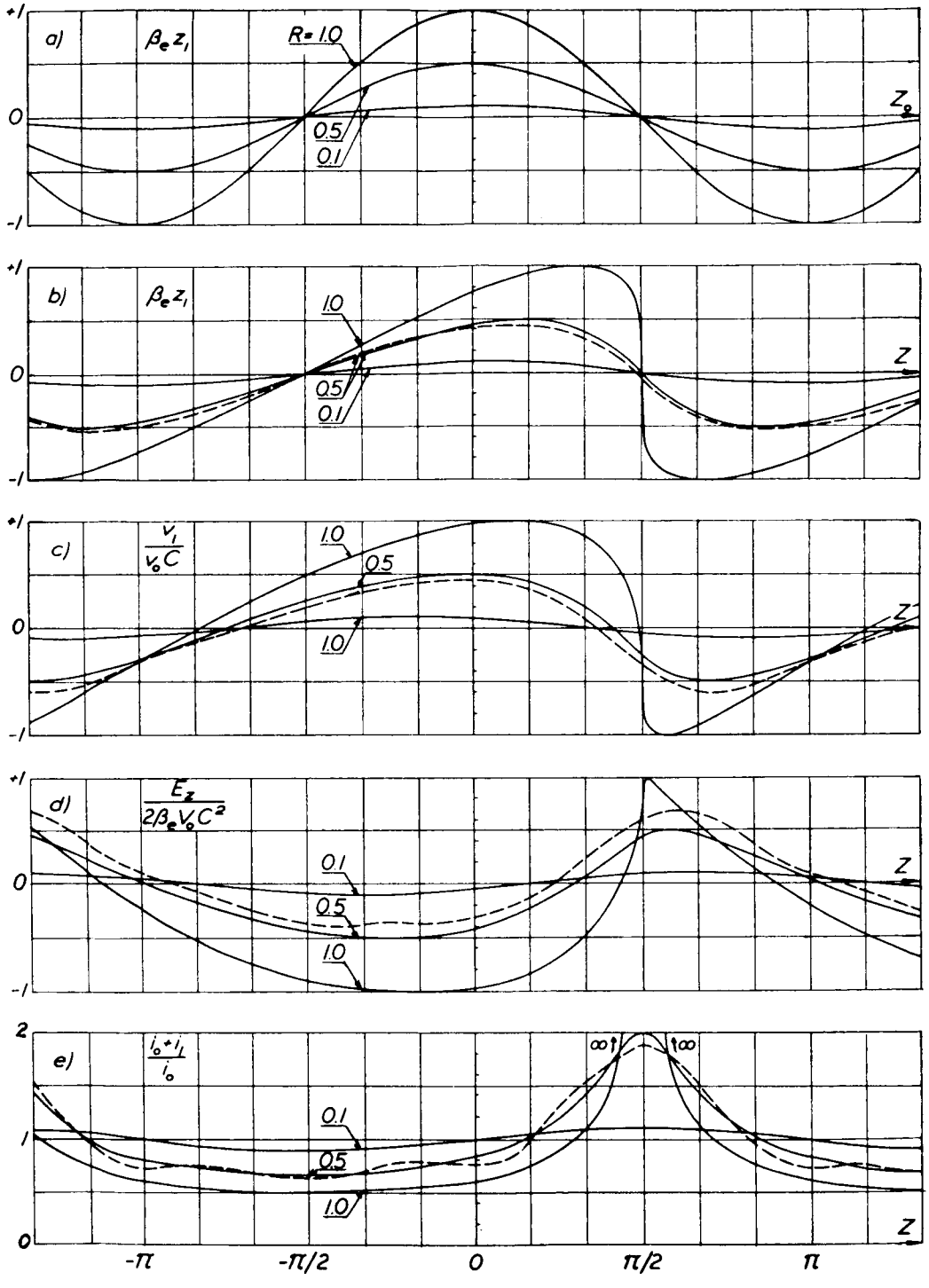

FIG. 8. For three values of amplitude parameter R: (a) displacement z_1 versus Z_0; and (b) displacement z_1, (c) excess velocity v_1, (d) axial electric field strength E_z, (e) total electron current density i (= i_0 + i_1), versus Z. Dashed curves, all for R = 0.5, taken from Fig. 4 for comparison.

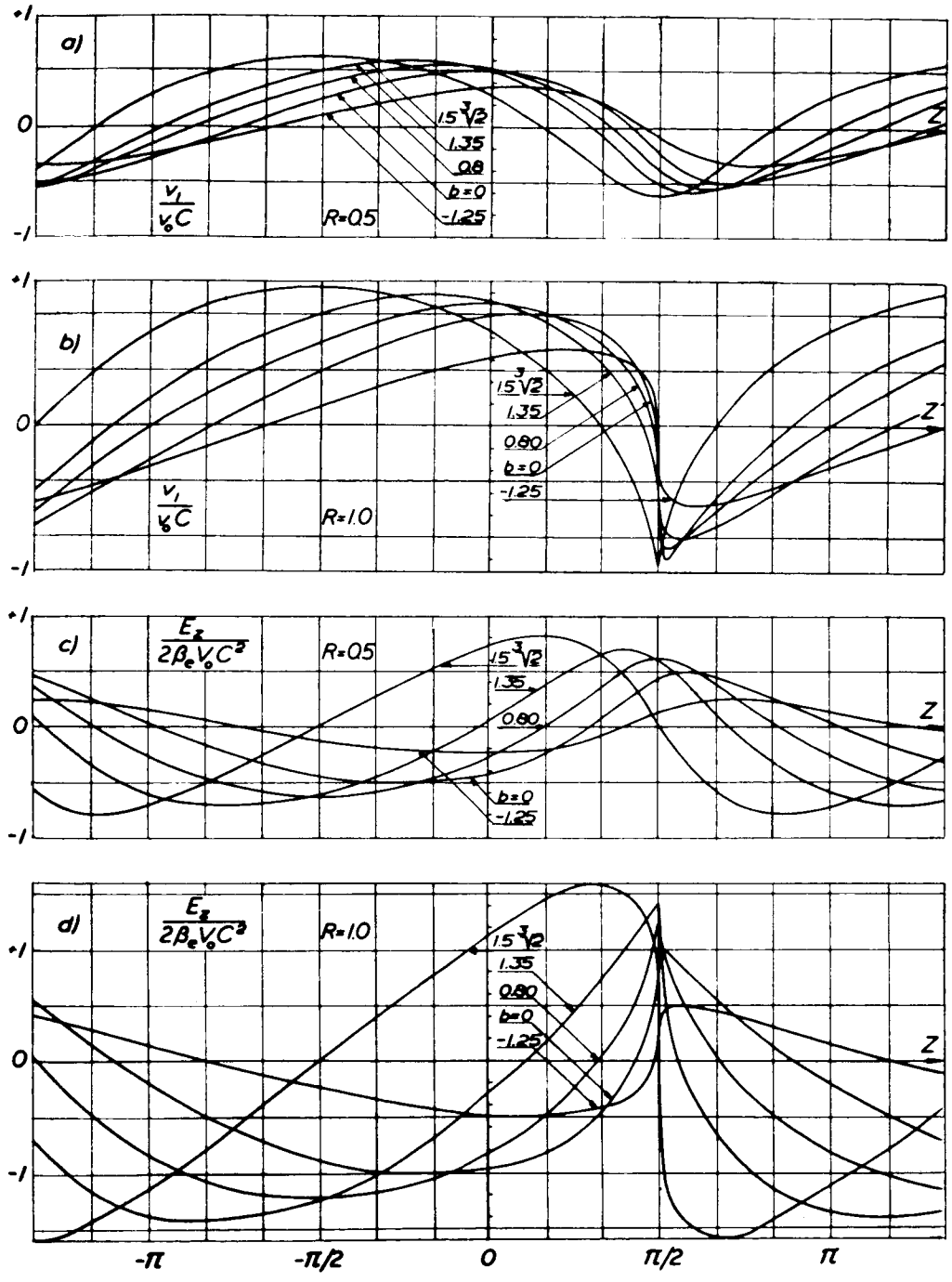

FIG. 9. For different values of R and b: (a,b) excess velocity v_1, and (c,d) axial electric field E_z, versus Z.

For b = 0 this yields

$$\frac{E_z}{2V_o\beta_e C^2} = R \sin (Z_o - 30°) \tag{74}$$

Equation 74 is plotted in (d) of Fig. 8, and Eq. 73 in (c) and (d) of Fig. 9. Observe that the electric field wave moves back in phase when the d-c velocity (parameter b) increases.

By the use of Eq. 4, one finally obtains from Eq. 70

$$\frac{i_o + i_1}{i_o} = \frac{1}{1 - R \sin Z_o} \tag{75}$$

Equation 75 is plotted versus Z in (e) of Fig. 8. As in (d) of Fig. 4, observe that a strong a-c bunch is built up around Z = $\pi/2$. From (c) and (d) of Fig. 9 we see that choosing b = 0.8 would center the retarding a-c field around the bunch. We may therefore expect to obtain good efficiencies if the d-c beam velocity is given a value somewhat higher than that corresponding to the maximum small signal gain. The experimental observations shown in Fig. 7 are in perfect agreement with this prediction.

In Fig. 10, finally, Eq. 72 is plotted for R = 2 and compared with Cutler's (8) measurement of the a-c velocity in an experimental TWT. In the situation shown, the drive is about 6 dB above overtaking and our theory is no longer valid. Nevertheless, the general shape of the two curves is essentially the same. It is beyond the scope of the present report to attempt to extrapolate the theory to the range beyond overtaking. Note, however, that overtaking occurs about 14 dB (6 dB + 8 dB) below saturation, leaving a large and important drive range untouched by analytical theories.

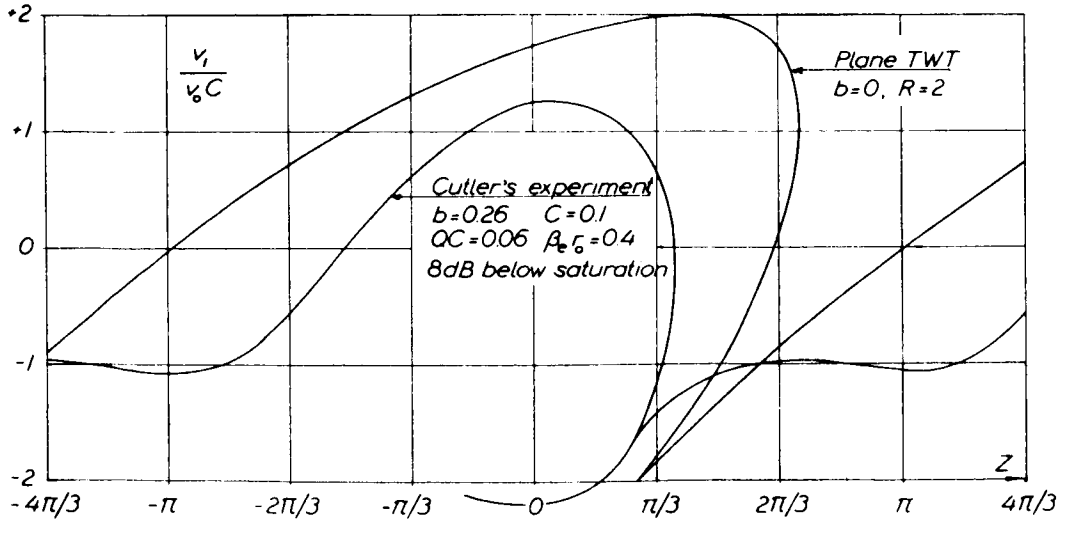

FIG. 10. The a-c velocity versus phase, a comparison of Cutler's experiment and our Eq. 72 in the range beyond overtaking.

7. CALCULATION OF THE DOMINANT TERMS

In Section 6 we reduced the exact fourth order wave equation (Eq. 60) to an approximate second order wave equation (Eq. 66). The exact solution (Eq. 67) of the latter was then studied in detail. This solution made it possible to give simple expressions for the various wave quantities of interest. The purpose of the present section is to extract the dominant terms. The exact solution is more convenient to handle than the series of dominant terms in order to obtain an over-all physical picture of the nonlinear phenomena, but it is nothing more than a reasonably good approximation to the series of dominant terms. These will now be computed.

Use will be made of the theory elsewhere developed for the plane klystron tube (12). The exact wave equation of the plane klystron tube is

$$\frac{d^2 z_1}{dt^2} + \omega_p^2 z_1 = 0 \tag{76}$$

If the undisturbed beam is modulated at the plane $z = 0$ in an ideal klystron gap producing an a-c velocity $v_1^o \cos \omega t$, the proper exact solution is

$$\beta_e z_1 = \frac{v_1^o \beta_e}{v_o \beta_p} \sin \beta_p z_o \cos (\omega t - \beta_e z_o) \tag{77}$$

If $|\beta_p z_1| \ll \pi/2$, Eq. 77 can be written in the approximate form

$$\beta_e z_1 \approx \frac{v_1^o \beta_e}{v_o \beta_p} \sin \beta_p z \cos (\omega t - \beta_e z + \beta_e z_1) \tag{78}$$

Equation 68, on the other hand, can be written

$$\beta_e z_1 \approx R \cos (\omega t - \beta z + \beta_e z_1) \tag{79}$$

Table 1 compares the corresponding equations concerned with the plane TWT (approximate) and with the plane klystron (exact). Equations 80 and 81 in the table are valid for both the TWT and the klystron, provided the proper expressions (given in the table) are used for R and T.

The series expansion for $\beta_e z_1$ (Eq. 80) is obtained by applying Fourier series to the formally identical Eqs. 78 and 79. The inversion procedure is given in detail in Ref. 12, Eqs. 37 through 45, and will not be repeated here.

It should be pointed out that the formula

$$Jn(nR) \approx \frac{1}{n!} \left(\frac{nR}{2}\right)^n$$

TABLE 1. Comparison of Equations for Plane TWT and Plane Klystron

Plane TWT	Plane Klystron
$\frac{d^2 z_1}{dt^2} + (\omega - \gamma v_o)^2 z_1 = 0$ (66)	$\frac{d^2 z_1}{dt^2} + \omega_p^2 z_1 = 0$ (76)
$R = A\beta_e e^{\alpha z} \quad T = \omega t - \beta z$	$R = \frac{v_1^o \beta_e}{v_o \beta_p} \sin \beta_p z \quad T = \omega t - \beta_e z$
$\beta_e z_1 \approx R \cos (T + \beta_e z_1)$ (79)	$\beta_e z_1 \approx R \cos (T + \beta_e z_1)$ (78)

$$\beta_e z_1 \approx \sum_{n=1}^{\infty} \frac{2}{n} J_n(nR) \sin [n(T + \tfrac{\pi}{2})]$$

$$\approx \sum_{n=1}^{\infty} \frac{R^n}{n!} (\tfrac{n}{2})^{n-1} \sin [n(T + \tfrac{\pi}{2})]$$

$$= R \cos T - \frac{1}{2} R^2 \sin 2T - \frac{3}{8} R^3 \cos 3T + \frac{1}{3} R^4 \sin 4T + \frac{125}{384} R^5 \cos 5T - \ldots \quad (80)$$

$$\frac{i_1}{i_o} = \frac{\partial(\beta_e z_1)}{\partial T} \approx \sum_{n=1}^{\infty} \frac{(nR)^n}{n!} (\tfrac{1}{2})^{n-1} \cos [n(T + \tfrac{\pi}{2})]$$

$$= - R \sin T - R^2 \cos 2T + \frac{9}{8} R^3 \sin 3T + \frac{4}{3} R^4 \cos 4T - \frac{625}{384} R^5 \sin 5T \ldots \quad (81)$$

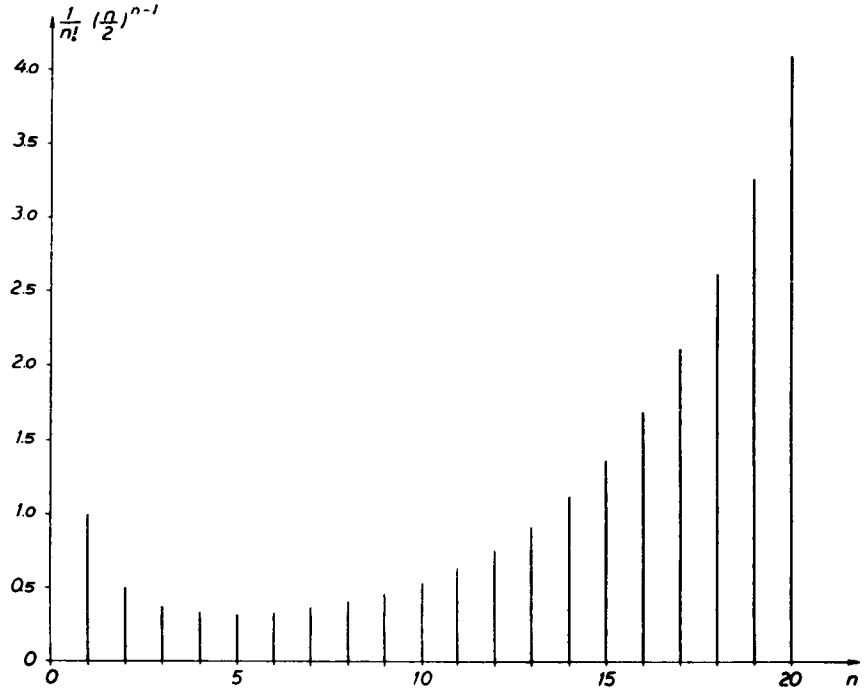

FIG. 11 Coefficients appearing in Eq. 80, versus n.

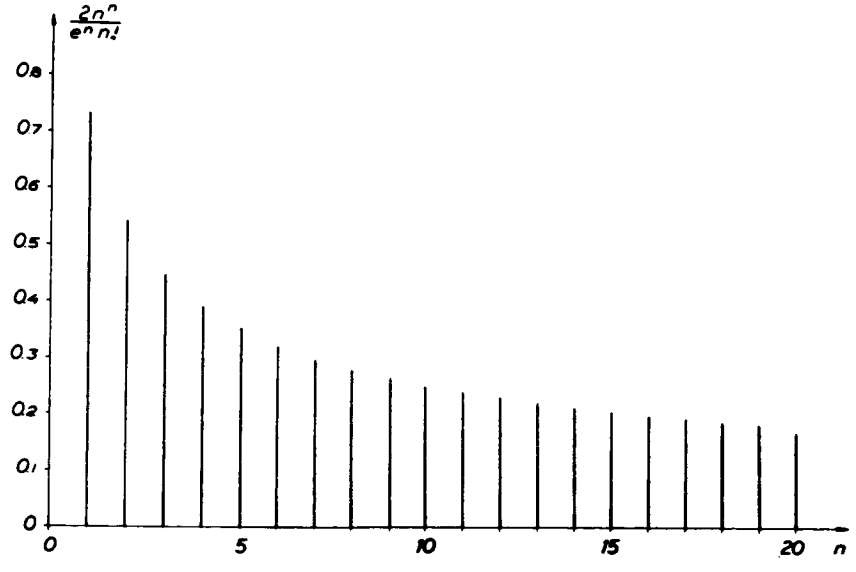

FIG. 12. Amplitudes of normalized a-c harmonic electron current waves $[(nR)^n/n!](1/2)^{n-1}$ at the limit of convergence of Eq. 81, that is, for R = 2/e.

which is valid when $R^2 \ll 1$, has been used in Eq. 80. Furthermore, a simple convergence test immediately gives the result that the series

$$\sum_{n=1}^{\infty} \frac{R^n}{n!} \left(\frac{n}{2}\right)^{n-1}$$

is convergent when $R < 2/e$. This, of course, does not tell us very much about the precise range of validity of Eq. 80, since the phase shift and saturation terms have been ignored anyway.

If we introduce the notation Z (= $\beta z - \omega t = -T$) into Eq. 80, we obtain

$$\beta_e z_1 = R \cos Z + \frac{1}{2} R^2 \sin 2Z - \frac{3}{8} R^3 \cos 3T$$

$$- \frac{1}{3} R^4 \sin 4Z + \frac{125}{384} R^5 \cos 5T \ldots \qquad (82)$$

The reader should now compare Eq. 82 with Eq. 40 and identify the three dominant terms that are common to these equations. Equation 40, which is limited to the third order, contains the three lowest dominant terms and the significant phase shift and saturation terms up to the third order. There is also a second order d-c term in Eq. 40. Equation 80 gives the dominant terms of all orders, but misses the phase shift and saturation terms completely.

From Eq. 81 and Fig. 12 one concludes that unless $R \ll 1$, the amplitudes of the harmonic frequency waves are large. This is expected, of course, on account of the development of the strong and narrow electron current bunch around the phase $Z = \pi/2$ when R is large enough. At the same time, the coupling between the electron beam and the slow wave medium is strong, for natural reasons, even at harmonic frequencies. In a real traveling-wave tube one should expect a much less pronounced generation of harmonic frequencies, owing to weak coupling.

8. CONCLUDING REMARKS

This report is concerned with a purely analytical nonlinear theory for a plane traveling-wave tube (TWT) model. The model, described in Section 1, consists of an infinitely wide confined single-velocity electron plasma stream of zero temperature, which interpenetrates an anisotropically conducting homogeneous medium. In the absence of the electron stream, the medium supports plane electromagnetic slow TM (transverse magnetic) waves, and thus plays the same role as the slow wave structure in a real TWT. A plane model was chosen to avoid the theoretical complications associated with the radial boundary conditions. This means, of course, that the present theory does not describe TWT effects caused by the radial finiteness of the beam or the slow wave structure. But the model allows one to study, in the simplest conceivable manner, the basic physical effects associated with the TWT amplification mechanism itself.

In Section 2 the exact nonlinear wave equation (Eq. 10) for the plane TWT is derived by the use of Maxwell's equations. It is assumed that the electron velocity is a one-valued function of distance; that is, electron overtaking is not allowed. This restriction considerably simplifies the analysis, but it limits the theory to drive levels well below saturation.

The results of a linearized theory of the plane TWT are briefly discussed in Section 3. For a detailed linear analysis of the device, the reader is referred to Refs. 1a and 1b. In Section 4 the method of successive approximations is applied to obtain a nonlinear third order solution. Some of the results are demonstrated in Fig. 4, which shows how the sinusoidal form of the various wave quantities is distorted by nonlinear processes when the wave amplitudes become large.

The nonlinear effects appearing in the amplitude and phase of the fundamental frequency wave are studied in Section 5 (Figs. 5 and 6). A number of new and rather interesting results are derived and discussed. Some of these have been checked experimentally by the use of a commercial TWT. The qualitative agreement between the theory and the experiments is good (Fig. 7).

Sections 6 and 7 are concerned with another method of dealing with the nonlinear fourth order wave equation (Eq. 10), the method of dominant terms. This method ignores some of the important nonlinear effects (saturation, phase shift), but it leads quickly and elegantly to simple implicit expressions for the wave quantities. Figure 8, depicting these expressions, shows that the agreement between the two methods (successive approximations and dominant terms) is close. In Section 7 the dominant-term-type approximate theory for the plane TWT is shown to be formally identical to the exact theory of the plane klystron tube, which is treated in Ref. 12. By the use of the plane klystron theory the dominant terms (the leading terms at each harmonic frequency $n\omega$, $n = 1, 2, 3, \ldots \infty$) are computed for the plane TWT.

ACKNOWLEDGMENTS

The author gratefully acknowledges the assistance given by M. Fischer, who checked the results and prepared most of the graphs, and by J.-I. Lindström and T. Srinivasan, who performed the measurements. The work was made possible through the support of the Rome Air Development Center, Air Force Systems Command, through the European Office, Aerospace Research, United States Air Force.

REFERENCES

1a. S. Olving, A New Method for Space Charge Wave Interaction Studies, Part I, Repts. Research Lab. Electronics No. 37, Trans. Chalmers Univ. Technol. No. 178, 1956.

1b. S. Olving, Part II, Repts. Research Lab. Electronics No. 51, Trans. Chalmers Univ. Technol. No. 228, 1960.

2. S. Olving, Non-linear Space Charge Wave Theory of the Radially Finite Electron Beam, Research Rept. EE 497, School Elec. Eng., Cornell Univ., 1961.

3. J. R. Pierce, Traveling Wave Tubes, Van Nostrand Co., New York, 1950.

4. O. E. H. Rydbeck, The Theory of the Travelling Wave Tube, Repts. Research Lab. Electronics No. 1, Chalmers Univ. Technol., 1948.

5. S. Olving, Electromagnetic and Space Charge Waves in a Sheath Helix, Repts. Research Lab. Electronics No. 49, Chalmers Univ. Technol., 1960.

6. C. K. Birdsall, G. R. Brewer, and A. V. Haeff, The Resistive-Wall Amplifier, Proc. IRE, 41:865-875, July 1953.

7. F. Paschke, On the Nonlinear Behavior of Electron-Beam Devices, RCA Rev., 18:221-242, June 1957.

8. C. C. Cutler, The Nature of Power Saturation in Traveling Wave Tubes, Bell System Tech. J., 35:841-876, July 1956.

9. S. Olving, The Kinetic A-C Power Flow in Nonhomogeneous Relativistic Electron Beams, Research Rept. EE 499, School Elec. Eng., Cornell Univ., 1961.

10. W. R. Beam and D. J. Blattner, Phase Angle Distortion in Traveling Wave Tubes, RCA Rev., 17:86-99, March 1956.

11. F. Paschke, New Results on Frequency Multiplication and Nonlinear Phase Distortion in Klystrons and Traveling-Wave Tubes, RCA Rev., 22:162-184, March 1961.

12. S. Olving, On the Nonlinear Theory of the Plane Klystron Tube, Research Rept. EE 500, School Elec. Eng., Cornell Univ., 1961.

13. P. McIsaac, Nonlinear Space-Charge-Wave Analysis, Research Rept. EE 513, School Elec. Eng., Cornell Univ., 1961.

U.Ed. 4-114